DYNAMIC AND STEADY-STATE ANALYSIS OF OXIDATIVE DEHYDROGENATION OF ETHANE

A THESIS SUBMITTED TO

THE GRADUATE SCHOOL OF NATURAL AND APPLIED SCIENCES

OF

MIDDLE EAST TECHNICAL UNIVERSITY

BY

GÜLSÜN KARAMULLAOĞLU

IN PARTIAL FULFILLMENT OF THE REQUIREMENTS
FOR
THE DEGREE OF DOCTOR OF PHILOSOPHY
IN
CHEMICAL ENGINEERING

JULY 2005

Approval of the Graduate School of Natural and Applied Sciences

_____

Prof. Dr. Canan Özgen
Director

I certify that this thesis satisfies all the requirements as a thesis for the degree of Doctor of Philosophy.

_____

Prof. Dr. Nurcan Baç
Head of Department

This is to certify that we have read this thesis and that in our opinion it is fully adequate, in scope and quality, as a thesis for the degree of Doctor of Philosophy.

_____

Prof. Dr. Timur Doğu
Supervisor

Examining Committee Members

Prof. Dr. H. Önder Özbelge (METU,Ch.E.) _____

Prof. Dr. Timur Doğu (METU, Ch.E.) _____

Prof. Dr. Gülşen Doğu (Gazi Univ., Ch.E.) _____

Prof. Dr. Hayrettin Yücel (METU,Ch.E.) _____

Prof. Dr. Güzide Çalık (Ankara Univ., Ch.E.) _____

I hereby declare that all information in this document has been obtained and presented in accordance with academic rules and ethical conduct. I also declare that, as required by these rules and conduct, I have fully cited and referenced all material and results that are not original to this work.

Name, Last name: Gülsün Karamulloğlu

Signature :

ABSTRACT

DYNAMIC AND STEADY-STATE
ANALYSIS OF
OXIDATIVE DEHYDROGENATION OF ETHANE

Karamullaoğlu, Gülsün
Ph.D., Department of Chemical Engineering
Supervisor: Prof. Dr. Timur Doğu

July 2005, 265 pages

In this research, oxidative dehydrogenation of ethane to ethylene was studied over Cr-O and Cr-V-O mixed oxide catalysts through steady-state and dynamic experiments. The catalysts were prepared by the complexation method. By XRD, presence of Cr_2O_3 phase in Cr-O; and the small Cr_2O_3 and V_2O_4 phases of Cr-V-O were revealed. In H_2-TPR, both catalysts showed reduction behaviour. From XPS the likely presence of Cr^{+6} on fresh Cr-O was found. On Cr-V-O, the possible reduction of V^{+5} and Cr^{+6} forms of the fresh sample to V^{+4}, V^{+3} and Cr^{+3} states by TPR was discovered through XPS.

With an O_2/C_2H_6 feed ratio of 0.17, Cr-O exhibited the highest total conversion value of about 0.20 at 447°C with an ethylene selectivity of 0.82. Maximum ethylene selectivity with Cr-O was obtained as 0.91 at 250°C. An ethylene selectivity of 0.93 was reached with the Cr-V-O at 400°C. In the experiments performed by using CO_2 as the mild oxidant, a yield value of 0.15 was achieved at 449°C on Cr-O catalyst.

In dynamic experiments performed over Cr-O, with C_2H_6 pulses injected into O_2-He flow, the possible occurrence of two reaction sites for the formation of CO_2 and H_2O was detected. By Gaussian fits to H_2O curves, the

presence of at least three production ways was thought to be probable. Different from Cr-O, no CO_2 formation was observed on Cr-V-O during pulsing C_2H_6 to O_2-He flow. In the runs performed by O_2 pulses into C_2H_6-He flow over Cr-V-O, formation of CO rather than C_2H_4 was favored.

Keywords: Oxidative Dehydrogenation, Ethane, Ethylene, Chromium Mixed Oxide Catalysts, Dynamic Analysis

öz

ETANIN OKSİDATİF DEHİDROJENASYONUNUN
DİNAMİK VE YATIŞKIN KOŞULLARDA ANALİZİ

Karamullaoğlu, Gülsün
Doktora, Kimya Mühendisliği Bölümü
Tez Yöneticisi: Prof. Dr. Timur Doğu

Temmuz 2005, 265 sayfa

Bu araştırmada, etanın etilene oksidatif dehidrojenasyonu Cr-O ve Cr-V-O karışık oksit katalizörleri üzerinde yatışkın ve dinamik deneylerle çalışılmıştır. Katalizörler kompleks metot ile hazırlanmıştır. XRD ile, Cr-O içinde Cr_2O_3 varlığı; ve Cr-V-O katalizörünün küçük Cr_2O_3 ve V_2O_4 yapıları ortaya çıkarılmıştır. H_2-TPR'de, her iki katalizör indirgenme davranışı göstermiştir. XPS'ten kullanılmamış Cr-O katalizöründe Cr^{+6}'nın olası varlığı bulunmuştur. Cr-V-O üzerinde, kullanılmamış örneğin V^{+5} ve Cr^{+6} formlarının TPR ile V^{+4}, V^{+3} ve Cr^{+3} durumlarına indirgenme olasılığı XPS ile ortaya çıkarılmıştır.

O_2/C_2H_6 besleme oranı 0.17 ile, Cr-O en yüksek toplam dönüşüm değeri olan yaklaşık 0.20'yi 447°C'de 0.82'lik etilen seçiciliği ile göstermiştir. Cr-O ile maksimum etilen seçiciliği 0.91 olarak 250°C'de elde edilmiştir. Cr-V-O ile 400°C'de 0.93'lük etilen seçiciliğine erişilmiştir. CO_2'in hafif oksidan olarak kullanıldığı deneylerde, Cr-O üzerinde 449°C'de, 0.15'lik etilen verim değeri elde edilmiştir.

Cr-O üzerinde yapılan dinamik deneylerde, O_2-He akışına verilen C_2H_6 vurularıyla, CO_2 ve H_2O oluşumu için iki reaksiyon konumunun olası varlığı

bulunmuştur. H_2O eğrilerine Gauss uygulaması ile, en az üç oluşum şeklinin muhtemel olduğu düşünülmüştür. Cr-O katalizöründen farklı olarak, Cr-V-O katalizörü üzerinde O_2-He akışına C_2H_6 vuru verilişi sırasında CO_2 oluşumu gözlenmemiştir. Cr-V-O katalizörü üzerinde C_2H_6-He akışına O_2 vurularıyla yapılan deneylerde, C_2H_4 yerine CO oluşumu tercih edilmiştir.

Anahtar Kelimeler: Oksidatif Dehidrojenasyon, Etan, Etilen, Krom Karışık Oksit Katalizörleri, Dinamik Analiz

To My Mother, My Sister, and
To the Memory of My Father and Uncle

ACKNOWLEDGEMENTS

First and foremost, I would like to express my deepest gratitute to my supervisor Prof. Dr. Timur Doğu for his invaluable guidance and help throughout this study. I would like to present my sincere and special thanks to my Ph.D. Committee Members Prof. Dr. Gülşen Doğu and Prof. Dr. Hayrettin Yücel for their constructive advices.

I would like to thank Dr.Sena Yaşyerli for her help in catalyst preparation and BET analysis. I am also thankful to Zuhal Göğebakan for XRD analysis. Thanks are also due to all the technicians and machine shop workers of the Department of Chemical Engineering who helped me in this study.

I would also like to thank Tanıl Tarhan, Almıla Bahar, Yusuf Göğebakan, Değer Şen, Burcu Mirkelamoğlu, Mustafa Karaman, Canan Şener, Berker Fıçıcılar, Zeynep Çulfaz, and Salih Obut for their various help.

Finally, my deepest gratitute is to my mother and sister for their love, support, patiance, encouragement, and faith in me.

TABLE OF CONTENTS

PLAGIARISM..... iii

ABSTRACT..... iv

ÖZ..... vi

ACKNOWLEDGEMENTS..... ix

TABLE OF CONTENTS..... x

LIST OF TABLES..... xiii

LIST OF FIGURES..... xvi

LIST OF SYMBOLS..... xxvi

CHAPTER

1. INTRODUCTION..... 1

1.1. Ethylene: an Important Chemical Feedstock..... 3

1.2. Oxidative Dehydrogenation Studies from Literature..... 6

1.3. Objectives of the Study..... 15

2. EXPERIMENTAL STUDIES..... 16

2.1. Experimental Set-up..... 16

2.1.1. Theory of Mass Spectrometer..... 20

2.2. Calibration of Mass Spectrometer..... 24

2.3. Catalyst Preparation..... 26

2.4. Catalyst Characterization..... 28

2.5. Catalyst Testing – Steady-state Experiments..... 29

2.6. Dynamic Experiments..... 29

3. RESULTS AND DISCUSSION..... 31

3.1. Catalyst Characterization..... 31

3.2. Catalyst Testing – Steady-state Experiments..... 50

3.2.1. Experiments with Cr-O Catalyst under O_2-C_2H_6-He Flow..... 53

3.2.2. Experiments with Cr-O Catalyst under CO_2-C_2H_6-He Flow..... 62

3.2.3. Experiments with Cr-V-O Catalyst under O_2-C_2H_6-He Flow..... 64

3.2.4. Experiments with Cr-V-O Catalyst under CO_2-C_2H_6-He Flow..... 72

3.2.5. Experiments with V-MCM-41 Catalyst under O_2-C_2H_6-He Flow..... 77

3.2.6. Comparison of Catalysts..... 80

3.2.6.1. Cr-O and Cr-V-O Catalysts..... 80

3.2.6.2. Cr-O, Cr-V-O, and V-MCM-41 Catalysts..... 80

3.3. Dynamic Experiments..... 84

3.3.1. Dynamic Experiments with Cr-O Catalyst..... 84

3.3.2. Dynamic Experiments with Cr-V-O Catalyst..... 97

3.3.3. Dynamic Experiments' Comparison of Cr-O and Cr-V-O Catalysts..... 103

4. CONCLUSIONS..... 105

5. RECOMMENDATIONS..... 111

REFERENCES..... 112

APPENDICES

A. CALIBRATION DATA FOR MASS SPECTROMETER..... 119

A.1. The Mass Spectrometer Cracking Patterns for the System Gases..... 119

A.2. Data of Mass Spectrometer Calibration Experiments..... 120

A.3. Data of Mass Spectrometer Calibration Experiments – Check after Blocking of Capillary..... 130

A.4. MS Calibration Charts – with Mean Values..... 143

A.5. MS Calibration Charts – with Normalized Mean Values..... 146

B. DEFINITIONS OF 'GOODNESS OF FIT STATISTICS' FOR MATLAB 6.5 CURVE FITS..... 149

C. EXPERIMENTAL DATA FOR STEADY-STATE EXPERIMENTS..... 150

C.1. Experimental Data for Cr-O Catalyst..... 150

C.2. Experimental Data for Cr-V-O Catalyst 151

C.3. Experimental Data for V-MCM-41 Catalyst..... 152

D. EXPERIMENTAL DATA FOR DYNAMIC EXPERIMENTS 153

D.1. Dynamic Experiments' Data for Cr-O Catalyst..... 153

D.1.1. Dynamic Experiments' Data for Cr-O Catalyst with C_2H_6 Pulses into O_2 and He Flow at 350°C..... 153

D.1.2. Dynamic Experiments' Data for Cr-O Catalyst with C_2H_6 Pulses into O_2 and He Flow at 401°C..... 165

D.1.3. Dynamic Experiments' Data for Cr-O Catalyst with C_2H_6 Pulses into O_2 and He Flow at 450°C..... 177

D.1.4. Dynamic Experiments' Data for Cr-O Catalyst with C_2H_6 pulses into He flow at 448°C..... 190

D.2. Dynamic Experiments' Data for Cr-V-O Catalyst..... 212

D.2.1. Dynamic Experiments' Data for Cr-V-O Catalyst with C_2H_6 Pulses into O_2 and He Flow at 400°C..... 212

D.2.2. Dynamic Experiments' Data for Cr-V-O Catalyst with O_2 Pulses into C_2H_6 and He Flow at 400°C..... 223

D.2.3. Dynamic Experiments' Data for Cr-V-O Catalyst with C_2H_6 Pulses into He Flow at 449°C..... 241

CURRICULUM VITAE..... 263

LIST OF TABLES

Table 1. Distribution of uses for ethylene..... 3

Table 2. Pulse-response experiments..... 30

Table 3. Parameters for the fitted TPR profile of Cr-V-O catalyst..... 40

Table 4. Atom percentages of Cr-O catalyst determined by XPS..... 45

Table 5. Binding energies for fresh and reduced Cr-O catalyst from XPS..... 45

Table 6. Atom percentages of Cr-V-O catalyst determined by XPS..... 46

Table 7. Binding energies for fresh and reduced Cr-V-O catalyst from XPS..... 48

Table 8. Average mean residence times of C_2H_6 and C_2H_4 for pulses of C_2H_6 into He and O_2 flow over Cr-O catalyst..... 85

Table 9. Average mean values of CO_2 and H_2O Gaussian curves for pulses of C_2H_6 into He and O_2 flow over Cr-O catalyst..... 91

Table 10. Product distribution for O_2 pulses into He and C_2H_6 flow over Cr-V-O catalyst at 400°C..... 99

Table A.1. Mass spectrometer calibration data for C_2H_6 in He..... 120

Table A.2. Mass spectrometer calibration data for C_2H_4 in He..... 122

Table A.3. Mass spectrometer calibration data for O_2 in He..... 124

Table A.4. Mass spectrometer calibration data for CO_2 in He..... 125

Table A.5. Mass spectrometer calibration data for CH_4 in He..... 126

Table A.6. Mass spectrometer calibration data for O_2 - C_2H_6 – He..... 128

Table A.7. Mass spectrometer calibration data for C_2H_6 in He (check-empty reactor) 130

Table A.8. Mass spectrometer calibration data for C_2H_6 in He (check - reactor filled with Cr-O catalyst) 132

Table A.9. Mass spectrometer calibration data for C_2H_4 in He (check- empty reactor) 134

Table A.10. Mass spectrometer calibration data for O_2 in He (check - reactor filled with Cr-O catalyst) 136

Table A.11. Mass spectrometer calibration data for CO_2 in He (check - reactor filled with Cr-O catalyst)..... 137

Table A.12. Mass spectrometer calibration data for CH_4 in He (check – empty reactor) 139

Table A.13. Mass spectrometer calibration data for CO in He (empty reactor) 141

Table A.14. Mass spectrometer calibration data for H_2 in He (reactor filled with Cr-O catalyst) 142

Table C.1. Experimental data for Cr-O catalyst with ~5% O_2 - 30% C_2H_6 – 65% He feed composition..... 150

Table C.2. Experimental data for Cr-O catalyst with ~10% O_2 - 30% C_2H_6 – 60% He feed composition..... 150

Table C.3. Experimental data for variation of O_2 mole fraction in feed with Cr-O catalyst (T = ~250°C) 150

Table C.4. Experimental data for Cr-O catalyst with ~10% CO_2 - 30% C_2H_6 – 60% He feed composition..... 151

Table C.5. Experimental data for Cr-V-O catalyst with ~5% O_2 - 30% C_2H_6 – 65% He feed composition..... 151

Table C.6. Experimental data for Cr-V-O catalyst with ~10% O_2 - 30% C_2H_6 – 60% He feed composition..... 151

Table C.7. Experimental data for Cr-V-O catalyst with ~10% CO_2 - 30% C_2H_6 – 60% He feed composition..... 152

Table C.8. Experimental data for Cr-V-O catalyst with ~45% CO_2 - 30% C_2H_6 – 25% He feed composition..... 152

Table C.9. Experimental data for V-MCM-41 catalyst with ~5% O_2 - 30% C_2H_6 – 65% He feed composition..... 152

Table D.1. C_2H_6 response data for C_2H_6 pulses into O_2 and He flow over Cr-O catalyst at 350°C..... 162

Table D.2. C_2H_4 response data for C_2H_6 pulses into O_2 and He flow over Cr-O catalyst at 350°C..... 162

Table D.3. CO_2 response data for C_2H_6 pulses into O_2 and He flow over Cr-O catalyst at 350°C..... 163

Table D.4. H_2O response data for C_2H_6 pulses into O_2 and He flow over Cr-O catalyst at 350°C..... 164

Table D.5. C_2H_6 response data for C_2H_6 pulses into O_2 and He flow over Cr-O catalyst at 401°C..... 174

Table D.6. C_2H_4 response data for C_2H_6 pulses into O_2 and He flow over Cr-O catalyst at 401°C..... 174

Table D.7. CO_2 response data for C_2H_6 pulses into O_2 and He flow over Cr-O catalyst at 401°C..... 175

Table D.8. H_2O response data for C_2H_6 pulses into O_2 and He flow over Cr-O catalyst at 401°C..... 176

Table D.9. C_2H_6 response data for C_2H_6 pulses into O_2 and He flow over Cr-O catalyst at 450°C..... 187

Table D.10. C_2H_4 response data for C_2H_6 pulses into O_2 and He flow over Cr-O catalyst at 450°C..... 187

Table D.11. CO_2 response data for C_2H_6 pulses into O_2 and He flow over Cr-O catalyst at 450°C..... 188

Table D.12. H_2O response data for C_2H_6 pulses into O_2 and He flow over Cr-O catalyst at 450°C..... 189

Table D.13. C_2H_6 response data for C_2H_6 pulses into He flow over Cr-O catalyst at 448°C..... 208

Table D.14. C_2H_4 response data for C_2H_6 pulses into He flow over Cr-O catalyst at 448°C..... 209

Table D.15. C_2H_6 response data for C_2H_6 pulses into O_2 and He flow over Cr-V-O catalyst at 400°C..... 220

Table D.16. C_2H_4 response data for C_2H_6 pulses into O_2 and He flow over Cr-V-O catalyst at 400°C..... 221

Table D.17. H_2O response data for C_2H_6 pulses into O_2 and He flow over Cr-V-O catalyst at 400°C..... 222

Table D.18. O_2 response data for O_2 pulses into C_2H_6 and He flow over Cr-V-O catalyst at 400°C..... 238

Table D.19. H_2O response data for O_2 pulses into C_2H_6 and He flow over Cr-V-O catalyst at 400°C..... 239

Table D.20. CO response data for O_2 pulses into C_2H_6 and He flow over Cr-V-O catalyst at 400°C..... 240

Table D.21. C_2H_6 response data for C_2H_6 pulses into He flow over Cr-V-O catalyst at 449°C..... 259

Table D.22. C_2H_4 response data for C_2H_6 pulses into He flow over Cr-V-O catalyst at 449°C..... 260

Table D.23. H_2O response data for C_2H_6 pulses into He flow over Cr-V-O catalyst at 449°C..... 262

LIST OF FIGURES

Figure 1. Ethylene products..... 4

Figure 2. Experimental set-up..... 16

Figure 3. Photograph of experimental set-up..... 17

Figure 4. HPR20 Gas Analysis System [56]..... 18

Figure 5. Vacuum line connections of the HPR20 mass spectrometer [56] 19

Figure 6. Block diagram of mass spectrometer [58] 21

Figure 7. Quadrupole mass analyzer [58] 22

Figure 8. Continuous dynode electron multiplier detector [58] 23

Figure 9. XRD patterns of the prepared Cr-O catalyst and Cr_2O_3..... 31

Figure 10. XRD patterns of the prepared Cr-V-O catalyst and $Cr_2VO_{5.5}$, V_2O_4, V_2O_3, and Cr_2O_3..... 32

Figure 11. XRD pattern of the V-MCM-41 catalyst..... 33

Figure 12. TPR profile of Cr-O catalyst..... 34

Figure 13. TPR profile of Cr-O catalyst (smoothed curve)..... 34

Figure 14. TPR profile of Cr-V-O catalyst..... 36

Figure 15. Formation of H_2O during TPR of Cr-V-O catalyst..... 36

Figure 16. H_2 consumed versus time for Cr-V-O catalyst..... 37

Figure 17. 'Summation of two Gaussian peaks' fit trial for H_2 consumed versus time for Cr-V-O catalyst..... 38

Figure 18. 'Summation of three Gaussian peaks' fit trial for H_2 consumed versus time for Cr-V-O catalyst..... 39

Figure 19. De-convolution of 'Summation of three Gaussian peaks' fit for H_2 consumption versus time for Cr-V-O catalyst..... 39

Figure 20. XPS spectrum of Cr-O catalyst..... 41

Figure 21. XPS spectrum of Cr-O catalyst after ion bombardment..... 42

Figure 22. XPS spectra of Cr-O catalyst before and after ion bombardment 42

Figure 23. XPS spectrum of reduced Cr-O catalyst after H_2-TPR..... 43

Figure 24. XPS spectrum of reduced Cr-O catalyst after after ion bombardment..... 44

Figure 25. XPS spectra of reduced Cr-O catalyst before and after ion bombardment..... 44

Figure 26. XPS spectrum of Cr-V-O catalyst..... 45

Figure 27. XPS spectrum of Cr-V-O catalyst after ion bombardment..... 46

Figure 28. XPS spectra of Cr-V-O catalyst before and after ion bombardment..... 47

Figure 29. XPS spectrum of reduced Cr-V-O catalyst after H_2-TPR..... 47

Figure 30. XPS spectrum of reduced Cr-V-O catalyst after ion bombardment..... 48

Figure 31. XPS spectra of reduced Cr-V-O catalyst before and after ion bombardment..... 49

Figure 32. **(a)** Total conversion-temperature data, **(b)** C_2H_4 selectivity-temperature data, **(c)** C_2H_4 yield-temperature data (catalyst: 0.2 g Cr-O, O_2/C_2H_6 = 0.50, feed: 50 cm^3/min) 54

Figure 33. **(a)** Total conversion-temperature data, **(b)** C_2H_4 selectivity-temperature data, **(c)** C_2H_4 yield-temperature data (catalyst: 0.2 g Cr-O, O_2/C_2H_6 = ~0.17, feed: 50 cm^3/min)..... 55

Figure 34. **(a)** CO_2 selectivity-temperature data, **(b)** CH_4 selectivity-temperature data (catalyst: 0.2 g Cr-O, O_2/C_2H_6 = ~0.17, feed: 50 cm^3/min) 56

Figure 35. **(a)** Total conversion-temperature data, **(b)** C_2H_4 selectivity-temperature data, **(c)** C_2H_4 yield-temperature data (catalyst: 0.2 g Cr-O, O_2/C_2H_6 = ~0.33, feed: 50cm^3/min).... 57

Figure 36. Comparison of **(a)** Total conversion-temperature data, **(b)** C_2H_4 selectivity-temperature data, **(c)** C_2H_4 yield-temperature data for Cr-O catalyst with 5% and 10% oxygen in feed (catalyst: 0.2 g Cr-O, O_2/C_2H_6 = ~0.17 and ~0.33, feed: 50 cm^3/min) 59

Figure 37. **(a)** CO_2 selectivity-temperature data, **(b)** CH_4 selectivity-temperature data, **(c)** CO selectivity-temperature data (catalyst: 0.2 g Cr-O, O_2/C_2H_6 = ~0.33, feed: 50 cm^3/min) 60

Figure 38. **(a)** Total conversion-O_2 compositon data, **(b)** C_2H_4 selectivity-O_2 compositon data, **(c)** C_2H_4 yield- O_2 compositon data (catalyst: 0.2 g Cr-O, T=~250°C, feed: 50 cm^3/min)..... 61

Figure 39. **(a)** Total conversion-temperature data, **(b)** C_2H_4 selectivity-temperature data, **(c)** C_2H_4 yield-temperature data (catalyst: 0.2 g Cr-O, CO_2/C_2H_6 = ~0.33, feed: 50 cm^3/min)..... 63

Figure 40. CH_4 selectivity-temperature data (catalyst: 0.2 g Cr-O, CO_2/C_2H_6 = ~0.33, feed: 50 cm^3/min)..... 64

Figure 41. Comparison of **(a)** Total conversion-temperature data, **(b)** C_2H_4 selectivity-temperature data, **(c)** C_2H_4 yield-temperature data for Cr-O catalyst with 10% O_2 and 10% CO_2 in feed (catalyst: 0.2 g Cr-O, feed: 50 cm^3/min)..... 65

Figure 42. **(a)** Total conversion-temperature data, **(b)** C_2H_4 selectivity-temperature data, **(c)** C_2H_4 yield-temperature data (catalyst: 0.2 g Cr-V-O, O_2/C_2H_6 = ~0.17, feed: 50 cm^3/min)..... 66

Figure 43. **(a)** CO_2 selectivity-temperature data, **(b)** CH_4 selectivity-temperature data, **(c)** CO selectivity-temperature data (catalyst: 0.2 g Cr-V-O, O_2/C_2H_6 = ~0.17, feed: 50 cm^3/min)..... 68

Figure 44. **(a)** Total conversion-temperature data, **(b)** C_2H_4 selectivity-temperature data, **(c)** C_2H_4 yield-temperature data (catalyst: 0.2 g Cr-V-O, O_2/C_2H_6 = ~0.33, feed: 50 cm^3/min)..... 69

Figure 45. Comparison of **(a)** Total conversion-temperature data, **(b)** C_2H_4 selectivity-temperature data, **(c)** C_2H_4 yield-temperature data for Cr-V-O catalyst with 5% O_2 and 10% O_2 in feed (catalyst: 0.2 g Cr-V-O, feed: 50 cm^3/min)..... 70

Figure 46. **(a)** CO_2 selectivity-temperature data, **(b)** CH_4 selectivity-temperature data, **(c)** CO selectivity-temperature data (catalyst: 0.2 g Cr-V-O, O_2/C_2H_6 = ~0.33, feed: 50 cm^3/min)..... 71

Figure 47. **(a)** Total conversion-temperature data, **(b)** C_2H_4 selectivity-temperature data, **(c)** C_2H_4 yield-temperature data (catalyst: 0.2 g Cr-V-O, CO_2/C_2H_6 = ~0.33, feed: 50 cm^3/min)..... 73

Figure 48. CH_4 selectivity-temperature data (catalyst: 0.2 g Cr-V-O, CO_2/C_2H_6 = ~0.33, feed: 50 cm^3/min) 74

Figure 49. Comparison of **(a)** Total conversion-temperature data, **(b)** C_2H_4 selectivity-temperature data, **(c)** C_2H_4 yield-temperature data for Cr-V-O catalyst with 10% O_2 and 10% CO_2 in feed (catalyst: 0.2 g Cr-V-O, O_2/C_2H_6 and CO_2/C_2H_6=~0.33 feed:50 cm^3/min)..... 75

Figure 50. **(a)** Total conversion-temperature data, **(b)** C_2H_4 selectivity-temperature data, **(c)** C_2H_4 yield-temperature data (catalyst: 0.2 g Cr-V-O, CO_2/C_2H_6 = ~1.5, feed: 50 cm^3/min)..... 76

Figure 51. **(a)** Total conversion-temperature data, **(b)** C_2H_4 selectivity-temperature data, **(c)** C_2H_4 yield-temperature data (catalyst: 0.2 g V-MCM-41, O_2/C_2H_6 = ~0.17, feed: 50 cm^3/min)..... 78

Figure 52. **(a)** CO_2 selectivity-temperature data, **(b)** CO selectivity-temperature data (catalyst: 0.2 g V-MCM-41, O_2/C_2H_6 = ~0.17, feed: 50 cm^3/min) 79

Figure 53. Comparison of **(a)** Total conversion-temperature data, **(b)** C_2H_4 selectivity-temperature data, **(c)** C_2H_4 yield-temperature data for Cr-O and Cr-V-O catalysts with 10% O_2 feed (catalyst: 0.2 g, O_2/C_2H_6=~0.33, feed:50 cm^3/min)..... 81

Figure 54. Comparison of **(a)** Total conversion-temperature data, **(b)** C_2H_4 selectivity-temperature data, **(c)** C_2H_4 yield-temperature data for Cr-O and Cr-V-O catalysts with 10% CO_2 feed (catalyst: 0.2 g, CO_2/C_2H_6=~0.33, feed:50 cm^3/min)..... 82

Figure 55. Comparison of **(a)** Total conversion-temperature data, **(b)** C_2H_4 selectivity-temperature data, **(c)** C_2H_4 yield-temperature data for Cr-O, Cr-V-O, and V-MCM-41 catalysts with 5% O_2-30%C_2H_6-60% He feed (catalyst: 0.2 g, O_2/C_2H_6=~0.17, feed:50 cm^3/min)..... 83

Figure 56. 'Pulse 3' C_2H_6 response data for C_2H_6 pulses into O_2 and He flow over Cr-O catalyst at 401°C..... 85

Figure 57. 'Pulse 3' C_2H_4 response data for C_2H_6 pulses into O_2 and He flow over Cr-O catalyst at 401°C..... 85

Figure 58. 'Pulse 4' CO_2 response data for C_2H_6 pulses into O_2 and He flow over Cr-O catalyst at 350°C..... 86

Figure 59. 'Pulse 4' H_2O response data for C_2H_6 pulses into O_2 and He flow over Cr-O catalyst at 350°C..... 86

Figure 60. **(a)** Gaussian fit **(b)** De-convolution of Gaussian fit for 'Pulse 4' CO_2 response data for C_2H_6 pulses into O_2 and He flow over Cr-O catalyst at 350°C..... 89

Figure 61. (a) Gaussian fit **(b)** De-convolution of Gaussian fit for 'Pulse 4' H_2O response data for C_2H_6 pulses into O_2 and He flow over Cr-O catalyst at 350°C..... 90

Figure 62. Variation of zeroth moments with pulse number for C_2H_6, C_2H_4, CO_2, and H_2O at **(a)** 350°C, **(b)** 401°C, and **(c)** 450°C for C_2H_6 pulses into O_2 and He flow over Cr-O catalyst..... 92

Figure 63. Variation of zeroth moments with pulse number for C_2H_4 at 350°C,401°C, and 450°C for C_2H_6 pulses into O_2 and He flow over Cr-O catalyst..... 93

Figure 64. Variation of zeroth moments with pulse number for CO_2 at 350°C,401°C, and 450°C for C_2H_6 pulses into O_2 and He flow over Cr-O catalyst..... 93

Figure 65. Variation of zeroth moments with pulse number for H_2O at 350°C,401°C, and 450°C for C_2H_6 pulses into O_2 and He flow over Cr-O catalyst..... 94

Figure 66. 'Pulse 6' C_2H_6 response data for C_2H_6 pulses into He flow over Cr-O catalyst at 448°C..... 95

Figure 67. 'Pulse 6' C_2H_4 response data for C_2H_6 pulses into He flow over Cr-O catalyst at 448°C..... 95

Figure 68. Variation of zeroth moments with pulse number for C_2H_6 and C_2H_4 at 448°C for C_2H_6 pulses into He flow over Cr-O catalyst 96

Figure 69. Variation of zeroth moments with time for C_2H_4 at about 450°C for C_2H_6 pulses into He and He-O_2 flow over Cr-O catalyst..... 96

Figure 70. 'Pulse 2' H_2O response data for C_2H_6 pulses into O_2 and He flow over Cr-V-O catalyst at 400°C..... 97

Figure 71. 'Pulse 2' O_2 response data for C_2H_6 pulses into O_2 and He flow over Cr-V-O catalyst at 400°C..... 98

Figure 72. Variation of zeroth moments with pulse number for C_2H_6, C_2H_4, and H_2O at about 400°C for C_2H_6 pulses into He and O_2 flow over Cr-V-O catalyst..... 98

Figure 73. 'Pulse 9' response data of H_2O, CO_2, CH_4, CO, and H_2 for O_2 pulses into He and C_2H_6 flow over Cr-V-O catalyst at 400°C..... 100

Figure 74. Variation of zeroth moments with pulse number for O_2, H_2O, and CO for O_2 pulses into He and C_2H_6 flow over Cr-V-O catalyst at 400°C..... 101

Figure 75. 'Pulse 6' response data of C_2H_4 for C_2H_6 pulses into He flow over Cr-V-O catalyst at 449°C..... 102

Figure 76. Variation of zeroth moments with pulse number for C_2H_6, C_2H_4, and H_2O for C_2H_6 pulses into He flow over Cr-V-O catalyst at 449°C..... 102

Figure 77. Variation of zeroth moments with time for C_2H_6, C_2H_4, CO_2, and H_2O for C_2H_6 pulses into He and O_2 flow over Cr-O and Cr-V-O catalysts at 400°C..... 103

Figure 78. Variation of zeroth moments with time for C_2H_6, C_2H_4, and H_2O for C_2H_6 pulses into He flow over Cr-O and Cr-V-O catalysts at about 449°C..... 104

Figure 79. Variation of zeroth moments with time for C_2H_4 and H_2O for C_2H_6 pulses into He flow over Cr-O and Cr-V-O catalysts at about 449°C..... 104

Figure A.4.1. Mass spectrometer caibration data with mean values..... 143

Figure A.5.1. Mass spectrometer caibration data with normalized mean values..... 146

Figure D.1.1. 'Pulse 1' response data for C_2H_6 pulses into O_2 and He flow over Cr-O catalyst at 350°C..... 154

Figure D.1.2. 'Pulse 2' response data for C_2H_6 pulses into O_2 and He flow over Cr-O catalyst at 350°C..... 155

Figure D.1.3. 'Pulse 3' response data for C_2H_6 pulses into O_2 and He flow over Cr-O catalyst at 350°C..... 156

Figure D.1.4. 'Pulse 4' response data for C_2H_6 pulses into O_2 and He flow over Cr-O catalyst at 350°C..... 157

Figure D.1.5. Gaussian fits and de-convolution of Gaussian fits for CO_2 response data for C_2H_6 pulses into O_2 and He flow over Cr-O catalyst at 350°C..... 158

Figure D.1.6. Gaussian fits and de-convolution of Gaussian fits for H_2O response data for C_2H_6 pulses into O_2 and He flow over Cr-O catalyst at 350°C..... 160

Figure D.1.7. 'Pulse 1' response data for C_2H_6 pulses into O_2 and He flow over Cr-O catalyst at 401°C..... 166

Figure D.1.8. 'Pulse 2' response data for C_2H_6 pulses into O_2 and He flow over Cr-O catalyst at 401°C..... 167

Figure D.1.9. 'Pulse 3' response data for C_2H_6 pulses into O_2 and He flow over Cr-O catalyst at 401°C..... 168

Figure D.1.10. 'Pulse 4' response data for C_2H_6 pulses into O_2 and He flow over Cr-O catalyst at 401°C..... 169

Figure D.1.11. Gaussian fits and de-convolution of Gaussian fits for CO_2 response data for C_2H_6 pulses into O_2 and He flow over Cr-O catalyst at 401°C..... 170

Figure D.1.12. Gaussian fits and de-convolution of Gaussian fits for H_2O response data for C_2H_6 pulses into O_2 and He flow over Cr-O catalyst at 401°C..... 172

Figure D.1.13. 'Pulse 1' response data for C_2H_6 pulses into O_2 and He flow over Cr-O catalyst at 450°C..... 178

Figure D.1.14. 'Pulse 2' response data for C_2H_6 pulses into O_2 and He flow over Cr-O catalyst at 450°C..... 179

Figure D.1.15. 'Pulse 3' response data for C_2H_6 pulses into O_2 and He flow over Cr-O catalyst at 450°C..... 180

Figure D.1.16. 'Pulse 4' response data for C_2H_6 pulses into O_2 and He flow over Cr-O catalyst at 450°C..... 181

Figure D.1.17. 'Pulse 5' response data for C_2H_6 pulses into O_2 and He flow over Cr-O catalyst at 450°C..... 182

Figure D.1.18. Gaussian fits and de-convolution of Gaussian fits for CO_2 response data for C_2H_6 pulses into O_2 and He flow over Cr-O catalyst at 450°C..... 183

Figure D.1.19. Gaussian fits and de-convolution of Gaussian fits for H_2O response data for C_2H_6 pulses into O_2 and He flow over Cr-O catalyst at 450°C..... 185

Figure D.1.20. 'Pulse 1' response data for C_2H_6 pulses into He flow over Cr-O catalyst at 448°C..... 191

Figure D.1.21. 'Pulse 2' response data for C_2H_6 pulses into He flow over Cr-O catalyst at 448°C..... 192

Figure D.1.22. 'Pulse 3' response data for C_2H_6 pulses into He flow over Cr-O catalyst at 448°C..... 193

Figure D.1.23. 'Pulse 4' response data for C_2H_6 pulses into He flow over Cr-O catalyst at 448°C..... 194

Figure D.1.24. 'Pulse 5' response data for C_2H_6 pulses into He flow over Cr-O catalyst at 448°C..... 195

Figure D.1.25. 'Pulse 6' response data for C_2H_6 pulses into He flow over Cr-O catalyst at 448°C..... 196

Figure D.1.26. 'Pulse 7' response data for C_2H_6 pulses into He flow over Cr-O catalyst at 448°C..... 197

Figure D.1.27. 'Pulse 8' response data for C_2H_6 pulses into He flow over Cr-O catalyst at 448°C..... 198

Figure D.1.28. 'Pulse 9' response data for C_2H_6 pulses into He flow over Cr-O catalyst at 448°C..... 199

Figure D.1.29. 'Pulse 10' response data for C_2H_6 pulses into He flow over Cr-O catalyst at 448°C..... 200

Figure D.1.30. 'Pulse 11' response data for C_2H_6 pulses into He flow over Cr-O catalyst at 448°C..... 201

Figure D.1.31. 'Pulse 12' response data for C_2H_6 pulses into He flow over Cr-O catalyst at 448°C..... 202

Figure D.1.32. 'Pulse 13' response data for C_2H_6 pulses into He flow over Cr-O catalyst at 448°C..... 203

Figure D.1.33. 'Pulse 14' response data for C_2H_6 pulses into He flow over Cr-O catalyst at 448°C..... 204

Figure D.1.34. 'Pulse 15' response data for C_2H_6 pulses into He flow over Cr-O catalyst at 448°C..... 205

Figure D.1.35. 'Pulse 16' response data for C_2H_6 pulses into He flow over Cr-O catalyst at 448°C..... 206

Figure D.1.36. 'Pulse 17' response data for C_2H_6 pulses into He flow over Cr-O catalyst at 448°C..... 207

Figure D.2.1. 'Pulse 1' response data for C_2H_6 pulses into O_2 and He flow over Cr-V-O catalyst at 400°C..... 213

Figure D.2.2. 'Pulse 2' response data for C_2H_6 pulses into O_2 and He flow over Cr-V-O catalyst at 400°C..... 214

Figure D.2.3. 'Pulse 3' response data for C_2H_6 pulses into O_2 and He flow over Cr-V-O catalyst at 400°C..... 215

Figure D.2.4. 'Pulse 4' response data for C_2H_6 pulses into O_2 and He flow over Cr-V-O catalyst at 400°C..... 216

Figure D.2.5. 'Pulse 5' response data for C_2H_6 pulses into O_2 and He flow over Cr-V-O catalyst at 400°C..... 217

Figure D.2.6. 'Pulse 6' response data for C_2H_6 pulses into O_2 and He flow over Cr-V-O catalyst at 400°C..... 218

Figure D.2.7. 'Pulse 7' response data for C_2H_6 pulses into O_2 and He flow over Cr-V-O catalyst at 400°C..... 219

Figure D.2.8. 'Pulse 2' response data for O_2 pulses into C_2H_6 and He flow over Cr-V-O catalyst at 400°C..... 224

Figure D.2.9. 'Pulse 3' response data for O_2 pulses into C_2H_6 and He flow over Cr-V-O catalyst at 400°C..... 225

Figure D.2.10. 'Pulse 4' response data for O_2 pulses into C_2H_6 and He flow over Cr-V-O catalyst at 400°C..... 226

Figure D.2.11. 'Pulse 5' response data for O_2 pulses into C_2H_6 and He flow over Cr-V-O catalyst at 400°C..... 227

Figure D.2.12. 'Pulse 6' response data for O_2 pulses into C_2H_6 and He flow over Cr-V-O catalyst at 400°C..... 228

Figure D.2.13. 'Pulse 7' response data for O_2 pulses into C_2H_6 and He flow over Cr-V-O catalyst at 400°C..... 229

Figure D.2.14. 'Pulse 8' response data for O_2 pulses into C_2H_6 and He flow over Cr-V-O catalyst at 400°C..... 230

Figure D.2.15. 'Pulse 9' response data for O_2 pulses into C_2H_6 and He flow over Cr-V-O catalyst at 400°C..... 231

Figure D.2.16. 'Pulse 10' response data for O_2 pulses into C_2H_6 and He flow over Cr-V-O catalyst at 400°C..... 232

Figure D.2.17. 'Pulse 11' response data for O_2 pulses into C_2H_6 and He flow over Cr-V-O catalyst at 400°C..... 233

Figure D.2.18. 'Pulse 12' response data for O_2 pulses into C_2H_6 and He flow over Cr-V-O catalyst at 400°C..... 234

Figure D.2.19. 'Pulse 13' response data for O_2 pulses into C_2H_6 and He flow over Cr-V-O catalyst at 400°C..... 235

Figure D.2.20 'Pulse 14' response data for O_2 pulses into C_2H_6 and He flow over Cr-V-O catalyst at 400°C..... 236

Figure D.2.21. 'Pulse 15' response data for O_2 pulses into C_2H_6 and He flow over Cr-V-O catalyst at 400°C..... 237

Figure D.2.22. 'Pulse 1' response data for C_2H_6 pulses into and He flow over Cr-V-O catalyst at 449°C..... 242

Figure D.2.23. 'Pulse 2' response data for C_2H_6 pulses into and He flow over Cr-V-O catalyst at 449°C..... 243

Figure D.2.24. 'Pulse 3' response data for C_2H_6 pulses into and He flow over Cr-V-O catalyst at 449°C..... 244

Figure D.2.25. 'Pulse 4' response data for C_2H_6 pulses into and He flow over Cr-V-O catalyst at 449°C..... 245

Figure D.2.26. 'Pulse 5' response data for C_2H_6 pulses into and He flow over Cr-V-O catalyst at 449°C..... 246

Figure D.2.27. 'Pulse 6' response data for C_2H_6 pulses into and He flow over Cr-V-O catalyst at 449°C..... 247

Figure D.2.28. 'Pulse 7' response data for C_2H_6 pulses into and He flow over Cr-V-O catalyst at 449°C..... 248

Figure D.2.29. 'Pulse 8' response data for C_2H_6 pulses into and He flow over Cr-V-O catalyst at 449°C..... 249

Figure D.2.30. 'Pulse 9' response data for C_2H_6 pulses into and He flow over Cr-V-O catalyst at 449°C..... 250

Figure D.2.31. 'Pulse 10' response data for C_2H_6 pulses into and He flow over Cr-V-O catalyst at 449°C..... 251

Figure D.2.32. 'Pulse 11' response data for C_2H_6 pulses into and He flow over Cr-V-O catalyst at 449°C..... 252

Figure D.2.33. 'Pulse 12' response data for C_2H_6 pulses into and He flow over Cr-V-O catalyst at 449°C..... 253

Figure D.2.34. 'Pulse 13' response data for C_2H_6 pulses into and He flow over Cr-V-O catalyst at 449°C..... 254

Figure D.2.35. 'Pulse 14' response data for C_2H_6 pulses into and He flow over Cr-V-O catalyst at 449°C..... 255

Figure D.2.36. 'Pulse 15' response data for C_2H_6 pulses into and He flow over Cr-V-O catalyst at 449°C..... 256

Figure D.2.37. 'Pulse 16' response data for C_2H_6 pulses into and He flow over Cr-V-O catalyst at 449°C..... 257

Figure D.2.38. 'Pulse 17' response data for C_2H_6 pulses into and He flow over Cr-V-O catalyst at 449°C..... 258

LIST OF SYMBOLS

C_{total} : Total gas concentration (kgmol/cm^3)

F^o : Inlet molar flow rate

h_i : Mass spectrometer mean value for the height of mass i

m_0 : Zeroth moment

m_2 : Second moment

P : Pressure (atm)

Q : Volumetric flow rate (cm^3/min)

R : Ideal gas constant

S_i : Selectivity to species i

t : Time (min)

t_m : Mean residence time (sec)

T : Temperature (K)

X_{total} : Total conversion

Y_i : Yield of species i

y_i : Mole fraction of species i

Greek Symbols:

μ_1 : First moment

η : Mean (sec)

σ^2 : Variance (sec^2)

σ : Standard deviation (sec)

CHAPTER 1

INTRODUCTION

Conversion of alkanes to unsaturated hydrocarbons is a major area of interest for paraffin utilization since olefins are important starting materials for many chemical industries. Three different ways can be carried out for the production of unsaturated hydrocarbons from alkanes, i.e., *thermal dehydrogenation*, *catalytic dehydrogenation*, and *catalytic oxidative dehydrogenation*.

The thermal dehydrogenation of alkane is highly endothermic and therefore requires high temperatures for obtaining acceptable conversions. Consequently, high-energy costs are required to supply the high reaction temperatures [1].

Compared to thermal dehydrogenation, the catalyst used in catalytic dehydrogenation process increases the selectivity for olefin production. However, operation at high temperatures results in undesirable side reactions such as cracking of the paraffin. Rapid coking of the catalyst and consequently rapid catalyst deactivation problems are the main disadvantages of catalytic dehydrogenation [1].

In comparison with the above-mentioned methods, catalytic oxidative dehydrogenation process is a promising alternative. This exothermic reaction of alkane with oxygen in the presence of a suitable catalyst offers many advantages such as execution at low temperatures, and absence of equilibrium limitations:

$C_nH_{2n+2} + 1/2O_2 \rightarrow C_nH_{2n} + H_2O$

Presence of a very stable compound, i.e, water, among the products, makes the oxidative dehydrogenation reaction thermodynamically favorable. Besides, since the reaction is carried out at lower temperatures, rapid catalyst deactivation problems can be prevented [1].

Catalytic dehydrogenation of paraffins has been in commercial use since the late 1930s. During World War II, for the production butenes, catalytic dehydrogenation of butanes over a chromia-alumina catalyst was utilized. Development of commercialized methods for the dehydrogenation of butanes over chromia-alumina catalyst started in the 1940s. The first companies which developed the process was Leuna in Germany and Universal Oil Products in the US and ICI in England. Companies such as Phillips Petroleum, Shell, Gulf, and Dow also improved technologies for dehydrogenation. Chromia-alumina catalysts were also started to be used for the dehyrogenation of propane to propylene and isobutane to isobutylene in the late 1980s [2]. As it can be deduced from these information, catalytic paraffin dehydrogenation is a 'well-established' and 'a mature technology' [2].

On the other hand, catalytic paraffin oxidative dehydrogenation for olefin production has not been commercialized yet [2]. Bhasin et al. [2] define the oxydehydrogenation process as to be 'still in its infancy'. However, the advantages of oxidative dehydrogenation process made it an attractive research area in recent years. The targets in researches include obtaining suitable paraffin conversions and olefin selectivities. The carbon oxides are thermodynamically more stable compared to the olefins, and therefore catalysts must be found that can both stop the reaction at the olefin step and prevent the formation of the oxides [2]. 'The success of oxidative dehydrogenation depends on the usage of a catalyst with high product selectivity and yield' [3].

1.1. Ethylene: an Important Chemical Feedstock

In the structure of the chemical industry, 'organic chemicals sector' own a considerable portion. One of the important raw materials used in this sector is 'ethylene' [4]. Due to double bond within its molecular structure, ethylene is a very reactive chemical and hence an important feedstock for the industry [5]. The commercially important reactions of ethylene are polymerization, oxidation, and addition including halogenation, alkylation, oligomerization, hydration and hydroformylation [6].

The products produced from ethylene are diverse. The distribution of uses for ethylene is summarized in Table 1 [4], and a flowchart of intermediates and major end-products produced from etyhlene is presented in Figure 1 [4].

Table 1. Distribution of uses for ethylene [4]

Product	**% of Ethylene Use**
Polyethylene	54
Ethylene dichloride	16
Ethylene oxide-glycol	13
Ethylbenzene-styrene	7
Linear olefins-alcohol	3
Vinyl acetate	2
Ethanol	1
Other	4

Source: Kirk-Othmer Encyclopedia of Chemical Technology

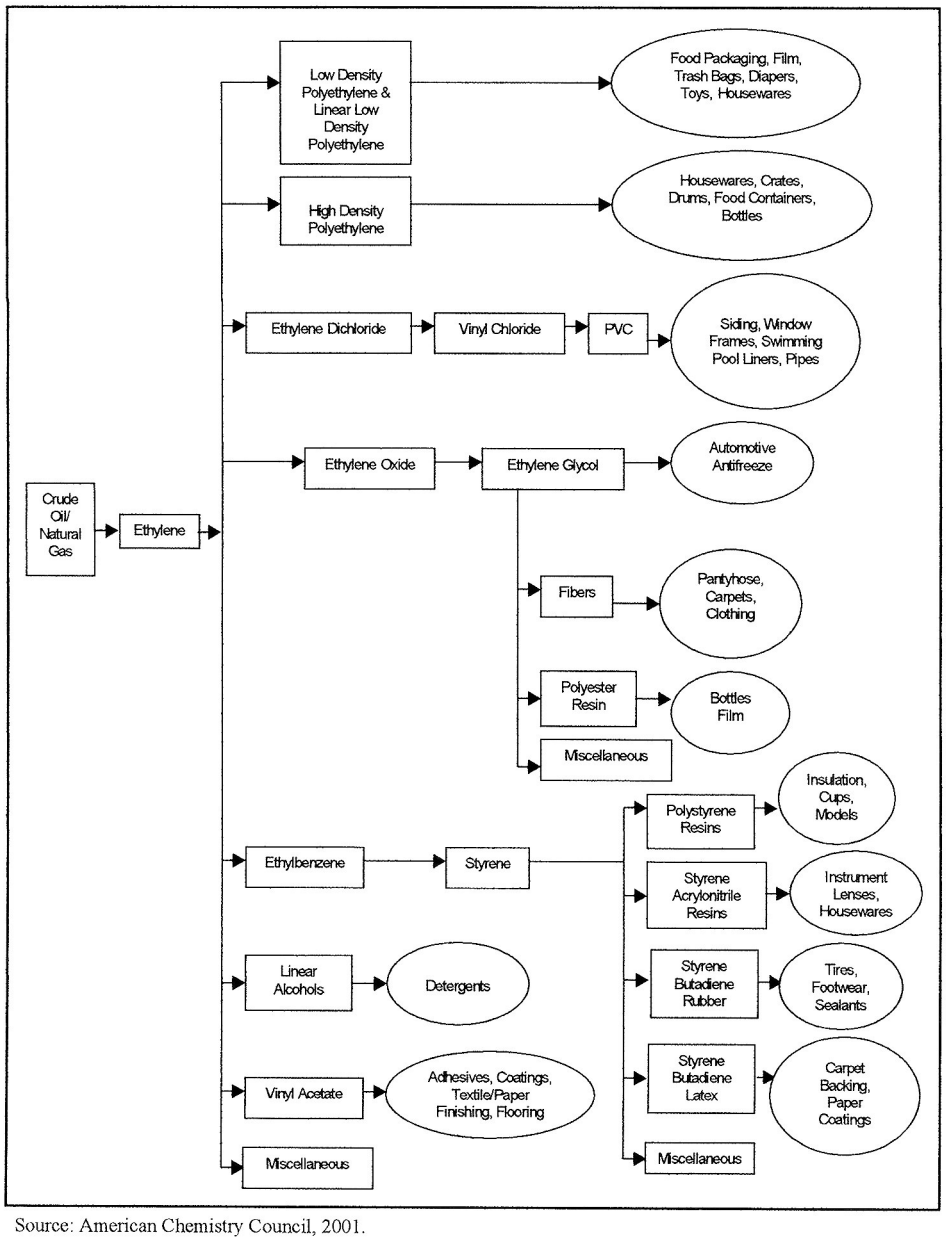

Source: American Chemistry Council, 2001.

Figure 1. Ethylene products [4]

The commercial method for ethylene production is thermal cracking of hydrocarbons in the presence of steam. The thermal cracking, i.e. pyrolysis of hydrocarbons, progresses using a free-radical mechanism [6]. The reactions involved are endothermic and are carried out at very high temperatures such as 800°C and above.

Other thermal and catalytic routes for ethylene production are also developed but none of them are yet commercialized. These include methods such as catalytic pyrolysis, membrane dehydrogenation of ethane, oxidative dehydrogenation, oxidative coupling of methane, methanol to ethylene, and dehydration of ethanol [6].

In the oxidative dehydrogenation of ethane to ethylene, ethane is reacted with oxygen over a suitable catalyst to produce ethylene and water:

$$C_2H_6 + 1/2O_2 \rightarrow C_2H_4 + H_2O$$

As stated earlier, formation of water removes the equilibrium constraint on conversion [2]. The challenge here is to avoid undesirable partial and/or total oxidation of ethane with oxygen to carbon oxides. Catalysts which are 'totally selective' for oxidation of ethane to ethylene will resolve this problem [2].

1.2. Oxidative Dehydrogenation Studies from Literature

Due to its above-mentioned advantages, oxidative dehydrogenation reaction has gained remarkable interest in the research area. Consequently a large number of catalysts has been studied for the oxidative dehydrogenation of various alkanes.

Mixed oxide catalysts containing Mo-V-Nb, or Mo-V together with other transition metal oxides were examined in many studies [7-13]. Vanadium based catalysts were tested intensely in recent years [14-21]. Viparelli et. al. [18] showed that the vanadium containing catalysts were very active but poorly selective to propylene in the oxidative dehydrogenation of propane; and the presence of niobium increased the catalyst performances at low V/Nb ratio.

Liu et al. [19] also studied the effect of Nb on the catalyst performance and reported that Nb did not affect the catalytic activity of the V-Al oxides in contrast to Mo-V-Nb oxides. Lemonidou et al. [17] investigated the oxidative dehydrogenation of propane over vanadia type catalysts supported on Al_2O_3, TiO_2, ZrO_2, and MgO at 450-550°C. V_2O_5/TiO_2 was found to be the most active catalyst while V_2O_5/Al_2O_3 was the most selective in propene.

In a similar study with propane, $V_2O_5/TiO_2/SiO_2$ catalysts were tested [20]. Mixed TiO_2/SiO_2 support was used to supply the advantages of both TiO_2 (good dispersion of the surface active species) and SiO_2 (high surface area) at the same time. At 500°C, a 50 mol% selectivity to propylene was obtained with a 27 mol% yield value.

The catalytic performance of $VO_x/\gamma\text{-}Al_2O_3$ materials (0.5-9.5 wt.% of vanadium) was tested for propane with O_2 and N_2O as oxidants [21]. Usage of N_2O instead of O_2 caused the overall activity to decrease and propene selectivity to increase for the same propane conversion. It was stated that this enhancement of selectivity was due to the reduction in the steady-state concentration of active lattice oxygen species.

Oxidative deydrogenation of isobutane was studied by Vislovskiy et al. [22] over vanadium-antimony catalysts. In this work, the yield of isobutene was improved by optimising the catalytic functions of oxide catalyst via variation of composition, support material (γ-Al_2O_3, α-Al_2O_3, SiO_2-Al_2O_3, SiO_2, MgO) and catalyst preparation method (citrate method, conventional co-precipitation, impregnation). Microspheric γ-alumina was found to be the best support. The optimal V-to-Sb atomic ratio was observed as 8.8 and the 'citrate' preparation technique was showed to be advantageous causing homogeneous distribution of components on the support surface. The optimized γ-alumina-supported V-Sb oxide catalyst was reported to demostrate very good activity with an olefin selectivity of 70% at 36% conversion; giving rise to an isobutene yield of 26% at 550°C.

Vanadia catalysts supported on mesoporous alumina (MAL) were found active and selective in the oxidative deydrogenation of ethane to ehylene [23]. The catalytic behaviour was showed to be dependent on the V-loading. At 570°C, the highest selectivity to ethylene (63.4%) was obtained on the catalyst with a V-coverage of 20% of the theoretical monolayer at an ethane conversion of 30%. The good results obtained by this sample were explained by the relatively high dispersion of vanadium causing lower formation of CO_x from deep oxidation of ethane and ethylene.

The nature and properties of the vanadium oxide species formed on the alumina support at vanadium loadings between 4.45 and 13.2 wt.% were characterized and tested in the oxidative dehydrogenation of propane within the work of Steinfeldt et al. [24]. The investigation of the effect of calcination temperature (in the range of 773-973 K) was also an objective of that study. The nature of vanadium species on alumina was found to be dependent both on vanadium loadings and calcination temperature. Higher dispersion of the tetrahedrally coordinated V^{5+} species was concluded to cause higher propene selectivity.

The catalytic performance of Mo and V catalysts supported on TiO_2 and Al_2O_3 for the oxidative dehydrogenation of ethane and propane was also investigated [25]. In their study, Heracleous et al. [25] examined the effect of

active metal at loadings equivalent to monolayer coverage; the effect of support and the nature of the alkane. The vanadia catalysts were found to be more active than the molybdena ones irrespective of the support used in both ethane and propane oxidative dehydrogenation. From support point of view, titania-supported catalysts were reported to exhibit higher activity but lower selectivity than the alumina-supported ones.

Vanadium-phosphorous-based catalysts, i.e. vanadium-exchanged Ti, Zr, and Sn cubic pyrophosphates, were tested for the oxidative dehydrogenation of ethane between 550-700°C [26]. All samples were active for the oxidative dehydrogenation reaction and vanadium-Ti-pyrophosphates exhibited the best catalytic performance. Isolated vanadium sites obtained by the ion-exchange method were concluded to show lower reducibility and thus, lower oxygen availibility inhibiting the total oxidation reactions.

Molybdenum based catalysts also constitute a wide area of interest for the oxidative dehydrogenation of various alkanes [27-30]. Dejoz et.al. [27] studied the influence of the addition of Mo ions to a selective MgO-supported vanadia catalyst for n-butane oxidation. The presence of molybdenum was shown to improve the yield of C_4-olefins. Despite molybdenum decreased the amount and the reducibility of the vanadium species which resulted in lower catalytic activity; it also decreased the amount of non-selective sites and hence improved the overall selectivity.

Mo-Mg-O catalysts [28] and MoO_3/γ-Al_2O_3 catalysts with different Mo loading [29] were studied in the oxidative dehydrogenation of isobutane and propane, respectively. Propane conversion increased, parallel to the acidity and the reducibility, with increasing Mo loading from 3.6 to 12.7 wt.% [29].

Hydrothermally synthesized Mo-V-M-O (M=Al, Ga, Bi, Sb, and Te) catalysts were tested by Ueda and Oshihara [30] for the selective oxidations of ethane to ethylene and/or acetic acid and of propane to acrylic acid. Mo-V-M-O (M= Al, possibly Ga and Bi) group of catalysts was moderately active for the ethane oxidation to ethene and to acetic acid; and Mo-V-M-O (M= Sb, and

Te) catalyst group was found extremely active for the oxidative dehydrogenation. At 340°C, with $Mo_6V_2Sb_1O_x$ catalyst, an ethylene selectivity value of 74.7% at 16.8% conversion was reported.

A comparative study on the catalytic performance in the oxidative dehydrogenation of ethane over Te-containing Mo-V-Nb mixed oxide catalysts, in which Te was incorporated by different procedures, was conducted by López Nieto et al. [31]. Mo-V-Nb-Te-O mixed oxide catalyst was shown to exhibit selectivity to ehylene values higher than 80% at ethane conversions greater than 80% in the temperature range of 340-400°C. Such catalytic behaviour was explained by the presence of high amounts of tellerium cations which favored the formation of a highly selective crystalline phase, i.e. $Te_2M_{20}O_{57}$ (M=Mo,V,Nb).

The interactions betwen Mo and V on alumina were studied for the oxidative dehydrogenation of propane by Bañares and Khatib [32]. The total Mo+V coverage and the reaction conditions were concluded to determine the resulting phases on alumina-supported mixed Mo-V oxides. Mo and V were found to contribute to the oxidative dehydrogenation reaction of propane with their own reactivity without significant cooperation between dispersed V and dispersed Mo oxides. The activity per vanadium site was reported to be nearly 10 times than that of Mo sites in supported oxides; and hence, vanadium was found dominant in performance.

The effect of chlorine on the redox and adsorption characteristics of Mo/Si:Ti catalysts in the oxidative dehydrogenation of ethane was tested [33]. Liu and Ozkan [33] studied a series of 10%Mo/Si:Ti=1:1 catalysts modified with Cl (Cl/Mo=0.1-2.0) and used various characterization techniques to understand the role of chlorine in the surface redox mechanism. At 550°C, an ethylene selectivity of 35.8% with an ethane conversion of 24.8% was obtained with the catalyst in which Cl/Mo=2.0. It was stated that the chlorine addition weakened the ethylene adsorption allowing it to escape to the gas phase more easily and thus, inhibited further reaction of ethylene. Consequently, selectivity for ethylene increased. Additionally, chlorine was seen to suppress the oxidation potential of the catalyst which in turn prevented total oxidation.

Oxidative dehydrogenation of ethane was investigated by in situ IR spectroscopy over a MoO_3/Al_2O_3 catalyst and pure alumina in order to obtain information about surface intermediate species in the work of Heracleous et al. [34]. Besides, selective and unselective routes of the oxidative dehydrogenation reaction was tried to be identified. Molybdena catalyst was highly selective to etylene (96% initial C_2H_4 selectivity) whereas mainly CO_x was formed with alumina. The selective activation of ethane was explained by the moderate acid strength introduced by molybdena. The strong acid sites on alumina were speculated to be responsible for the unselective conversion of ethane to CO_x. From the spectroscopic data, it was deduced that, MoO_3/Al_2O_3 favored the route in which activation of the ethane C-H bond proceeded through the formation of alkoxides which, in turn, decomposed to ethylene; whereas, pure alumina favored formation of oxygenates and full oxidation.

Additionally, the catalytic performance of chromium oxide based catalysts was attractive in recent years for oxidative dehydrogenation reaction [3, 35-38]. Oxidative dehydrogenation of ethane and isobutane was investigated using chromium-vanadium-niobium mixed oxide catalyts in our previous study [3]. CH_4 formation was observed in the oxidative dehydrogenation of ethane different from that of isobutane. Reaction mechanisms for the two reactions were also proposed according to the DRIFTS studies.

The work of Grzybowska et al. [37] for oxidation of ethane, propane, n-butane and isobutane on chromium oxide supported on alumina and on unsupported chromia showed that the main reaction products depended on the structure of the hydrocarbon; i.e., carbon oxides for ethane, propane, n-butane; and isubutene for isobutane. Unsupported Cr_2O_3 was found to be more active but less selective than the alumina-supported catalyst in the oxidative dehydrogenation of isobutane.

In another study with isobutane, 'the performance of chromium oxide catalysts supported on Al_2O_3 was evaluated' [35] and the optimum loading of Cr on Al_2O_3 was determined to be between 5 and 15%. Jiménez-López et al. [38] investigated propane oxidative dehydrogenation with chromium oxide

supported on Zr- and La-doped mesoporous silica (1-5wt.% Cr). SiZr5-3Cr (Si/Zr=5 and 3 wt.% Cr) was found to be the most active catalyst with 22.7% conversion and 17.5% selectivity to propene at 450°C.

Selection of optimum chromium oxide-based catalyst for propane oxidative dehydrogenation was made with respect to chromium loading (between 0.1-20 wt.%), support, and catalyst precursor in the research of Al-Zahrani et al. [39]. Propane conversion and selectivity to propene was seen to increase with chromium loadings up to 10 wt.%. Among the various supports tested (MgO, TiO_2, SiO_2, γ-Al_2O_3), γ-Al_2O_3 was found to exhibit the best performance. With the chromium oxide (10 wt.%) γ-Al_2O_3 catalyst, a propene selectivity of 61% and a propene yield value of 18% was observed at 500°C.

In a similar study by Jibril [40], supported chromium oxide catalysts were tested for propane oxidative dehydrogenation for the effects of various supports (MgO, TiO_2, SiO_2, γ-Al_2O_3) and feed composition. As in the work of Al-Zahrani et al. [39], γ-Al_2O_3 was seen to exhibit the best performance. At 450°C, on the 10 wt.% chromium oxide on alumina, a propylene selectivity of 54.1% was obtained with a propene conversion of 16.7%.

In another oxidative dehydrogenation of propane study, Cs-doped Cr-Mo/Al_2O_3 catalyst was tested in the temperature range of 300-340°C [41]. The catalyst was found to be active in propane oxidehydrogenation reaction. At 340°C, selectivity to propene values were above 70% at propane conversions of about 5%. Propane consumption and propene production rates were reported to be not dependent significantly on oxygen partial pressure.

Recently, another approach is the use of carbon dioxide as a mild oxidant for catalytic dehydrogenation of hydrocarbons [36, 42-44]. 'CO_2 is expected to increase equilibrium conversion by diluting light alkanes, and to maintain the activity of the catalyst over a long time by removing coke formed on the catalyst' [45]. In the researches made, CO_2 was either used alone as the oxidant itself (instead of O_2) or added to the feed besides O_2 in small amounts to increase selectivity and yield.

Over LaBaSm oxide catalyst, the influence of the addition of CO_2 into the feed was investigated for isobutane [42].The promoting effect of CO_2 addition on selectivity and conversion was explained by the decrease of adsorbed molecular oxygen which was responsible for total oxidation. For propane dehydrogenation by CO_2, Cr_2O_3 catalysts supported on Al_2O_3, active carbon and SiO_2 were tested by Takahara et al. [43] and it was reported that only over SiO_2-supported catalyst, CO_2 enhanced the yield and prevented catalyst deactivation. Similarly, Cr_2O_3 catalysts (unsupported and supported on Al_2O_3, SiO_2, TiO_2 and ZrO_2) were used for dehydrogenation of ethane with CO_2 [36]. And as in the work of Takahara et al. [43], Cr_2O_3/SiO_2 exhibited higher conversion and selectivity for ethylene. The optimum Cr_2O_3 loading was found as 8 wt.%. At 650°C, 8 wt.% Cr_2O_3/SiO_2 catalysts were reported to give 55.5% ethylene yield with 61% ethane conversion.

Mimura et al. [45] reported the effects of CO_2 on the dehydrogenation of ethane over Cr/H-ZSM-5 catalysts. Cr/H-ZSM-5 (SiO_2/Al_2O_3 ≥190) catalyst was observed to exhibit the highest performance in the dehydrogenation of ethane with CO_2 as the oxidant. At 650°C, the Cr/H-ZSM-5 (SiO_2/Al_2O_3 ≥190) catalyst resulted in 51.6% conversion of ethane and 79.1% selectivity to ethene. It was stated that CO_2 maintained the activity of the catalyst by removing coke from the surface of the catalyst.

The results obtained by the introduction of small amounts of CO_2 (3 vol.%) in the oxidative dehydrogenation of propane on $NiMoO_4$ catalysts were given by Dury et al. [46]. Within the temperature range of 400-480°C, CO_2 was observed to be not inert during the reaction. Dissociation of CO_2 to CO and an active oxygen species on the surface of $NiMoO_4$ was concluded to induce the oxidation of reduced Mo-containing oxides.

To improve selectivity and yield to C_4 products in the oxidative dehydrogenation of n-butane, addition of CO_2 into the feed mixture was investigated by Ge et al. [47]. 70.2% selectivity to C_4 products and 34.1% yield were obtained by adding CO_2 at 600°C. This high catalytic performance was attributed to a similar explanation reported by Bi et al. [42], that is, the competition between molecular O_2 and CO_2 adsoption on catalyst surface and

the decrease of adsorbed molecular O_2 which is believed to be responsible for the total oxidation of alkanes.

Most of the studies done in this research area are carried out in steady-state for determining different catalyst performances, 'for the measurement of reaction kinetics and the determination of rate expressions and constants' [48]. However, it is difficult to deduce reaction mechanisms from steady-state kinetic data [49]. Compared to steady-state experiments, transient experiments can supply more information about the short-lived reaction intermediates and hence the reaction mechanism in a few number of experiments. The adsorption-desorption equilibrium is not reached during the transient behaviour and thus, adsorption and desorption constants of the individual reaction steps can be determined [48]. Besides steady-state works, there are also a few transient studies of oxidative dehydrogenation in the literature [48-52]. In these studies, it is also aimed to improve the selectivity by minimizing undesired side reactions of the alkane with oxygen resulting carbon oxides.

Creaser et al. [49] studied the oxidative dehydrogenation of propane on a MgO-$Mg_3(VO_4)_2$ catalyst with various transient techniques such as start-up, reaction interuption and pulsing. To minimize the complete oxidation of propane by unsteady-state operation was also an objective of that study. In another transient study with propane, V_2O_5/TiO_2 catalysts were tested [50]. Similarly, to limit the total oxidation reactions, the catalyst was exposed to alternating concentration steps of propane and oxygen in He separeted by He flow. The cyclic operation of propane oxydehydrogenation was also studied by Creaser et al. [51] over V-Mg-O catalyst. By the alternate feeding of propane and oxygen mixtures, time-average propene yields higher than that of steady-state were obtained. The oxygen half-cycle was used to reoxidize the catalyst. Kondratenko et al. [52] performed pulse experiments in a TAP reactor to derive the type of interaction of oxygen with the Na_2O/CaO, Sm_2O_3/CaO and Sm_2O_3 catalysts during the oxidative dehydrogetaion of ethane. Rate constants and activation energies of the elementary reaction steps of oxygen adsorption and desorption were also estimated.

Oxidative dehyrogenation of propane over V_2O_5/TiO_2 catalysts was carried out by both steady-state and transient experiments [53]. The steady-state experiments were performed between 225-280°C, and transient tests were done in the temperature range of 166-446°C by alternating concentration steps of O_2 in He and C_3H_8 in He, separated with steps of pure He. Within the transient experiments, the influence of reaction temperature and C_3H_8 partial pressure on reaction products was studied. From the interpretation of the experimental data, C_3H_6 formation was decided to proceed through a Eley-Rideal sequence of steps, i.e. without participation of any adsorbed propane (propyl) intermediate. Additionally, two reaction models were proposed considering the lattice oxygen as the only oxygen species participating in the reaction.

Throughout the case studies performed by van Veen et al. [54], 'a paralled TAP (temporal-analysis-of-product) reactor with multisample holder' was used to acquire adsorption/desorption parameters for a series of zeolite materials. The zeolites were 'tested to evaluate their potential as catalyst supports in the oxidative dehydrogenation of ethane' [54]. ('In the temporal-analysis-of-product reactor, concentration transients are generated by pulsing small and known amounts of reactants through a catalyst bed maintained under vacuum, and the pulse expansion and relaxation are analysed at the reactor exit' [54].)

A comparative study of oxidative dehyrogenation of ethane over Pt/ Al_2O_3 catalysts, under steady-state and TAP reactor conditions was performed by Silberova et al. [55]. 'During TAP studies, no ethene was produced whereas under flow conditions small but significant ethene formation was observed'. It was concluded that since TAP reactor excluded gas-phase reactions, ethene produced in the flow reactor was formed in the gas-phase and not via a surface reaction.

As it is seen, many studies have been carried out for the oxidative dehydrogenation reaction and there is still way for industrial application both from catalyst and reaction mechanism point of view. The selectivity to ethylene from ethane in steam cracking was reported to be about 84% at

54% ethane conversion at 800°C [2]. Hence to compete with the currently applied steam cracking method, catalysts with high olefin selectivity and yield must be found.

1.3. Objectives of the Study

Oxidative dehydrogenation of ethane is a promising alternate to the currently applied routes for the production of ethylene. It is both 'energy saving' [45] and 'thermodynamically favourable' [1].

The objective of this study was to investigate the oxidative dehydrogenation of ethane on chromium-based mixed oxide catalysts, through steady-state and dynamic analysis. For this purpose, chromium-oxide and chromium-vanadium-oxide catalysts were prepared, characterized and tested for their catalytic performance at various temperatures at steady-state. The effect of usage CO_2 as a mild oxidant, instead of O_2, was also studied.

For the dynamic analysis, a pulse-response (single pulse-multiple response) system was developed. Experiments with pulses of C_2H_6 to O_2-He flow, C_2H_6 to He flow and O_2 to C_2H_6-He flow were performed on both catalysts.

CHAPTER 2

EXPERIMENTAL STUDIES

2.1. Experimental Set-up

The experimental set-up consists of reactant (C_2H_6, O_2, CO_2) and diluent (He) gas cylinders joined to a differential fixed-bed reactor placed into a temperature-controlled furnace and a mass spectrometer connected on line to the outlet stream leaving the reactor for the simultaneous analysis of the products. The scheme of the experimental set-up is shown in Figure 2. A quartz tube with 73 cm length and 17 mm inside diameter was used to place the powder catalysts inside within quartz wool. The catalyst part was 1-1.5 cm in length. The flow rate of O_2 and He were measured by flowmeters (Aalborg model GFM171) and that of C_2H_6 and CO_2 by rotameters (Cole-Palmer). Figure 3 presents the photograph of the set-up.

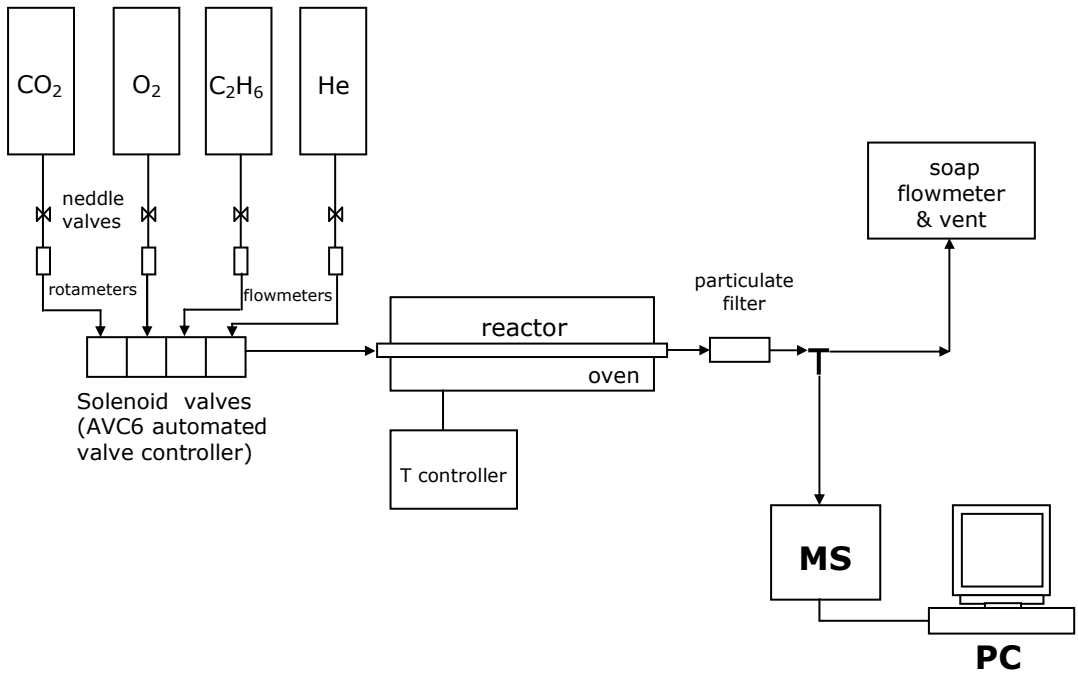

Figure 2. Experimental set-up

Figure 3. Photograph of experimental set-up

The mass spectrometer which was used in the system is 'Hiden Analytical HPR20 Gas Analysis System'. Its basic system comprises an ultra-high vacuum (UHV) housing, inlet system, turbo molecular pump and gauges. The inlet system is by-pass pumped and has a heated capillary sampling line. Figure 4 shows the HPR20 Gas Analysis System [56].

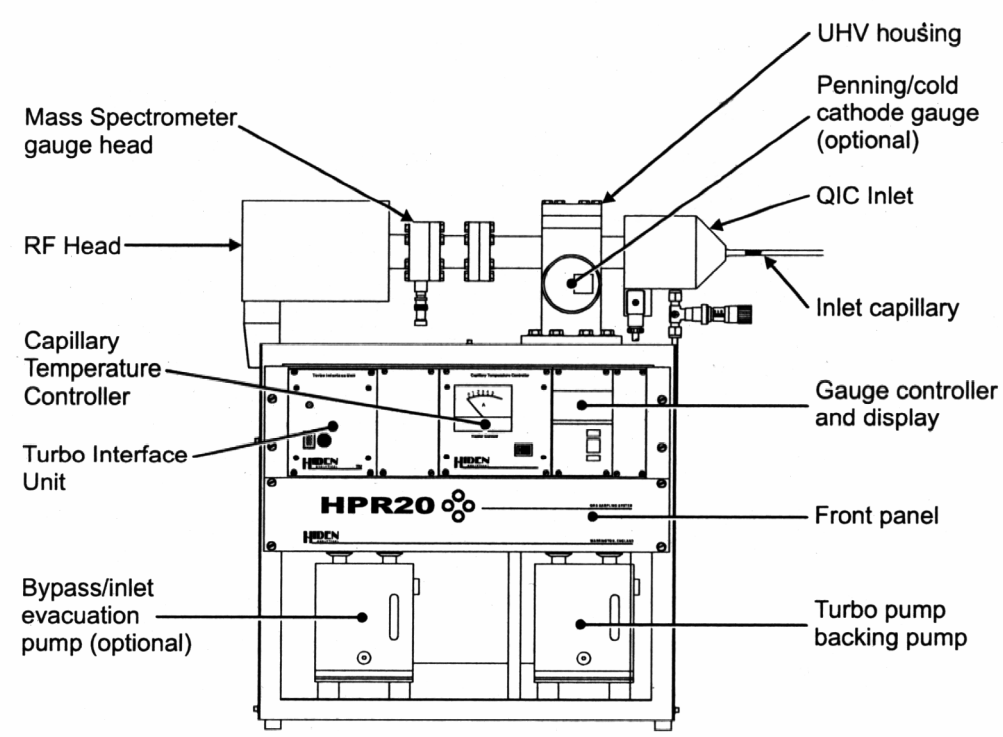

Figure 4. HPR20 Gas Analysis System [56]

The ultra-high vacuum pumping system comprises the turbo pump, turbo pump backing pump (which is a two-stage rotary pump), turbo controller interface unit (TCIU) and the venting device. The pumping system is illustrated in Figure 5 [56]. The mass spectrometer is operated when pressure is below $5x10^{-6}$ torr [57]. For a number of different reasons high vacuum is necessary for the components of the mass spectrometer:

1. High vacuum makes certain that the molecules entering the ion source will be in the gas phase and will not condense on the surfaces of the spectrometer [58].

2. The mean free path of ions formed under high vacuum is long so that the chance of collisions with other ions or molecules are rare. This provides the occurence of intramolecular fragmentation reactions (decomposition of individual ions) rather than intermolecular ones (reaction of ions with other ions or neutral molecules or fragments) [58].

3. High vacuum protects the metal surfaces of the ion source, analyzer and the detector from the corrosion of air and water vapor [58].

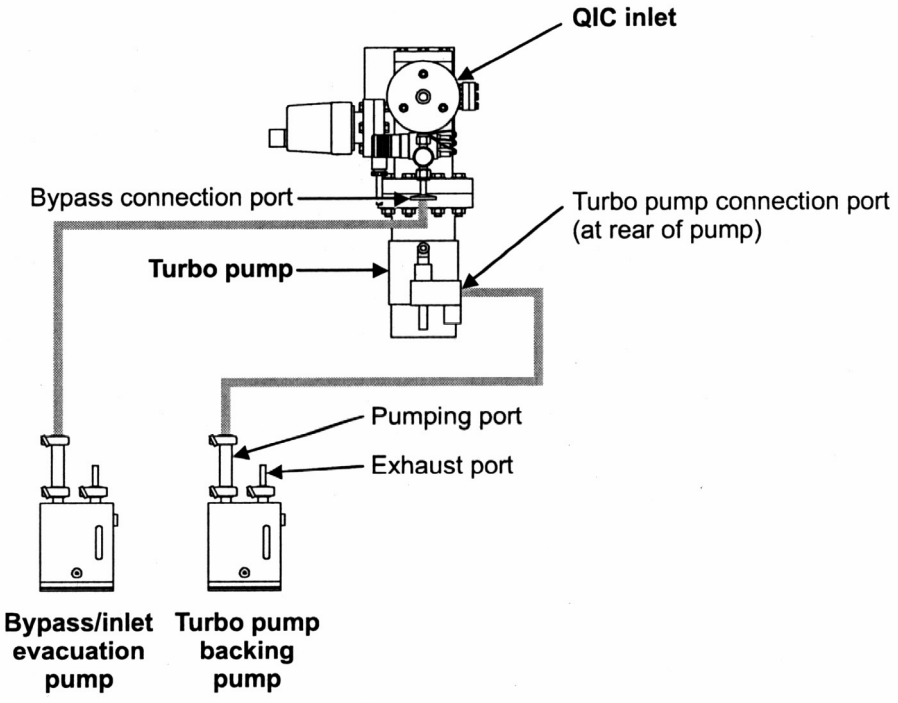

Figure 5. Vacuum line connections of the HPR20 mass spectrometer [56]

The QIC (Quartz Inert Capillary) fast sampling capillary inlet of the system provides a dynamic method of sampling of the gases by the mass spectrometer. Two pressure reduction stages are employed to reduce the sample pressure to an acceptable level for the operation of the mass spectrometer ion source. In the first stage, the sample gas to be analysed is drawn down the silica capillary by the sample bypass pumping line. The sample gas which exits the capillary at low pressure and high velocity impinges on a platinum orifice providing the second stage pressure reduction. The flow then directly enters the mass spectrometer ion source. Continuous heating of the inlet capillary, orifice and sample bypass regions minimises the condensation of vapors and the adsorption of the sample gas. The pressure at the capillary/orifice interface depends on the sample bypass line pumping speed which is adjusted by the sample bypass control valve [56].

The system also has the AVC6 Automated Valve Controller which provides the control of four solenoid valves. In the steady-state experiments, these solenoid valves were used as a mixing chamber for the gases in the system. During the pulse-response runs they were used for giving pulses to the reactor.

2.1.1. Theory of Mass Spectrometer

A simple block diagram of the mass spectrometer is shown in Figure 6. The three main parts are the ion source, mass analyzer and the detector. 'During mass spectral analysis, sample molecules first undergo reaction with an ionizing agent', which in our case is 'a beam of high-energy electrons' (electron ionization mass spectrometry). In the ion source, 'sample molecules are bombarded with a beam of highly energetic electrons (70 eV; 1eV=23kcal)' [58]. The electron beam is produced by an oxide coated iridium filament at 1500 K [57]. The loss of an electron by the sample molecule during ionization generates the molecular ion. The charged molecular ion has the same molecular weight as the sample molecule. 'The bond strengths in

organic compounds range from 10 to 20 eV', therefore, the excess energy present in 70-eV electrons may be satisfactory to overcome the second or third ionization potential of the molecule (leading to ions with +2 or +3 charges) or to fragment the molecular ion (first-formed ion) [58].

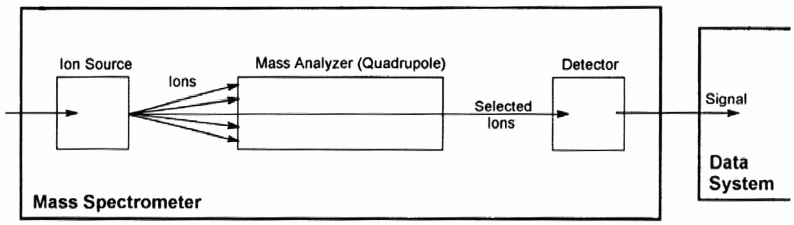

Figure 6. Block diagram of mass spectrometer [58]

The positive ions produced by the electron impact are attracted through the slits of the ion source (the extractor at –90V pulls the ions from the ion source) and the mass analyzer. These ions are mass analyzed for differentiation according to their mass-to-charge ratio. The mass analyzer, (which in our MS is the quadrupole mass filter), 'uses the fact that, in certain environments, charged particles have motions that are directly related to their mass-to-charge ratio (m/e)' [58]. The quadrupole mass filter consists of four stainless steel rods which are 12.5cm in length and 6.3mm in diameter [57]. 'The opposing rods are connected in pairs to radio frequency (RF) and direct current (dc) generators' (Figure 7, [58]). By this way the ions are bathed in a combined electric and radio frequency field during their passage through rods. With the right dc voltage and RF, one chooses which ions to travel along the rods [57].

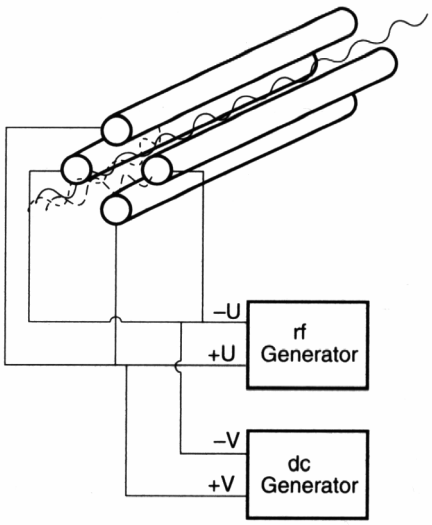

Figure 7. Quadrupole mass analyzer [58]

The detection of the ions which pass through the quadrupole mass analyzer is done by either the 'Faraday Cup' or the 'Secondary Electron Multiplier (SEM)'. These detectors convert the beam of ions into an electrical signal that can be processed by a computer and presented in graphical form.

In electron ionization mass spectrometry, ionization is so inefficient and because of this, the number of ions reaching the detector is small. Therefore, amplification of the signal is needed and the electron multiplier detector amplifies the ion current by several orders of magnitude [58, 59]. 'When the positive ions formed in the ion source and sorted by the analyzer strike the multiplier surface, electrons are ejected from the surface' [58]. A continuous dynode electron multiplier detector, which is actually a channeltron, is shown in Figure 8 [58]. The channeltron is made of a circular glass tube coated with a conducting material. Its shape allows a continuous cascading effect by the cycloidal motion of ions and electrons [59]. The top surface of the electron multiplier is kept at a highly negative potential (usually -1.2 to –3 kV) whereas the bottom is referenced to ground (0 V). By this way, the ejected electrons find the rest of the multiplier after the top surface more positive, and they are further attracted into the multiplier. The collision of each ion or

electron with the multiplier surface results an average of two electrons' ejection. The total signal magnification is approximately 2^n, where n is the total number of collisions with the surface. The electrons generated in the last collision form the signal current output of the multiplier. This current is sent to the signal amplifier and finally to the data system [58].

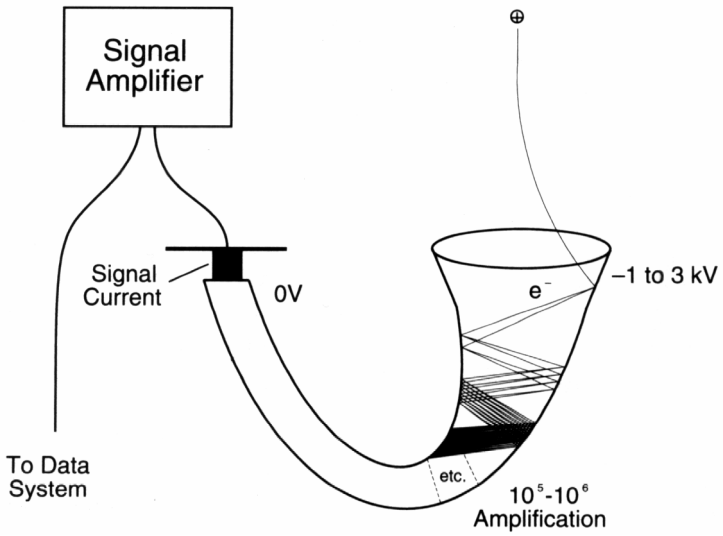

Figure 8. Continuous dynode electron multiplier detector [58]

The Faraday Cup is actually an ion collector which is placed after the ion analyzer [59]. There is no signal amplification in the Faraday Cup. Actually SEM is used for very sensitive measurements where the ion partial pressures ranges between 10^{-13} -10^{-6} torr whereas the Faraday Cup is ideal for 10^{-10} -10^{-4} torr [57].

2.2. Calibration of Mass Spectrometer

For quantitative analysis the mass spectrometer was calibrated for the reactant and the possible product gases by gas mixtures of various compositions. The gases used for calibration include C_2H_6, C_2H_4, O_2, CO_2, CH_4, CO, and He.

Before the start of the calibration runs, the system was purged with He for about 3-5 hours. During these runs, 15-20 minutes were waited after the set of each flowmeter and the analysis of the mass spectrometer was continued till the mass spectrometer signal reached to steady-state.

The mass spectrometer calibration experiments' data are given in Appendix A2. The 'mean' values in these tables are the mean value of the peak heights at an interval where the data reach to steady-state. The reference data obtained from the database of Hiden Analytical HPR20 Mass Spectrometer's software 'MASsoft' are presented in Appendix A1.

During the catalyst testing experiments the mass spectrometer's capillary was blocked; and this error caused a change in the calibration of the mass spectrometer. Due to this, all the calibration experiments were performed again to obtain the new calibration data presented in Appendix A3. The variation of the new curves compared with the previous ones can be seen on the calibration graphs in Appendix A4.

Some calibration experiments were also performed with the reactor containing the catalyst to see whether the catalyst present make any difference in the calibration curves. From the ethane calibration curve, it can be seen that there is no significant difference between the two (Appendix A4).

The curves with the normalized mean values were obtained by dividing the actual mean values by the mean value for He for that specific experiment. Using the curve equations, the outlet gas mole fractions were calculated as follows:

1. **O_2** : from the mean value of the peak at mass 32 $\rightarrow h_{32}$
2. **C_2H_6** : from the mean value of the peak at mass 30 $\rightarrow h_{30}$
3. **CO_2** : from the mean value of the peak at mass 44 $\rightarrow h_{44}$
4. **CH_4** : from the mean value of the peak at mass 15 after subtracting the ethane contribution. (the mean value at mass 30 is multiplied with 0.143 which is obtained from ethane calibration experiments and subtracted from the mean value at mass 15) $\rightarrow h_{15}$ - (h_{30} x 0.143)
5. **C_2H_4** : from the mean value of the peak at mass 27 after subtracting the ethane contribution. (the mean value at mass 30 is multiplied with 1 which is obtained from ethane calibration experiments and subtracted from the mean value at mass 27) $\rightarrow h_{27}$ - (h_{30} x 1)
6. **CO and H_2O** : from C and H balances.
   $(C/O)_{in}$ and $(H/O)_{in}$ are calculated from the inlet gas compositions, and using the following equations, CO and H_2O mole fractions are calculated:

$$\left(\frac{C}{O}\right)_{in} = \frac{2y_{C_2H_6} + 2y_{C_2H_4} + y_{CO} + y_{CO_2} + y_{CH_4}}{y_{H_2O} + y_{CO} + 2y_{CO_2} + 2y_{O_2}}$$

$$\left(\frac{H}{O}\right)_{in} = \frac{2y_{H_2O} + 6y_{C_2H_6} + 4y_{C_2H_4} + 4y_{CH_4}}{y_{H_2O} + y_{CO} + 2y_{CO_2} + 2y_{O_2}}$$

CO and H_2O mole fractions calculations for the experiments performed with CO_2 are as follows:

$$\left(\frac{C}{O}\right)_{in} = \frac{2y_{C_2H_6} + 2y_{C_2H_4} + y_{CO} + y_{CO_2} + y_{CH_4}}{y_{H_2O} + y_{CO} + 2y_{CO_2}}$$

$$\left(\frac{H}{O}\right)_{in} = \frac{2y_{H_2O} + 6y_{C_2H_6} + 4y_{C_2H_4} + 4y_{CH_4}}{y_{H_2O} + y_{CO} + 2y_{CO_2}}$$

After the blocking of the mass spectrometer's capillary, the factors were calculated as given below. Additionally calibrations for CO and H_2 were made.

C_2H_4 : $h_{27} - (h_{30} \times 1)$

CH_4 : $h_{15} - (h_{30} \times 0.148)$

CO : h_{28} – (C_2H_6 contribution) – (C_2H_4 contribution) – (CO_2 contribution)
CO : $h_{28} - (h_{30} \times 4.06) - (h_{27} \times 2.13) - (h_{44} \times 0.34)$

H_2 : h_2 – (He contribution) – (C_2H_6 contribution)
H_2 : $h_2 - (h_4 \times 0.006) - (h_{30} \times 0.027)$

2.3. Catalyst Preparation

Chromium-based mixed oxide catalysts (Cr-O, Cr-V-O) were prepared for this study by using the complexation method as the preparation technique. In the complexation method, chemical reactions are used to transform the homogeneous solution of catalyst precursors into a homogeneous, amorphous phase (with either a glassy, jelly-like, or foamy appearance) slowly and without phase separation [60]. 'To obtain a smooth gelation of the solution of catalyst precursors, they are complexed with multifunctional organic reagents that are capable of entering in a successive series of intermolecular polycondensation reactions. The gelation process results in a three-dimensional organic network with the metallic components entrapped in this structure' [60]. The textural properties such as pore structure and the surface area of the catalyst are caused by the organic matrix [60]. During preparation the metallic elements are added as water-soluble salts and several α-hydroxy acids are used as complexing agents. Citric acid is the most commonly used one among the others (such as malic, tartaric, glycolic, lactic); and because of this the complexing method is also called the 'citrate method'. The organic ingredient is removed during the catalyst activation step [60].

The catalysts were prepared according to the procedure given by Yaşyerli [61]. For catalyst preparation, a molar ratio of 1:1 of citric acid to total metals was used.

In the preparation of the Cr-O catalyst, 25ml, 0.5M aqueous solutions of chromium(III)nitrate nonahydrate and citric acid were prepared separately by dissolving the necessary amounts in water at room temperature (that is, 5g of $Cr(NO_3)_3.9H_2O$ and 2.6g of citric acid monohydrate). The solutions were then mixed and slowly evaporated at 60-70°C under continuous stirring for 53 h (at 60°C for 22 h and at 70°C for 31 h) till a viscous liquid was obtained. Then, this viscous solution was slowly dehydrated in an oven at 70-80°C for 88 h. At the end, the solid was calcined at 550°C for 8 h.

Similarly, the Cr-V-O catalyst was prepared by using chromium(III)nitrate nonahydrate and ammonium metavanadate as precursors. The used amounts were arranged in order to make the mole ratio of chromium to vanadium as 1. Aqueous solutions of 12.5ml, 0.5M chromium(III)nitrate nonahydrate (2.5g) and 12.5ml, 0.5M ammonium metavanadate (0.73g) were prepared and mixed with 25ml, 0.5M citric acid (2.6g) solution. The total 50ml aqueous solution was evaporated by stirring continuously at magnetic hot plate at 65-70°C for 52 h. The sample was placed into the oven at 70±2°C for 89 h to obtain further dehydration. The calcination was again performed at 550°C for 8 h.

2.4. Catalyst Characterization

Brunauer-Emmet-Teller (BET), X-ray diffraction (XRD), temperature programmed reduction (TPR) measurements, and X-Ray Photoelectron Spectroscopy (XPS) were employed for the characterization of the prepared catalysts. The BET surface area was measured by the Monosorb-Quanta Chrome apparatus at Gazi University. X-ray diffraction for the identification of the crystalline phases was performed by Philips PW 1840 X-Ray Diffractometer.

The TPR experiments with H_2 were carried out in the experimental set-up given in Figure 2 after some modifications. 0.2 g catalyst samples were used in the analysis. The inlet total flow was 50 cm^3/min with a composition of 5% H_2 in He.

Used Cr-V-O catalyst was treated with oxygen prior to TPR by passing over O_2, at a temperature starting from 30°C to 550°C, and kept at 550°C for about 3 hours. The temperature was incresed linearly from room temperature (21.5°C) to 577°C. O_2 was not passed over the Cr-O catalyst and temperature was increased linearly from 20°C to 535°C.

The XPS spectra of Cr-O and Cr-V-O catalysts before and after H_2-TPR were obtained. The XPS measurements were performed with the SPECS instrument at the Central Laboratory in METU. The analyses were also made after ion bombardment (Ar^+) at 5000 eV for 2 min. The binding energy of the C 1s at 284.6 eV was taken as reference in the XPS measurements.

2.5. Catalyst Testing – Steady-state Experiments

Oxidative dehydrogenation of ethane experiments were performed with the prepared Cr-O and Cr-V-O catalysts. Addionally, the catalytic performance of V-MCM-41 catalyst was tested for the oxidative dehydrogenation reaction. This catalyst was prepared by Y. Güçbilmez in another ongoing research [62]. One-pot synthesis method (direct hydrothermal synthesis) was used as the preparation technique for V-MCM-41 catalyst.

A total feed flow rate of 50 cm^3/min and a catalyst amount of 0.2 g were used throughout these experiments. The space time was $4x10^{-3}$g.min/cm^3. Inside the reactor, the powder catalyst was placed between pieces of quartz wools. Before each run the reactor was heated to the desired temperature under He flow and the reactor outlet was heated to about 150°C to prevent condensation of water.

2.6. Dynamic Experiments

The dynamic experiments include the pulse-response experiments performed with the Cr-O and Cr-V-O catalysts. These runs were performed in the same experimental set-up of stedy-state experiments after making some modifications. The solenoid valves of the AVC6 Automated Valve Controller were used to give 15-second pulses to the system. The catalyst amount used was 0.2g.

With Cr-O catalyst, pulses of C_2H_6 to O_2 and He flow at different temperatures (350, 401, 450°C) and C_2H_6 pulses to He flow at 450°C were studied. Pulses of C_2H_6 to O_2 and He flow at 400°C, and C_2H_6 pulses to He flow at 449°C were performed with Cr-V-O catalyst. Additionally, at 400°C, O_2 pulses to C_2H_6 and He flow was given to Cr-V-O catalyst. The summary of these runs are presented in Table 2. The ones that were done at the same conditions with different catalysts are signed with red arrows. Pulse-response experiments without catalyst were also carried out at temperatures 350, 400, and 450°C.

Table 2. Pulse-response experiments

Cr-O Catalyst					Cr-V-O Catalyst				
Temp. (°C)	**Pulse**	**Flowing Gas**	**ml/min**	**% comp.**	**Temp. (°C)**	**Pulse**	**Flowing Gas**	**ml/min**	**% comp.**
350	C_2H_6	He O_2	42.9 2.7	94.1% 5.9%					
401	C_2H_6	He O_2	42.6 2.7	94% 6%	400	C_2H_6	He O_2	42.6 2.7	94% 6%
450	C_2H_6	He O_2	42.5 2.7	94% 6%					
448	C_2H_6	He	45		449	C_2H_6	He	45	
					400	O_2	He C_2H_6	42.6 5.5	88.6% 11.4%

CHAPTER 3

RESULTS AND DISCUSSION

3.1. Catalyst Characterization

BET: The BET surface areas of Cr-O and Cr-V-O catalysts were measured to be 52.8 m^2/g and 28.8 m^2/g, respectively. The BET area of V-MCM-41 catalyst was 481 m^2/g [62].

XRD: Figure 9 shows the XRD pattern of the prepared Cr-O catalyst. Below the figure, XRD patterns of Cr_2O_3 and CrO_3 are seen. The comparison of these reveals that the characteristic peaks of Cr_2O_3 are present in the Cr-O catalyst and Cr_2O_3 phase is formed successfully.

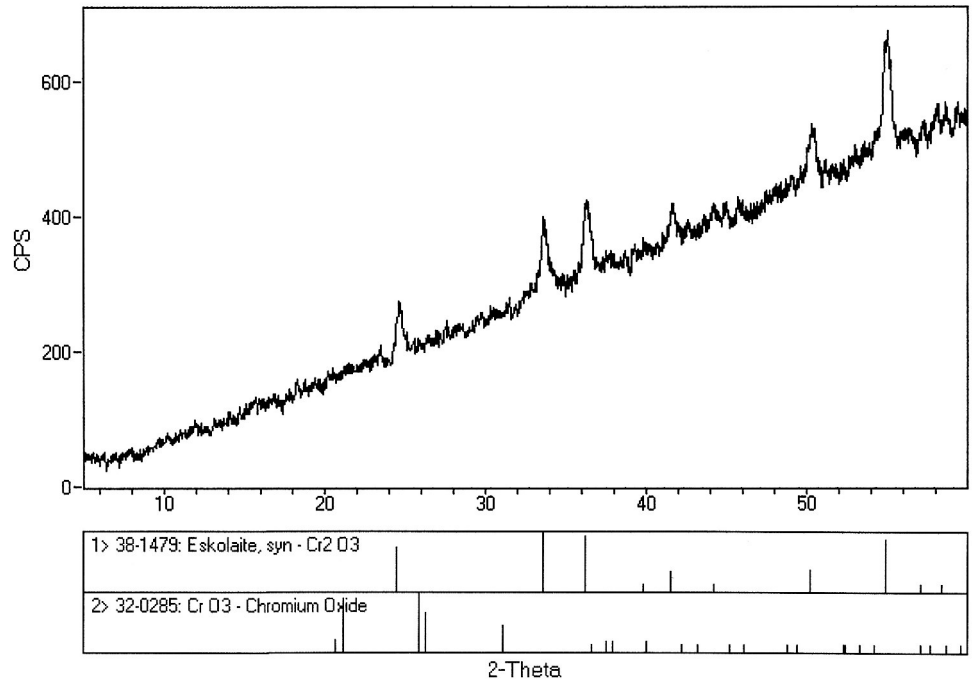

Figure 9. XRD patterns of the prepared Cr-O catalyst, Cr_2O_3, and CrO_3

The XRD pattern of the Cr-V-O catalyst is shown in Figure 10. For comparison, below the figure, XRD patterns of $Cr_2VO_{5.5}$, V_2O_4, V_2O_3, Cr_2O_3, CrO_3, V_2O_5 are also presented. From the XRD pattern, it appears that this catalyst has an amorpous structure. The Cr_2O_3 and V_2O_4 phases are present in the Cr-V-O catalyst in small amount.

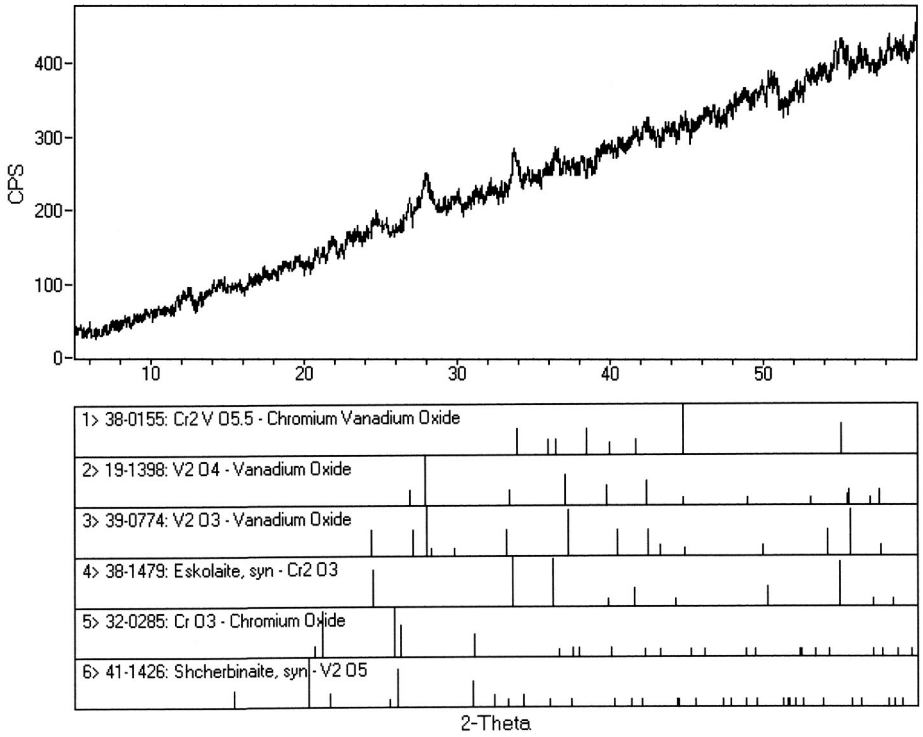

Figure 10. XRD patterns of the prepared Cr-V-O catalyst, $Cr_2VO_{5.5}$, V_2O_4, V_2O_3, Cr_2O_3, CrO_3, and V_2O_5

Figure 11 presents the XRD pattern of the V-MCM-41 catalyst.

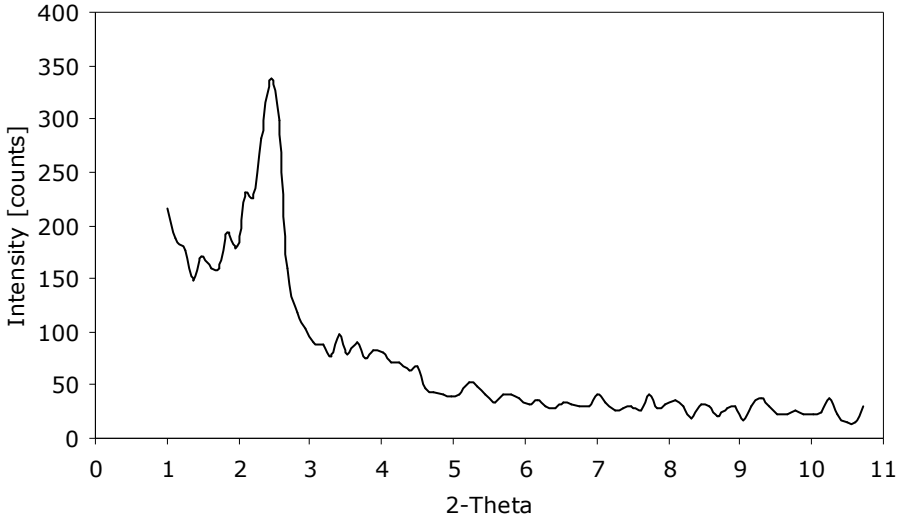

Figure 11. XRD pattern of the V-MCM-41 catalyst

H_2-TPR: Information about the reduction behaviour of Cr-O and Cr-V-O catalysts was provided by TPR analysis. Generally, the oxidative dehydrogenation reaction is accepted to take place through a redox cycle; that is the catalyst's lattice oxygen takes part in the oxidation reaction and then the reduced catalyst is re-oxidized by the gas phase oxygen [27], following a Mars-van Krevelen mechanism [21, 33, 34, 41, 46]. Hence the reducibility of the active sites is very important for the explanation of the catalytic behaviour [27].

The TPR profile of Cr-O catalyst is shown in Figure 12.

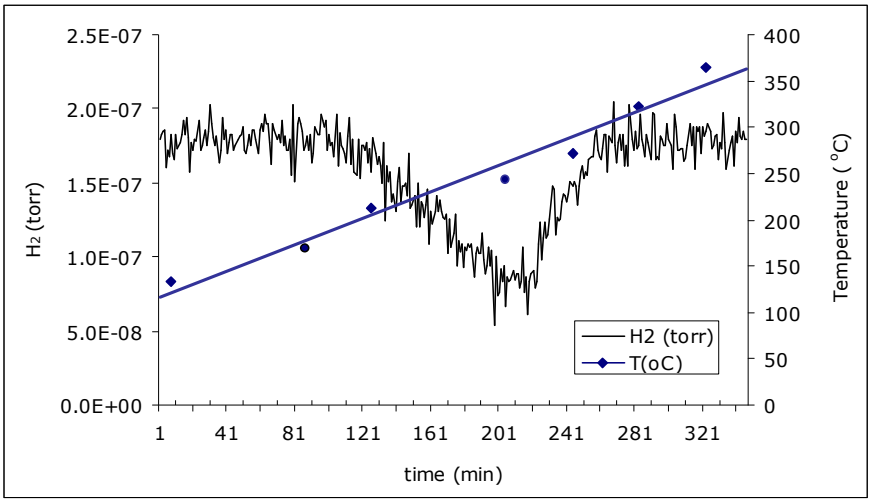

Figure 12. TPR profile of Cr-O catalyst

As it can be seen from the decrease of H_2 (Figure 12), the Cr-O catalyst started to show a reduction peak at about 213°C with a maximum H_2 consumption at about 243°C. Increasing temperature up to 535°C did not cause any further reduction in the catalyst sample. The H_2 consumption of this run was calculated as 1.01×10^{-4}gmol H_2/min from the smoothed curve of Figure 13. The calculations are given below.

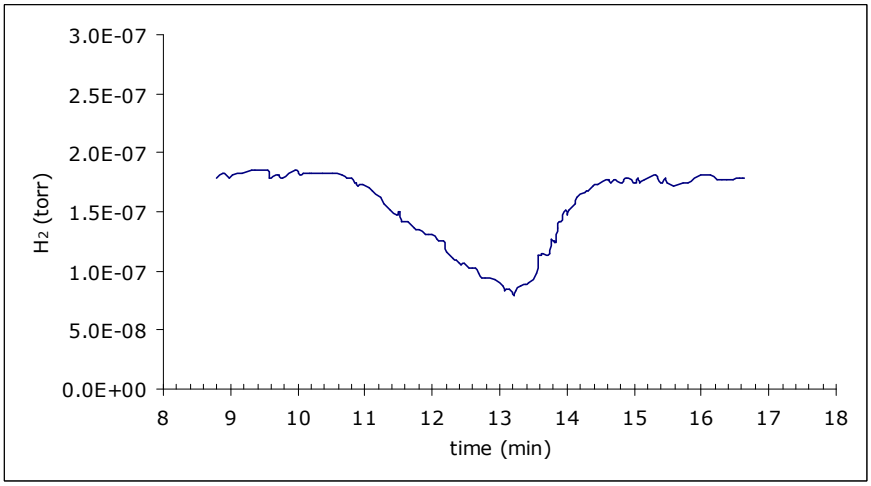

Figure 13. TPR profile of Cr-O catalyst (smoothed curve)

$$H_2 \text{ consumption} = C_{total} Q \int_{t_1}^{t_2} (y_{H_{2_0}} - y_{H_2})\, dt$$

$$y_{H_{2_0}} = 0.05$$

and,

$$y_{H_2} = 0.05 \frac{h_{H_2}}{h_{H_{2_0}}}$$

Therefore,

$$H_2 \text{ consumption} = C_{total} Q \frac{0.05}{h_{H_{2_0}}} \int_{t_1}^{t_2} (h_{H_{2_0}} - h_{H_2})\, dt$$

From Figure 13:

$h_{H_{2_0}}$ =1.8x10^{-7}, t_1=10.52, t_2=14.69

$$\int_{t_1}^{t_2} (h_{H_{2_0}} - h_{H_2})\, dt = 1.96 \text{x} 10^{-7}$$

$$C_{total} = \frac{P}{RT} = 0.037 \text{x} 10^{-6} \text{kgmol} / \text{cm}^3$$

where P=678mmHg and T=21°C.

Q = 50cm^3/min

H_2 consumed with Cr-O catalyst = 1.01x10^{-4}gmol H_2

H_2 consumed per g of Cr-O catalyst = 5.05x10^{-4}gmol H_2/g of Cr-O

The TPR profile of Cr-V-O catalyst is shown in Figure 14. Figure 15 also shows the formation of H_2O with the depletion of H_2.

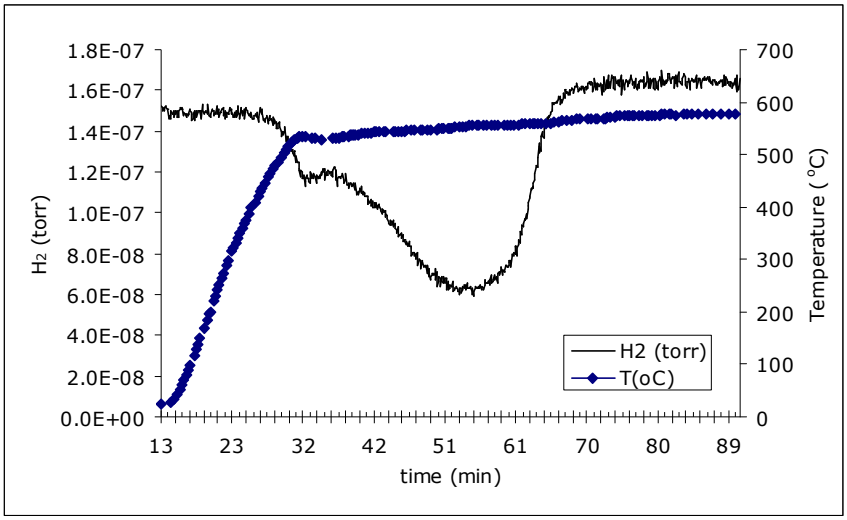

Figure 14. TPR profile of Cr-V-O catalyst

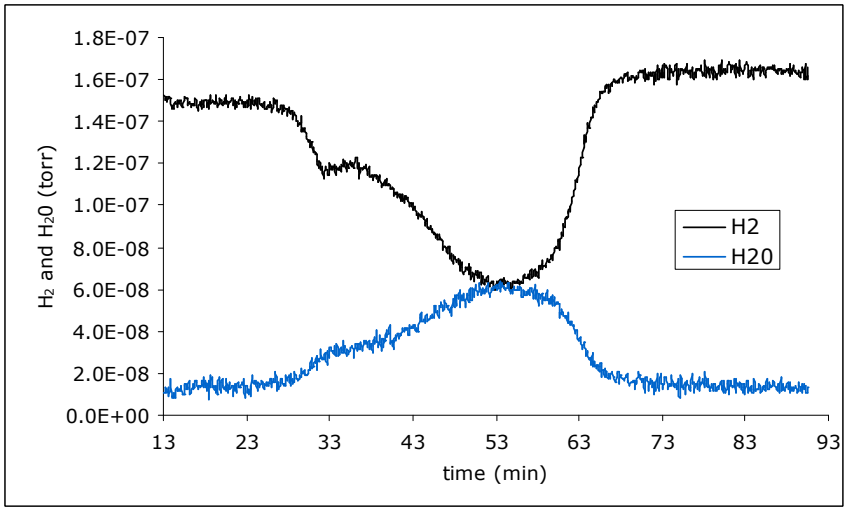

Figure 15. Formation of H_2O during TPR of Cr-V-O catalyst

Different from the TPR profile of the Cr-O, Cr-V-O catalyst exhibited two peaks in the H_2-TPR curve (Figure 14). Reduction of Cr-V-O started at a temperature of about 444°C. The maximum of H_2 consumption for the small and the big peaks were at about 535°C and 555°C, respectively.

The peaks resembled 'two poorly resolved Gaussian peaks' [63]. Deconvolution of this TPR profile was made by fitting Gaussian curves using the software MATLAB 6.5. The MATLAB software utilizes the following type of equation:

$$y = \sum_{i=1}^{n} a_i e^{\left[-\left(\frac{x-b_i}{c_i}\right)^2\right]}$$

'where *a* is the amplitude, *b* is the centroid (location), *c* is related to the peak width, and *n* is the number of peaks to fit' [63].

To fit the peaks, first, the symmetrical curve of the original data was drawn as shown in Figure 16 by adjusting the baseline to zero.

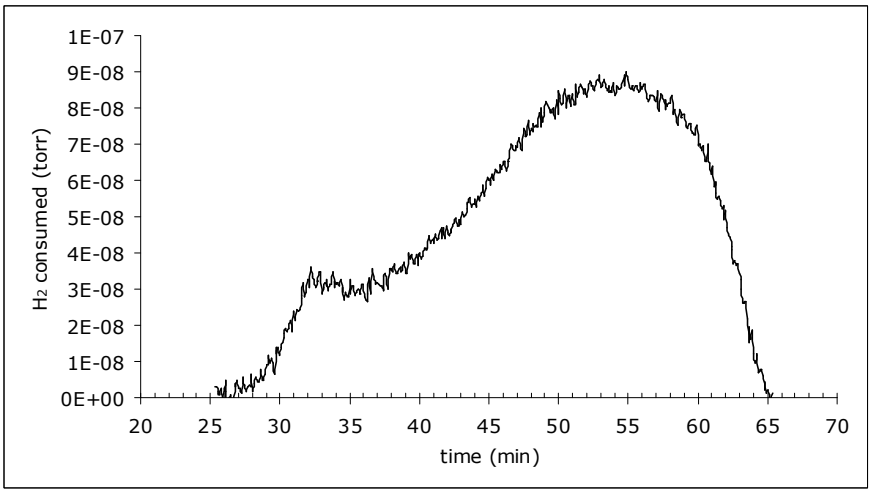

Figure 16. H_2 consumed versus time for Cr-V-O catalyst

Initially, addition of two Gaussian curves was tried to be fitted as the model; but this did not match well with experimental data. Figure 17 shows this trial with the model equation and the goodness of fit. The definitions of these goodness of fit statistics are given in Appendix B.

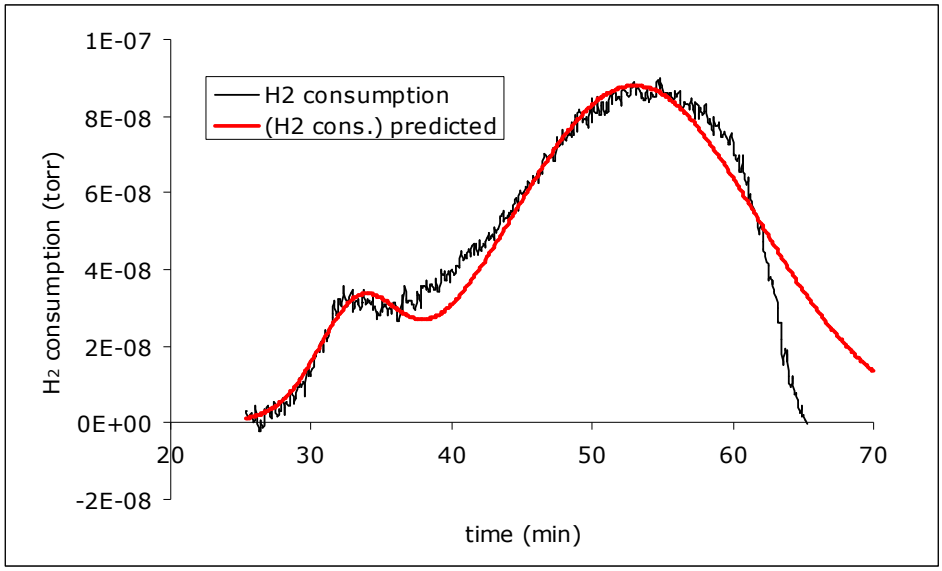

Figure 17. 'Summation of two Gaussian peaks' fit trial for H_2 consumed versus time for Cr-V-O catalyst

Equation of the Gaussian-shaped peak in Figure 17 was:

$$y = 2.601x10^{-8} e^{-\left(\frac{x-33.3}{4}\right)^2} + 8.798x10^{-8} e^{-\left(\frac{x-53}{12.4}\right)^2}$$

Goodness of fit:

SSE: $2.507x10^{-14}$

R-square: 0.9239

Adjusted R-square: 0.923

RMSE: $7.772x10^{-9}$

As a next trial, Gaussian curve with three peaks was fitted. Figure 18 depicts the modelling of the TPR profile of Cr-V-O with the equation of the sum of three Gauss peaks. This model was better than the two-Gauss fit. In order to make the pattern of the TPR spectra more rational, the plot was de-convoluted into three separate Gaussian peaks. The separated peaks drawn by the equation of the fit is given in Figure 19. The three peaks of this fitted curve indicate that there are probably three different forms of reduction sites on the Cr-V-O catalyst surface.

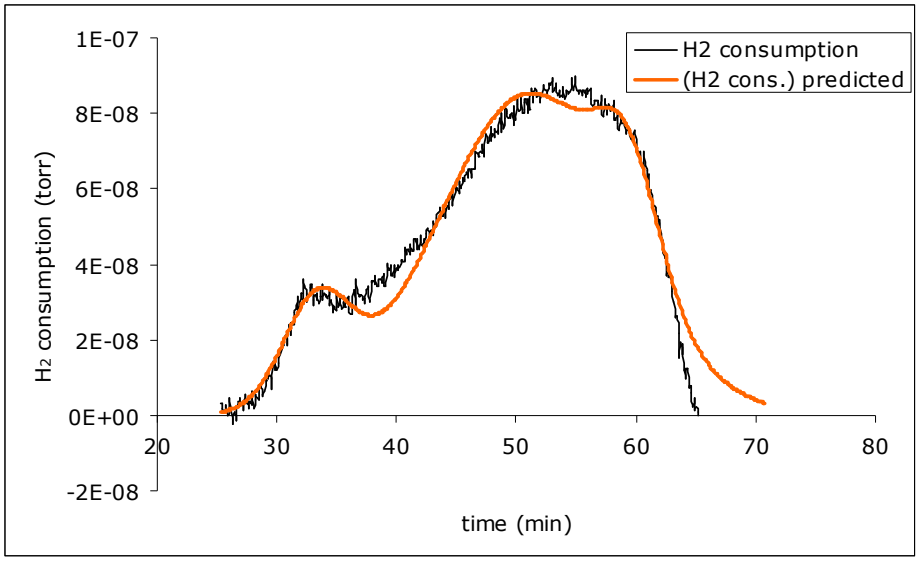

Figure 18. 'Summation of three Gaussian peaks' fit trial for H_2 consumed versus time for Cr-V-O catalyst.

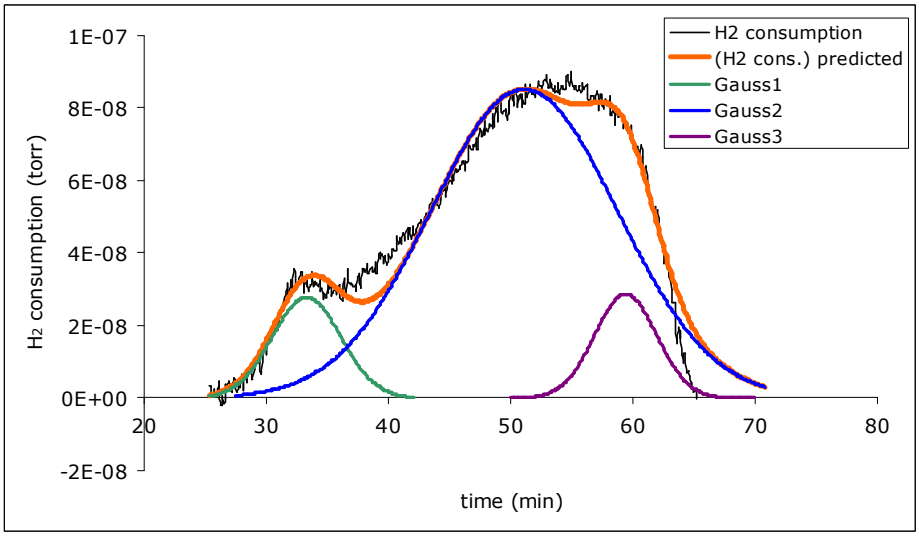

Figure 19. De-convolution of 'Summation of three Gaussian peaks' fit for H_2 consumption versus time for Cr-V-O catalyst.

The equation of the Gaussian-shaped peak in Figure 18 was:

$$y = 2.769x10^{-8} e^{-\left(\frac{x-33.3}{4}\right)^2} + 8.515x10^{-8} e^{-\left(\frac{x-51.1}{10.8}\right)^2} + 2.859x10^{-8} e^{-\left(\frac{x-59.4}{3.6}\right)^2}$$

Goodness of fit:

SSE: $1.019x10^{-14}$

R-square: 0.9691

Adjusted R-square: 0.9685

RMSE: $4.973x10^{-9}$

The maximum temperatures of these peaks (Figure 19), the areas, and the percentages of the areas are presented in Table 3.

Table 3. Parameters for the fitted TPR profile of Cr-V-O catalyst

	Area	% area	T_{max} of peak (°C)
Gauss 1	$2.0x10^{-7}$	9.8	532
Gauss 2	$1.6x10^{-6}$	81.1	550
Gauss 3	$1.8x10^{-7}$	9.1	557
Total:	*$1.98x10^{-6}$*		

The H_2 consumed by Cr-V-O catalyst during TPR is calculated as follows:

$$H_2 \text{ consumption} = C_{total} Q \frac{0.05}{h_{H_{2_0}}} \int_{t_1}^{t_2} h_{H_2} \, dt$$

$$h_{H_{2_0}} = 1.49x10^{-7} \text{ and } \int_{t_1}^{t_2} h_{H_2} \, dt = 1.98x10^{-6}$$

$$C_{total} = \frac{P}{RT} = 0.037x10^{-6} \text{kgmol} / \text{cm}^3$$

where P=678mmHg and T=21.5°C.

Q = $50 cm^3/min$

H_2 consumed with Cr-V-O catalyst = $1.23x10^{-3}$gmol H_2

H_2 consumed per g of Cr-V-O catalyst = $6.15x10^{-3}$gmol H_2/g of Cr-V-O

The three Gaussian curves show that there are three diffrent reduction sites for oxygen on Cr-V-O catalyst. The first 9.8% part may be due to the reduction of adsorbed oxygen. The highest percentage of them, i.e. 81.1%, may possibly be due to the reduction V species, and the final 9.1% portion may be caused by the reduction of Cr species present in Cr-V-O (Table 3).

***XPS*:** In X-Ray Photoelectron Spectroscopy (XPS) monoenergetic soft X rays bombard the sample material, causing electrons to be ejected. From the kinetic energies of these ejected photoelectrons, identification of the elements present in the sample can be made [64]. Besides, 'the relative concentrations of elements can be determined from the measured photoelectron intensities' [64]. 'For a solid, XPS probes 2-20 atomic layers deep' (5-50Å). Greater depths require sputter profiling [64].

The XPS spectrum of the fresh Cr-O catalyst is presented in Figure 20. The peak at 534.4 eV corresponds to O 1s level (Figure 20). The average value of Cr $2p_{3/2}$ binding energy for CrO_3 is reported as 579.37 eV (reference C 1s 285 eV) [71]. The spectrum of Cr $2p_{3/2}$ level of fresh Cr-O catalyst was measured at 580.7 eV (Figure 20). Comparison of this value with the literature one shows that Cr species in +6 oxidation state are present on the surface of the Cr-O catalyst.

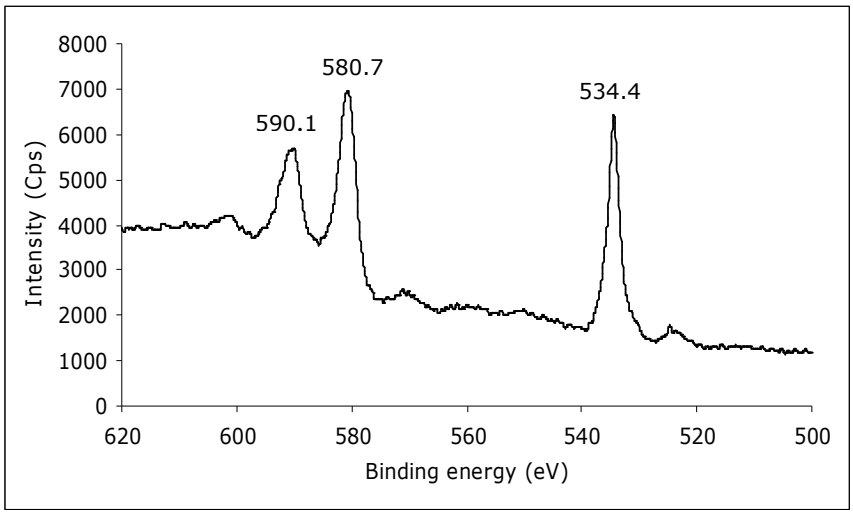

Figure 20. XPS spectrum of Cr-O catalyst

Figure 21 depicts the XPS spectrum of fresh Cr-O catalyst after 2 min. Ar^+ ion bombardment at 5000 eV. By this way it is aimed to remove the adsorbed oxygen species from the surface and move further away from the top surface. The Cr $2p_{3/2}$ binding energy was detected at 579.6 eV which is close to the value of before ion bombardment spectrum (580.7 eV, Figure 20). The peak at 533.4 eV corresponds to O 1s binding energy. The comparison of the spectra before and after ion bombardment can be seen in Figure 22.

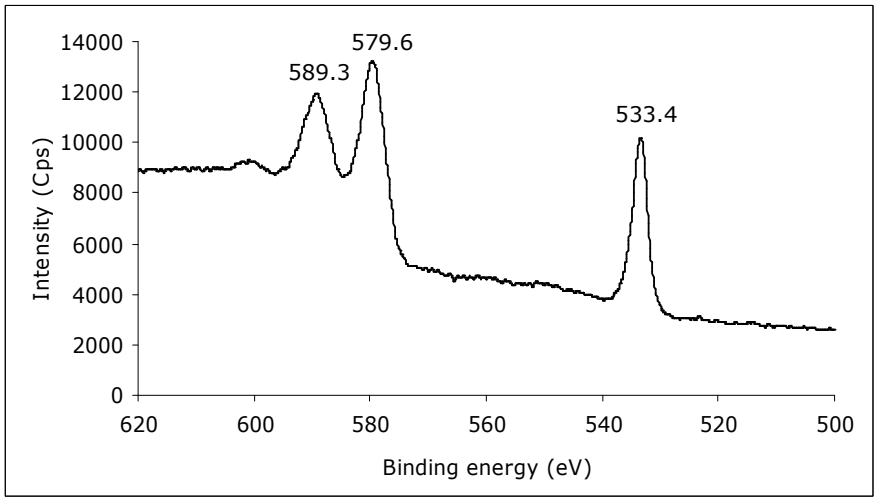

Figure 21. XPS spectrum of Cr-O catalyst after ion bombardment

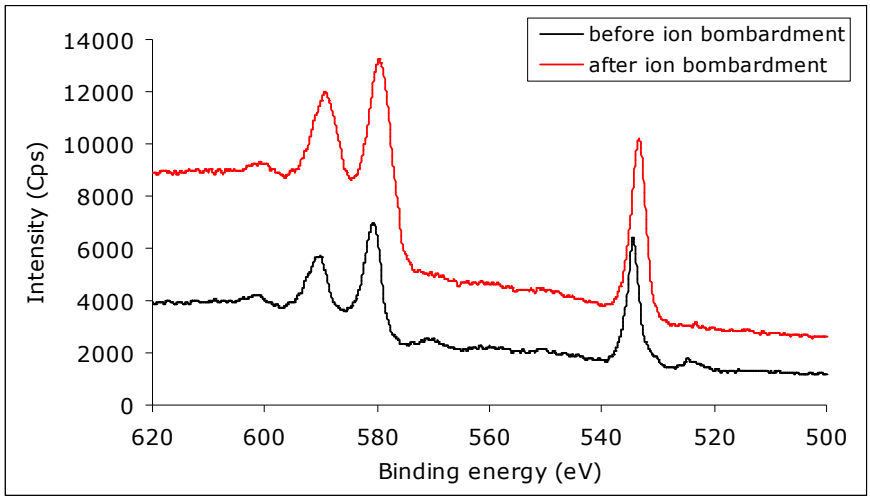

Figure 22. XPS spectra of Cr-O catalyst before and after ion bombardment

On the surface of the fresh Cr-O catalyst the Cr and O atom percentages were found as 17.7 and 82.3%, respectively; that is the O/Cr ratio was 4.6. After ion bombardment, the O atom percentange was decreased to 79.2, as expected. The Cr percentage was 20.8. The O atom amount was 3.8 times the Cr amount after ion bombardment.

The XPS spectrum of the Cr-O catalyst after H_2-TPR is given in Figure 23. The Cr $2p_{3/2}$ level of fresh Cr-O catalyst was measured at 580.7 eV (Figure 20). Comparing this value with the reduced catalyst's Cr $2p_{3/2}$ level of 578.8 (Figure 23) and the reported literature Cr $2p_{3/2}$ average value of 579.37 eV for CrO_3 shows that the Cr-O catalyst after H_2-TPR treatment still contained some Cr^{+6} species. The catalyst is only partly reduced. Perhaps the H_2 consumption seen during TPR (Figure 12) may be majorly due to the reduction of adsorbed oxygen species.

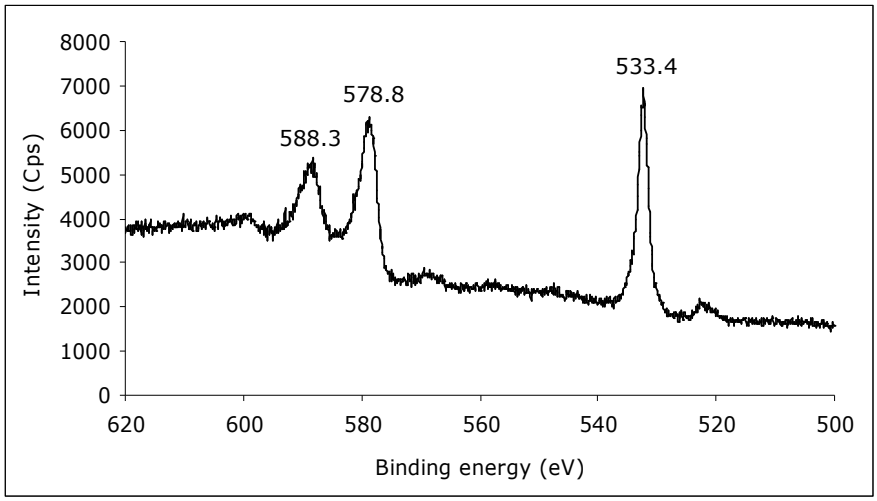

Figure 23. XPS spectrum of reduced Cr-O catalyst after H_2-TPR

Figure 24 gives the spectrum of reduced Cr-O catalyst after ion bombardment. In this sample, the Cr $2p_{3/2}$ level was detected at 578.2 eV. The spectra obtained before and after ion bombardment are compared in Figure 25. When after ion bombardment Cr $2p_{3/2}$ value for the fresh and reduced Cr-O catalyst are examined; that is, 579.6 eV for fresh and 578.2 eV for reduced catalysts (Figure 21 and Figure 24), the change in the level towards a lower value is an indication of its partial reduction. A complete reduction to Cr^{+2} would result in an average Cr $2p_{3/2}$ value of 576.6 eV (reference C 1s 285 eV) as reported for Cr_2O_3 [71].

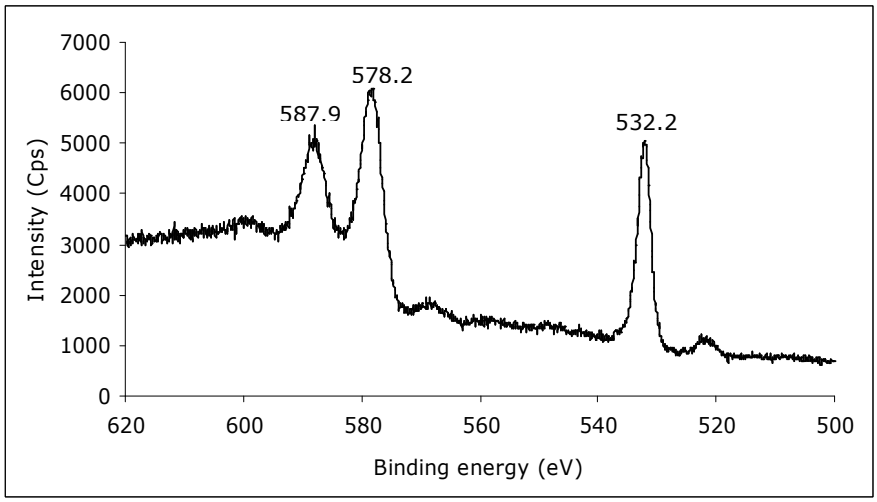

Figure 24. XPS spectrum of reduced Cr-O catalyst after after ion bombardment

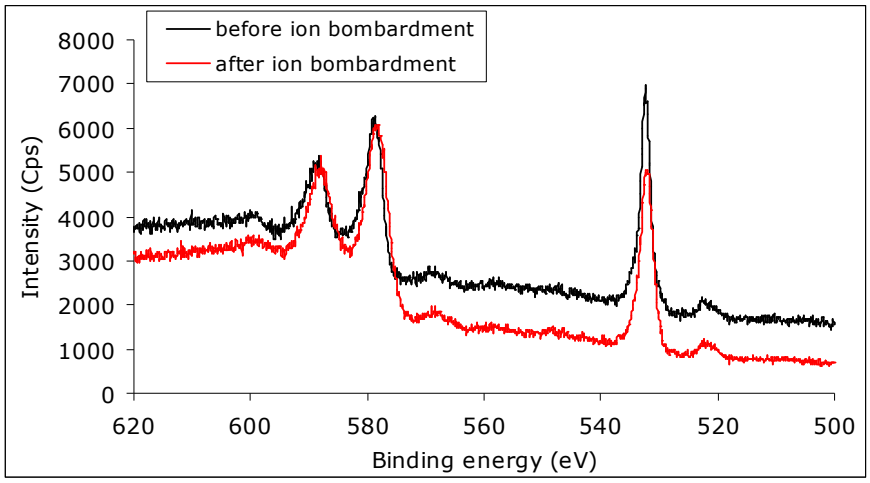

Figure 25. XPS spectra of reduced Cr-O catalyst before and after ion bombardment

Table 4 and 5 summarizes the binding energy values of Cr $2p_{3/2}$ level for the fresh and reduced Cr-O catalyst both before and after ion bombardment, and the atom percentages obtained by XPS, respectively. The O/Cr ratio in the reduced Cr-O catalyst was 5.5 before ion bombardment. After ion bombardment this value was reduced to 2.7 (Table 4).

Table 4. Atom percentages of Cr-O catalyst determined by XPS

	Fresh Cr-O		Cr-O after TPR	
	Before ion bombardment	After ion bombardment	Before ion bombardment	After ion bombardment
Cr %	17.7	20.8	15.5	26.9
O %	82.3	79.2	84.6	73.1

Table 5. Binding energies for fresh and reduced Cr-O catalyst from XPS

	Fresh Cr-O		Cr-O after TPR	
	Before ion bombardment	After ion bombardment	Before ion bombardment	After ion bombardment
Cr $2p_{3/2}$ BE (eV)	580.7	579.6	578.8	578.2

The XPS spectrum of the fresh Cr-V-O catalsyt (Figure 26), reveals the presence of Cr, V, and O species on the surface. The elemental composion of the surface shows that V is 1.5 times the Cr amount (Table 6). During preparation of the Cr-V-O catalyst, the mole ratio of V to Cr was arranged to be 1. This calculation aims the bulk composition. Therefore, according to XPS results, the surface contains more vanadium than chromium compared to the bulk of the catalyst.

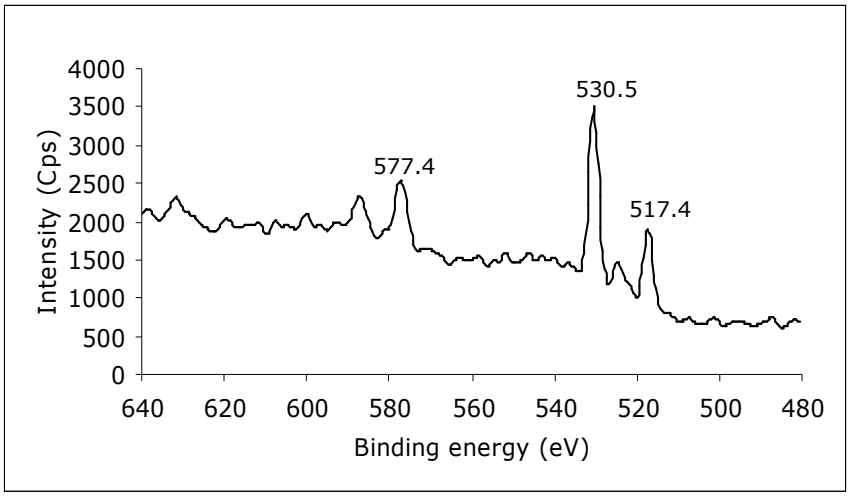

Figure 26. XPS spectrum of Cr-V-O catalyst

The V $2p_{3/2}$ binding energy value of V_2O_5 is reported as 517.3 eV (reference C 1s 285 eV) [65] and as 517.7 eV (reference C 1s 284.6 eV) [66]. The Cr $2p_{3/2}$ binding energy value for CrO_3 is 578.7 eV (reference C 1s 283.8 eV) [71]. Comparison of these data with the spectrum (Figure 26), shows that these species may probably be present in the Cr-V-O catalyst, and hence the V^{+5} and Cr^{+6} forms.

After ion bombardment, that is when the surface O is removed and moved closer to the bulk, the V amount is 1.4 times the Cr; not much different from the surface (Table 6). The spectrum obtained after 2 min. Ar^+ ion bombardment at 5000 eV is given in Figure 27. The comparison of the spectra before and after ion bombardment can be seen from Figure 28.

Table 6. Atom percentages of Cr-V-O catalyst determined by XPS

	Fresh Cr-V-O		**Cr-V-O after TPR**	
	Before ion bombardment	After ion bombardment	Before ion bombardment	After ion bombardment
Cr %	8.0	11.7	12.6	18.5
V %	12.3	16.7	12.6	14.4
O %	79.6	71.6	74.8	67.1

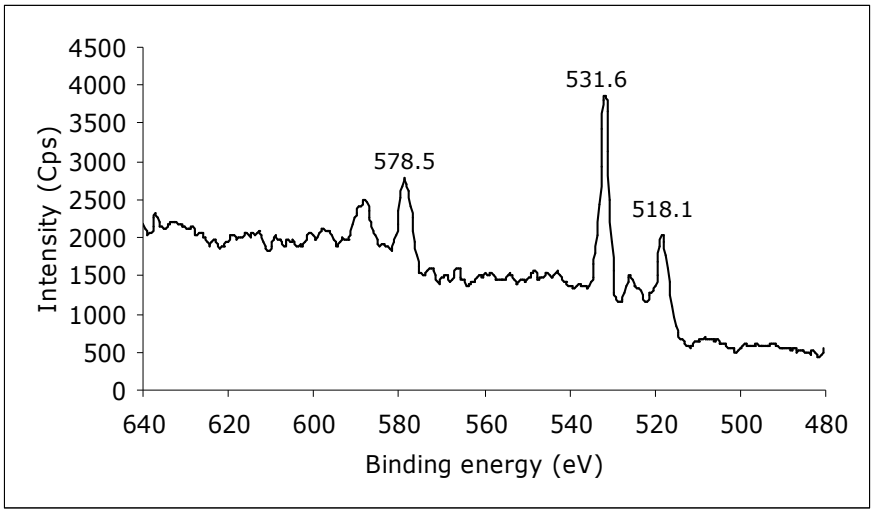

Figure 27. XPS spectrum of Cr-V-O catalyst after ion bombardment

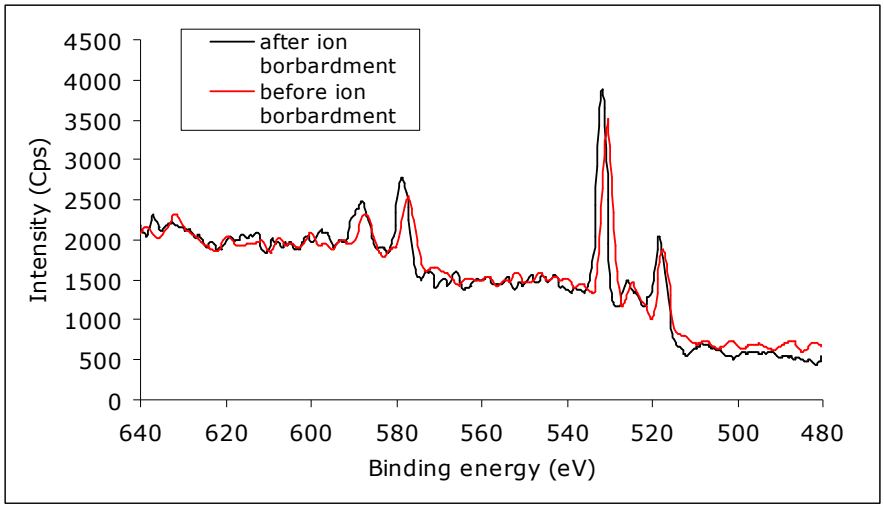

Figure 28. XPS spectra of Cr-V-O catalyst before and after ion bombardment

Figure 29 depicts the XPS spectrum of the Cr-V-O catalyst after H_2-TPR. In this reduced sample the surface atomic concentration of V and Cr is the same (Cr/V=1). The spectrum of reduced Cr-V-O catalyst after ion bombardment is presented in Figure 30. The Cr/V ratio became 1.3 after ion bombardment. The increase of percentages of Cr and V after ion bombardment is due to the removal of O species (Table 6).

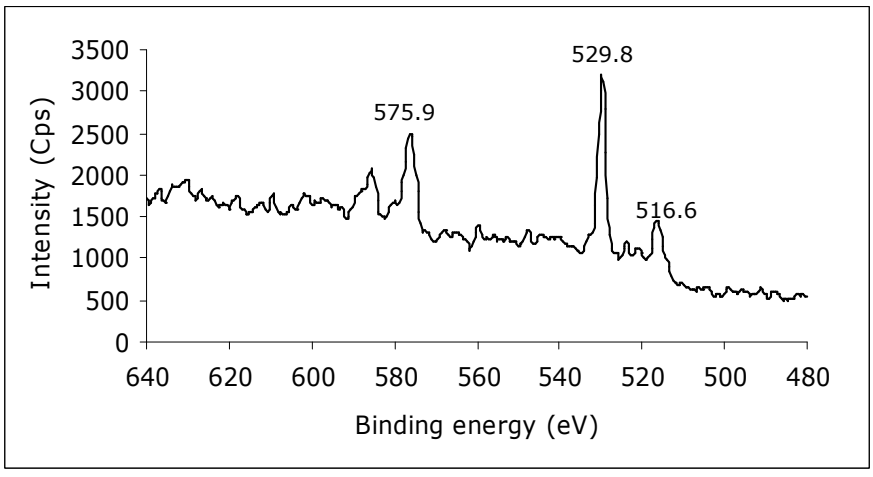

Figure 29. XPS spectrum of reduced Cr-V-O catalyst after H_2-TPR

The V $2p_{3/2}$ binding energy values for VO_2 were reported to be 516 eV and for V_2O_3 515.9 eV (reference C1s 285 eV) [66]. The peaks corresponding to V $2p_{3/2}$ value of the reduced sample before and after ion bombardment were seen at 516.6 and 515.5 eV, respectively (Figures 29 and 30). Therefore, by TPR, the Cr-V-O catalyst's V species are probably reduced from V^{+5} to V^{+4} and V^{+3} states. Table 7 summarizes the binding energy values for the XPS of the fresh and the reduced Cr-V-O catalysts.

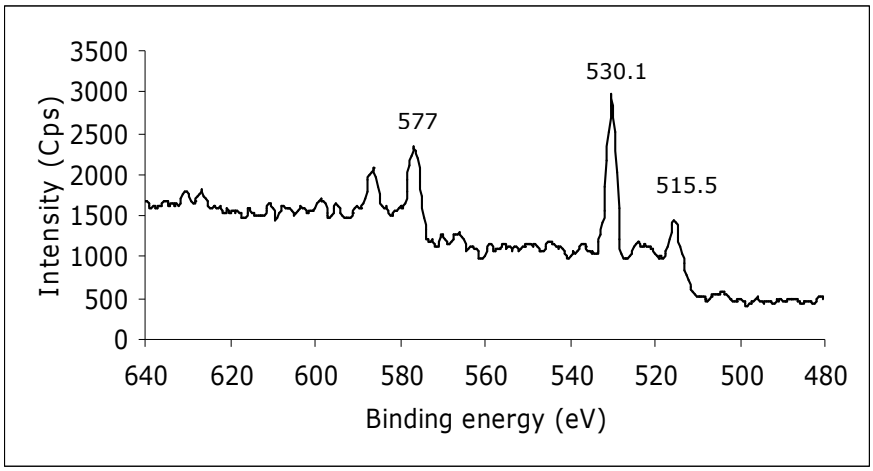

Figure 30. XPS spectrum of reduced Cr-V-O catalyst after ion bombardment

Table 7. Binding energies for fresh and reduced Cr-V-O catalyst from XPS

	Fresh Cr-V-O		**Cr-V-O after TPR**	
	Before ion bombardment	After ion bombardment	Before ion bombardment	After ion bombardment
Cr $2p_{3/2}$ BE (eV)	577.4	578.5	575.9	577
V $2p_{3/2}$ BE (eV)	517.4	518.1	516.6	515.5

The spectra of the reduced Cr-V-O before and after ion bombardment are compared in Figure 31.

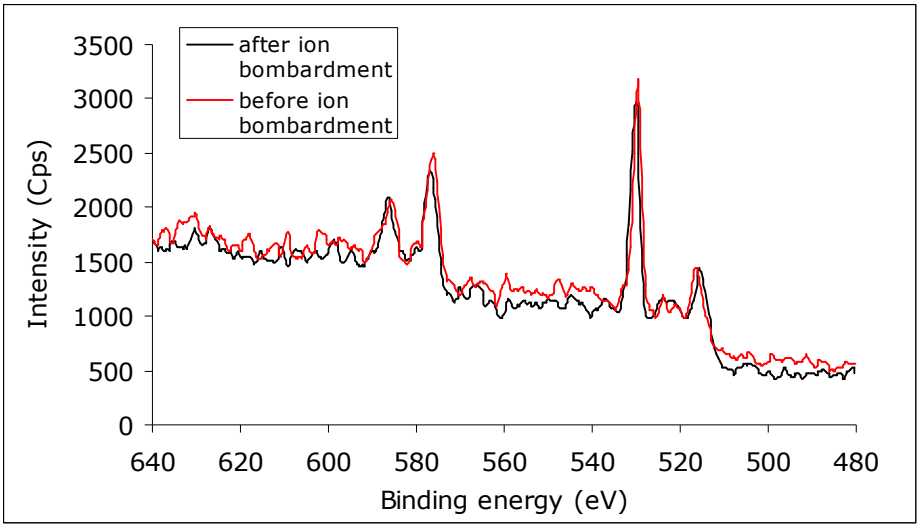

Figure 31. XPS spectra of reduced Cr-V-O catalyst before and after ion bombardment

The Cr $2p_{3/2}$ binding energy value for Cr_2O_3 is reported as 575.6 eV (reference C1s 283.8 eV) [71] and 575.7 eV (reference C1s 285 eV) [65]. When the before ion bombardment Cr $2p_{3/2}$ binding energies of the fresh (577.4 eV) and reduced (575.9 eV) Cr-V-O (Table 7) are compared with the literature data, the Cr^{+6} species present in the fresh catalyst seem to be reduced to its lower oxidation state of Cr^{+3}.

According to XPS results, the possible reactions occuring during reduction of Cr-V-O catalyst may be as follows:

$$V_2O_5 + H_2 \rightarrow 2VO_2 + H_2O$$
$$V_2O_5 + 2H_2 \rightarrow V_2O_3 + 2H_2O$$
$$2CrO_3 + 3H_2 \rightarrow Cr_2O_3 + 3H_2O$$

This is consistent with the TPR results in which the presence of three reduction sites was revealed from the Gaussian fits (Table 3). Therefore, from XPS and TPR, it can be deduced that, pure Cr-O was not reduced to its lower oxidation states, whereas Cr-V-O was. These results showed that vanadium is much more easily reduced and it is probably involved in the oxidative dehyrogenation reaction through a redox mechanism.

3.2. Catalyst Testing – Steady-state Experiments

There are seven species in the system (C_2H_6, C_2H_4, O_2, H_2O, CO_2, CO, and CH_4) and three elemental species conservation equations can be written for C, H, and O. Therefore, four (7-3=4) independent reactions identify the system. Consequently, the following reactions were considered for the analysis of the results:

$$C_2H_6 + \tfrac{1}{2}\, O_2 \rightarrow C_2H_4 + H_2O \quad (1)$$

$$C_2H_6 + 7/2\, O_2 \rightarrow 2CO_2 + 3H_2O \quad (2)$$

$$C_2H_6 + 5/2\, O_2 \rightarrow 2CO + 3H_2O \quad (3)$$

$$C_2H_6 + O_2 \rightarrow CH_4 + CO + H_2O \quad (4)$$

The overall conversion, selectivity and yield values were defined as follows:

$$\text{Total Conversion} = \frac{\text{Moles of ethane reacted}}{\text{Moles of ethane fed to the system}}$$

$$X_{total} = \frac{F_{C_2H_6}^{\ 0} - F_{C_2H_6}}{F_{C_2H_6}^{\ 0}}$$

$$F_{C_2H_6}^{\ o} = F_{C_2H_6} + F_{C_2H_4} + \frac{1}{2}F_{CO_2} + \frac{1}{2}F_{CO} + \frac{1}{2}F_{CH_4}$$

$$X_{total} = \frac{\left(F_{C_2H_6} + F_{C_2H_4} + \frac{1}{2}F_{CO_2} + \frac{1}{2}F_{CO} + \frac{1}{2}F_{CH_4}\right) - F_{C_2H_6}}{F_{C_2H_6} + F_{C_2H_4} + \frac{1}{2}F_{CO_2} + \frac{1}{2}F_{CO} + \frac{1}{2}F_{CH_4}}$$

Dividing by F_{total}:

$$X_{total} = \frac{y_{C_2H_4} + \frac{1}{2}y_{CO_2} + \frac{1}{2}y_{CO} + \frac{1}{2}y_{CH_4}}{y_{C_2H_6} + y_{C_2H_4} + \frac{1}{2}y_{CO_2} + \frac{1}{2}y_{CO} + \frac{1}{2}y_{CH_4}}$$

$$\text{Selectivity} = \frac{\text{Moles of ethylene formed}}{\text{Moles of ethane reacted}}$$

$$S_{C_2H_4} = \frac{F_{C_2H_4}}{F_{C_2H_6}^{0} - F_{C_2H_6}}$$

$$S_{C_2H_4} = \frac{y_{C_2H_4}}{y_{C_2H_4} + \frac{1}{2} y_{CO_2} + \frac{1}{2} y_{CO} + \frac{1}{2} y_{CH4}}$$

Similarly,

$$S_{CO_2} = \frac{(y_{CO_2}/2)}{y_{C_2H_4} + \frac{1}{2} y_{CO_2} + \frac{1}{2} y_{CO} + \frac{1}{2} y_{CH4}} \quad \text{and}$$

$$S_{CH_4} = \frac{(y_{CH4}/2)}{y_{C_2H_4} + \frac{1}{2} y_{CO_2} + \frac{1}{2} y_{CO} + \frac{1}{2} y_{CH4}}$$

$$\text{Yield} = (\text{Selectivity}) \times (\text{Total Conversion}) = \frac{\text{Moles of ethylene formed}}{\text{Moles of ethane fed to the system}}$$

$$Y_{C_2H_4} = \frac{y_{C_2H_4}}{y_{C_2H_6} + y_{C_2H_4} + \frac{1}{2} y_{CO_2} + \frac{1}{2} y_{CO} + \frac{1}{2} y_{CH4}}$$

For the experiments conducted with CO_2 instead of O_2, total conversion, selectivity, and yield values were calculated using the following equations:

$$(X_{total})_{withCO_2} = \frac{y_{C_2H_4} + \frac{1}{2}y_{CO} + \frac{1}{2}y_{CH_4}}{y_{C_2H_6} + y_{C_2H_4} + \frac{1}{2}y_{CO} + \frac{1}{2}y_{CH_4}}$$

$$(S_{C_2H_4})_{withCO_2} = \frac{y_{C_2H_4}}{y_{C_2H_4} + \frac{1}{2}y_{CO} + \frac{1}{2}y_{CH4}}$$

$$(Y_{C_2H_4})_{withCO_2} = \frac{y_{C_2H_4}}{y_{C_2H_6} + y_{C_2H_4} + \frac{1}{2}y_{CO} + \frac{1}{2}y_{CH4}}$$

All the experimental data used for the graphs presented in the following sections are given in Appendix C.

3.2.1. Experiments with Cr-O Catalyst under O_2-C_2H_6-He Flow

Oxidative dehydrogenation experiments were performed with the prepared Cr-O catalyst under O_2-C_2H_6-He flow. As a first trial, an O_2/C_2H_6 feed ratio of 0.5 was used (15% O_2, 30% C_2H_6, 55% He) and experiments were carried out at room temperature, 153°C and 251°C. The total conversion, ethylene selectivity and yield values are given in Figure 32. Since a high amount of CO_2 formation, i.e. 0.65 CO_2 selectivity, and the consumption of all the feed O_2 at 251°C were observed, the O_2 amount in this trial was concluded to be too high.

Consequently, the O_2 amount in the feed was decreased and an O_2/C_2H_6 feed ratio of 0.17 was used (5% O_2, 30% C_2H_6, 65% He) as the next trial. The experiments for this feed composition were done at a temperature range of 148-447°C. The variation of total conversion, selectivity to ethylene, and ethylene yield with temperature are presented in Figures 33a-c, respectively.

The total fractional conversion values increased with temperature and reached to 0.2 at 447°C (Figure 33a). As it can be seen from Figure 33b, the selectivity to ethylene values were almost constant, i.e. 0.8, in the temperature range of 250-450°C. No CO formation was observed in these experiments. The variation of selectivity to CO_2 and CH_4 with temperature for ~5% O_2 in feed are illustrated in Figures 34a and 34b, respectively. Selectivity to CO_2 started to decrease above 350°c (Figure 34a), and CH_4 selectivity values were constant at a value of 0.05 in the temperature range of 300-450°C (Figure 34b).

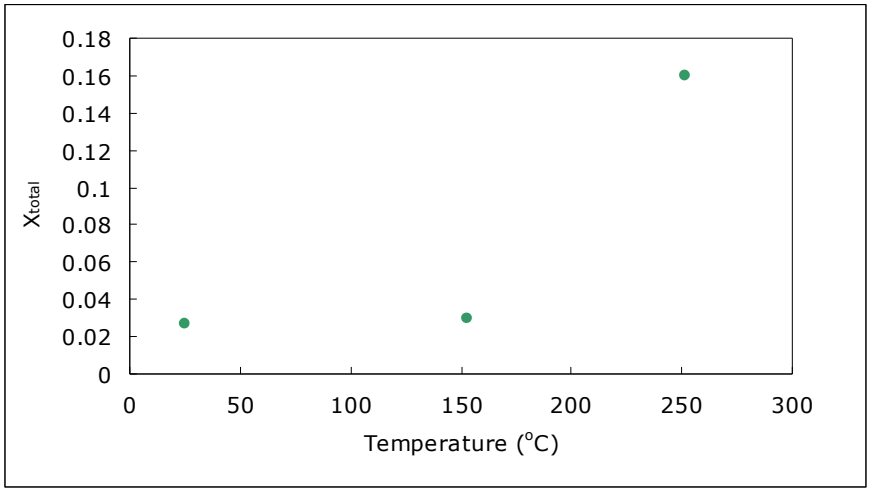

(a)

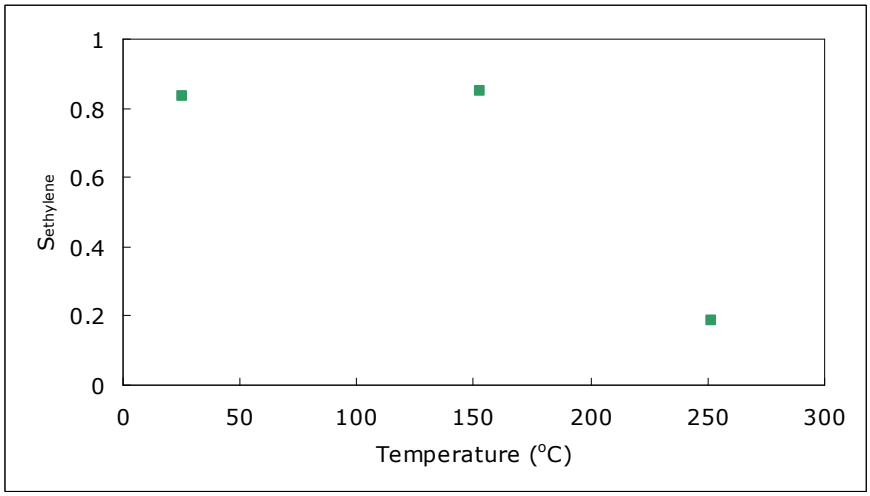

(b)

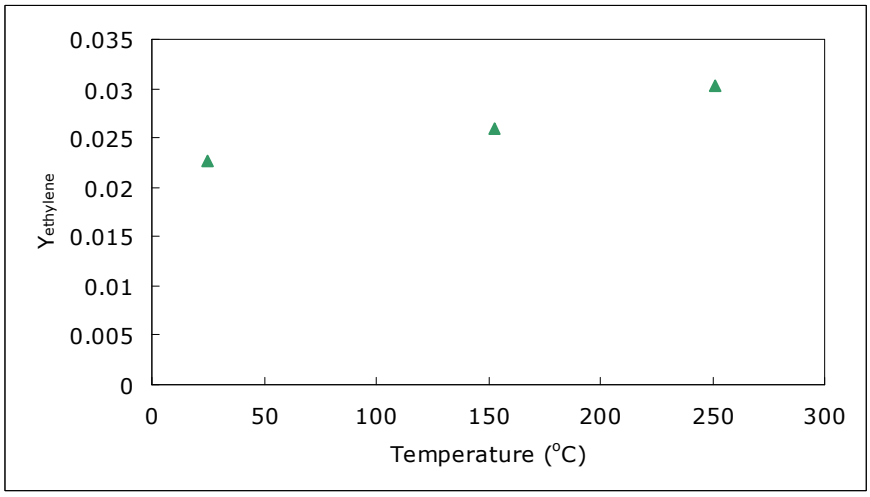

(c)

Figure 32. (a) Total conversion-temperature data, **(b)** C_2H_4 selectivity-temperature data, **(c)** C_2H_4 yield-temperature data (catalyst: 0.2 g Cr-O, O_2/C_2H_6 = 0.50, feed: 50 cm^3/min)

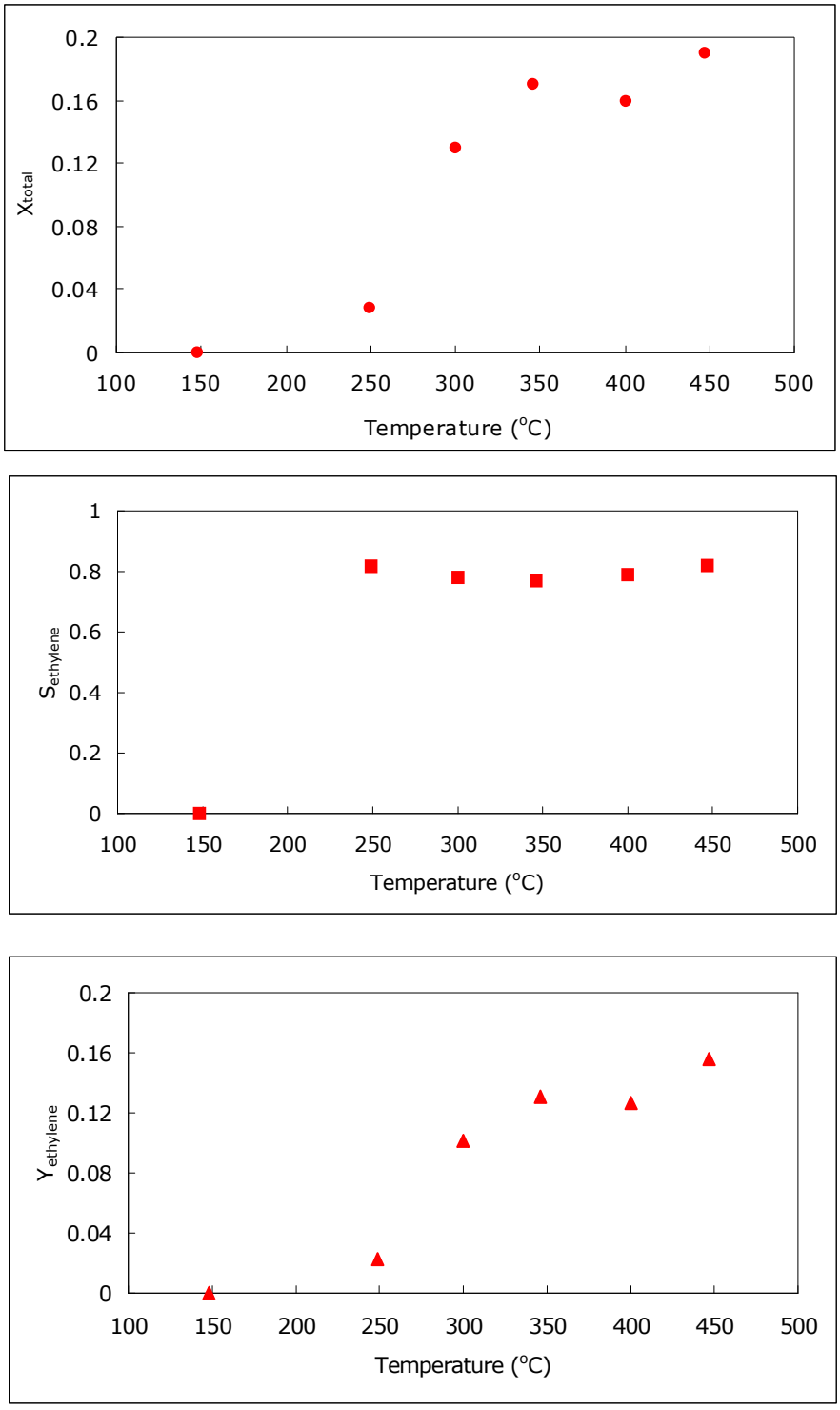

Figure 33. (a) Total conversion-temperature data, **(b)** C_2H_4 selectivity-temperature data, **(c)** C_2H_4 yield-temperature data (catalyst: 0.2 g Cr-O, O_2/C_2H_6 = ~0.17, feed: 50 cm^3/min)

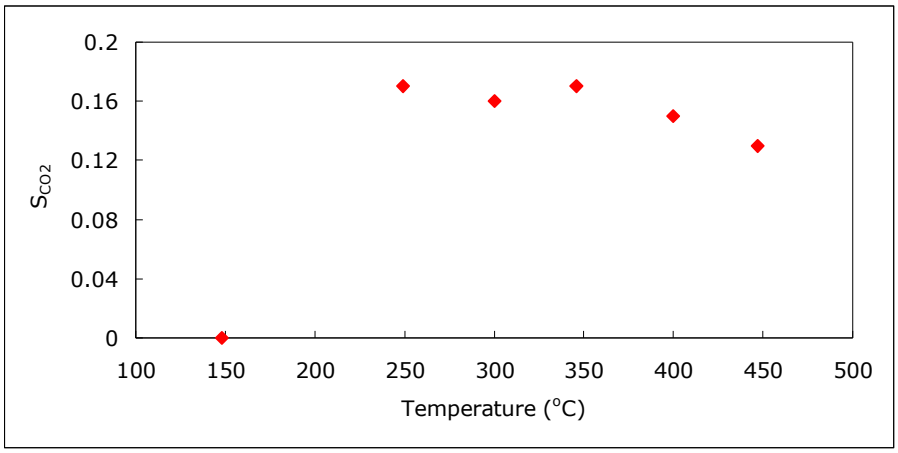

(a)

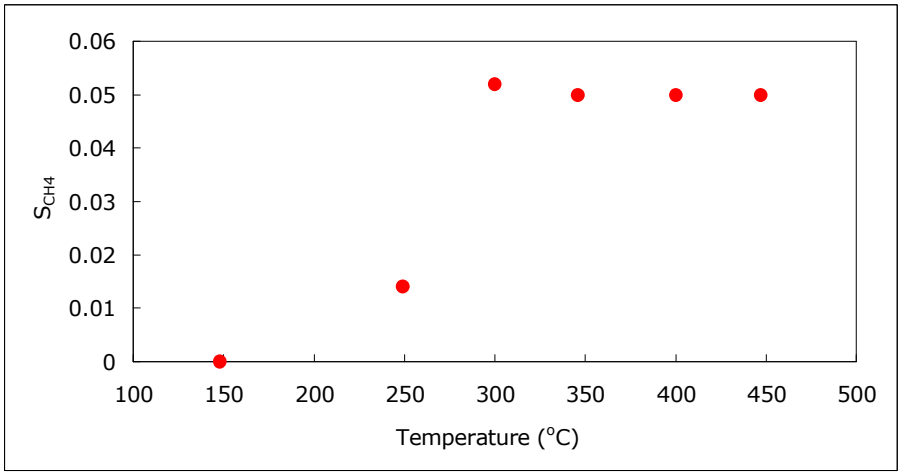

(b)

Figure 34. (a) CO_2 selectivity-temperature data, **(b)** CH_4 selectivity-temperature data (catalyst: 0.2 g Cr-O, O_2/C_2H_6 = ~0.17, feed: 50 cm^3/min)

Following these runs, the O_2 amount in the feed was increased to 10% keeping the C_2H_6 percentage constant at 30% (O_2/C_2H_6 = ~0.33). For the temperature range of 250-400°C, the variation of total conversion, selectivity to ethylene, and ethylene yield with temperature are given in Figures 35a-c, respectively.

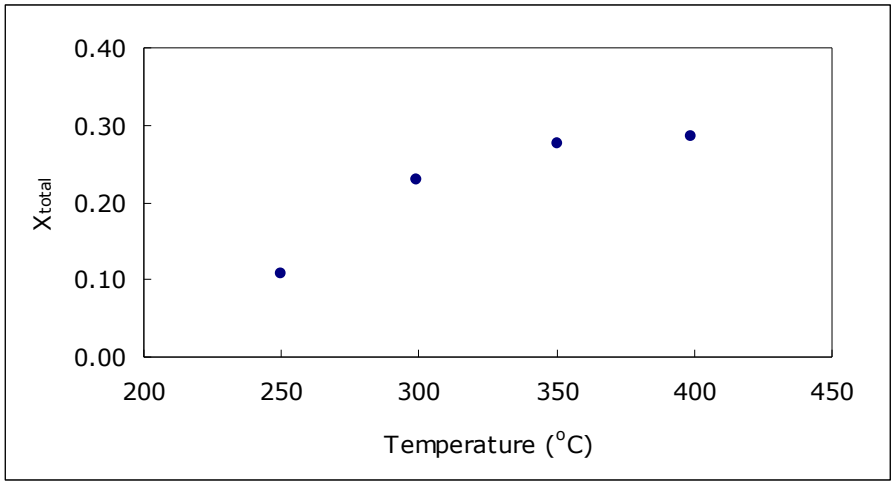

(a)

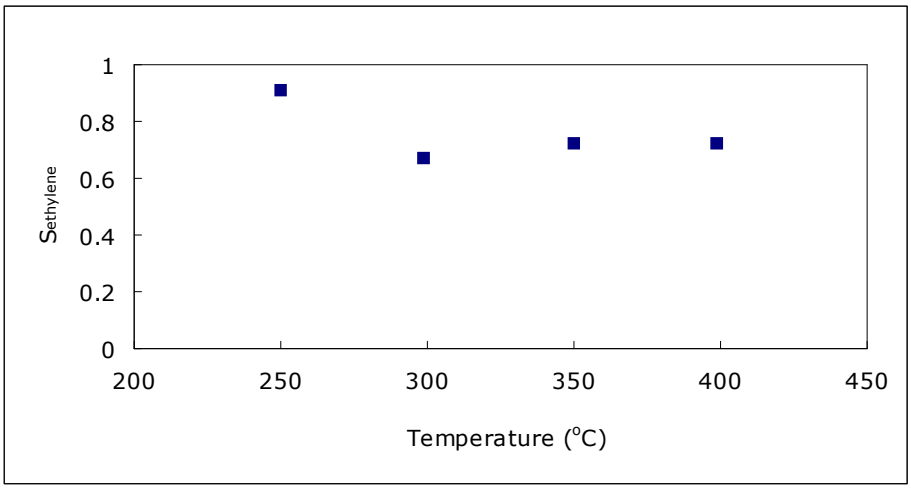

(b)

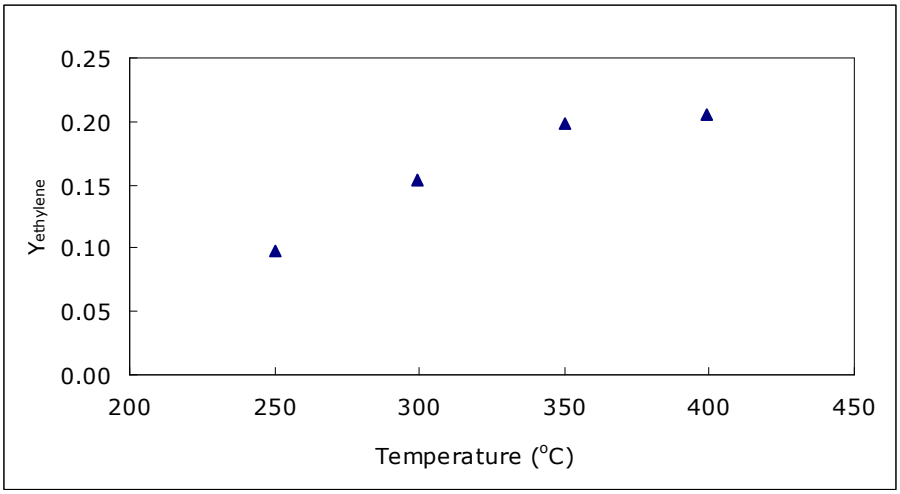

(c)

Figure 35. (a) Total conversion-temperature data, **(b)** C_2H_4 selectivity-temperature data, **(c)** C_2H_4 yield-temperature data (catalyst: 0.2 g Cr-O, O_2/C_2H_6 = ~0.33, feed: 50cm^3/min)

When data in Figures 33a and 35a are compared, it can be seen that the increase of O_2 in the feed enhanced the total conversion (Figure 36a). The comparison of ethylene selectivity and yield for feed containing 5% and 10% O_2 can be seen in Figure 36b and 36c, respectively.

At 250°C, with ~10% O_2 – 30% C_2H_6 feed composition, a total fractional conversion value of 0.11 was obtained with an C_2H_4 selectivity of 0.91. The variation of selectivity to CO_2, CH_4, and CO with temperature for ~10% O_2 in feed are illustrated in Figures 37a, b, and c, respectively. The CH_4 selectivity values were about 0.05 for this feed composition (Figure 37b) and the CO_2 selectivities were constant above 300 °C with a value of 0.2 (Figure 37a).

For 250°C, the effect of O_2 mole fraction variation in the feed to total conversion, C_2H_4 selectivity and yield are presented in Figures 38a-c. As expected, total conversion increased with O_2 amount in the feed (Figure 38a); whereas, selectivity to ethylene decreased significantly above 10% O_2 due to increase in formation of CO_2 (Figure 38b). Figure 38 shows that at ~250°C, the highest ethylene selectivity value of 0.91 was obtained at a feed composition of 10% O_2 with total conversion and yield values of 0.11 and 0.1, respectively.

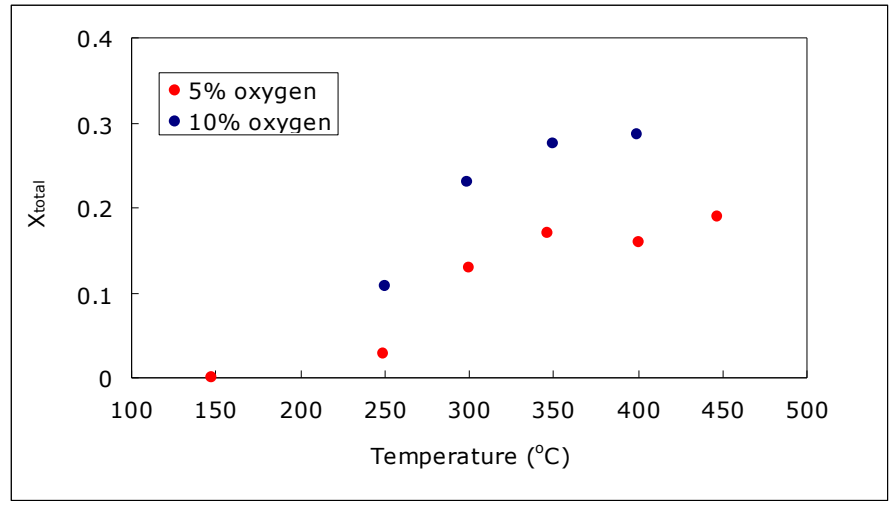

(a)

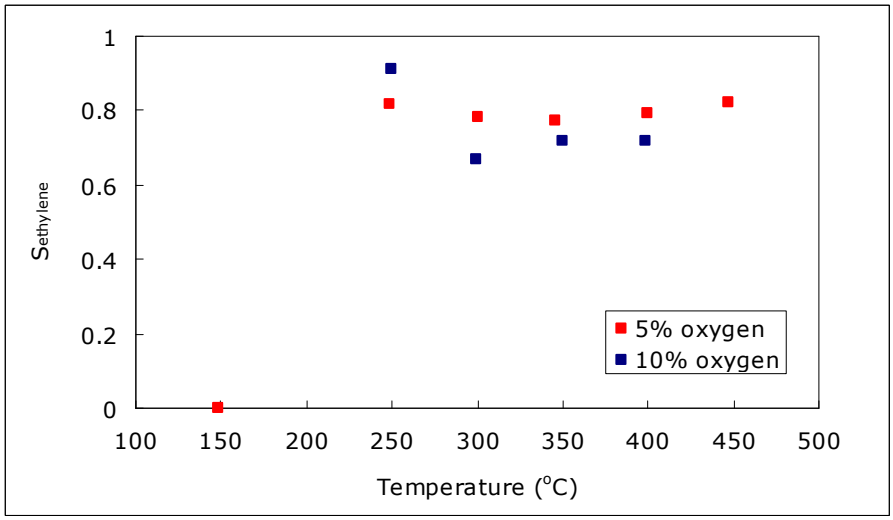

(b)

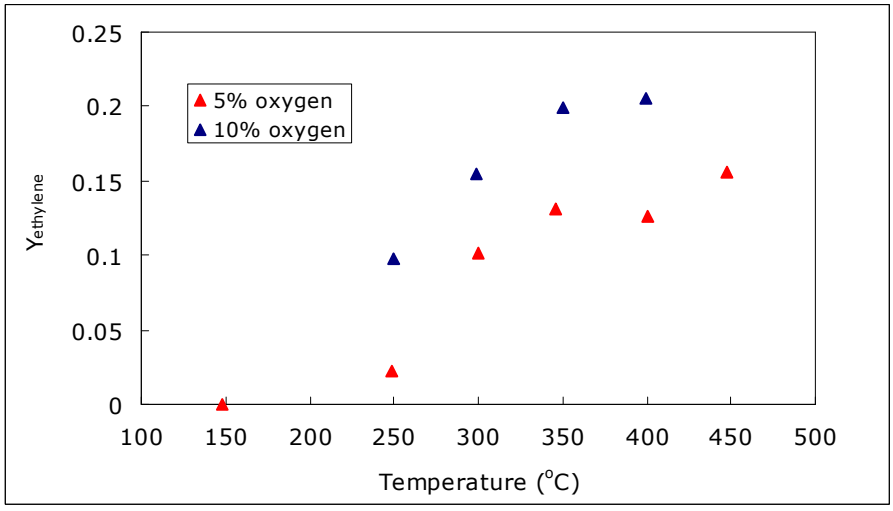

(c)

Figure 36. Comparison of **(a)** Total conversion-temperature data, **(b)** C_2H_4 selectivity-temperature data, **(c)** C_2H_4 yield-temperature data for Cr-O catalyst with 5% and 10% oxygen in feed (catalyst: 0.2 g Cr-O, O_2/C_2H_6 = ~0.17 and ~0.33, feed: 50 cm^3/min)

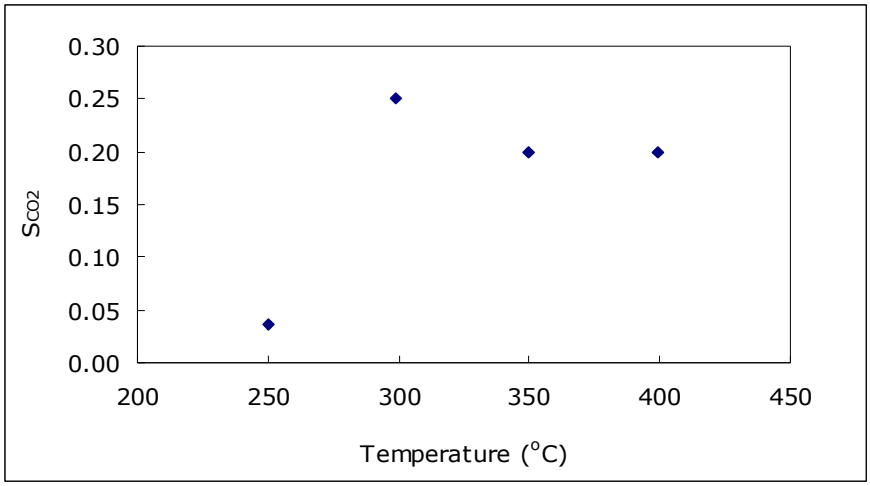

(a)

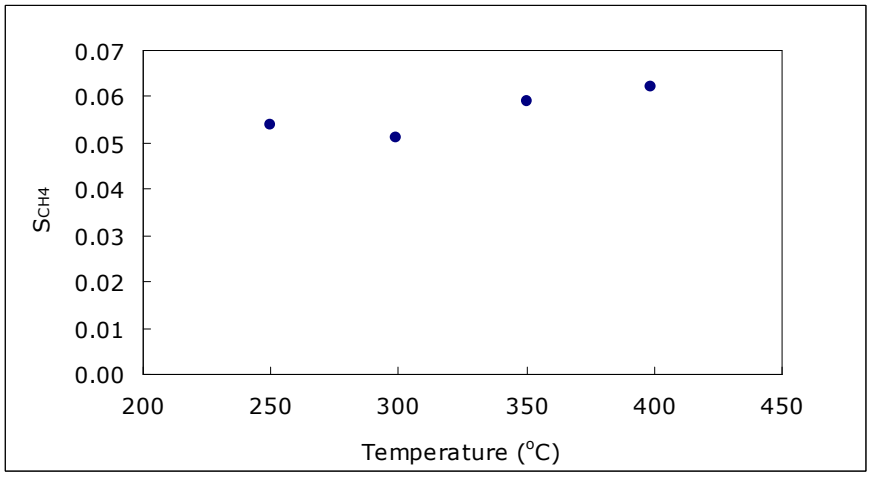

(b)

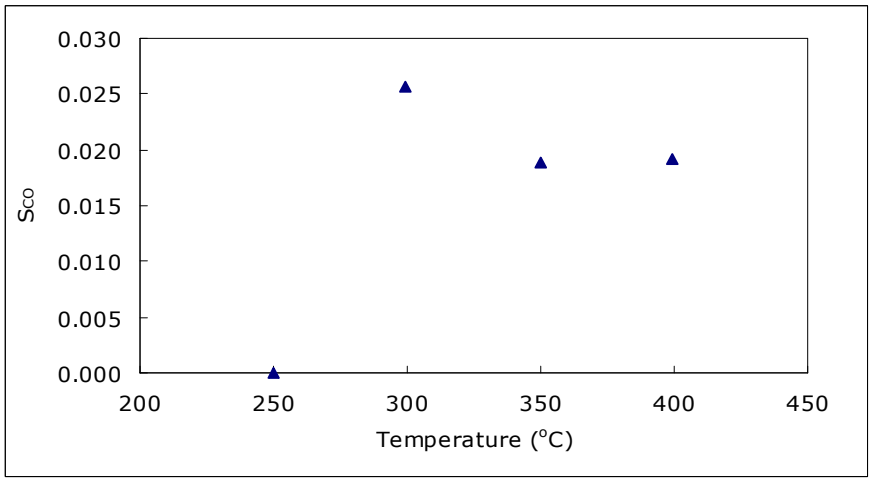

(c)

Figure 37. (a) CO_2 selectivity-temperature data, **(b)** CH_4 selectivity-temperature data, **(c)** CO selectivity-temperature data
(catalyst: 0.2 g Cr-O, O_2/C_2H_6 = ~0.33, feed: 50 cm^3/min)

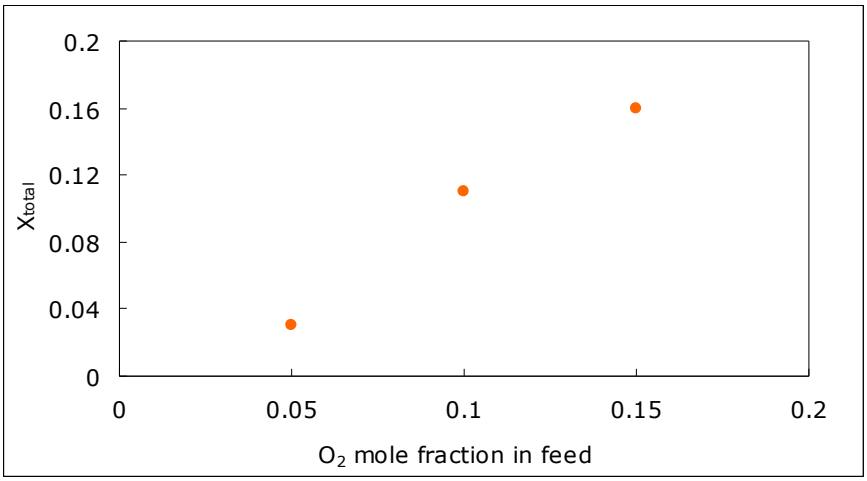

(a)

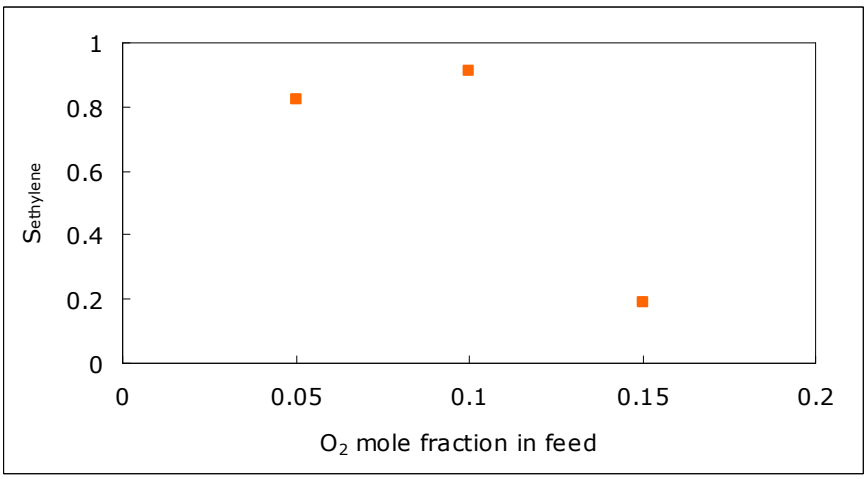

(b)

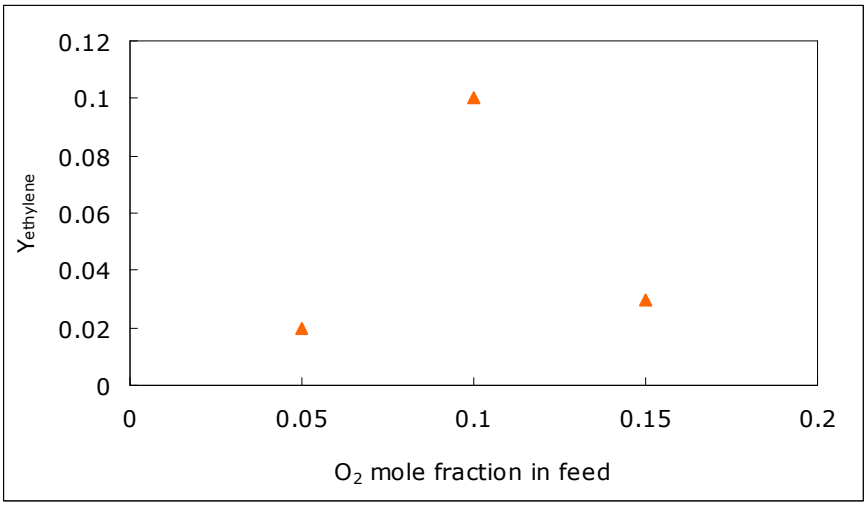

(c)

Figure 38. (a) Total conversion-O_2 mole fraction in feed data, **(b)** C_2H_4 selectivity-O_2 mole fraction in feed data, **(c)** C_2H_4 yield-O_2 mole fraction in feed data (catalyst: 0.2 g Cr-O, T=~250°C, feed: 50 cm^3/min)

3.2.2. Experiments with Cr-O Catalyst under CO_2-C_2H_6-He Flow

In addition to the experiments with O_2, ethane dehydrogenation with CO_2 was also tried with the Cr-O catalyst. These runs were performed with ~10% CO_2-30% C_2H_6 –60% He feed mixtures at a temperature range of 250-450°C. The variation of total conversion, selectivity to ethylene, and ethylene yield with temperature are given in Figures 39a-c, respectively. Total fractional conversion values of about 0.16 were obtained with ethylene selectivity values of ~0.93 at 300-450°C. The CH_4 selectivity – temperature data are presented in Figure 40. Above 300°C, selectivity to CH_4 values were about 0.07.

For the dehydrogenation of ethane with CO_2, the following reactions were proposed in the literature [2, 36]:

$$C_2H_6 \rightarrow C_2H_4 + H_2 \quad (5)$$

$$CO_2 + H_2 \rightarrow CO + H_2O \quad (6)$$

$$C_2H_6 + 2CO_2 \rightarrow 4CO + 3H_2 \quad (7)$$

$$C_2H_6 + H_2 \rightarrow 2CH_4 \quad (8)$$

No CO formation was seen through the experiments performed with CO_2. From the calculations made with the MS data, it was found that the CO_2 mole fraction did not change at the reactor outlet for 250-350°C. The C_2H_4 formed during these runs may be due to the simple dehydrogenation reaction (5).

According to the reaction mechanism proposed in our previous studies [3] for the oxidative dehydrogenation of ethane, 'ethane was considered to be dissociatively adsorbed on the catalyst surface with the elimination of a hydrogen atom' [3]. β-hydrogen elimination of this adsorbed ethyl species formed a vinyl species; desorption of which yielded ethylene. Formation of CH_4 was proposed through the formation of methyl species from adsorbed ethyl species. Such kind of reaction mechanism might also be proceeding here.

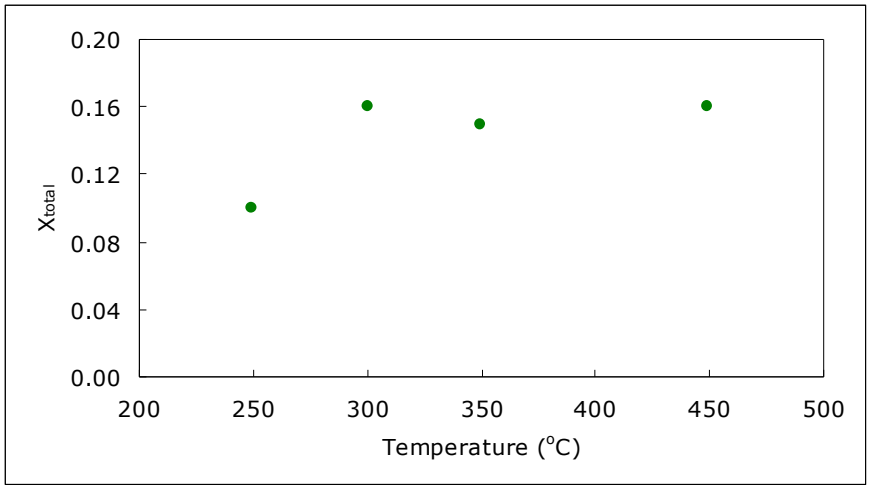

(a)

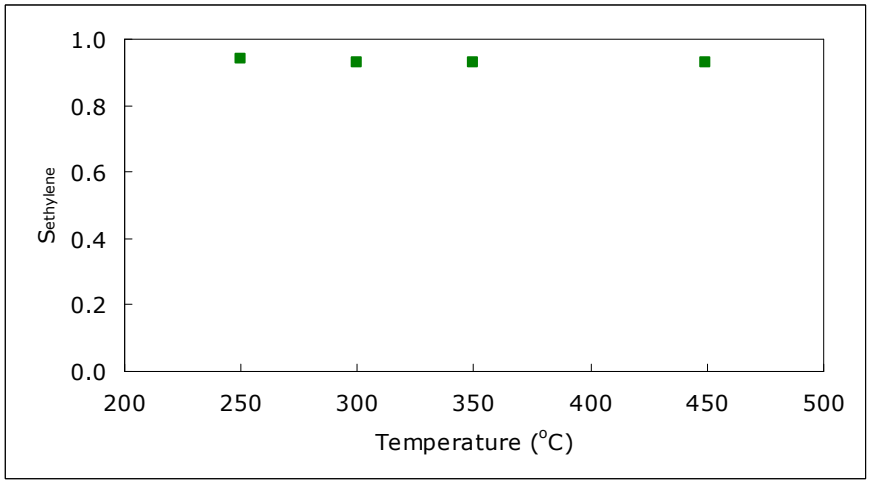

(b)

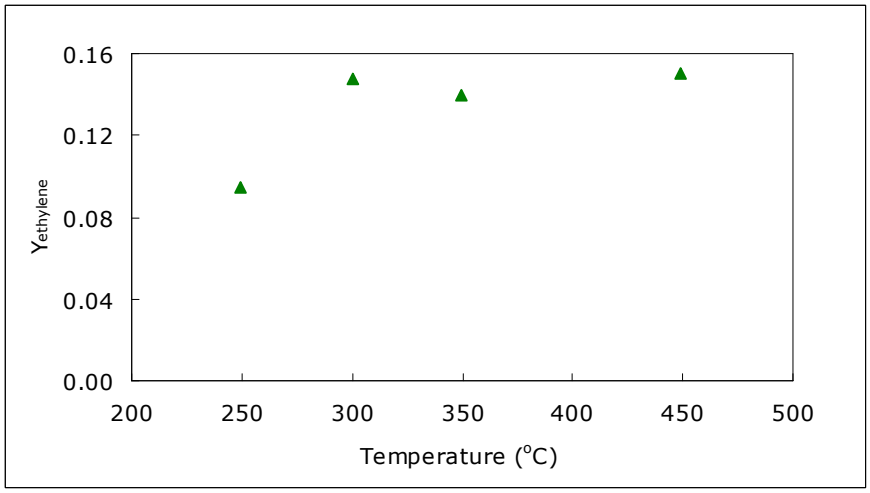

(c)

Figure 39. (a) Total conversion-temperature data, **(b)** C_2H_4 selectivity-temperature data, **(c)** C_2H_4 yield-temperature data
(catalyst: 0.2 g Cr-O, CO_2/C_2H_6 = ~0.33, feed: 50 cm^3/min)

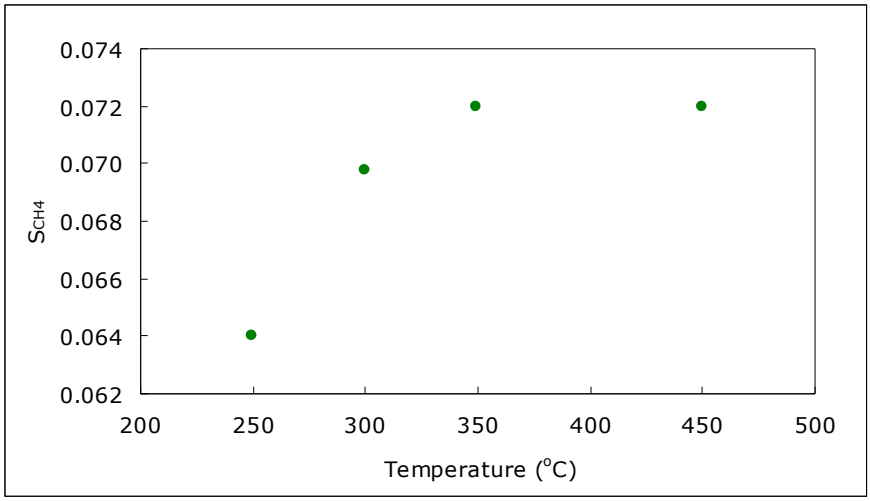

Figure 40. CH_4 selectivity-temperature data
(catalyst: 0.2 g Cr-O, CO_2/C_2H_6 = ~0.33, feed: 50 cm^3/min)

The comparison of the catalytic performance of Cr-O catalyst under feed containing 10% O_2 and 10% CO_2 is presented in Figure 41a-c. Above 250°C, the total conversion values were about 1.7 times higher in the experiments performed with 10% O_2 than 10% CO_2 (Figure 41a). Ethylene selectivities were higher in 10% CO_2 runs than the ones with 10% O_2 in the feed (Figure 41b).

3.2.3. Experiments with Cr-V-O Catalyst under O_2-C_2H_6-He Flow

The steady-state experiments which were performed with the Cr-O catalyst were also performed with the Cr-V-O catalyst. For a feed mixture containing an O_2/C_2H_6 feed ratio of ~0.17 (5% O_2, 30% C_2H_6 and 65% He), experiments were performed at a temperature range of 150-525°C. The variation of total conversion, selectivity to ethylene, and ethylene yield with temperature are presented in Figures 42a-c, respectively.

As it can be seen from Figure 42a and 42b, the total fractional conversion values were about 0.03 till 350°C with an average corresponding ethylene selectivity value of about 0.87. Increasing temperature further, caused an increase in the total ethane conversion values at the expense of selectivity to ethylene. The ethylene yield values reached up to 0.09 at 525°C (Figure 42c).

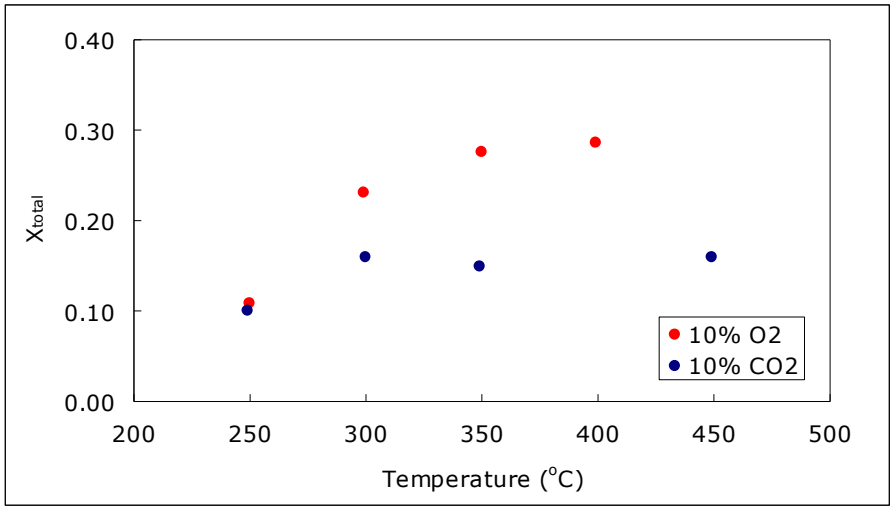

(a)

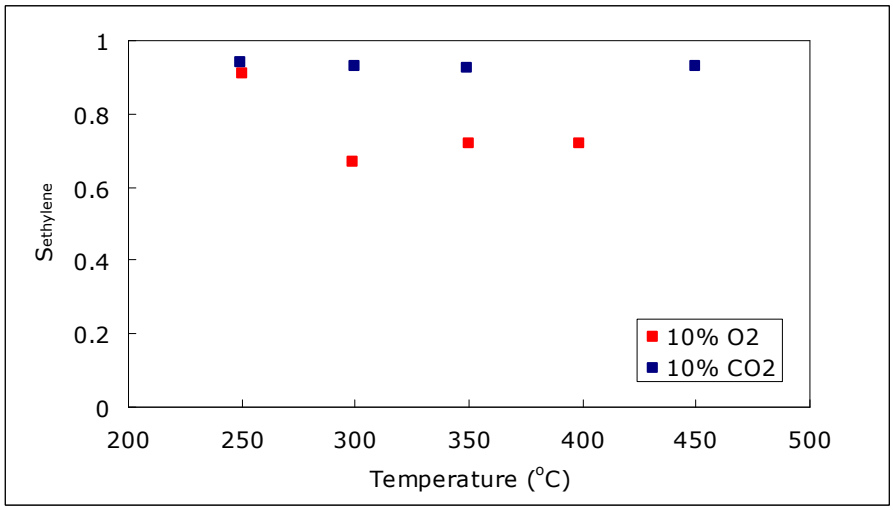

(b)

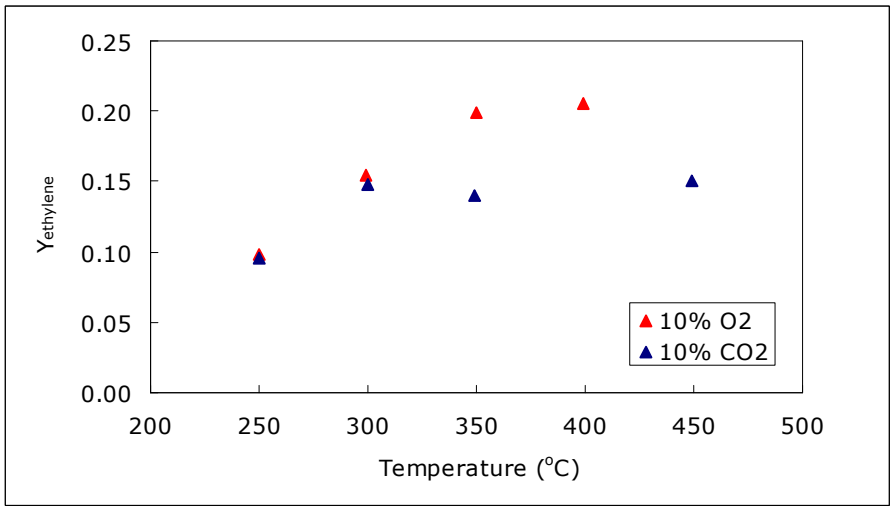

(c)

Figure 41. Comparison of **(a)** Total conversion-temperature data, **(b)** C_2H_4 selectivity-temperature data, **(c)** C_2H_4 yield-temperature data for Cr-O catalyst with 10% O_2 and 10% CO_2 in feed (catalyst: 0.2 g Cr-O, feed: 50 cm^3/min)

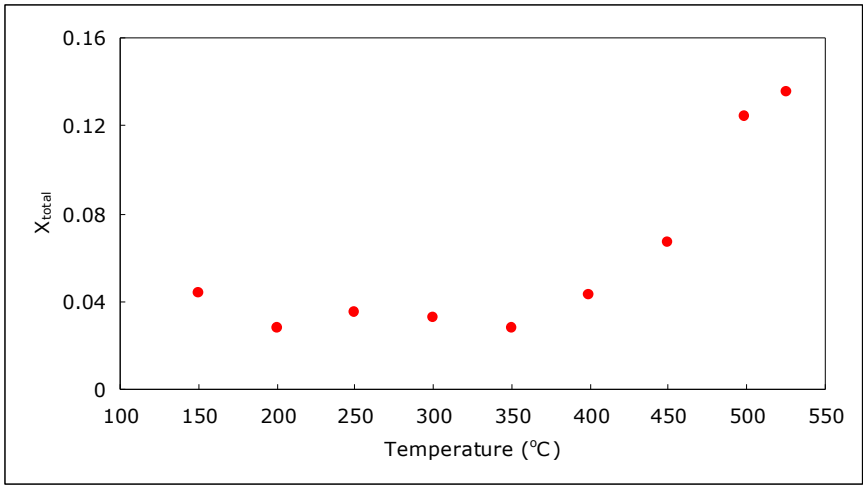

(a)

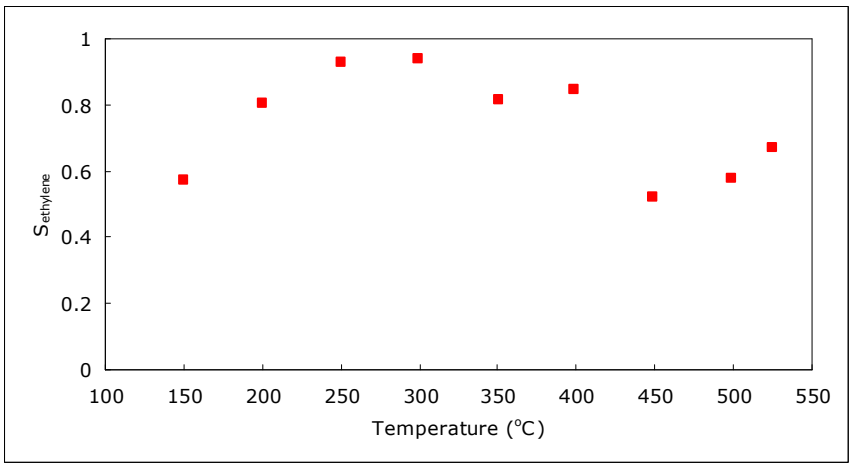

(b)

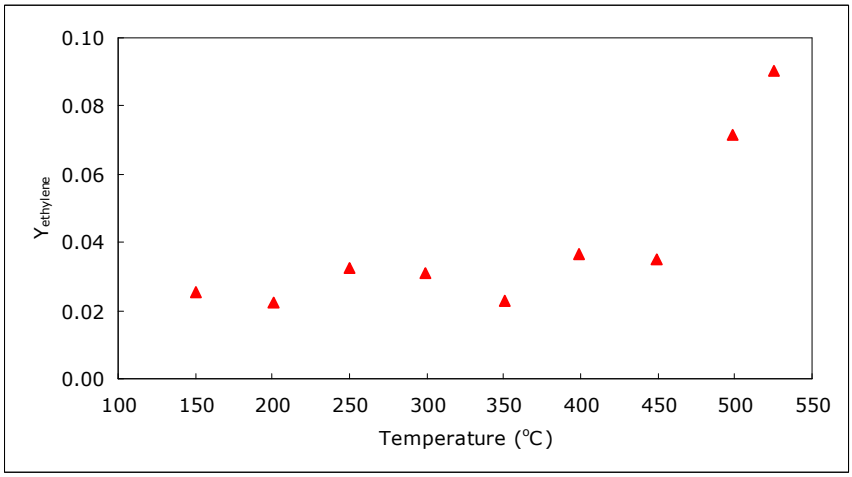

(c)

Figure 42. (a) Total conversion-temperature data,
(b) C_2H_4 selectivity-temperature data, **(c)** C_2H_4 yield-temperature data
(catalyst: 0.2 g Cr-V-O, O_2/C_2H_6 = ~0.17, feed: 50 cm^3/min)

The variations of selectivity to CO_2, CH_4 and CO with temperature are shown in Figures 43a-c, respectively. The formation of CO_2 increased with temperature and gave a maximum selectivity value of 0.07 at 525°C (Figure 43a). CO formation showed a fluctuating trend increasing above 400°C (Figure 43c) and CH_4 selectivities were around 0.023 with fluctuations through the temperature range studied (Figure 43b).

With increasing O_2 amount in the feed to 10%, experiments were performed for the temperature range of 151-497°C. The feed composition was 10% O_2, 30% C_2H_6 and 60% He (O_2/C_2H_6 = ~0.33). The corresponding results for the variation of total conversion, selectivity to ethylene, and ethylene yield with temperature are given in Figures 44a-c, respectively.

Increasing O_2 amount to 10% in the feed, enhanced total conversion. At 448°C, a fractional conversion value of 0.22 was obtained (Figure 44a). The ethylene selectivity values decreased above 400°C from values of about 0.95 to 0.6-0.5 (Figure 44b). Within the temperature range studied, a maximum ethylene yield value of 0.14 was obtained at 448°C (Figure 44c). Figure 45a-c depicts the comparison of total conversion, ethylene selectivity and yield for Cr-V-O catalyst under feed containing 5% and 10% O_2. Till 500°C, the selectivity values in the runs performed with 10% O_2 were higher than with 5% O_2 (Figure 45b). Higher ethylene yields were obtained with 10% O_2 feed composition (Figure 45c).

The variations of selectivity to CO_2, CH_4 and CO with temperature for an O_2/C_2H_6 feed ratio of ~0.33 are shown in Figures 46a-c, respectively. Similar to 5% O_2 percentage in feed, the CO_2 selectivity values showed an increasing trend with temperature (Figure 46a). The values for selectivity to CH_4 were around 0.03 (Figure 46b). CO formation was observed above 400°C (Figure 46c).

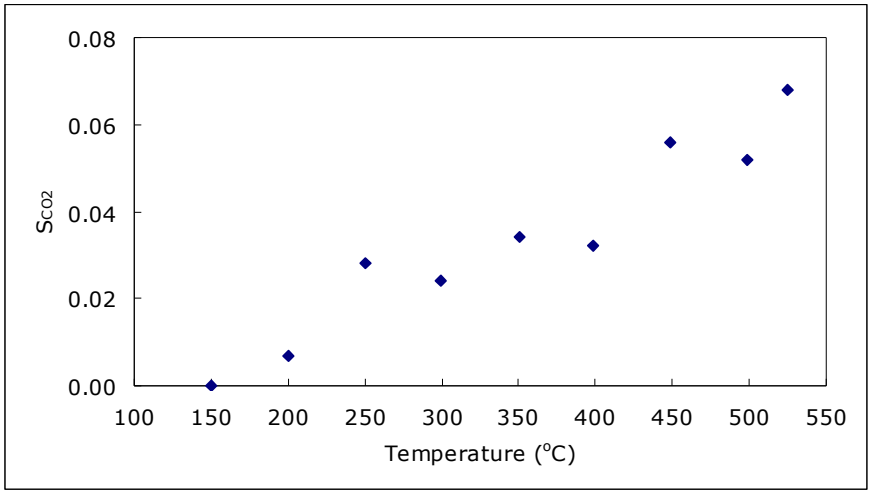

(a)

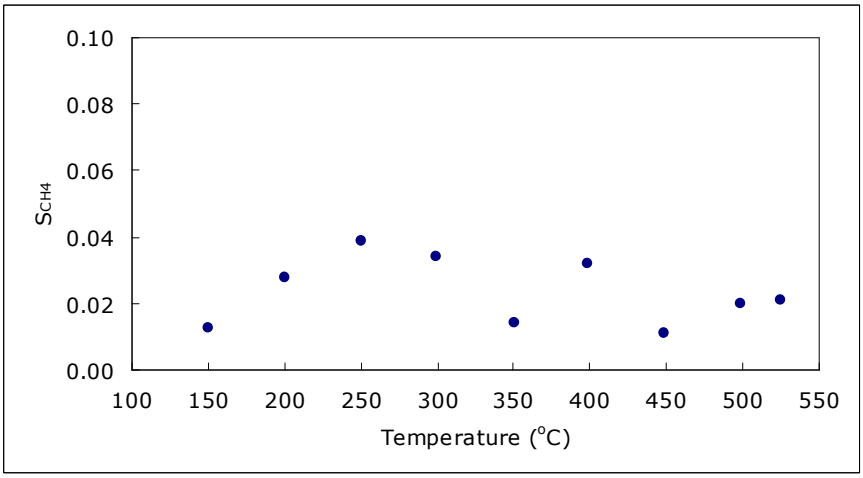

(b)

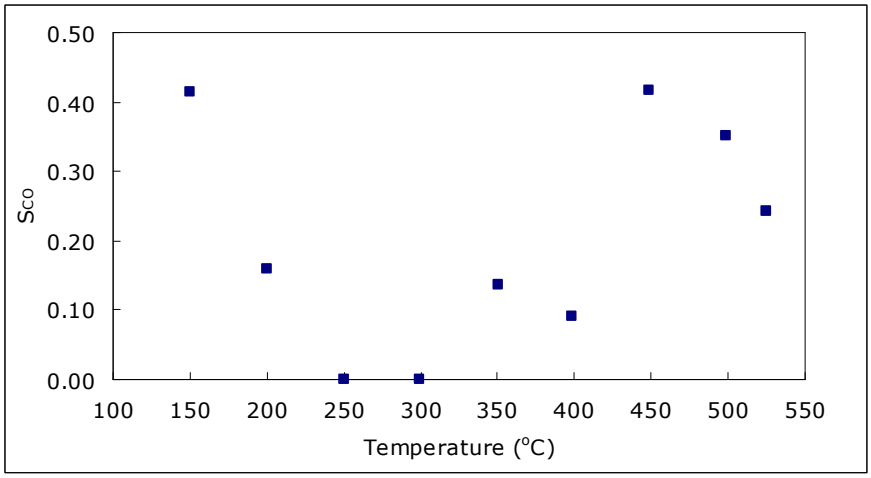

(c)

Figure 43. (a) CO_2 selectivity-temperature data,
(b) CH_4 selectivity-temperature data, **(c)** CO selectivity-temperature data
(catalyst: 0.2 g Cr-V-O, O_2/C_2H_6 = ~0.17, feed: 50 cm^3/min)

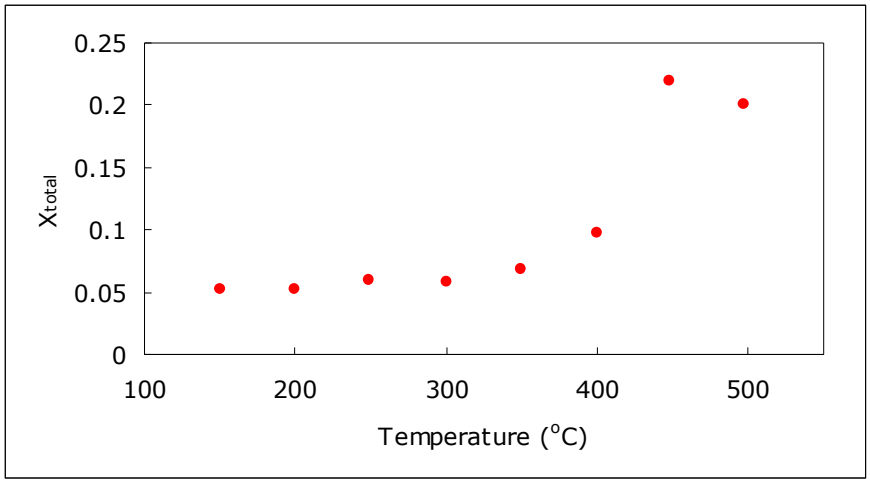

(a)

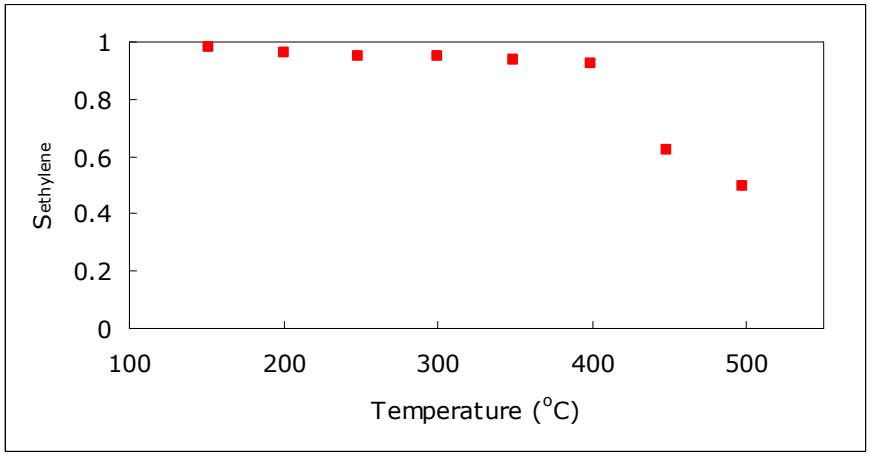

(b)

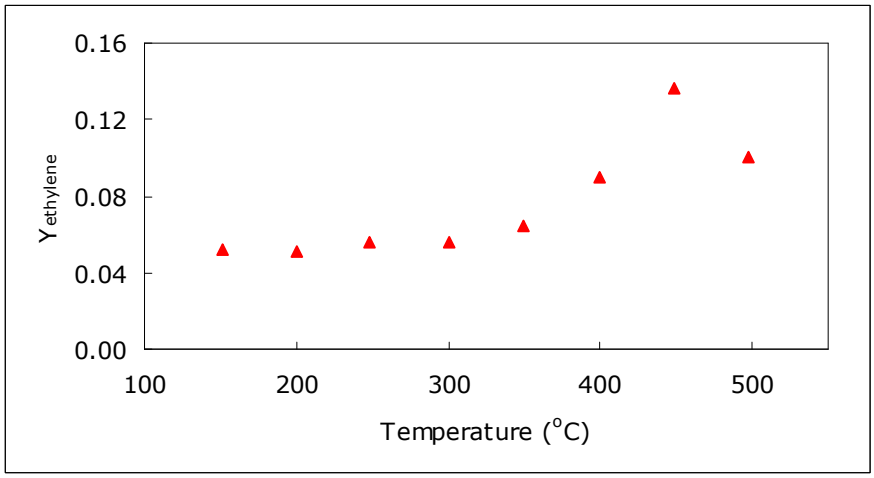

(c)

Figure 44. (a) Total conversion-temperature data,
(b) C_2H_4 selectivity-temperature data, **(c)** C_2H_4 yield-temperature data
(catalyst: 0.2 g Cr-V-O, O_2/C_2H_6 = ~0.33, feed: 50 cm^3/min)

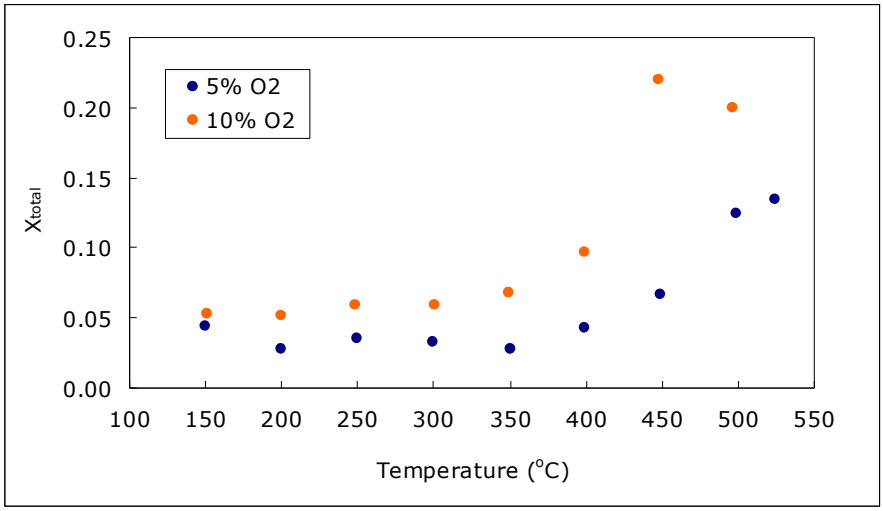

(a)

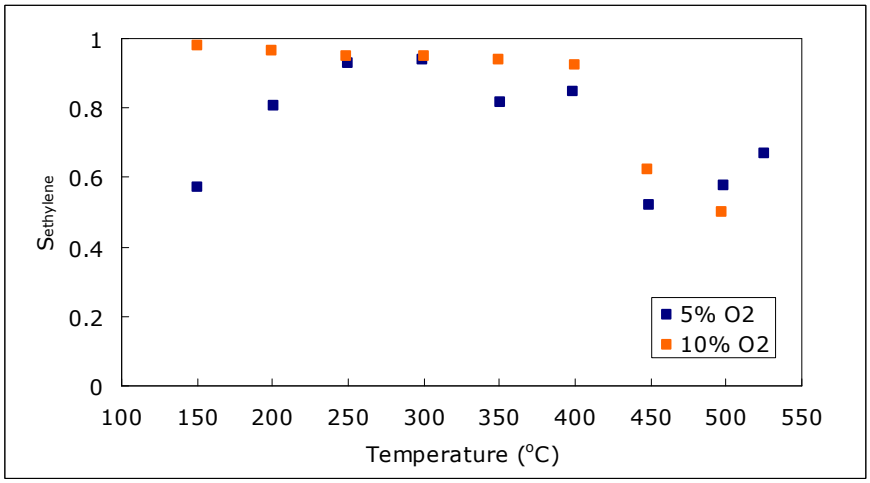

(b)

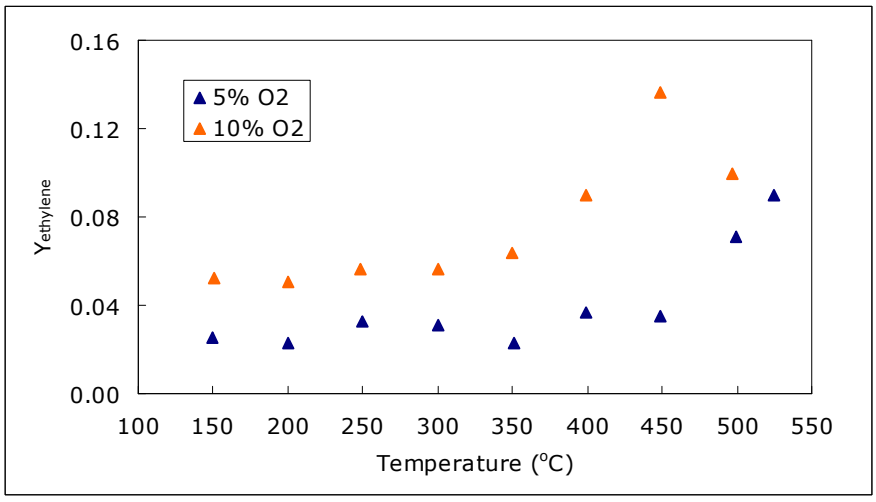

(c)

Figure 45. Comparison of **(a)** Total conversion-temperature data, **(b)** C_2H_4 selectivity-temperature data, **(c)** C_2H_4 yield-temperature data for Cr-V-O catalyst with 5% O_2 and 10% O_2 in feed (catalyst: 0.2 g Cr-V-O, feed: 50 cm^3/min)

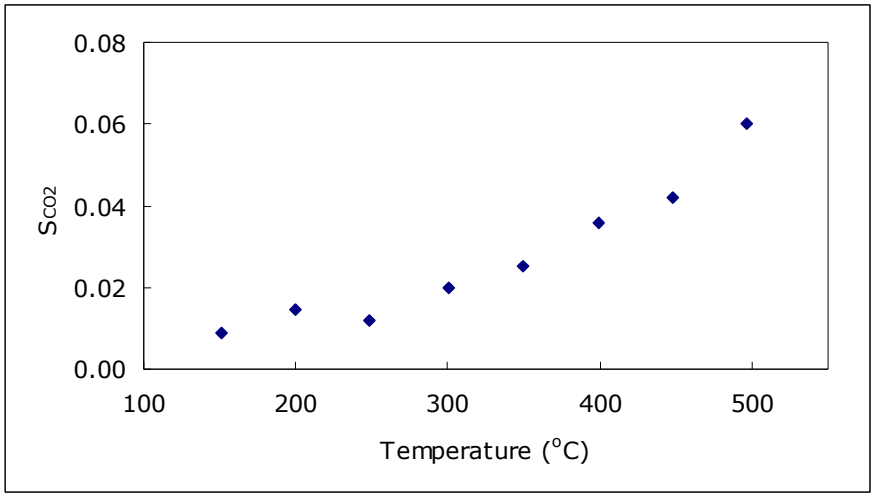

(a)

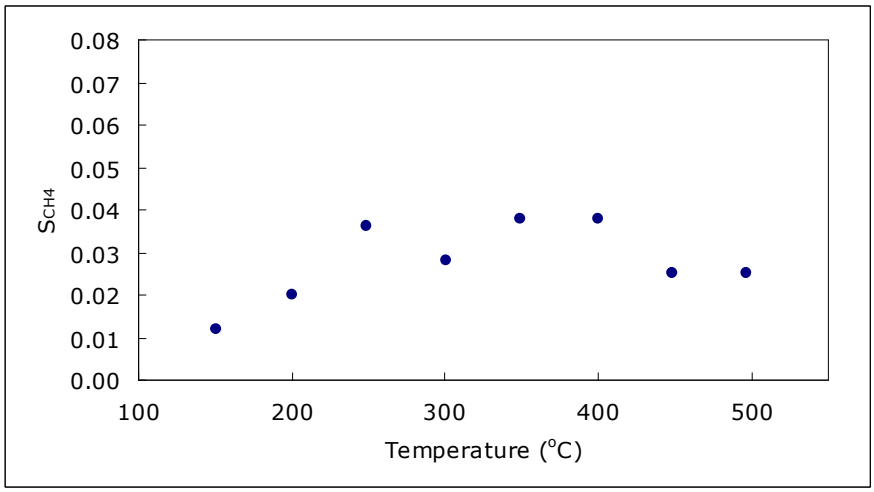

(b)

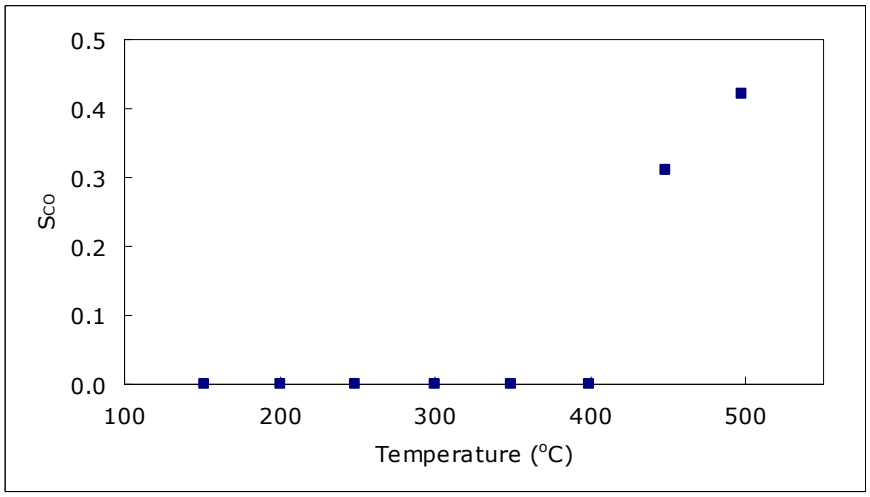

(c)

Figure 46. (a) CO_2 selectivity-temperature data,
(b) CH_4 selectivity-temperature data, **(c)** CO selectivity-temperature data
(catalyst: 0.2 g Cr-V-O, O_2/C_2H_6 = ~0.33, feed: 50 cm^3/min)

3.2.4. Experiments with Cr-V-O Catalyst under CO_2-C_2H_6-He Flow

Ethane oxidative dehydrogenation reaction was also carried out with the mild oxidant, CO_2 over the Cr-V-O catalyst. These runs were performed with feed mixtures containing 10% CO_2 and 45% CO_2 keeping C_2H_6 percentage constant at 30%.

With a total feed flow rate of 50 cm^3/min and a feed composition of 10% CO_2 - 30% C_2H_6 - 60% He, experiments were performed at the temperature range of 200-592°C. The results for these runs as the variation of total conversion, selectivity to ethylene, and ethylene yield with temperature are given in Figures 47a-c, respectively.

The total fractional conversion values were very low and at around 0.03 above 400°C (Figure 47a). Higher total conversion values were detected in the experiments with feed containing O_2. In the experiments done with the feed composition of 10% O_2 - 30% C_2H_6 - 60% He, a total conversion value of 0.22 was obtained at 448°C (Figure 44a) which is 5.5 times of the value observed by the feed with 10% CO_2 , i.e. 0.04 at 451°C (Figure 47a). The ethylene selectivity values were almost constant with an average value of 0.96 (Figure 47b). Similar to the experiments carried out with Cr-O catalyst, formation of CO was not detected also with Cr-V-O catalyst under CO_2 containing feed mixture. Figure 48 presents the CH_4 selectivity–temperature data. The average of the selectivity to CH_4 values was about 0.04 in the temperature range studied.

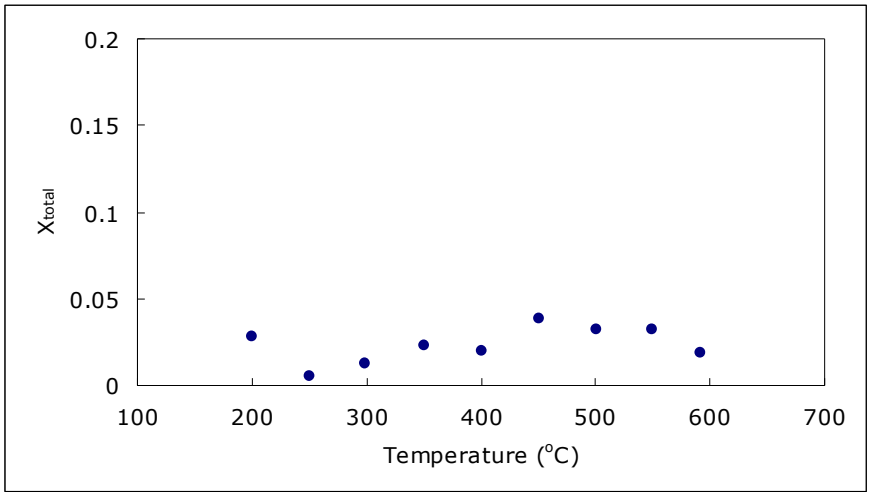

(a)

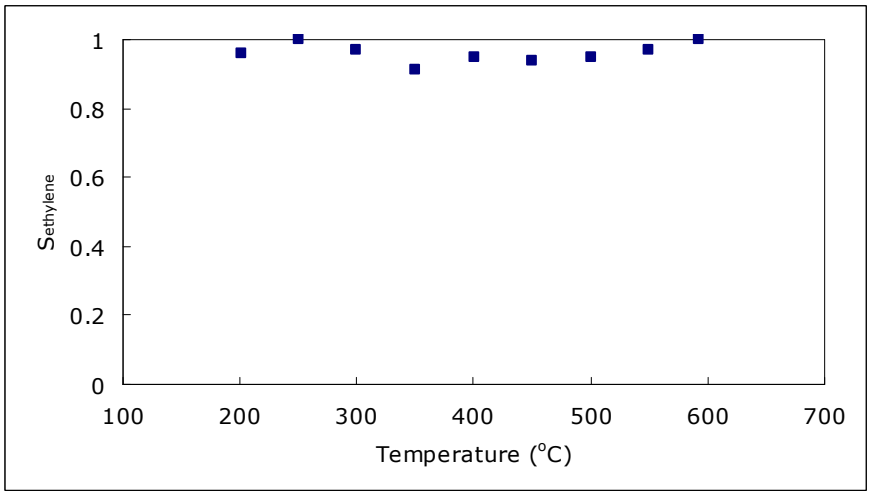

(b)

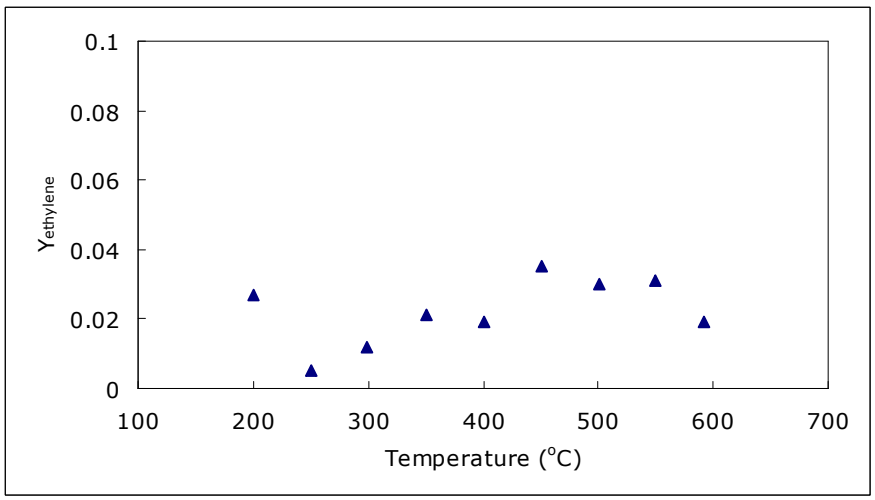

(c)

Figure 47. (a) Total conversion-temperature data, **(b)** C_2H_4 selectivity-temperature data, **(c)** C_2H_4 yield-temperature data
(catalyst: 0.2 g Cr-V-O, CO_2/C_2H_6 = ~0.33, feed: 50 cm^3/min)

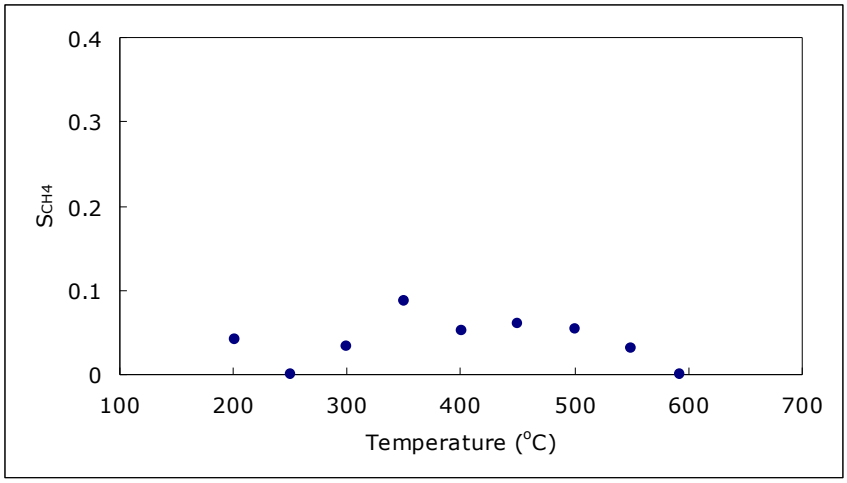

Figure 48. CH_4 selectivity-temperature data
(catalyst: 0.2 g Cr-V-O, CO_2/C_2H_6 = ~0.33, feed: 50 cm^3/min)

The variation of total conversion, selectivity to ethylene and yield values for Cr-V-O catalyst under feed with 10% O_2 and 10% CO_2 can be explicitly seen in Figure 49a-c. Although the total fractional conversion values were higher in the runs with O_2/C_2H_6 feed ratio of ~0.33; the ethylene selectivity values started to decrease above 400°C compared with CO_2 containing feed (i.e. CO_2/C_2H_6 = ~0.33).

With Cr-V-O catalyst, increasing CO_2 percentage in the feed to 45%, some more trials were made for the temperature range of 350-500°C. The total fractional conversion and ethylene yield values did not increase. The variation of total conversion, selectivity to ethylene, and ethylene yield with temperature are given in Figures 50a-c, respectively.

To summarize, over Cr-V-O catalyst, in the experiments performed by CO_2, higher and almost constant selectivity values (~0.96) were obtained compared with the runs in which O_2 was used as the gas phase oxidant (Figure 49b). However, the yield values obtained by feed consisting of CO_2 (0.04 at 451°C) were much lower than the ones reached by feed containing O_2 (0.14 at 448°C) (Figure49c). Therefore, within the experimental conditions utilized here, CO_2 was not good enough to act as a functional oxidant compared with O_2.

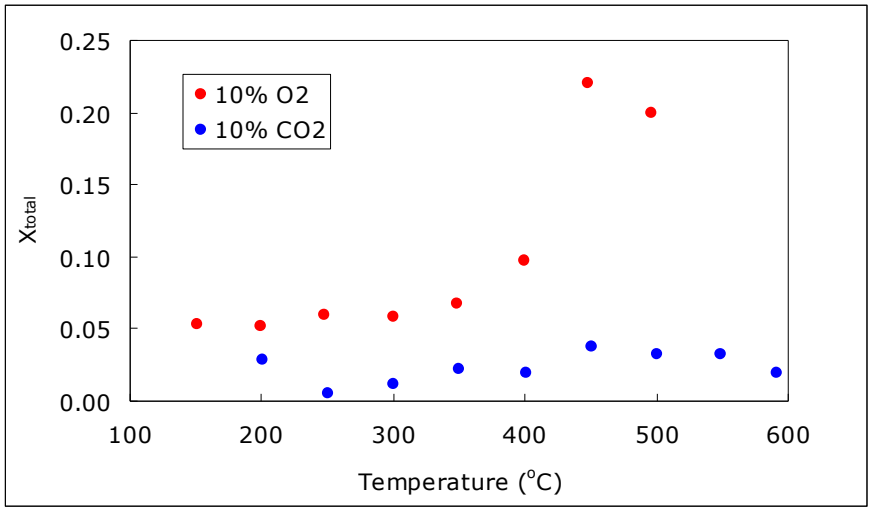

(a)

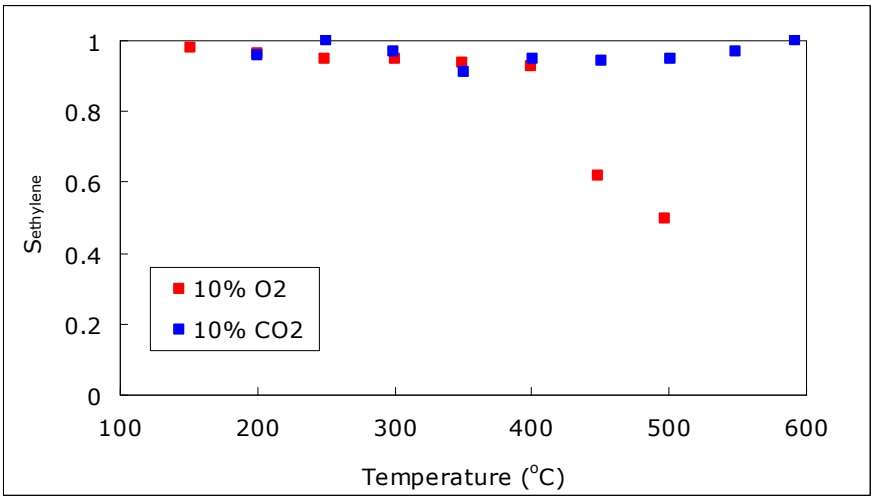

(b)

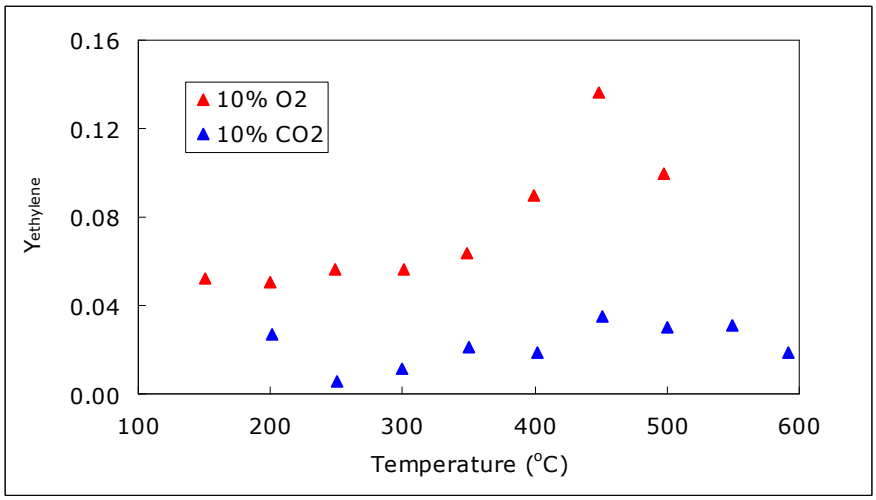

(c)

Figure 49. Comparison of **(a)** Total conversion-temperature data, **(b)** C_2H_4 selectivity-temperature data, **(c)** C_2H_4 yield-temperature data for Cr-V-O catalyst with 10% O_2 and 10% CO_2 in feed (catalyst: 0.2 g Cr-V-O, O_2/C_2H_6 and CO_2/C_2H_6=~0.33 feed:50 cm^3/min)

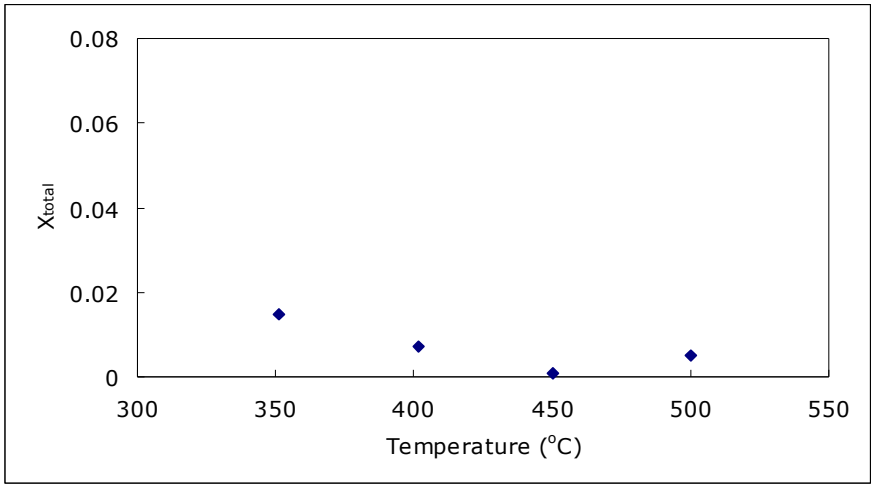

(a)

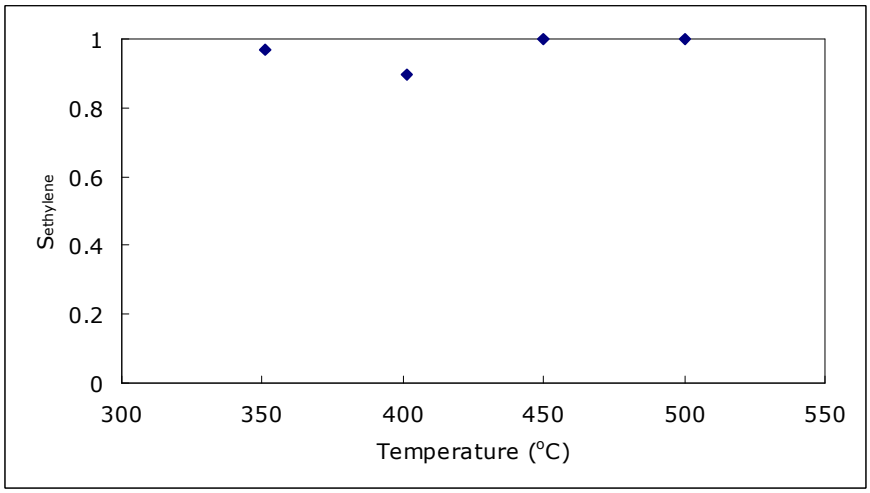

(b)

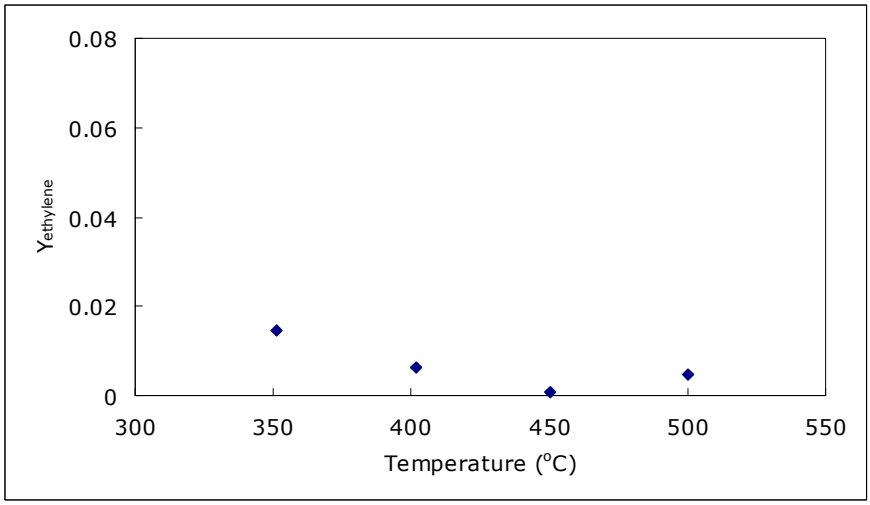

(c)

Figure 50. (a) Total conversion-temperature data, **(b)** C_2H_4 selectivity-temperature data, **(c)** C_2H_4 yield-temperature data
(catalyst: 0.2 g Cr-V-O, CO_2/C_2H_6 = ~1.5, feed: 50 cm^3/min)

3.2.5. Experiments with V-MCM-41 Catalyst under O_2-C_2H_6-He Flow

Vanadium containing mesoporous molecular sieves were studied for the oxidative dehydrogenation of alkanes [67-69]. In addition to Cr-O and Cr-V-O catalysts, V-MCM-41 catalyst was tried for the oxidative dehydrogenation of ethane reaction.

The experiments with 0.2 g V-MCM-41 were performed at the temperature range of 150-500°C. The feed mixture composed of ~5% O_2, 30% C_2H_6 and 65% He, that is, a O_2/C_2H_6 feed ratio of ~0.17. The graphs for total fractional conversion, selectivity to ethylene, and ethylene yield versus temperature are given in Figures 51a-c, respectively.

The total conversion was almost constant in the range of 200-350°C at the value of 0.02 and started to increase at 400°C. At ~500°C, a conversion value of 0.03 was reached (Figure 51a). Selectivity to ethylene increased with temperature and gave a maximum value of 0.81 at ~500°C (Figure 51b). CO_2 selectivity values were below 0.1 till 400°C (Figure 52a). Formation of CO decreased with increasing temperature (Figure 52b). Formation CH_4 was not observed in the experiments performed by V-MCM-41 catalyst.

The low conversion and selectivity values of this catalyst are probably due to the high V/Si ratio of it; i.e. 0.16. High vanadium content catalysts were reported to give low selectivity values for oxidative dehydrogenation of ethane to ethene [67, 68]. Besides, the synthesis method of V-MCM-41 was considered to be effective in its catalytic performance. Direct hydrothermal method (which was used for this catalyst [62]) led to poor selectivity for ethane oxidative dehydrogenation compared to template-ion exchange method [67].

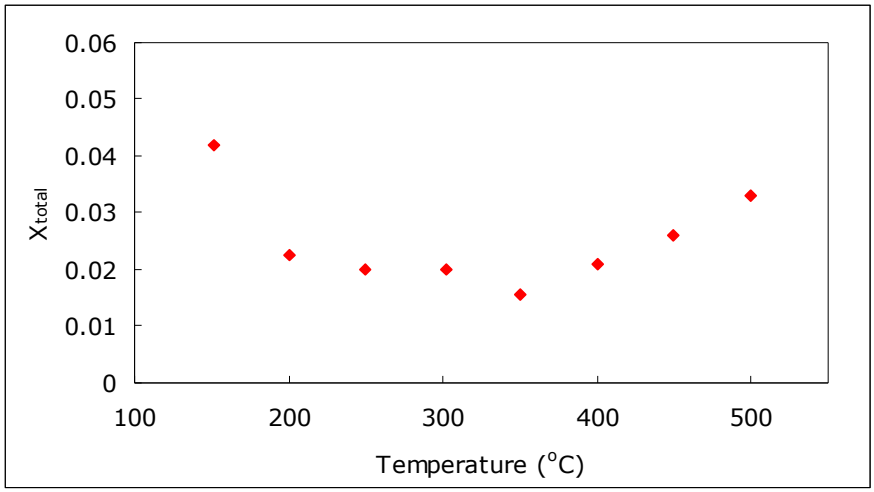

(a)

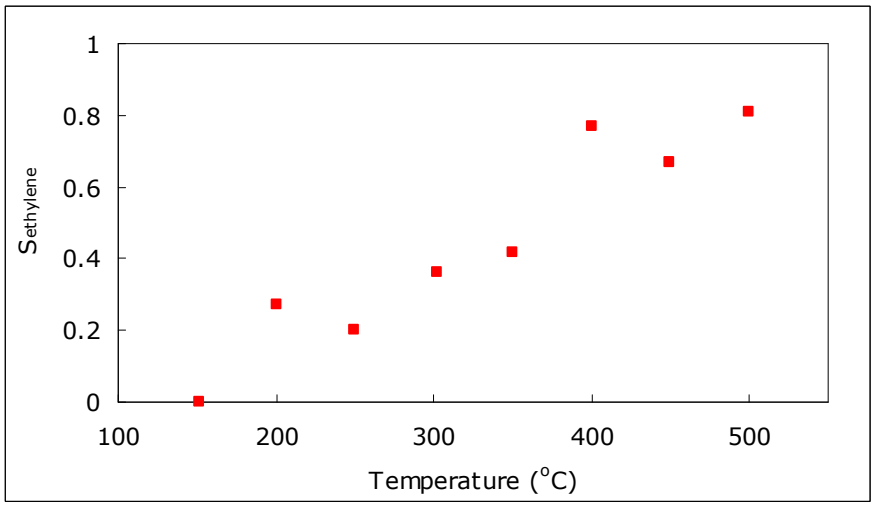

(b)

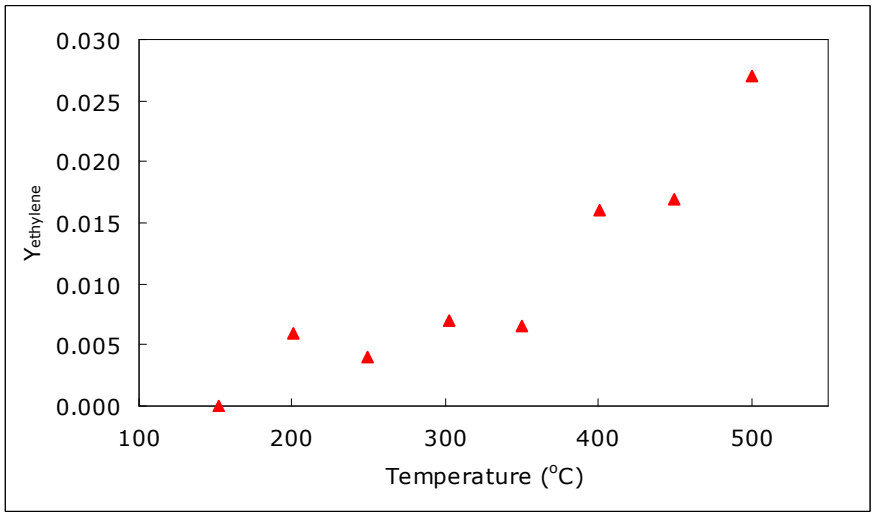

(c)

Figure 51. (a) Total conversion-temperature data, **(b)** C_2H_4 selectivity-temperature data, **(c)** C_2H_4 yield-temperature data (catalyst: 0.2 g V-MCM-41, O_2/C_2H_6 = ~0.17, feed: 50 cm^3/min)

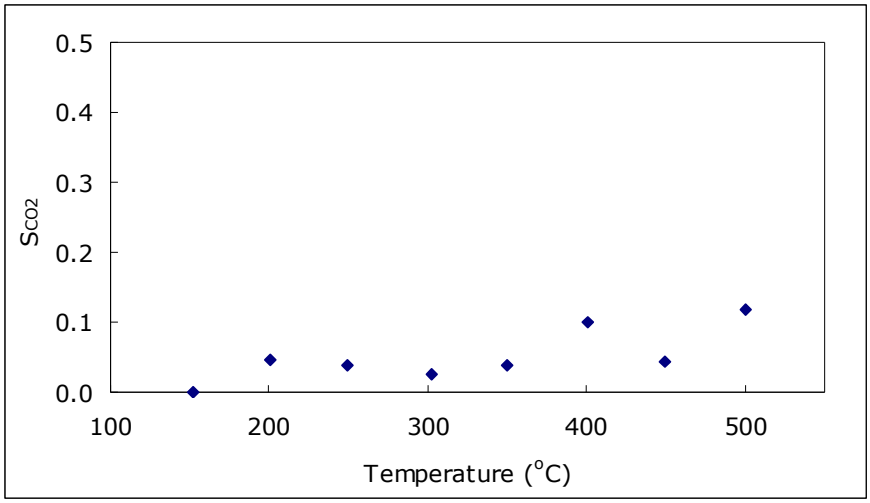

(a)

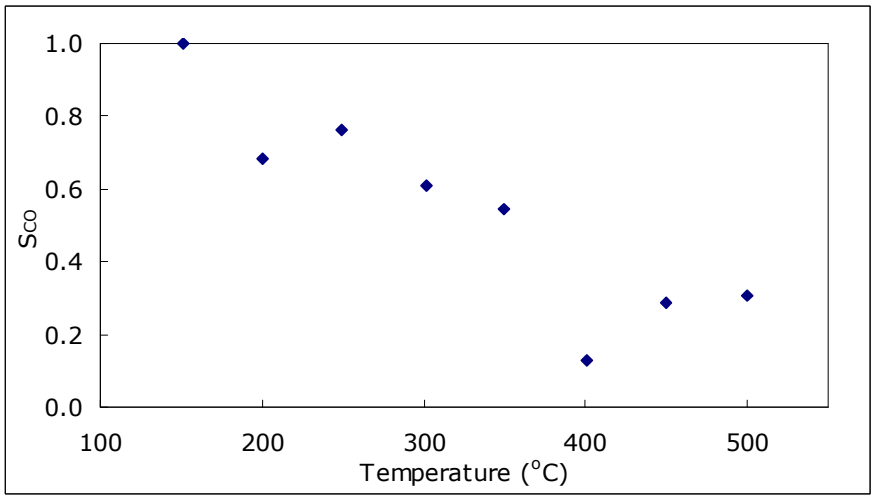

(b)

Figure 52. (a) CO_2 selectivity-temperature data, **(b)** CO selectivity-temperature data (catalyst: 0.2 g V-MCM-41, O_2/C_2H_6 = ~0.17, feed: 50 cm^3/min)

3.2.6. Comparison of Catalysts

3.2.6.1. Cr-O and Cr-V-O Catalysts

The comparison of the catalytic performance of Cr-O and Cr-V-O catalysts for the oxidative dehydrogenation of ethane reaction with feed composition of 10% O_2-30% C_2H_6-60% He is presented in Figure 53a-c. The Cr-O catalyst was more active with total conversion values higher than that of Cr-V-O in the temperature range of 250-400°C (Figure 53a). Higher ethylene yields were observed over Cr-O compared to Cr-V-O with the feed containing an O_2/C_2H_6 ratio of ~0.33 (Figure 53c).

In Figure 54a-c, the variation of total conversion, selectivity to ethylene and ethylene yield values for Cr-O and Cr-V-O catalysts with 10% CO_2-30% C_2H_6-60% He are shown. Similar to the results with O_2, higher conversions and yields were obtained with Cr-O than with Cr-V-O (Figure 54a and 54c). The selectivities with both catalysts were quite high and close to each other in the temperature range of 250-450°C, i.e. over 0.90 (Figure 54b).

3.2.6.2. Cr-O, Cr-V-O, and V-MCM-41 Catalysts

The Cr-O, Cr-V-O, and V-MCM-41 catalysts are compared in Figure 55a-c for their total conversion, selectivity, and yield variations with 5% O_2-30% C_2H_6-65%He feed. Above 300°C, Cr-O catalyst showed the highest total conversion values among the catalysts with a maximum of about 0.20 at 447°C (Figure 55a). Within 250-450°C, ethylene selectivity values were about 0.8 and 0.9 for Cr-O and Cr-V-O catalysts, respectively. The selectivity with V-MCM-41 reached to 0.8 with increasing temperature to 500°C (Figure 55b). Consequently, higher yield values were reached by the Cr-O catalyst (Figure 55c). At 447°C, over Cr-O, a yield value of 0.16 was obtained (Figure 55c) with an ethylene selectivity of 0.82 (Figure 55b) for the O_2/C_2H_6 feed ratio of ~0.17.

By increasing the catalyst amount and consequently the space time, it can be possible to increase the obtained conversion values. Usage of a different kind of reactor, such as membrane, can be another way to enhance yield. Or, by feeding small amounts of O_2 along the reactor, conversion can be increased and selectivity values can be held at high levels.

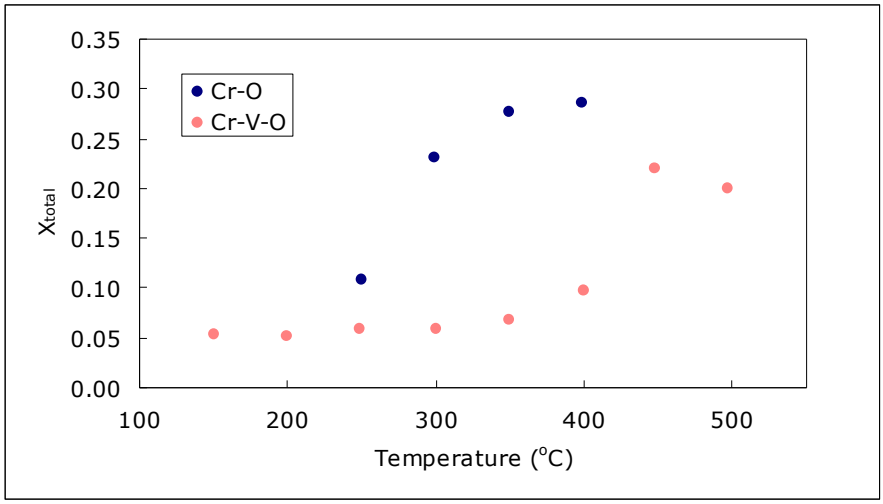

(a)

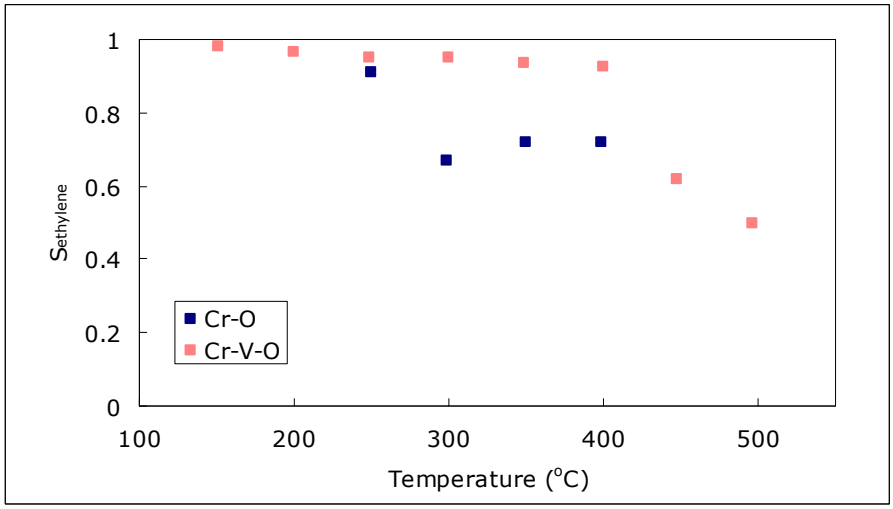

(b)

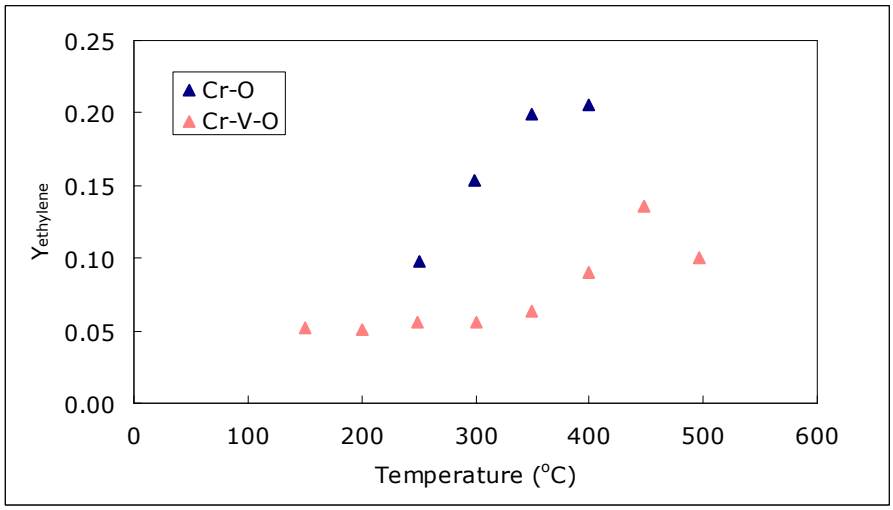

(c)

Figure 53. Comparison of **(a)** Total conversion-temperature data, **(b)** C_2H_4 selectivity-temperature data, **(c)** C_2H_4 yield-temperature data for Cr-O and Cr-V-O catalysts with 10% O_2 feed (catalyst: 0.2 g, O_2/C_2H_6=~0.33, feed:50 cm^3/min)

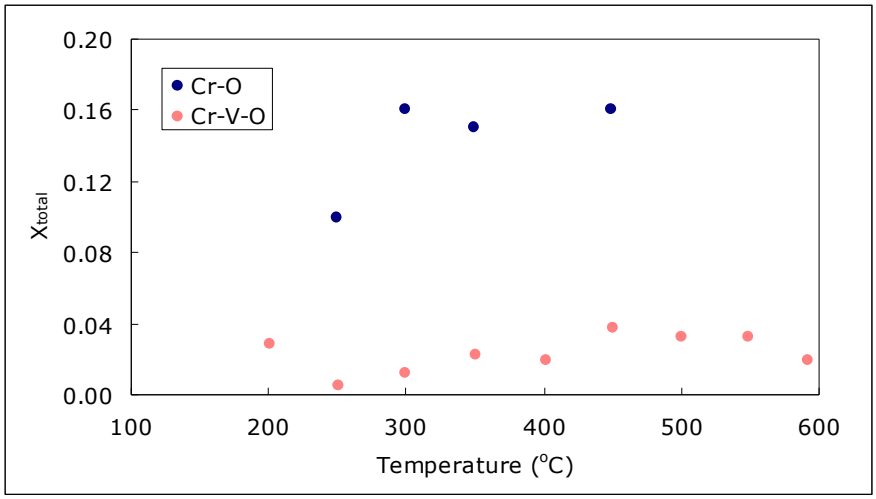

(a)

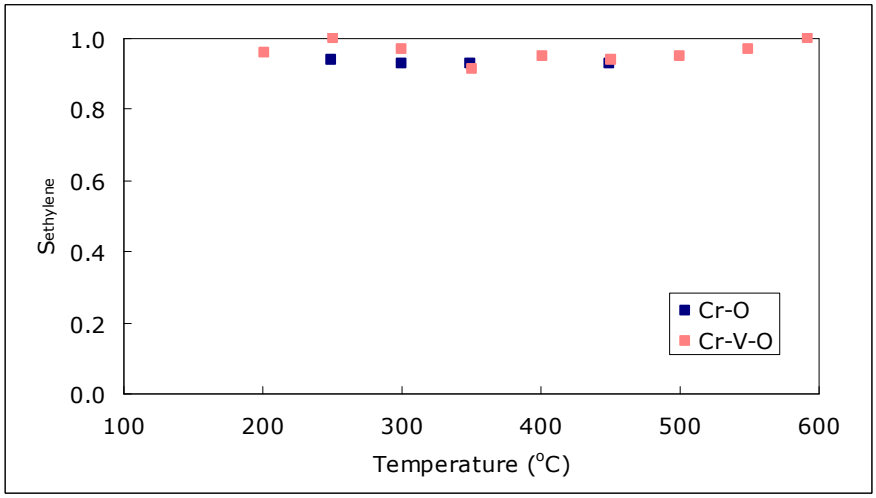

(b)

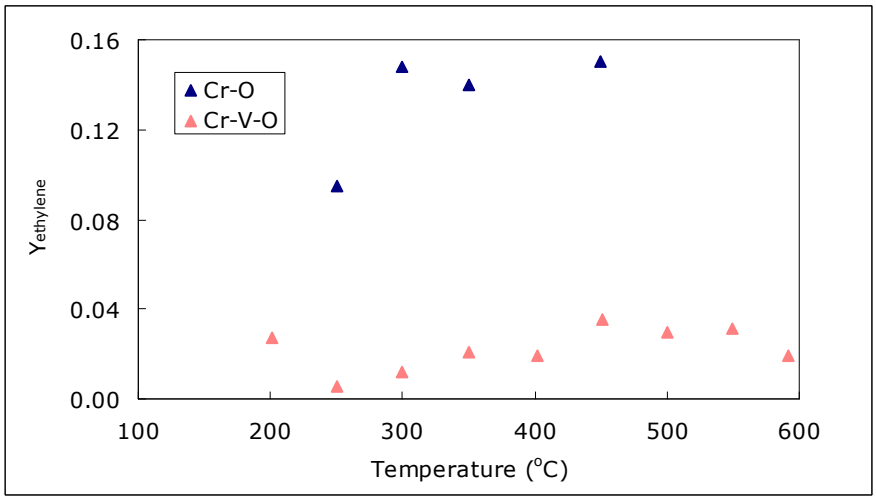

(c)

Figure 54. Comparison of **(a)** Total conversion-temperature data, **(b)** C_2H_4 selectivity-temperature data, **(c)** C_2H_4 yield-temperature data for Cr-O and Cr-V-O catalysts with 10% CO_2 feed (catalyst: 0.2 g, CO_2/C_2H_6=~0.33, feed: 50 cm^3/min)

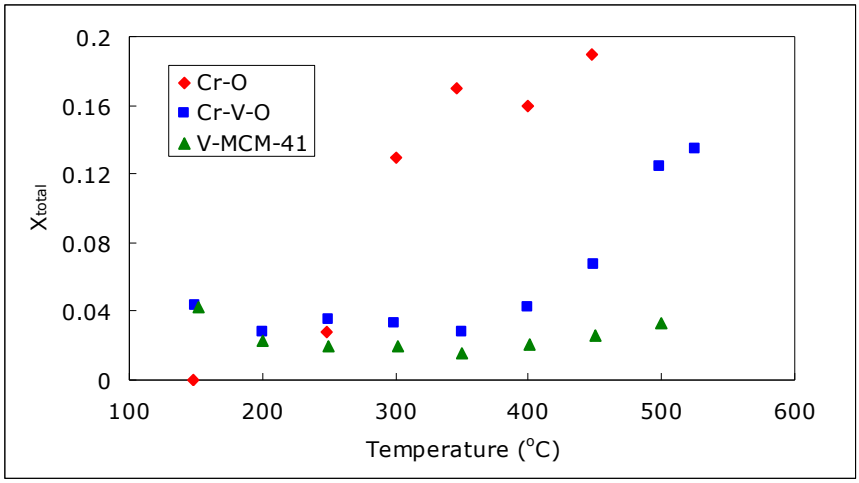

(a)

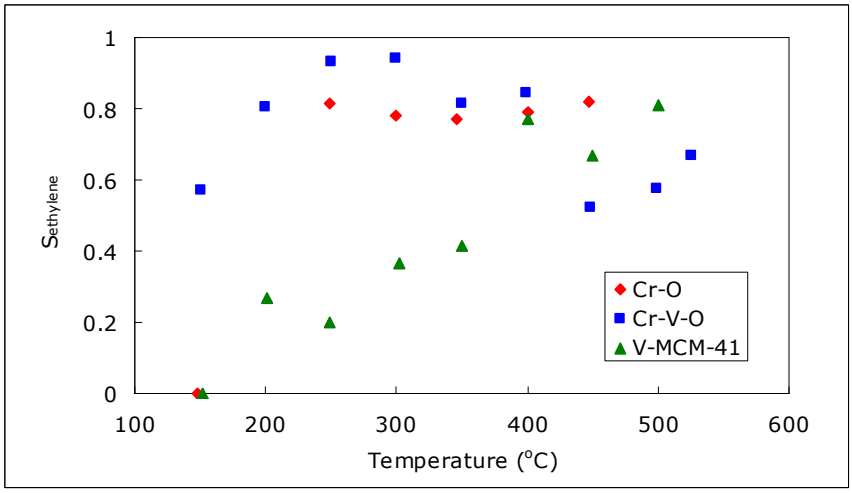

(b)

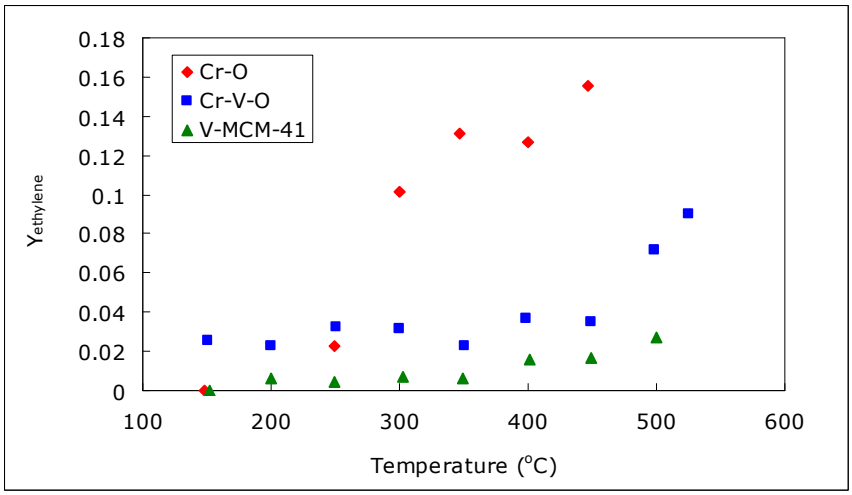

(c)

Figure 55. Comparison of **(a)** Total conversion-temperature data, **(b)** C_2H_4 selectivity-temperature data, **(c)** C_2H_4 yield-temperature data for Cr-O, Cr-V-O, and V-MCM-41 catalysts with 5% O_2-30%C_2H_6-65% He feed (catalyst: 0.2 g, O_2/C_2H_6=~0.17, feed:50 cm^3/min)

3.3. Dynamic Experiments

Various pulse-response experiments were performed with the Cr-O and Cr-V-O catalysts. Within these runs, pulses of C_2H_6 to O_2 and He flow, C_2H_6 to only He flow, and O_2 to C_2H_6 and He flow were carried out. The responses of these pulses and the formation of the instant products were observed through the mass spectrometer analysis. The multi-responses obtained by the single-pulse were analysed for their moments, mean residence times, and variances.

3.3.1. Dynamic Experiments with Cr-O Catalyst

15-second four or five pulses of C_2H_6 with about 10 min. intervals were given to O_2 and He flow at temperatures of 350, 401, and 450°C over Cr-O catalyst. The flowing gas for these experiments was at a total flow rate of about 45 ml/min containing 94% He and 6% O_2. The figures for response data of the pulses at 350°C, 401, and 450°C for C_2H_6, C_2H_4, H_2O, CO_2, CH_4, H_2, O_2, and He are presented in Appendix D.1.1, D.1.2, and D.1.3, respectively.

Formation of C_2H_4, H_2O, CO_2, and trace amounts of H_2 and CH_4 were detected in these runs (Figures D.1.1 to D.1.4 for 350°C, Figures D.1.7 to D.1.10 for 401°C, and Figures D.1.13 to D.1.17 for 450°C). The ethane response curves of these pulses had a tail denoting that some of ethane was adsorbed on the catalyst and reached to the mass spectrometer after desorption. An example for this is shown in Figure 56 for 'pulse 3' of C_2H_6 pulses into O_2 and He flow over Cr-O catalyst at 401°C.

The ethylene peaks were composed of two different parts; a bigger first part followed by a smaller piece. The separation of these two was more significant in some runs. Figure 57 presents the ethylene peak for 3rd pulse of C_2H_6 pulses into O_2-He flow over Cr-O catalyst at 401°C. The second part of the ethylene peak can be due to the reaction of the adsorbed ethane. The variation of average mean residence times of given pulses for ethane and the two curves of ethylene at 350, 401, and 450°C are given in Table 8.

The decrease in O_2 peak showed both its usage in the reactions and the composition change. He depletion was due to variation of gas composition.

Table 8. Average mean residence times of C_2H_6 and C_2H_4 for pulses of C_2H_6 into He and O_2 flow over Cr-O catalyst

	C_2H_6	**C_2H_4**	
T (°C)	t_m (sec)	t_{m1} (sec)	t_{m2} (sec)
350	37	33.2	59.9
401	36.3	32.6	61.7
450	36.2	32.3	61.8

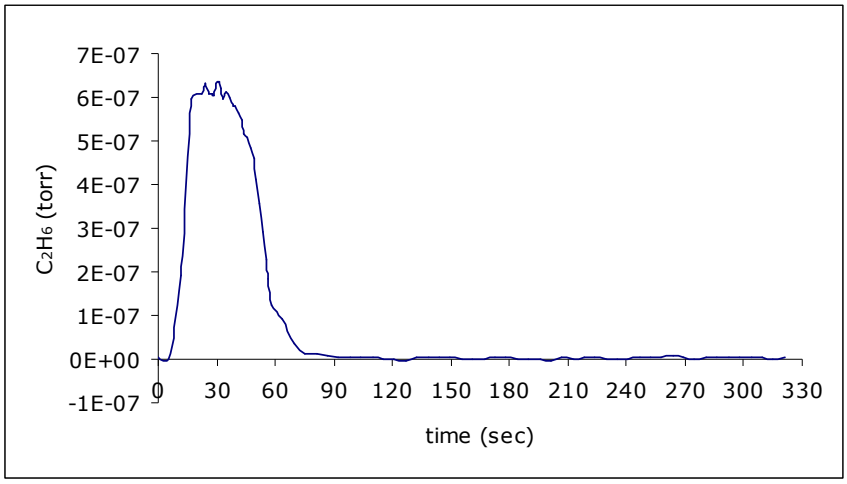

Figure 56. 'Pulse 3' C_2H_6 response data for C_2H_6 pulses into O_2 and He flow over Cr-O catalyst at 401°C

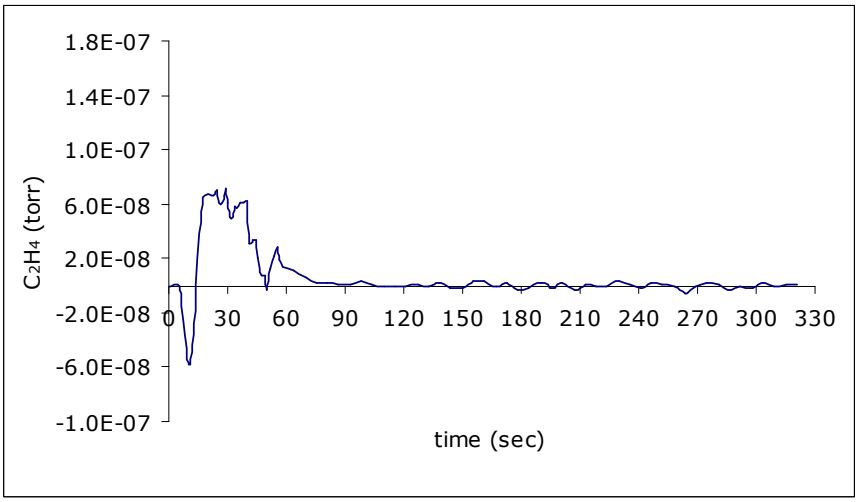

Figure 57. 'Pulse 3' C_2H_4 response data for C_2H_6 pulses into O_2 and He flow over Cr-O catalyst at 401°C

The most interesting observation of these runs was the two distinct peaks of CO_2 and H_2O. Examples of these peaks can be seen in Figures 58 and 59. At first sight, these peaks suggested the occurrence of either two reaction sites on the Cr-O catalyst or the presence of two reaction pathways for the formation of CO_2 and H_2O. The long tail of H_2O was the indication of its strong adsorption on the catalyst surface.

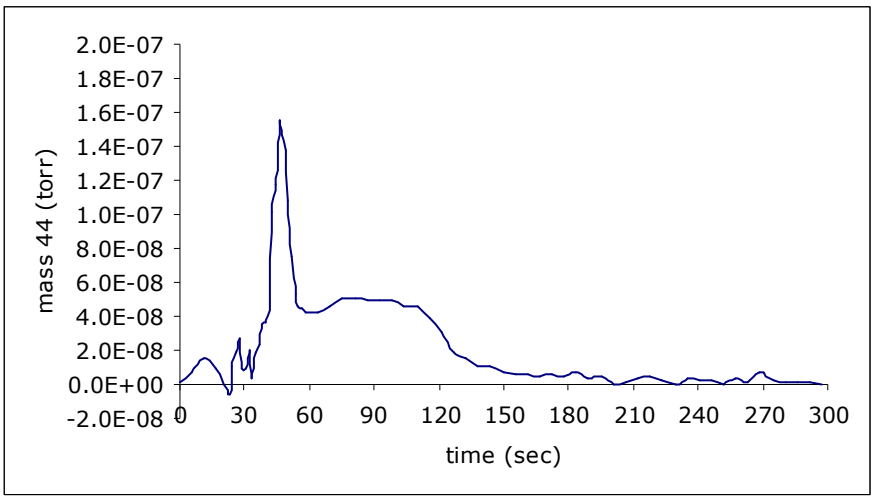

Figure 58. 'Pulse 4' CO_2 response data for C_2H_6 pulses into O_2 and He flow over Cr-O catalyst at 350°C

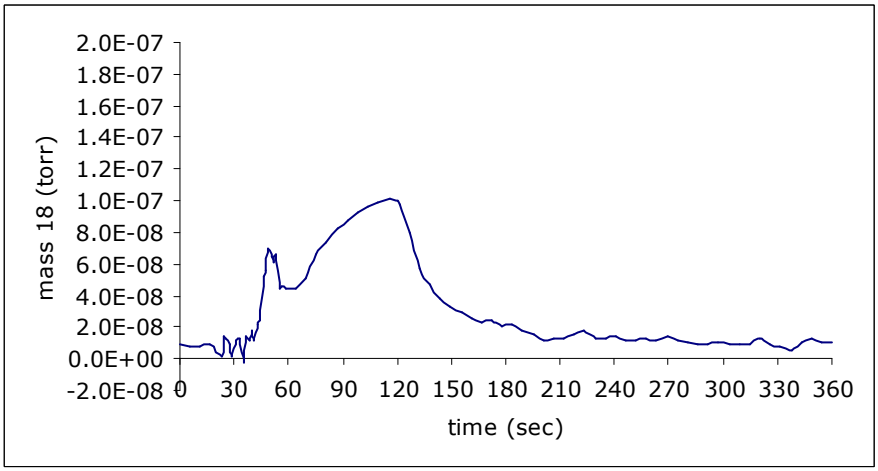

Figure 59. 'Pulse 4' H_2O response data for C_2H_6 pulses into O_2 and He flow over Cr-O catalyst at 350°C

To identify the distributions, zeroth and first moments, mean residence times, variances, and standard deviations were calculated for C_2H_6, C_2H_4, CO_2, and H_2O. Tabulated data for these values are given in Appendix D, Tables D.1-D.12. For ethylene, the moments and mean residence times were calculated for the two peaks separately. The following equations were used for the calculation of mean values and variances:

$$\mu_1 = t_m = \frac{\int_0^\infty tCdt}{\int_0^\infty Cdt} = \frac{m_1}{m_0}$$

$$\sigma^2 = \frac{\int_0^\infty t^2Cdt}{\int_0^\infty Cdt} = \frac{m_2}{m_0} - t_m^2$$

where C is the mass spectrometer response, μ_1 is the first moment, t_m is the mean residence time, and σ^2 is the variance. The locus of distribution is given by the mean residence time, and the spread of distribution is described by the variance.

Gaussian curves were fitted to CO_2 and H_2O peaks by the software MATLAB 6.5. The form of the equation used is as follows:

$$y = \sum_{i=1}^{n} a_i e^{\left[-\left(\frac{x-b_i}{c_i}\right)^2\right]}$$

'where *a* is the amplitude, *b* is the centroid (location), *c* is related to the peak width, and *n* is the number of peaks to fit' [63].

Summation of two and four Gaussian peaks were used for CO_2 and H_2O, respectively. These plots were then deconvoluted into separate Gaussian peaks and their means, variances, standard deviations, peak amplitudes,

areas, and area percentages were calculated using the model equations. The means and variances were found by comparing the above equation with the Gaussian distribution equation given below [70].

$$y = constant \frac{1}{\sigma} e^{-\left[\frac{(x-\eta)^2}{2\sigma^2}\right]}$$

where σ^2 is the variance, σ is the standard deviation, and η is the mean value.

The examples of these fits together with their equations for CO_2 and H_2O for 4th pulse of 350°C are shown in Figures 60 and 61, respectively. The Gaussian curves, their separated forms, and the fit equations for CO_2 and H_2O in all pulses over Cr-O catalyst are given in Appendix D.1 (Figures D.1.5 and D.1.6 for 350°C, Figures D.1.11 and D.1.12 for 401°C, and Figures D.1.18 and D.1.19 for 450°C).

The fit of H_2O peaks with summation of four Gaussian curves shows the presence of at least three production ways for water. The last curve can be due to adsorbed water on the catalyst surface. Similarly, the two fitted Gaussian curves of CO_2 indicate two routes for its formation.

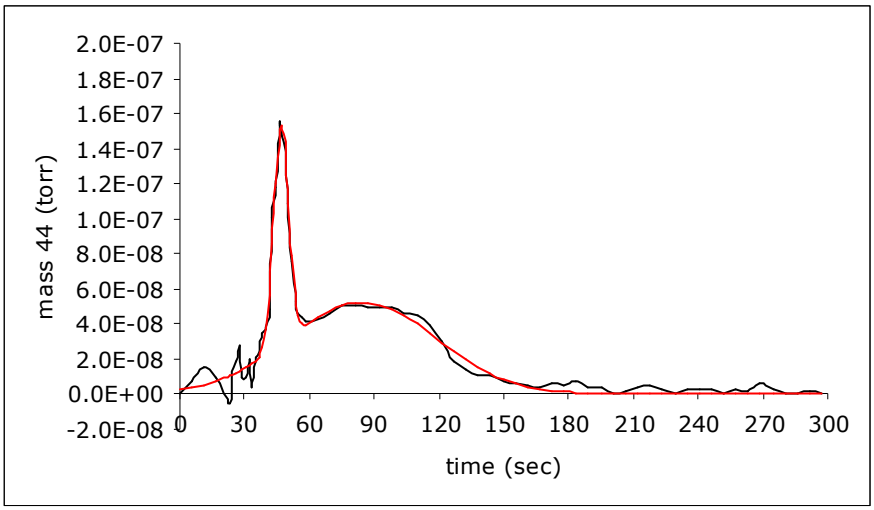

(a)

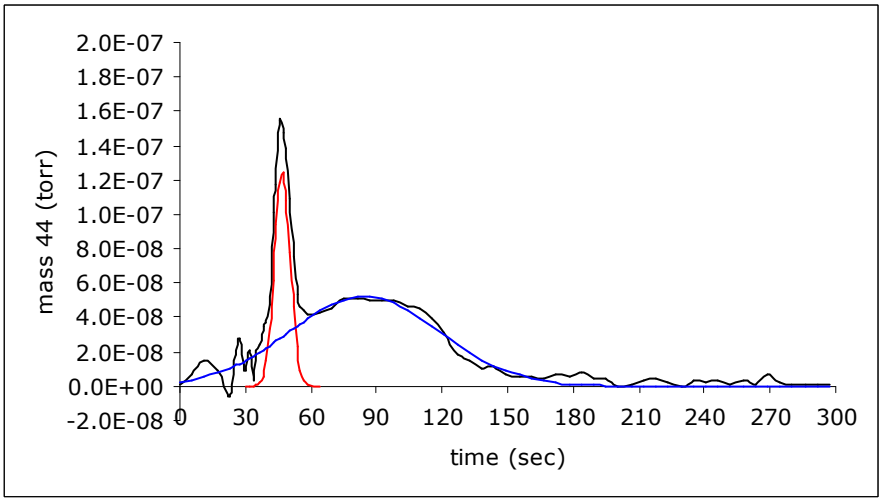

(b)

$$y = 1.25x10^{-7}e^{-\left(\frac{x-47}{5}\right)^2} + 5.226x10^{-8}e^{-\left(\frac{x-84.5}{48.5}\right)^2}$$

Goodness of fit:

SSE: $1.766x10^{-15}$

R-square: 0.9809

Adjusted R-square: 0.9794

RMSE: $5.252x10^{-9}$

Figure 60. (a) Gaussian fit **(b)** De-convolution of Gaussian fit for 'Pulse 4' CO_2 response data for C_2H_6 pulses into O_2 and He flow over Cr-O catalyst at 350°C

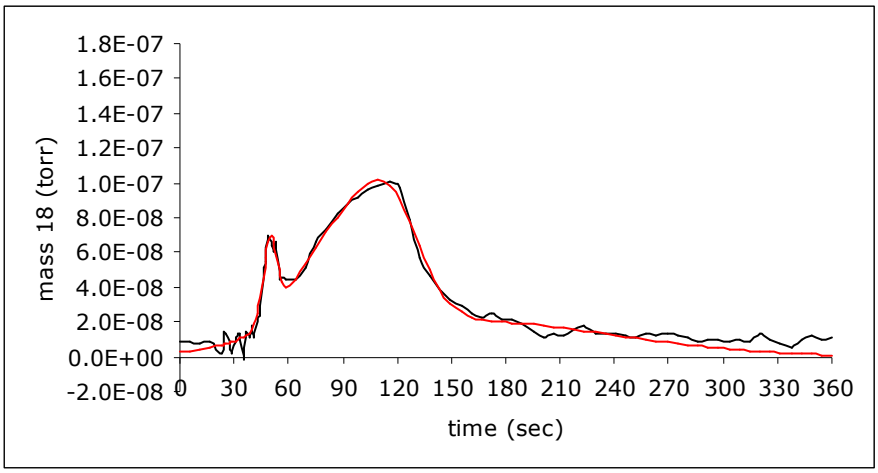

(a)

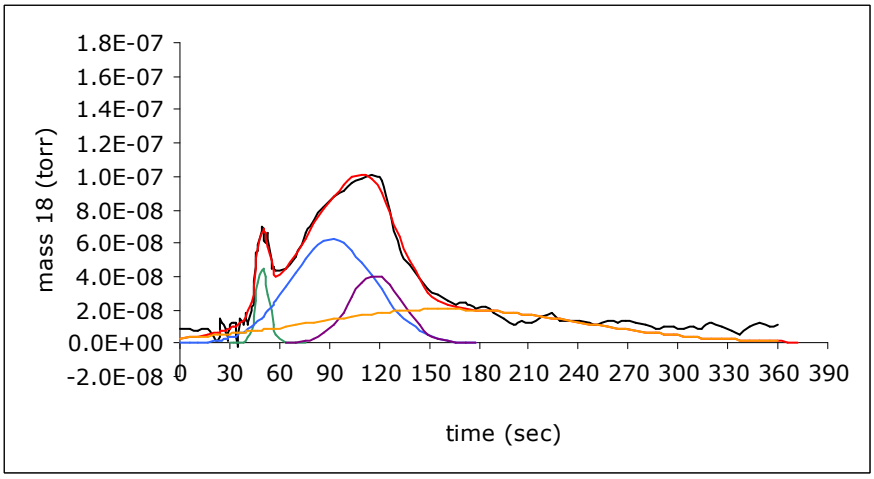

(b)

$$y = 4.49\text{x}10^{-8}e^{-\left(\frac{x-50}{5.5}\right)^2} + 6.214\text{x}10^{-8}e^{-\left(\frac{x-92}{36}\right)^2} + 4.094\text{x}10^{-8}e^{-\left(\frac{x-118}{22.5}\right)^2} + 2.035\text{x}10^{-8}e^{-\left(\frac{x-160}{115}\right)^2}$$

Goodness of fit:

SSE: $1.766\text{x}10^{-15}$

R-square: 0.9809

Adjusted R-square: 0.9794

RMSE: $5.252\text{x}10^{-9}$

Figure 61. (a) Gaussian fit **(b)** De-convolution of Gaussian fit for 'Pulse 4' H_2O response data for C_2H_6 pulses into O_2 and He flow over Cr-O catalyst at 350°C

Inspecting more the behaviour of species during these ethane pulses, Figure 62a, b, and c show the variations of zeroth moments with pulse number for C_2H_6, C_2H_4, CO_2, and H_2O at 350, 401, and 450°C, respectively. These plots also give an idea about the amounts of the products formed during the oxidative dehydrogenation reaction. At each temperature the variation of products between pulses seem constant.

In more detail, the variation of ethylene formed is depicted in Figure 63 as zeroth moment versus pulse number. Formation of ethylene decreases with increasing temperature. Similar plots for CO_2 and H_2O are given in Figures 64, and 65, respectively. CO_2 formed increases with increasing temperature within a small range (Figure 64), and highest H_2O formation is seen at 450°C (Figure 65).

The variation of average mean values of the fitted Gaussian curves to CO_2 and H_2O distributions obtained by the given pulses of ethane at 350, 401, and 450°C are presented in Table 9.

Table 9. Average mean values of CO_2 and H_2O Gaussian curves for pulses of C_2H_6 into He and O_2 flow over Cr-O catalyst

	CO_2		**H_2O**			
T (°C)	η_{Gauss1}	η_{Gauss2}	η_{Gauss1}	η_{Gauss2}	η_{Gauss3}	η_{Gauss4}
350	47	84.3	50.5	90.8	118.8	167.8
401	46.5	90	50.3	86.9	124	175
450	45	91	49	93	130	191

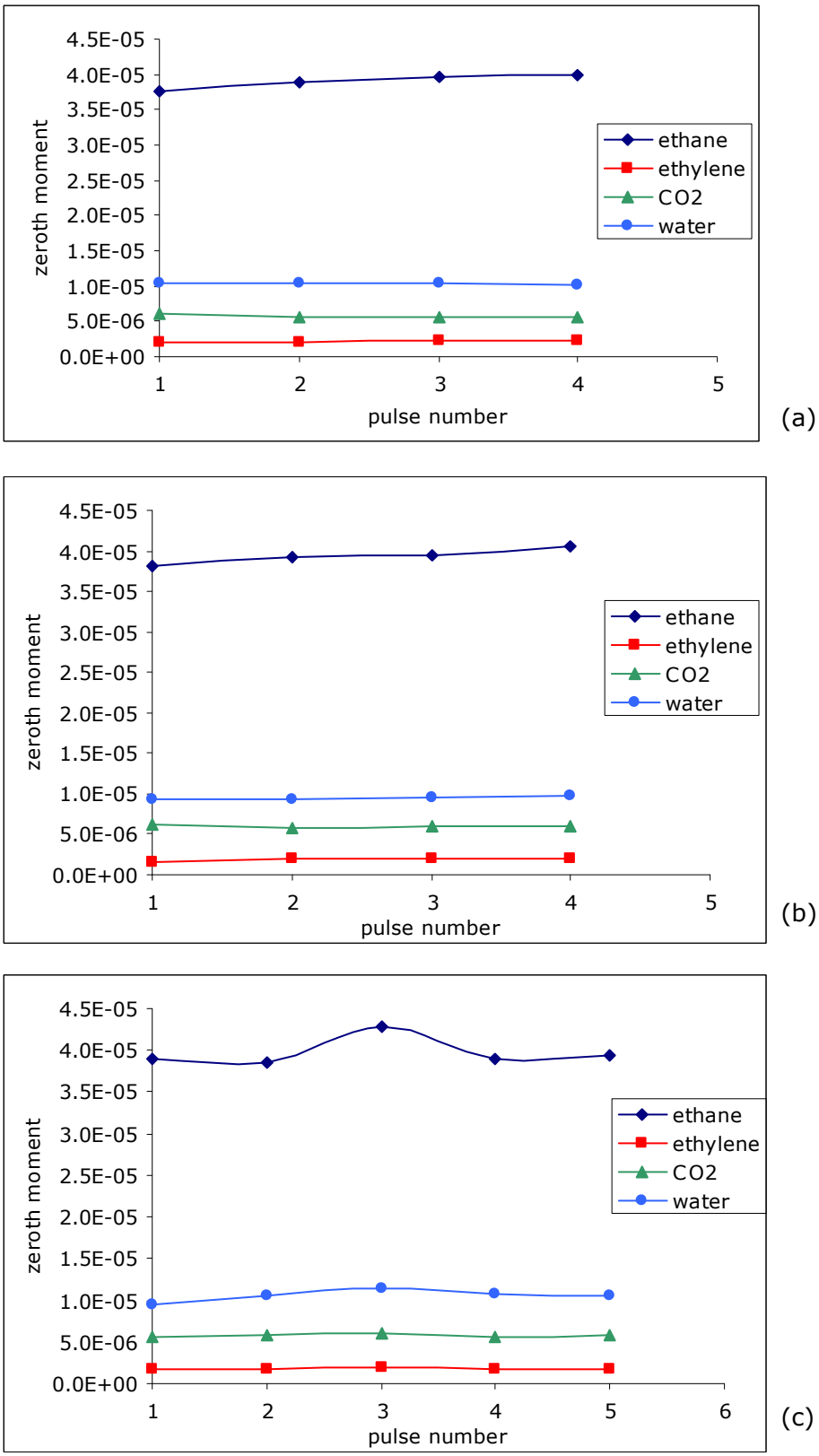

Figure 62. Variation of zeroth moments with pulse number for C_2H_6, C_2H_4, CO_2, and H_2O at **(a)** 350°C, **(b)** 401°C, and **(c)** 450°C for C_2H_6 pulses into O_2 and He flow over Cr-O catalyst

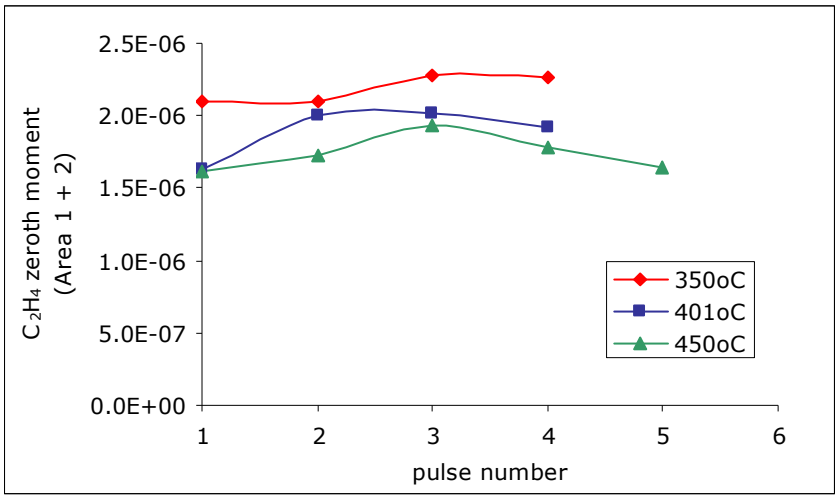

Figure 63. Variation of zeroth moments with pulse number for C_2H_4 at 350°C, 401°C, and 450°C for C_2H_6 pulses into O_2 and He flow over Cr-O catalyst

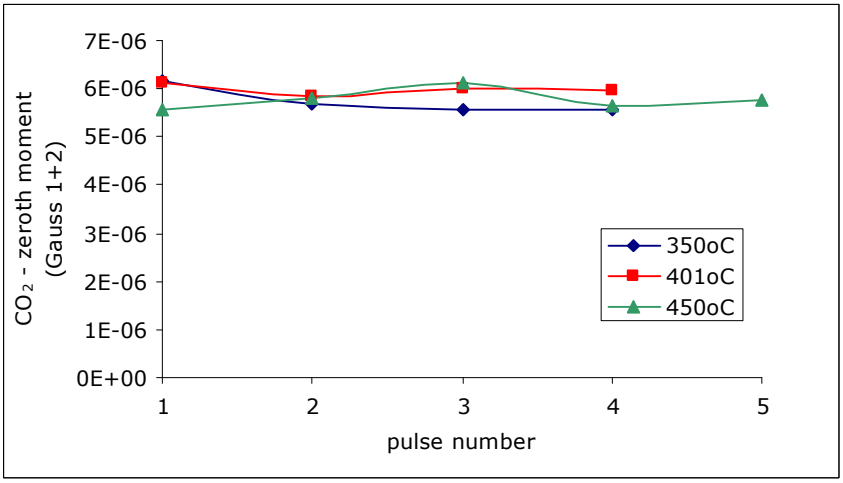

Figure 64. Variation of zeroth moments with pulse number for CO_2 at 350°C, 401°C, and 450°C for C_2H_6 pulses into O_2 and He flow over Cr-O catalyst

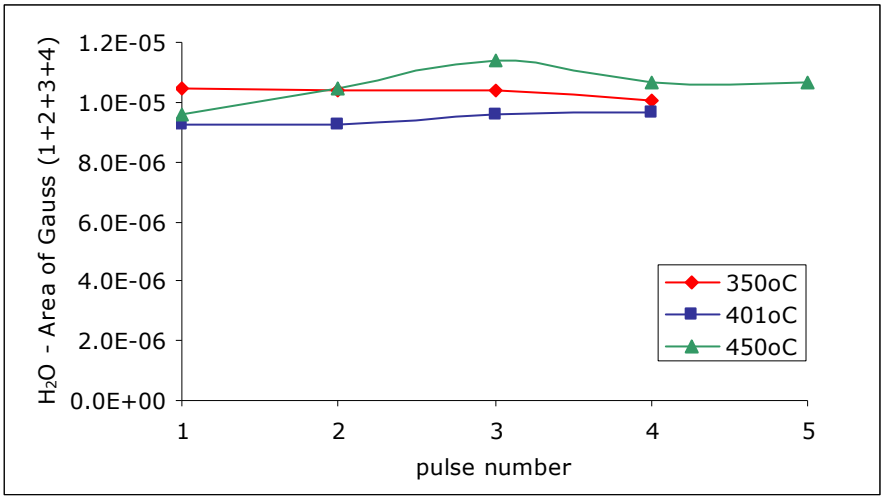

Figure 65. Variation of zeroth moments with pulse number for H_2O at 350°C, 401°C, and 450°C for C_2H_6 pulses into O_2 and He flow over Cr-O catalyst

In addition to the above O_2 containing runs, pulse-response experiments without gas phase oxidant were performed with the Cr-O catalyst at 448°C. Within these tests, 15-second 17 C_2H_6 pulses with 3 min. periods were given to He, flowing at 45 ml/min. The mass spectrometer response data for these pulses are presented in Appendix D.1.4, Figures D.1.20-D.1.36. The response of ethane pulses had tails similar to the runs performed with flows containing oxygen (Figure 66). The tails indicated again the possibility of ethane adsorbing on the catalyst surface. Formation of ethylene was detected within all pulses. Like previous runs, ethylene responses showed two curves. The separation of these curves was more distinguishable in some pulses. An example to this is shown in Figure 67. Trace amounts of H_2O, CO_2, and H_2 formation were also observed. The tabulated data for zeroth moment, first moment, mean residence time, variance, and standard deviation for C_2H_6 and C_2H_4 are given in Tables D.13 and D.14, respectively. The average mean residence time for ethane was calculated as 41.5 sec; and 39.3 and 58.8 sec for the first and second part of ethylene curve, respectively.

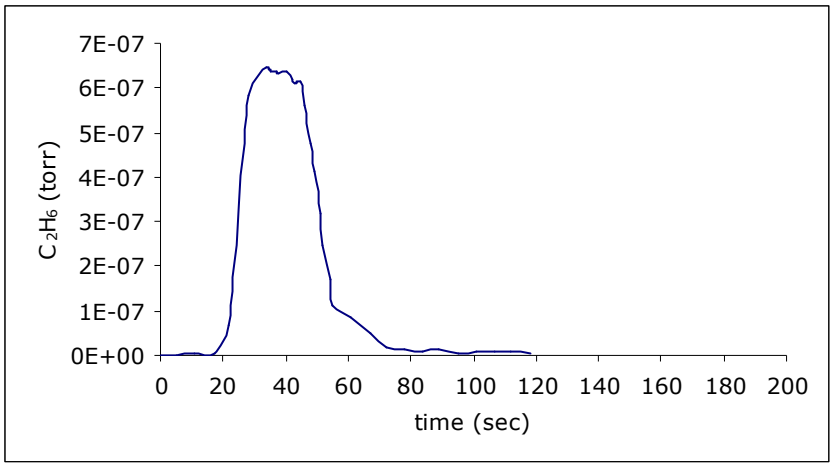

Figure 66. 'Pulse 6' C_2H_6 response data for C_2H_6 pulses into He flow over Cr-O catalyst at 448°C

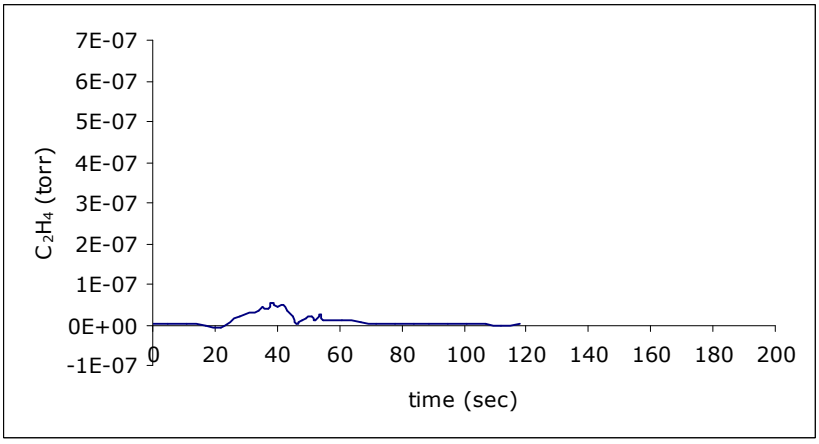

Figure 67. 'Pulse 6' C_2H_4 response data for C_2H_6 pulses into He flow over Cr-O catalyst at 448°C

As an indication of the amount of ethylene formed from the ethane pulses given, the variation of zeroth moments with the pulses for ethane and ethylene is given in Figure 68. The ethylene formation was very small compared with the supplied ethane pulse amount.

Figure 69 presents the comparison of the amount of the ethylene formed during the pulses given to O_2 containing flow with the one without O_2 at about 450°C. Obviously the ethylene formation is favoured more in the runs containing O_2 within the time range studied (Figure 69).

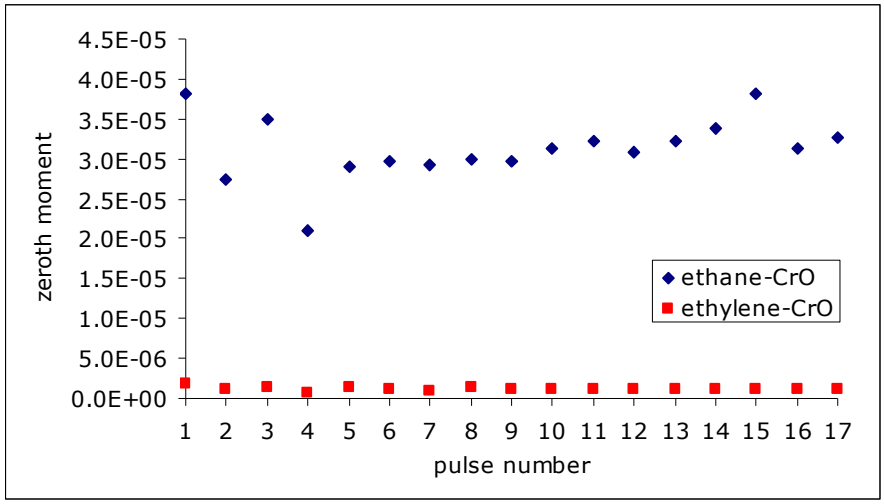

Figure 68. Variation of zeroth moments with pulse number for C_2H_6 and C_2H_4 at 448°C for C_2H_6 pulses into He flow over Cr-O catalyst

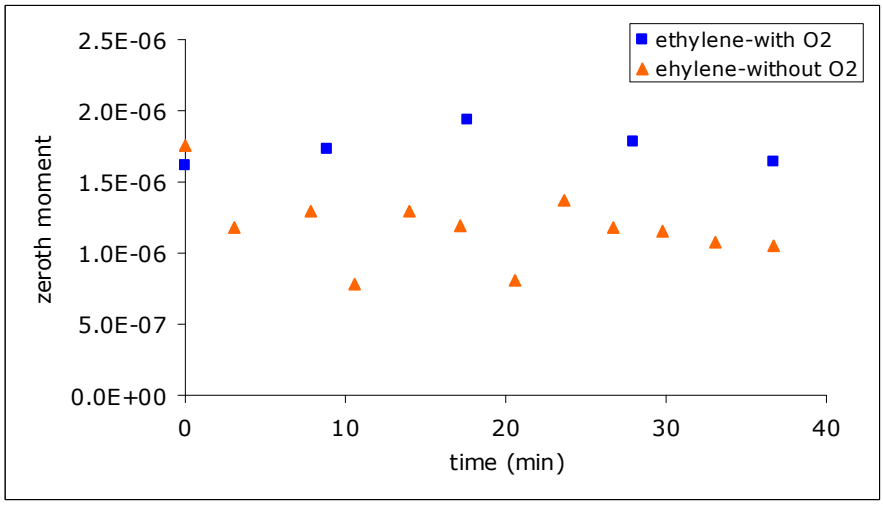

Figure 69. Variation of zeroth moments with time for C_2H_4 at about 450°C for C_2H_6 pulses into He and He-O_2 flow over Cr-O catalyst

3.3.2. Dynamic Experiments with Cr-V-O Catalyst

Seven 15-second ethane pulses were given to the flow containing 94% He and 6% O_2 over Cr-V-O catalyst at 400°C. The flow rate of He-O_2 mixture was about 45 ml/min. The intervals between the pulses were about 10 minutes. The responses of reactants and possible products are presented in Appendix D.2.1, Figures D.2.1-D.2.7. Inspection of these figures shows that ethylene and water were formed as reaction products. Ethane curves had the same occurance just as in the pulses with Cr-O catalyst; i.e. a tail as an indication of adsorption on the catalyst. The long tails of water peaks were a sign of the water adsorbing on the surface of the catalyst (Figure 70). The ethylene curves showed two combined peaks. Oxygen displayed two different decreasing curves (Figure 71). This behaviour may be due to two adsorption sites for oxygen or two different reaction pathways consuming oxygen. Additionally, trace amount of CO_2 formation was observed.

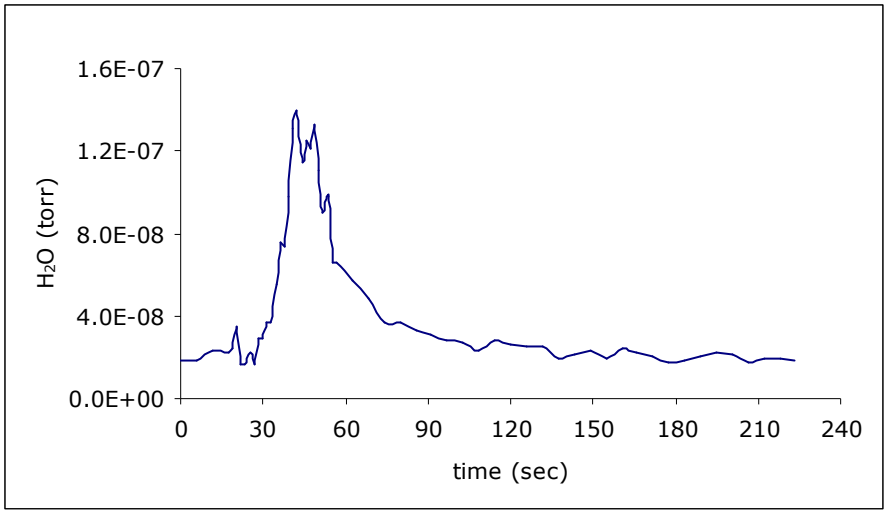

Figure 70. 'Pulse 2' H_2O response data for C_2H_6 pulses into O_2 and He flow over Cr-V-O catalyst at 400°C

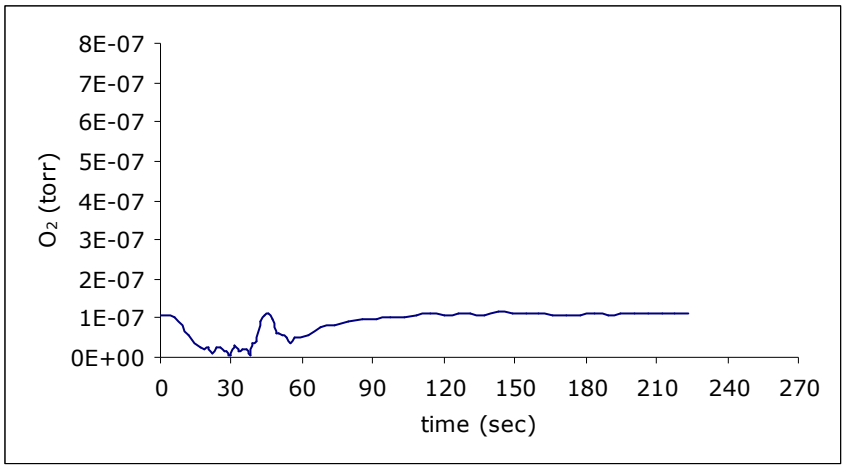

Figure 71. 'Pulse 2' O_2 response data for C_2H_6 pulses into O_2 and He flow over Cr-V-O catalyst at 400°C

The values for zeroth moment, first moment, mean residence time, and variance for ethane, ethylene, and water distributions are tabulated in Tables D.13, D.14, and D.15, respectively. The average value of mean residence times was found as 33.7 sec for ethane and 49.1 sec for water. For ethylene the mean residence time average was 31.4 and 58.4 sec for the first and second parts, respectively. The variation of zeroth moments with pulses for C_2H_6, C_2H_4, and H_2O is presented in Figure 72. The amounts of C_2H_6 pulses and formed C_2H_4 and H_2O were constant for these 7 pulses.

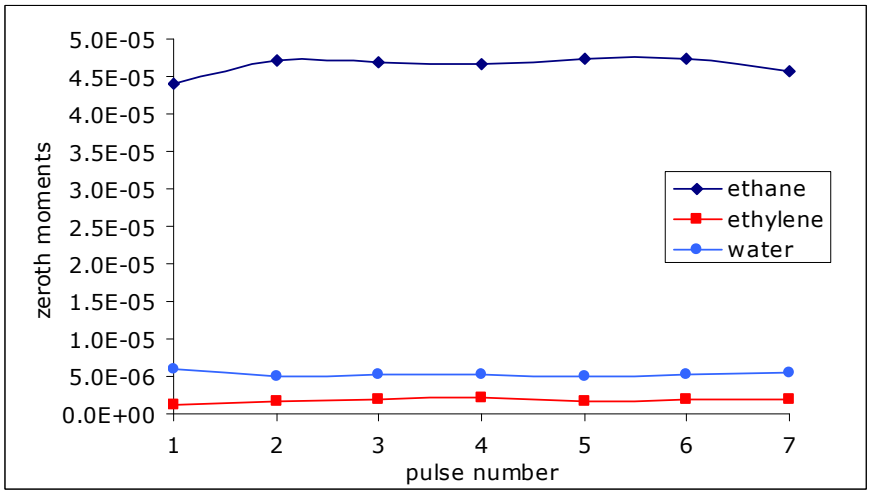

Figure 72. Variation of zeroth moments with pulse number for C_2H_6, C_2H_4, and H_2O at about 400°C for C_2H_6 pulses into He and O_2 flow over Cr-V-O catalyst

With Cr-V-O catalyst, 15 O_2 pulses were given to He and C_2H_6 flow at 400°C. The pulses' duration was 15 seconds and the time interval between them was 5 minutes. The flowing gas composition was 11.4% C_2H_6 and 88.6% He. In all pulses formation of CO and H_2O was observed. Trace amount of ethylene formation was seen in 7^{th}, 8^{th}, and 10^{th} pulses. The product distribution for all pulses is shown in Table 10. The first pulse had an error; therefore, it was not included in the calculations. The response curves for the reactants and products are presented in Appendix D.2.2, Figures D.2.8-D.2.21. Formation of CO rather than C_2H_4 indicated that oxygen pulse amount was high, so that, partial combustion of C_2H_6 was favoured.

Table 10. Product distribution for O_2 pulses into He and C_2H_6 flow over Cr-V-O catalyst at 400°C

Pulse no	H_2O	CO	CH_4	CO_2	H_2	C_2H_4
2	x	x				
3	x	x				
4	x	x				
5	x	x	x	x	x	
6	x	x			x	
7	x	x	x	x	x	x
8	x	x		x	x	x
9	x	x	x	x	x	
10	x	x	x	x	x	x
11	x	x	x	x		
12	x	x	x	x	x	
13	x	x	x	x	x	
14	x	x	x	x	x	
15	x	x	x	x	x	

As seen in Table 10, in some pulses small amounts of CH_4, CO_2, and H_2 were also obtained. When CH_4, H_2, and CO_2 were detected in the mass spectrometer response data, they had the same kind of shaped peaks occurring at almost the same times. H_2O and CO had also similar second peaks. The long tail of water was possibly again due to adsorption of it on the catalyst surface. Examples to this behaviour are presented in Figure 73 for pulse 9. These characteristic peaks suggest the possibility of occurrence of the following reactions on the Cr-V-O catalyst in some pulses:

$C_2H_6 + 5/2O_2 \rightarrow 2CO + 3H_2O$

$C_2H_6 + 7/2O_2 \rightarrow 2CO_2 + 3H_2O$

$C_2H_6 + O_2 \rightarrow CO + CH_4 + H_2O$

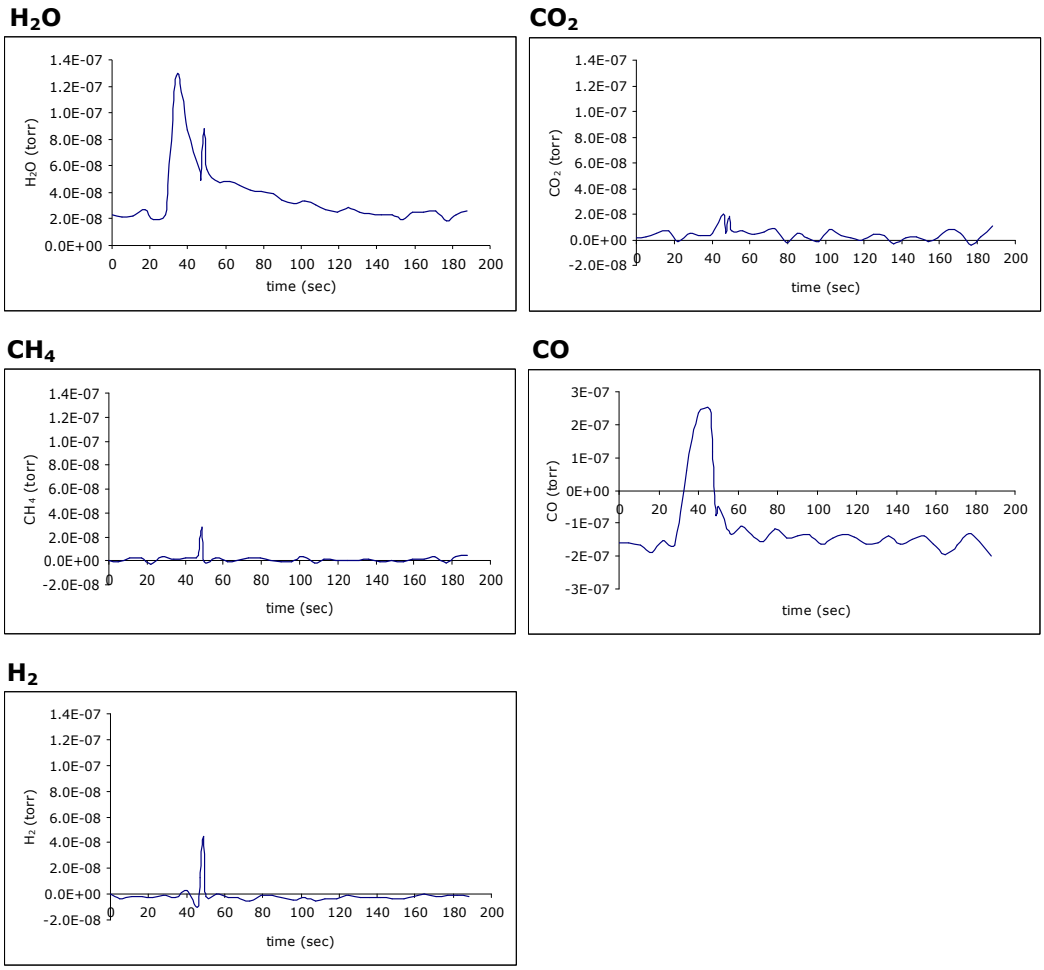

Figure 73. 'Pulse 9' response data of H_2O, CO_2, CH_4, CO, and H_2 for O_2 pulses into He and C_2H_6 flow over Cr-V-O catalyst at 400°C

The calculated zeroth moment, first moment, mean residence time, and variance data for O_2, H_2O, and CO are given in Tables D.16, D.17, and D.18, respectively. In Figure 74, the variation of zeroth moments with pulse number for O_2, H_2O, and CO for O_2 pulses into He and C_2H_6 flow over Cr-V-O catalyst at 400°C is depicted. Formation of CO decreased a little bit after the 6th pulse whereas, water amount was almost constant in the pulse range; that is, for about 70 minutes. The average mean residence times for O_2, CO, and H_2O were 44.5, 47.7, and 58.2 sec, respectively.

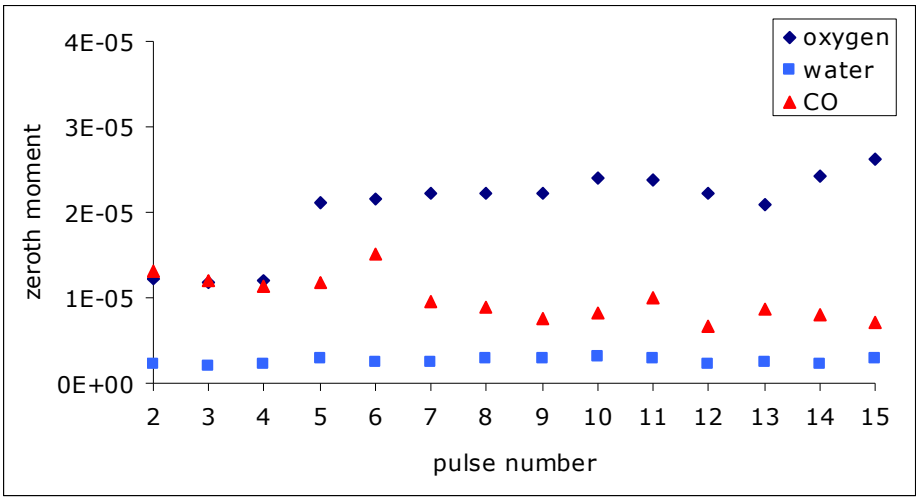

Figure 74. Variation of zeroth moments with pulse number for O_2, H_2O, and CO for O_2 pulses into He and C_2H_6 flow over Cr-V-O catalyst at 400°C

Moreover, pulses without O_2 were also performed with the Cr-V-O catalyst. At 449°C, 17 C_2H_6 pulses were given to He flowing at 45 ml/min. The 15-second pulses were given to the system at 3 minute time intervals. The distributions of responses to these pulses are exhibited in Appendix D.2.3, Figures D.2.21-D.2.28.

In these runs noticeable ethylene and water formation was detected after 4^{th} pulse. Trace amount of CO_2 and H_2 were also observed in some pulses. Ethylene peaks were again composing of two parts. Figure 75 depicts the C_2H_4 response data for the 6^{th} pulse as an example of this behaviour. The calculated moment and mean residence time data for C_2H_6, C_2H_4, and H_2O are shown in Tables D.19, D.20, and D.21, respectively. The average mean residence time for C_2H_6 was 41.1 sec and that of H_2O was 57.7 sec. The first and second parts of C_2H_4 peak had average means of 29.2 sec and 41.3 sec, respectively.

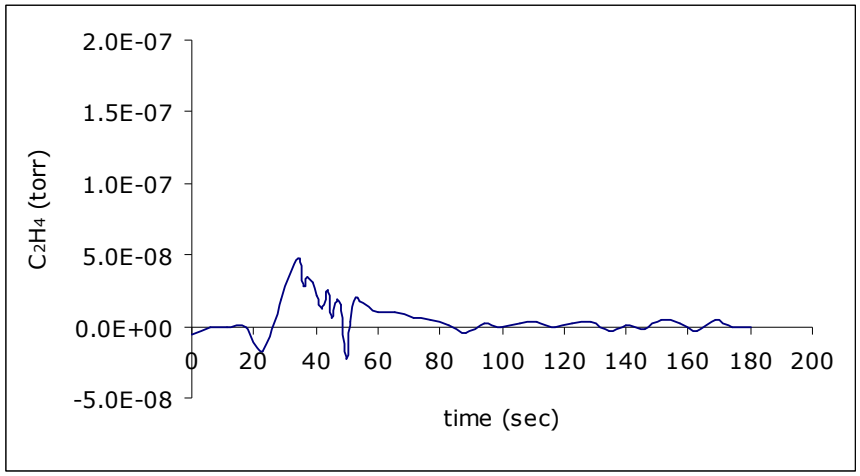

Figure 75. 'Pulse 6' response data of C_2H_4 for C_2H_6 pulses into He flow over Cr-V-O catalyst at 449°C

The zeroth moment versus pulse number for C_2H_6, C_2H_4, and H_2O is given in Figure 76. The amount of formed C_2H_4 and H_2O were almost the same within this 17-pulse period.

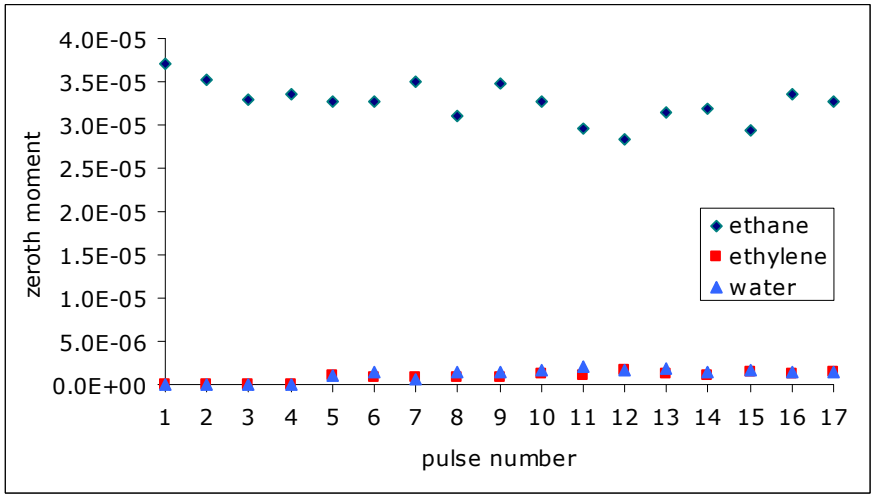

Figure 76. Variation of zeroth moments with pulse number for C_2H_6, C_2H_4, and H_2O for C_2H_6 pulses into He flow over Cr-V-O catalyst at 449°C

3.3.3. Dynamic Experiments' Comparison of Cr-O and Cr-V-O Catalysts

The zeroth moment versus time for the products and reactants of C_2H_6 pulses to He and O_2 flow over Cr-O and Cr-V-O catalysts at 400°C is shown in Figure 77. The zeroth moments were almost constant for the time ranges studied. Different from the Cr-V-O catalyst, CO_2 formation was seen in the runs with the Cr-O catalyst. Consequently, the H_2O amount was higher than that of Cr-V-O. Accordingly, for Cr-O, ethane zeroth moments were lower than for Cr-V-O. Ethylene amounts were almost the same over both catalysts. This may be due to consecutive reactions occuring on Cr-O catalyst; that is, the ethylene formed on Cr-O might be acting as an intermediate product and forming CO_2.

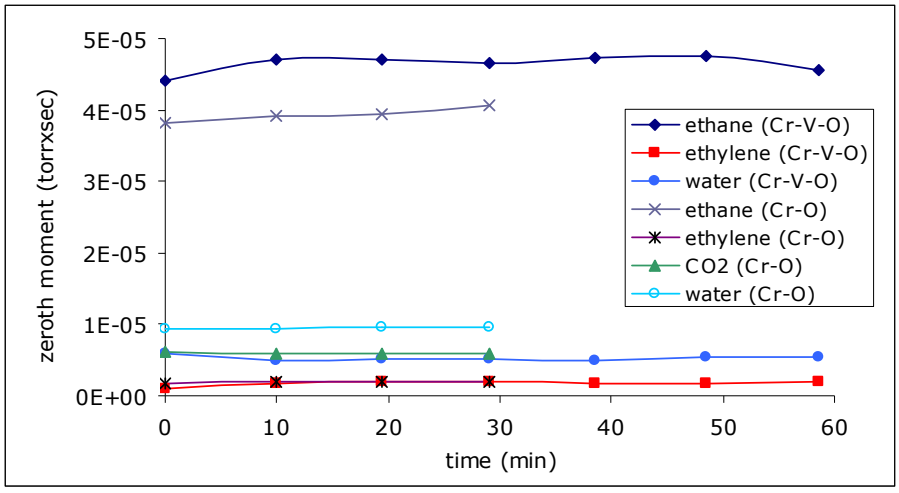

Figure 77. Variation of zeroth moments with time for C_2H_6, C_2H_4, CO_2, and H_2O for C_2H_6 pulses into He and O_2 flow over Cr-O and Cr-V-O catalysts at 400°C

For ethane pulses into only He flow over Cr-O and Cr-V-O catalysts at about 449°C, the variation of zeroth moment with time for all pulses is presented in Figure 78. The products formed in these without gas phase oxidant runs were small in amount compared with the ethane pulse supplied. Over Cr-O catalyst trace amount of water was produced. To see the trends of products in detail, Figure 79 is depicted. The zeroth moment for ethylene formed on both catalysts were within close range.

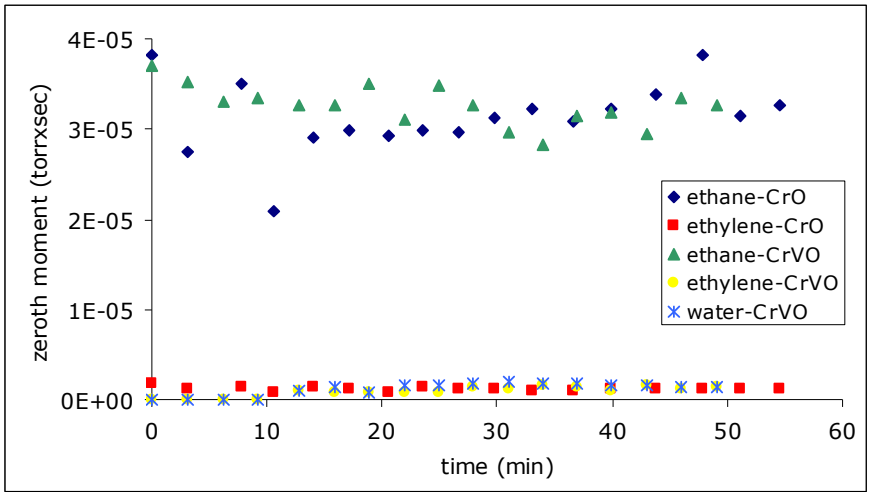

Figure 78. Variation of zeroth moments with time for C_2H_6, C_2H_4, and H_2O for C_2H_6 pulses into He flow over Cr-O and Cr-V-O catalysts at about 449°C

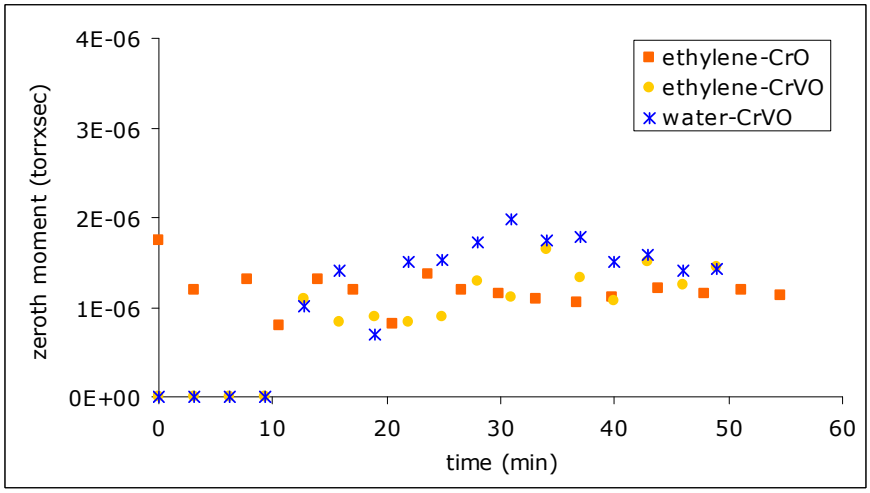

Figure 79. Variation of zeroth moments with time for C_2H_4 and H_2O for C_2H_6 pulses into He flow over Cr-O and Cr-V-O catalysts at about 449°C

CHAPTER 4

CONCLUSIONS

In this study, the oxidative dehydrogenation of ethane over mixed oxide catalysts, i.e. Cr-O, Cr-V-O, was examined through steady-state and dynamic analysis. Additionally V-MCM-41 catalyst was tested for oxidehyrogenation reaction. Within steady-state experiments, the effect of variation of temperature, gas composition, and gas phase oxidant on catalytic performance was investigated. In dynamic studies, single-pulse multi-response runs were performed with ethane and oxygen pulses over Cr-O and Cr-V-O catalysts at different temperatures.

Throughout the characterization studies for Cr-O and Cr-V-O catalysts BET, XRD, TPR, and XPS were utilized. The complexation method which was used as the preparation route for the mixed oxide catalysts was found to generate mildly high surface areas. From XRD analysis, Cr_2O_3 phase was detected to be formed successfully on Cr-O catalyst. The Cr-V-O catalyst was revealed to have an amorpous structure with little Cr_2O_3 and V_2O_4 phases.

Within H_2-TPR analysis both catalysts showed reduction peaks. Cr-O exhibited this behavior at a much lower temperature than Cr-V-O. The Cr-O catalyst's maximum H_2 consumption was at about 243°C. For the Cr-V-O catalyst the possibility of presence of three reduction sites was shown through the deconvoluted Gaussian curve fit analysis. The maximum H_2 consumption for the two peaks of Cr-V-O was seen at about 535°C and 555°C.

XPS technique was used to find out the oxidation states and the surface atom concentrations of both fresh and reduced Cr-O and Cr-V-O. On fresh Cr-O surface the presence of Cr^{+6} was discovered to be probable and O/Cr ratio was found to be 4.6. After ion bombardment O/Cr ratio was decreased to 3.8. The reduced Cr-O catalyst still contained Cr^{+6} species which brought about the possibility that the H_2 consumption in TPR might be by reduction of

adsorbed oxygen species. O/Cr ratio in the reduced Cr-O catalyst before and after ion bombardment was 5.5 and 2.7, respectively.

By the XPS of the fresh Cr-V-O, V/Cr ratio of the surface was found as 1.5, which was higher than the aimed bulk ratio of 1.0. Hence, the surface of Cr-V-O was concluded to contain more V than Cr compared to its bulk. After ion bombardment, the V/Cr ratio was 1.4. The V/Cr ratio of the reduced Cr-V-O before and after ion bombardment was 1.0 and 0.8, respectively. On the surface of the fresh Cr-V-O catalyst, the V^{+5} and Cr^{+6} forms were likely present. Over reduced Cr-V-O sample, possible existence of V^{+4}, V^{+3}, and Cr^{+3} states was found. Consequently, by TPR analysis, it is probable that the vanadium species of Cr-V-O mixed oxide catalyst were reduced from V^{+5} to V^{+4} and V^{+3} forms; and the chromium in the form of Cr^{+6} was partially reduced to Cr^{+3}.

In steady-state runs, experiments were performed by both feed containing O_2 and CO_2 as oxidant at various temperatures with the space time value of $4x10^{-3}$g.min/cm^3. Over Cr-O catalyst, different feed compositions with O_2/C_2H_6 feed ratios of 0.5, 0.33, and 0.17 were tested. With O_2/C_2H_6 feed ratio of 0.5 at 251°C, a CO_2 selectivity value of 0.65 was obtained together with the consumption of all the feed O_2. Lowering the O_2/C_2H_6 feed ratio to 0.17, a total fractional conversion of 0.20 was reached at 447°C. Almost constant selectivity to ethylene values of 0.8 were achieved in the temperature range of 250-450°C. No CO formation was observed in these experiments. O_2/C_2H_6 feed ratio was also increased further to ~0.33; and at 250°C, a total fractional conversion value of 0.11 was obtained with an C_2H_4 selectivity of 0.91.

Ethane dehydrogenation with CO_2 over Cr-O catalyst was also performed with ~10% CO_2-30% C_2H_6 –60% He feed mixtures. In the temperature range of 300-450°C, total fractional conversion and selectivity values of about 0.16 and 0.93 were obtained, respectively. When the experiments over Cr-O catalysts with 10% O_2 and 10% CO_2 were compared, above 250°C, higher total conversion values were obtained in the runs performed by O_2; i.e. the total conversion values were about 1.7 times higher in the experiments

performed with 10% O_2 than 10% CO_2. On the other hand, selectivity to ethylene values were higher with CO_2 runs than the ones with O_2.

With the Cr-V-O catalyst, experiments were done with feed containing O_2/C_2H_6 feed ratios of about 0.17 and 0.33. For the feed mixture with O_2/C_2H_6 ratio of ~0.17, till 350°C, total fractional conversion values of about 0.03 with an average ethylene selectivity value of about 0.87 were attained. Further temperature increment resulted an increase in the total ethane conversion at the expense of selectivity to ethylene. Higher total conversion values were obtained when the O_2/C_2H_6 feed ratio was increased to 0.33 over Cr-V-O. In the temperature range studied, maximum ethylene yield value of 0.14 was obtained at 448°C.

Over Cr-V-O catalyst CO_2 was also utilized as the mild oxidant. With feed mixtures containing 10% CO_2 and 45% CO_2 keeping C_2H_6 percentage constant at 30%, very small total fractional conversion values which were around 0.03 above 400°C were observed. The ethylene selectivity values were almost constant with an average value of 0.96. At 448°C, with feed containing 10% O_2, a total conversion value 5.5 times higher than that with 10% CO_2 was obtained. Increasing CO_2 percentage in the feed to 45% did not improve total fractional conversion and ethylene yield values for the temperature range of 350-500°C.

For the test of V-MCM-41 catalyst, an O_2/C_2H_6 feed ratio of ~0.17 was used. In the temperature range of 200-350°C, the total conversion values were nearly constant at 0.02; and started to increase at 400°C. At ~500°C, a conversion value of 0.03 with the maximum selectivity value of 0.81 was reached. No CH_4 formation was observed in these experiments. The low conversion and selectivity values observed by the V-MCM-41 catalyst were possibly due to the high V/Si ratio of 0.16.

When Cr-O, Cr-V-O, and V-MCM-41 catalysts were compared about their catalytic performances, with 5%O_2 - 30%C_2H_6 - 65%He feed, Cr-O catalyst showed the highest total conversion values with a maximum of about 0.20 at 447°C. In the temperature range of 250-450°C, ethylene selectivity values

were about 0.8 for Cr-O catalyst. The yield values obtained by Cr-O were also higher compared to Cr-V-O, and V-MCM-41 catalysts. Within all steady-state experiments, the maximum ethylene yield was obtained over Cr-O catalyst as 0.21 at 399°C with a total conversion value of 0.29 for an O_2/C_2H_6 feed ratio of 0.33.

In the dynamic analysis part, pulses of C_2H_6 to O_2 and He flow, C_2H_6 to only He flow, and O_2 to C_2H_6 and He flow were given over Cr-O and Cr-V-O catalysts. The responses of these pulses were analysed to observe the behaviour of products and reactants. Besides the moments, mean residence times, and variances were calculated to characterize the distributions.

Over Cr-O catalyst C_2H_6 pulses were given to O_2 and He flow at temperatures of 350, 401, and 450°C. Formation of C_2H_4, H_2O, CO_2, and trace amounts of H_2 and CH_4 were observed. Response curves of ethane had a tail denoting that some of ethane was adsorbed on the catalyst. The ethylene peaks were composed of two different parts. CO_2 and H_2O had two distinct peaks which evoked the possibility of the occurrence of either two reaction sites or the presence of two reaction pathways. The long tail of H_2O indicated its likely adsorption on the catalyst surface. Gaussian fits were utilized to de-convolute these curves and the presence of at least three production ways for H_2O was found to be probable. Through the variation of zeroth moments with pulses, the amounts of products formed at each temperature were constant. Besides, formation of ethylene decreased with increasing temperature.

At 448°C, pulse-response experiments without gas phase oxygen were also performed. C_2H_6 pulses were given to He flow over Cr-O. Although ethylene formed was very small compared with the supplied ethane pulse, it was detected in all pulses. Besides, trace amounts of H_2O, CO_2, and H_2 formation were observed. Ethylene formation was favoured more in the runs containing O_2.

Over Cr-V-O catalyst, C_2H_6 pulses were given to O_2 and He flow at 400°C. Ethylene and water were formed as reaction products. Moreover, trace amounts of CO_2 formation were observed. Ethane and water curves had

similar tails to ones obtained by Cr-O catalyst. The two different decreasing curves of oxygen was thought to be due to two adsorption sites for oxygen or two different reaction pathways consuming oxygen.

Different from Cr-O catalyst, O_2 pulses were given to Cr-V-O catalyst over which C_2H_6 and He were flowing at 400°C. In these runs formation of CO rather than C_2H_4 was observed. Therefore, oxygen pulse amount was concluded to be high, so that, partial combustion of C_2H_6 to CO was favoured. In three pulses trace amounts of ethylene formation were detected. Small amounts of CH_4, CO_2, and H_2 were also obtained in some pulses. These three had the similar shaped peaks occurring at almost the same times suggesting the proceeding of same reactions. At these times H_2O and CO had also similar second peaks. From the zeroth moment variation with pulses, it was seen that after the 6^{th} pulse, CO amount decreased a little; however, water amount was almost constant for about 70 minutes.

Besides, without oxygen, C_2H_6 pulses were given to He flow over Cr-V-O catalyst at 449°C. Noticeable amount of ethylene and water were observed after the 4^{th} pulse, and trace amounts of CO_2 and H_2 were detected. The amount of C_2H_4 and H_2O formed were almost the same within the pulse range.

When Cr-O and Cr-V-O catalysts were compared at 400°C for C_2H_6 pulses to He and O_2 flow, the most significant difference was the formation of CO_2 on Cr-O catalyst. The H_2O amount obtained by Cr-O was consequently higher than that of Cr-V-O. On both catalysts, nearly the same amount of ethylene were reached. The possible occurence of series reactions on Cr-O catalyst may be the cause of this.

With Cr-O and Cr-V-O catalysts, at about 449°C, for ethane pulses into He flow, the products formed were small in amount compared with the provided ethane. The amounts of ethylene formed on both catalysts with ethane pulses without O_2 were close to each other.

To sum up, among the catalysts tested, Cr-O is the promising one for the oxidative dehydrogenation of ethane to ethylene. The highest yield value

obtained by this catalyst (0.21) at 399°C with feed containing 10% O_2-30% C_2H_6-60%He can be enhanced further by increasing the used catalyst amount and the space time accordingly. From the results of TPR and XPS analysis, it can be deduced that, probably, during oxidative dehydrogenation reaction adsorbed oxygen is being used on Cr-O catalyst whereas a lattice oxygen involved redox mechanism is proceeding on Cr-V-O catalyst.

CHAPTER 5

RECOMMENDATIONS

The study carried out here contributed useful findings to the oxidative dehydrogenation of ethane to ethylene over chromium-based mixed oxide catalysts. Absolutely additional improvements can be made both in experimental set-up and procedures to enhance the results obtained. Moreover, modelling studies can be carried out for further identification of the dynamic system part.

The conversion values obtained within steady-state experiments may be increased via increasing the catalyst amount. Besides, other types of reactors can be utilized to improve the total conversion and selectivity. For instance, the limiting reactant, i.e. O_2, can be fed in small amounts along the reactor, so that it can be supplied for the reaction as soon as it is depleted. Usage of a membrane reactor which is permeable to oxygen can be another alternative. Additionally, through kinetic studies, the activation energy calculations can be made.

In dynamic analysis part, modelling studies by moment techniques can be applied to investigate the diffusion, adsorption, and reaction behaviours of the reactant and product gases in the system. The results obtained in single-pulse multi-response experiments can be employed to find adsorption rates, equilibrium constants and diffusivities.

Needless to say, the recommendations presented above will form the basis of our future studies. Further experiments and calculations to be done in the light of the stated suggestions will enrich the research and supply additional data to this field.

REFERENCES

[1] H.H. Kung, 'Oxidative dehydrogenation of light (C_2 to C_4) alkanes', *Advances in Catalysis*, 40 (1994)1.

[2] M.M. Bhasin, J.H. McCain, B.V. Vora, T. Imai, P.R. Pujado 'Dehydrogenation and oxidehydrogenation of parafins to olefins', *Applied Catalysis A Gen.*, 221 (2001) 397.

[3] G. Karamullaoglu, S. Onen, T. Dogu, 'Oxidative dehydrogenation of ethane and isobutene with chromium-vanadium-niobium mixed oxide catalysts', *Chem. Eng. Proc.,* 41 (2002) 337.

[4] EPA Office of Compliance sector Notebook Project, 'Profile of the Organic Chemical Industry', 2nd Ed., www.epa.gov/compliance/resources /publications/assistance/sectors/notebooks, November 2004.

[5] L. Kniel, O. Winter, K. Stork, Ethylene-Keystone to the Petrochemical Industry, Marcel Dekker, Inc., New York, 1980.

[6] Kirk-Othmer Encyclopedia of Chemical Technology, 'Ethylene', www.mrv.interscience.wiley.com/kirk/articles/ethysund.a01/sect9-fs.html, December 2004.

[7] G. Karamullaoğlu, Oxidative Dehydrogenation of Ethane, Middle East Technical University, Turkey, 1999 Master Thesis.

[8] E.M. Thorsteinson, T.P. Wilson, F.G. Young, P.H. Kasai, 'The oxidative dehydrogenation of ethane over catalysts containing mixed oxides of molybdenum and vanadium', *J. Catal.* 52 (1978) 116.

[9] R. Burch, R. Swarnakar, 'Oxidative dehydrogenation of ethane on vanadium-molybdenum oxide and vanadium-niobium-molybdenum oxide catalysts', *Appl. Catal.* 70 (1991) 129.

[10] O. Desponds, R.L. Keiski, G.A. Somorjai, 'The oxidative dehydrogenation of ethane over molybdenum-vanadium-niobium oxide catalysts: the role of catalyst composition', *Catal. Lett.* 19 (1993) 17.

[11] G. Karamullaoglu, T. Dogu, 'Oxidative dehydrogenation of ethane over a monolith coated by molybdenum-vanadium-niobium mixed-oxide catalyst', *Chem. Eng. Comm.* 190 (2003) 1427.

[12] K. Ruth, R. Burch, R. Kieffer, 'Mo-V-Nb catalysts for the partial oxidation of ethane', *J. Catal.* 175 (1998) 27.

[13] S. Önen, Kinetic Studies for the Catalytic Oxidative Dehydrogenation of Isobutane, Middle East Technical University, Turkey, 1997 Ph.D Thesis.

[14] K. Chen, A. Khodakov, J. Yang, A.T. Bell, E. Iglesia, 'Isotopic tracer and kinetic studies of oxidative dehydrogenation pathways on vanadium oxide catalysts', *J. Catal.* 186 (1999) 325.

[15] D. Creaser, B. Andersson, R.R. Hudgins, P.L. Silveston, 'Oxygen partial pressure effects on the oxidative dehydrogenation of propane', *Chem. Eng. Sci.* 54 (1999) 4365.

[16] G. Martra, F. Arena, S. Coluccia, F. Frusteri, A. Parmaliana, 'Factors controlling the selectivity of V_2O_5 supported catalysts in the oxidative dehydrogenation of propane', *Catal. Today* 63 (2000) 197.

[17] A.A. Lemonidou, L. Nalbandian, I.A. Vasalos, 'Oxidative dehydrogenation of propane over vanadium oxide based catalysts Effect of support and alkali promoter', *Catal. Today* 61 (2000) 333.

[18] P. Viparelli, P. Ciambelli, L. Lisi, G. Ruoppolo, G. Russo, J.C. Volta, 'Oxidative dehydrogenation of propane over vanadium and niobium oxides supported catalysts', *Appl. Catal. A: Gen.* 184 (1999) 291.

[19] Y. Liu, P. Cong, R.D. Doolen, H.W. Turner, W.H. Weinberg, 'High-throughput synthesis and screening of V-Al-Nb and Cr-Al-Nb oxide libraries for ethane oxidative dehydrogenation to ethylene', *Catal. Today* 61 (2000) 87.

[20] R. Monaci, E. Rombi, V. Solinas, A. Sorrentino, E. Santacesaria, G. Colon, 'Oxidative dehydrogenation of propane over $V_2O_5/TiO_2/SiO_2$ catalysts obtained by grafting titanium and vanadium alkoxides on silica', *Appl. Catal. A: Gen.* 214 (2001) 203.

[21] E.V. Kondratenko, M. Baerns, 'Catalytic oxidative dehydrogenation of propane in the presence of O_2 and N_2O – the role of vanadia distribution and oxidant activation', *Appl. Catal. A: Gen.* 222 (2001) 133.

[22] V.P. Vislovskiy, N.T. Shamilov, A.M. Sardarly, V.Yu. Bychkov, M.Yu. Sinev, P. Ruiz, R.X. Valenzuela, V. Cortés Corberán, 'Improvement of catalytic functions of binary V-Sb oxide catalysts for oxidative conversion of isobutane to isobutene', *Chem. Eng. J.* 95 (2003) 37.

[23] P. Concepción, M.T. Navarro, T. Blasco, J.M. López Nieto, B. Panzacchii, F. Rey, 'Vanadium oxida supported on mesoporous Al_2O_3 - Preparation, characterization and reactivity', *Catal. Today* 96 (2004) 179.

[24] N. Steinfeldt, D. Müller, H. Berndt, 'VO_x species on alumina at high vanadia loadings and calcination temperature and their role in the ODP reaction', *Appl. Catal. A: Gen.* 272 (2004) 201.

[25] E. Heracleous, M. Machli, A.A. Lemonidou, I.A. Vasalos, 'Oxidative dehydrogenation of ethane and propane over vanadia and molybdena supported catalysts', *J. Mol. Cat. A: Chem.* 232 (2005) 29.

[26] L. Lisi, G. Ruoppolo, M.P. Casaletto, P. Galli, M.A. Massucci, P. Patrono, F. Pinzari, 'Vanadium-metal(IV)phosphates as catalysts for the oxidative dehydrogenation of ethane', *J. Mol. Cat. A: Chem.* 232 (2005) 127.

[27] A. Dejoz, J.M. López Nieto, F. Márquez, M.I. Vázquez, 'The role of molybdenum in Mo-doped V-Mg-O catalysts during the oxidative dehydrogenation of n-butane', *Appl. Catal. A: Gen.* 180 (1999) 83.

[28] Y.J. Zhang, I. Rodríguez-Ramos, A. Guerrero-Ruiz, 'Oxidative dehydrogenation of isobutane over magnesium molybdate catalysts', *Catal. Today* 61 (2000) 377.

[29] M.C. Abello, M.F. Gomez, O. Ferretti, 'Mo/γ-Al_2O_3 catalysts for the oxidative dehydrogenation of propane. Effect of Mo loading', *Appl. Catal. A: Gen.* 207 (2001) 421.

[30] W. Ueda, K. Oshihara, 'Selective oxidation of light alkanes over hydrothermally synthesized Mo-V-M-O (M=Al, Ga, Bi, Sb, and Te) oxide catalysts', *Appl. Catal. A: Gen.* 200 (2000) 135.

[31] J.M. López Nieto, P. Botella, P. Concepción, A. Dejoz, M.I. Vázquez, 'Oxidative dehydrogenation of ethane on Te-containing MoVNbO catalysts', *Catal. Today* 91-92 (2004) 241.

[32] M.A. Bañares, S.J. Khatib, 'Structure-activity relationships in alumina-supported molybdena-vanadia catalysts for propane oxidative dehydrogenation', *Catal. Today* 96 (2004) 251.

[33] C. Liu, U.S. Ozkan, 'Effect of chlorine on redox and adsorption characteristics of Mo/Si:Ti catalysts in the oxidative dehydrogenation of ethane', *J. Mol. Cat. A: Chem.* 220 (2004) 53.

[34] E. Heracleous, A.A. Lemonidou, J.A. Lercher, ' Mechanistic features of the ethane oxidative dehydrogenation by in situ FTIR spectroscopy over a MoO_3/Al_2O_3 catalyst', *Appl. Catal. A: Gen.* 264 (2004) 73.

[35] S.M. Al-Zahrani, N.O. Elbashir, A.E. Abasaeed, M. Abdulwahed, 'Catalytic performance of chromium oxide supported on Al_2O_3 in oxidative dehyrogenation of isobutane to isobutene', *Ind. Eng. Chem. Res.* 40 (2001) 781.

[36] S. Wang, K. Murata, T. Hayakawa, S. Hamakawa, K. Suzuki, 'Dehyrogenation of ethane with carbon dioxide over supported chromium oxide catalysts', *Appl. Catal. A: Gen.* 196 (2000) 1.

[37] B. Grzybowska, J. Sloczynski, R. Grabowski, K. Kerommes, K. Wcislo, T. Bobinska, 'Oxidation of C_2-C_4 alkanes on chromium oxide/alumina and on Cr_2O_3 : catalytic and TPD studies', *Appl. Catal. A: Gen.* 209 (2001) 279.

[38] A. Jiménez-López, E. Rodríguez-Castellón, P. Maireles-Torres, L. Díaz, J. Mérida-Robles, 'Chromium oxide supported on zirconium- and lanthanum-doped mesoporous silica for oxidative dehyrogenation of propane', *Appl. Catal. A: Gen.* 218 (2001) 295.

[39] S.M. Al-Zahrani, B.Y. Jibril, A.E. Abasaeed, 'Selection of optimum chromium oxide-based catalysts for propane oxidehydrogenation', *Catal. Today* 81 (2003) 507.

[40] B.Y. Jibril, 'Propane oxidative hydrogenation over chromium oxide-based catalysts', *Appl. Catal. A: Gen.* 264 (2004) 193.

[41] B.Y. Jibril, S.M. Al-Zahrani, A.E. Abasaeed, R. Hughes, 'Propane oxidative hydrogenation on Cs-doped Cr-Mo-Al-O catalyst: kinetics and mechanism', *Chem. Eng. J.* 103 (2004) 59.

[42] Y. Bi, K. Zhen, R.X. Valenzuela, M. Jia, V.C. Corberán 'Oxidative dehydrogenation of isobutane over LaBaSm oxide catalyst- Influence of the addition of CO_2 in the feed', *Catal. Today* 61 (2000) 369.

[43] I. Takahara, W.-C. Chang, N. Mimura, M. Saito, 'Promoting effects of CO_2 dehydrogenation of propane over a SiO_2-supported Cr_2O_3 catalyst', *Catal. Today* 45 (1998) 55.

[44] O.V. Krylov, A.Kh. Mamedov, S.R. Mirzabekova, 'The regularities in the interaction of alkanes with CO_2 on oxide catalyst', *Catal. Today* 24 (1995) 371.

[45] N. Mimura, I. Takahara, M. Inaba, M. Okamoto, K. Murata, 'High performance Cr/H-ZSM-5 catalysts for oxidative dehydrogenation of ethane to ethylene with CO_2 as an oxidant', *Catal. Comm.* 3 (2002) 257.

[46] F. Dury, E.M. Gaigneaux, P. Ruiz, 'The active role of CO_2 at low temperature in oxidation processes: the case of the oxidative dehydrogetaion of propane on $NiMoO_4$ catalysts', *Appl. Catal. A: Gen.* 242 (2003) 187.

[47] S. Ge, C. Liu, S. Zhang, Z. Li, 'Effect of carbon dioxide on the reaction performance of oxidative dehydrogenation of *n*-butane over V-Mg-O catalyst', *Chem. Eng. J.* 94 (2003) 121.

[48] A. Hinz, B. Nilsson, A. Andersson, 'Simulation of transients in heterogeneous catalysis: a comparison of the step- and pulse-transient techniques for the study of hydrocarbon oxidation on metal oxide catalysts', *Chem. Eng. Sci.* 55 (2000) 4385.

[49] D. Creaser, B. Andersson, R.R. Hudgins, P.L. Silveston, 'Transient study of oxidative dehydrogenation of propane' , *Appl. Catal. A: Gen.* 187 (1999) 147.

[50] F. Genser, S. Pietrzyk, 'Oxidative dehydrogenation of propane on V_2O_5/TiO_2 catalysts under transient conditions', *Chem. Eng. Sci.* 54 (1999) 4315.

[51] D. Creaser, B. Andersson, R.R. Hudgins, P.L. Silveston, 'Cyclic operation of the oxidative dehydrogenation of propane' , *Chem. Eng. Sci.* 54 (1999) 4437.

[52] E.V. Kondratenko, O. Buyevskaya, M. Baerns, 'Mechanistic insights in the activation of oxygen on oxide catalysts for the oxidative dehydrogenation of ethane from pulse experiments and contact potential difference measurements' , *J. Mol. Cat. A: Chem.* 158 (2000) 199.

[53] R. Grabowski, S. Pietrzyk, J. Słoczyński, F. Genser, K. Wcisło, B. Grzybowska-Świerkosz, 'Kinetics of the propane oxidative dehydrogenation on vanadia/titania catalysts from steady-state and transient experiments', *Appl. Catal. A: Gen.* 232 (2002) 277.

[54] A.C. van Veen, D. Farrusseng, M. Rebeilleau, T. Decamp, A. Holzwarth, Y. Schuurman, C. Mirodatos, 'Acceleration in catalysts development by fast transient kinetic investigation', *J. Catal.* 216 (2003) 135.

[55] B. Silberova, R. Burch, A. Goguet, C. Hardacre, A. Holmen, 'Low-temperature oxidation reactions of ethane over a Pt/ Al_2O_3 catalyst', *J. Catal.* 219 (2003) 206.

[56] Hiden Analytical RC System Manuals, Warrington, 2000.

[57] M.E.Buckley (from Hiden Analytical Limited), Quadrupole Mass Spectrometry Lectures, Ankara, 2000.

[58] R.M. Smith, K.L. Busch, Understanding Mass Spectra-A Basic Approach, John Wiley & Sons, Inc., USA, 1999.

[59] B. Imelik, J.C. Vedrine, Catalyst Characterization-Physical Techniques for Solid Materials, Plenum Press, New York, 1994.

[60] J.A. Schwarz, C. Contescu, A. Contescu, 'Methods for Preparation of Catalytic Materials', *Chem. Rev.* 95 (1995) 477.

[61] S. Yaşyerli, Kimyasal Proseslerde Oluşan H_2S'ün Yenilenebilir Adsorbentler ile Tutulması, Gazi University, Turkey, 2001 PhD. Thesis.

[62] Y. Güçbilmez, Novel Mesoporous Materials, Middle East Technical University, Turkey, 2005 PhD. Thesis.

[63] MATLAB 6.5, Curve Fitting Toolbox User's Guide CD, 2001-2002, The Math Works, Inc.

[64] I.E. Wachs, Characterization of Catalytic Materials, Butterworth-Heinemann and Manning Publications Co., USA, 1992.

[65] Handbooks of Monochromatic XPS Spectra (DEMO version), Vol.1-The Elements and Native Oxides, XPS Internatiol Inc., www.xpsdata.com, June, 2005.

[66] G. Silversmit, D. Depla, H. Poelman, G.B. Marin, R. De Gryse, 'Determination of the V2p XPS binding energies for different vanadium oxidation states (V^{5+} to V^{0+})', *J. Electron. Spectrosc. Relat. Phenom.* 135 (2004) 167.

[67] Q. Zhang, Y. Wang, Y. Ohishi, T. Shishido, K. Takehira, 'Vanadium-containing MCM-41 for partial oxidation of lower alkanes', *J. Catal.* 202 (2001) 308.

[68] B. Solsona, T. Blasco, J.M. López Nieto, M.L. Peña, F. Rey, A. Vidal-Moya, 'Vanadium oxide supported Mesoporous MCM-41 as selective catalysts in the oxidative dehydrogenation of alkanes', *J. Catal.* 203 (2001) 443.

[69] M.J. Jia, R.X. Valenzuela, P. Amorós, D. Beltrán-Porter, J. El-Haskouri, M.D. Marcos, V. Cortés Corberán, 'Direct oxidation of isobutane to methacrolein over V-MCM-41 catalysts', *Catal. Today* 91-92 (2004) 43.

[70] G.E.P. Box, W.G. Hunter, J.S. Hunter, Statistics for Experimenters – An Introduction to Design, Data Analysis, and Model Building, John Wiley & Sons, Inc., USA, 1978.

[71] B. Liu, M. Terano, 'Investigation of the physico-chemical state and aggregation mechanism of surface Cr species on a Phillips CrO_x/SiO_2 catalyst by XPS and EPMA', *J. Mol. Catal. A: Chem.* 172 (2001) 227.

APPENDIX A

CALIBRATION DATA FOR MASS SPECTROMETER

A.1. The mass spectrometer cracking patterns for the system gases

The following data is obtained from the library of the Hiden Analytical HPR20 Mass Spectrometer's software 'MASsoft'.

C_2H_6

Mass	Intensity
28	100
27	33.3
30	26.2
26	23
25	4.2
12	4.6
14	3.4

C_2H_4

Mass	Intensity
28	100
27	64.8
26	62.3
25	11.7
14	6.3
24	3.7
13	3.5
29	2.2
12	2.1

CH_4

Mass	Intensity
16	100
15	85.8
14	15.6
13	7.7
2	3
12	2.4
17	1.2

CO

Mass	Intensity
28	100
12	4.5
16	0.9
14	0.6
29	1.1
30	0.2

CO_2

Mass	Intensity
44	100
28	11.4
16	8.5
12	6
45	1.3
22	1.2
46	0.4
13	0.1
29	0.1

He

Mass	Intensity
4	100
2	10

O_2

Mass	Intensity
32	100
16	11.4
34	0.4
33	0.1

A.2. Data of mass spectrometer calibration experiments

Table A.1. Mass spectrometer calibration data for C_2H_6 in He

		Ref.:*	*3.82*	*4.76*	*0.81*		*1.27*
Experiment	Mass	Mean	**28/30**	**28/29**	**29/30**	**15/30**	**27/30**
9.7% C_2H_6 90.3% He	4	1.478E-06	3.87	4.40	0.88	0.15	1.07
	15	3.537E-08					
	26	1.586E-07					
	27	2.482E-07					
	28	8.974E-07					
	29	2.039E-07					
	30	2.320E-07					
12.5% C_2H_6 87.5% He	4	1.376E-06	3.84	4.36	0.88	0.15	1.07
	15	4.277E-08					
	26	1.966E-07					
	27	3.101E-07					
	28	1.118E-06					
	29	2.566E-07					
	30	2.911E-07					
19.2% C_2H_6 80.8% He	4	1.275E-06	3.76	4.30	0.87	0.14	1.04
	15	5.431E-08					
	26	2.507E-07					
	27	3.983E-07					
	28	1.436E-06					
	29	3.339E-07					
	30	3.822E-07					
20% C_2H_6 80% He	4	1.120E-06	3.48	4.29	0.81	0.13	0.94
	15	6.527E-08					
	26	2.952E-07					
	27	4.746E-07					
	28	1.749E-06					
	29	4.073E-07					
	30	5.023E-07					
30% C_2H_6 70% He	4	9.062E-07	3.46	4.26	0.81	0.13	0.95
	15	7.598E-08					
	26	3.398E-07					
	27	5.480E-07					
	28	1.990E-06					
	29	4.666E-07					
	30	5.752E-07					

Table A.1. (Cont'd.)

		Ref.:*	*3.82*	*4.76*	*0.81*		*1.27*
Experiment	Mass	Mean	**28/30**	**28/29**	**29/30**	**15/30**	**27/30**
40% C_2H_6 60% He	4	7.286E-07	3.45	4.25	0.81	0.13	0.96
	15	8.780E-08					
	26	3.948E-07					
	27	6.342E-07					
	28	2.282E-06					
	29	5.371E-07					
	30	6.610E-07					
50% C_2H_6 50% He	4	5.686E-07	3.53	4.24	0.83	0.14	0.99
	15	1.026E-07					
	26	4.532E-07					
	27	7.245E-07					
	28	2.57E-06					
	29	6.064E-07					
	30	7.291E-07					
60% C_2H_6 40% He	4	4.442E-07	3.56	4.25	0.84	0.15	1.01
	15	1.177E-07					
	26	5.160E-07					
	27	8.213E-07					
	28	2.885E-06					
	29	6.789E-07					
	30	8.100E-07					
		Avr:	*3.62*	*4.30*	*0.84*	*0.14*	*1.01*

Table A.2. Mass spectrometer calibration data for C_2H_4 in He

			C_2H_4	C_2H_4	C_2H_4	C_2H_4/He	C_2H_4/He
		Ref.:*	*1.54*	*1.61*	*8.55*		
Experiment	Mass	Mean	**28/27**	**28/26**	**28/25**	**27/4**	**26/4**
9.3% C_2H_4 90.7% He	4	1.21E-06	1.90	2.04	13.31	0.28	0.26
	25	4.84E-08					
	26	3.15E-07					
	27	3.38E-07					
	28	6.44E-07					
	29	1.73E-08					
14.5%C_2H_4 85.5% He	4	1.65E-06	1.91	2.04	14.18	0.36	0.34
	25	7.97E-08					
	26	5.55E-07					
	27	5.94E-07					
	28	1.13E-06					
	29	2.86E-08					
21% C_2H_4 79% He	4	1.49E-06	1.98	2.18	16.24	0.66	0.60
	25	1.19E-07					
	26	8.88E-07					
	27	9.77E-07					
	28	1.94E-06					
	29	5.02E-08					
41% C_2H_4 59% He	4	9.86E-07	1.98	2.17	16.27	1.31	1.20
	25	1.57E-07					
	26	1.18E-06					
	27	1.29E-06					
	28	2.56E-06					
	29	6.64E-08					
51% C_2H_4 49% He	4	7.10E-07	1.95	2.13	15.56	2.08	1.90
	25	1.85E-07					
	26	1.35E-06					
	27	1.48E-06					
	28	2.88E-06					
	29	7.77E-08					

Table A.2. (Cont'd.)

			C_2H_4	C_2H_4	C_2H_4	C_2H_4/He	C_2H_4/He
		Ref.:*	*1.54*	*1.61*	*8.55*		
Experiment	Mass	Mean	**28/27**	**28/26**	**28/25**	**27/4**	**26/4**
60% C_2H_4 40% He	4	5.89E-07	1.93	2.10	15.03	2.68	2.46
	25	2.03E-07					
	26	1.45E-06					
	27	1.58E-06					
	28	3.05E-06					
	29	8.24E-08					
70% C_2H_4 30% He	4	4.44E-07	1.90	2.06	14.53	3.82	3.52
	25	2.21E-07					
	26	1.56E-06					
	27	1.69E-06					
	28	3.22E-06					
	29	8.84E-08					
		Avr:	*1.94*	*2.10*	*15.01*	*1.60*	*1.47*

Table A.3. Mass spectrometer calibration data for O_2 in He

				O_2	
		Ref.:*		*0.014*	O_2/He
Experiment	Mass	Mean	**28/32**	**16/32**	**32/4**
5% O_2 95% He	4	2.084E-06	0.96	0.12	0.07
	16	1.84E-08			
	28	1.43E-07			
	32	1.50E-07			
10% O_2 90% He	4	1.825E-06	0.25	0.07	0.22
	16	2.688E-08			
	28	1.004E-07			
	32	4.056E-07			
20% O_2 80% He	4	1.571E-06	0.10	0.06	0.48
	16	4.166E-08			
	28	7.118E-08			
	32	7.474E-07			
30% O_2 70% He	4	1.119E-06	0.05	0.05	0.86
	16	4.874E-08			
	28	5.146E-08			
	32	9.637E-07			
40% O_2 60% He	4	8.768E-07	0.04	0.05	1.28
	16	5.959E-08			
	28	4.246E-08			
	32	1.121E-06			
50% O_2 50% He	4	6.928E-07	0.03	0.06	1.81
	16	6.966E-08			
	28	3.641E-08			
	32	1.257E-06			
60% O_2 40% He	4	5.685E-07	0.02	0.06	2.54
	16	8.187E-08			
	28	3.242E-08			
	32	1.445E-06			
		Avr.:		*0.07*	

Table A.4. Mass spectrometer calibration data for CO_2 in He

			CO_2	CO_2	CO_2/He	CO_2/He
		Ref.:*	*11.76*	*8.77*		
Experiment	Mass	Mean	**44/16**	**44/28**	**44/4**	**28/4**
6.4% CO_2 93.6% He	4	1.070E-06	11.86	8.19	0.36	0.04
	16	3.207E-08				
	28	4.643E-08				
	44	3.804E-07				
9.4% CO_2 90.6% He	4	9.515E-07	11.74	8.88	0.44	0.05
	16	3.564E-08				
	28	4.712E-08				
	44	4.183E-07				
12.5% CO_2 87.5% He	4	4.736E-07	9.18	8.11	0.49	0.06
	16	2.549E-08				
	28	2.884E-08				
	44	2.339E-07				
15.8% CO_2 84.2% He	4	4.752E-07	9.66	8.73	0.60	0.07
	16	2.953E-08				
	28	3.267E-08				
	44	2.852E-07				
30% CO_2 70% He	4	1.090E-06	13.91	12.53	1.76	0.14
	16	1.375E-07				
	28	1.527E-07				
	44	1.913E-06				
40% CO_2 60% He	4	9.622E-07	13.75	13.88	2.29	0.17
	16	1.604E-07				
	28	1.589E-07				
	44	2.205E-06				
50% CO_2 50% He	4	7.256E-07	13.82	14.09	3.40	0.24
	16	1.785E-07				
	28	1.750E-07				
	44	2.466E-06				
60% CO_2 40% He	4	5.284E-07	14.16	14.40	5.22	0.36
	16	1.948E-07				
	28	1.916E-07				
	44	2.759E-06				
70% CO_2 40% He	4	3.232E-07	14.34	14.76	8.98	0.61
	16	2.025E-07				
	28	1.967E-07				
	44	2.903E-06				
		Avr:	*12.49*	*11.51*		

Table A.5. Mass spectrometer calibration data for CH_4 in He

			CH_4	CH_4	CH_4/He	CH_4/He
		Ref.:*	*1.17*	*6.41*		
Experiment	Mass	Mean	**16/15**	**16/14**	**16/4**	**15/4**
7.2% CH_4 92.1% He	4	1.643E-06	1.22	11.55	0.40	0.33
	14	5.673E-08				
	15	5.359E-07				
	16	6.551E-07				
	18	5.135E-08				
	28	3.134E-08				
10.9% CH_4 89.1% He	4	1.514E-06	1.22	11.99	0.51	0.42
	14	6.462E-08				
	15	6.331E-07				
	16	7.747E-07				
	18	3.110E-08				
	28	2.972E-08				
16.4% CH_4 83.6% He	4	1.433E-06	1.23	12.26	0.69	0.56
	14	8.039E-08				
	15	8.042E-07				
	16	9.856E-07				
	18	2.527E-08				
	28	2.892E-08				
20% CH_4 80% He	4	1.358E-06	1.22	12.38	1.16	0.95
	14	1.271E-07				
	15	1.287E-06				
	16	1.573E-06				
	18	4.354E-08				
	28	3.004E-08				
30% CH_4 70% He	4	1.245E-06	1.22	12.68	1.56	1.27
	14	1.532E-07				
	15	1.587E-06				
	16	1.943E-06				
	18	2.977E-08				
	28	2.824E-08				
39.5% CH_4 60.5% He	4	1.110E-06	1.23	13.01	2.12	1.72
	14	1.807E-07				
	15	1.911E-06				
	16	2.351E-06				
	18	2.415E-08				
	28	2.706E-08				

Table A.5. (Cont'd.)

			CH_4	CH_4	CH_4/He	CH_4/He
		Ref.:*	*1.17*	*6.41*		
Experiment	Mass	Mean	**16/15**	**16/14**	**16/4**	**15/4**
50% CH_4 50% He	4	9.680E-07	1.24	13.37	2.95	2.38
	14	2.133E-07				
	15	2.305E-06				
	16	2.852E-06				
	18	1.785E-08				
	28	2.537E-08				
60% CH_4 40% He	4	7.862E-07	1.24	13.61	4.35	3.50
	14	2.512E-07				
	15	2.753E-06				
	16	3.418E-06				
	18	1.708E-08				
	28	2.339E-08				
70% CH_4 30% He	4	6.063E-07	1.25	13.76	6.47	5.20
	14	2.851E-07				
	15	3.151E-06				
	16	3.923E-06				
	18	1.568E-08				
	28	2.250E-08				
80% CH_4 20% He	4	3.974E-07	1.25	13.83	11.40	9.14
	14	3.277E-07				
	15	3.631E-06				
	16	4.531E-06				
	18	1.541E-08				
	28	1.996E-08				
		Avr.:	*1.23*			

Table A.6. Mass spectrometer calibration data for O_2 - C_2H_6 - He

			C_2H_6	C_2H_6	C_2H_6	O_2	O_2/He
		Ref.:*	*3.82*	*1.27*	*0.8*	*8.77*	
Experiment	Mass	Mean	**28/30**	**27/30**	**29/30**	**32/16**	**32/4**
5% O_2 10% C_2H_6 85% He	4	1.34E-06	3.65	0.98	0.83	10.65	0.09
	16	1.10E-08					
	26	2.21E-07					
	27	3.53E-07					
	28	1.31E-06					
	29	3.00E-07					
	30	3.60E-07					
	32	1.18E-07					
10% O_2 20% C_2H_6 70% He	4	9.69E-07	3.64	1.00	0.84	13.56	0.24
	16	1.74E-08					
	26	2.64E-07					
	27	4.21E-07					
	28	1.54E-06					
	29	3.56E-07					
	30	4.22E-07					
	32	2.36E-07					
15% O_2 25% C_2H_6 60% He	4	8.00E-07	3.58	0.99	0.83	14.34	0.43
	16	2.41E-08					
	26	2.85E-07					
	27	4.53E-07					
	28	1.64E-06					
	29	3.83E-07					
	30	4.59E-07					
	32	3.45E-07					
20% O_2 30% C_2H_6 50% He	4	1.10E-06	3.94	1.03	0.86	16.63	0.67
	16	4.41E-08					
	26	1.45E-07					
	27	2.30E-07					
	28	8.76E-07					
	29	1.92E-07					
	30	2.22E-07					
	32	7.34E-07					

Table A.6. (Cont'd.)

			C_2H_6	C_2H_6	C_2H_6	O_2	O_2/He
		Ref.:*	*3.82*	*1.27*	*0.8*	*8.77*	
Experiment	Mass	Mean	**28/30**	**27/30**	**29/30**	**32/16**	**32/4**
	4	6.45E-07	3.75	1.02	0.86	17.97	1.78
	16	6.39E-08					
30% O_2	26	2.08E-07					
40% C_2H_6	27	3.28E-07					
30% He	28	1.21E-06					
	29	2.76E-07					
	30	3.21E-07					
	32	1.15E-06					
	4	1.98E-07	3.68	1.02	0.86	16.97	7.06
	16	8.25E-08					
40% O_2	26	2.49E-07					
50% C_2H_6	27	3.95E-07					
10% He	28	1.43E-06					
	29	3.35E-07					
	30	3.88E-07					
	32	1.40E-06					
		Avr.:	*3.71*	*1.01*	*0.85*	*15.02*	

A.3. Data of mass spectrometer calibration experiments - check after blocking of capillary

Table A.7. Mass spectrometer calibration data for C_2H_6 in He (check-empty reactor)

		Ref.:*	*3.82*	*4.76*	*0.81*	*1.27*
Experiment	Mass	Mean	**28/30**	**28/29**	**29/30**	**27/30**
6.7% C_2H_6 93.3% He	4	1.093E-06	5.29	5.85	0.90	1.08
	26	8.360E-08				
	27	1.303E-07				
	28	6.358E-07				
	29	1.086E-07				
	30	1.202E-07				
13.5% C_2H_6 86.5% He	4	1.061E-06	4.73	5.32	0.89	1.05
	26	1.164E-07				
	27	1.839E-07				
	28	8.278E-07				
	29	1.555E-07				
	30	1.751E-07				
19.7% C_2H_6 80.3% He	4	9.774E-07	4.47	5.06	0.88	1.05
	26	1.469E-07				
	27	2.339E-07				
	28	9.964E-07				
	29	1.968E-07				
	30	2.229E-07				
29.8% C_2H_6 70.2% He	4	8.175E-07	4.03	4.65	0.87	1.01
	26	2.331E-07				
	27	3.747E-07				
	28	1.495E-06				
	29	3.217E-07				
	30	3.710E-07				
40.6% C_2H_6 59.4% He	4	7.049E-07	3.88	4.52	0.86	1.00
	26	2.777E-07				
	27	4.495E-07				
	28	1.751E-06				
	29	3.874E-07				
	30	4.510E-07				

Table A.7. (Cont'd.)

		Ref.:*	*3.82*	*4.76*	*0.81*	*1.27*
Experiment	Mass	Mean	**28/30**	**28/29**	**29/30**	**27/30**
49.6% C_2H_6 50.4% He	4	5.814E-07	3.82	4.44	0.86	1.00
	26	3.126E-07				
	27	5.038E-07				
	28	1.925E-06				
	29	4.334E-07				
	30	5.037E-07				
60.3% C_2H_6 39.7% He	4	4.302E-07	3.80	4.40	0.86	1.02
	26	3.489E-07				
	27	5.595E-07				
	28	2.087E-06				
	29	4.744E-07				
	30	5.491E-07				
		Avr.:	*4.29*	*4.89*	*0.87*	*1.03*

Table A.8. Mass spectrometer calibration data for C_2H_6 in He
(check - reactor filled with Cr-O catalyst)

		Ref.:*	*0.81*	*1.27*		*0.027*	*0.176*
Experiment	Mass	Mean	**29/30**	**27/30**	**15/30**	**2/30**	**12/30**
7.1% C_2H_6 92.9% He	4	1.12E-06	0.88	1.05	0.16	0.06	0.03
	2	8.46E-09					
	12	4.03E-09					
	15	2.17E-08					
	26	9.06E-08					
	27	1.43E-07					
	28	6.46E-07					
	29	1.19E-07					
	30	1.35E-07					
13.8% C_2H_6 86.2% He	4	1.06E-06	0.87	1.04	0.15	0.05	0.02
	2	1.05E-08					
	12	3.21E-09					
	15	2.87E-08					
	26	1.26E-07					
	27	2.00E-07					
	28	8.47E-07					
	29	1.68E-07					
	30	1.93E-07					
20.6% C_2H_6 79.4% He	4	9.80E-07	0.86	1.03	0.15	0.05	0.02
	2	1.24E-08					
	12	4.90E-09					
	15	3.79E-08					
	26	1.63E-07					
	27	2.61E-07					
	28	1.06E-06					
	29	2.20E-07					
	30	2.55E-07					
31.3% C_2H_6 68.7% He	4	7.90E-07	0.87	1.01	0.15	0.04	0.02
	2	1.63E-08					
	12	5.99E-09					
	15	5.56E-08					
	26	2.40E-07					
	27	3.86E-07					
	28	1.49E-06					
	29	3.32E-07					
	30	3.82E-07					

Table A.8. (Cont'd.)

		Ref.:*	*0.81*	*1.27*		*0.027*	*0.176*
Experiment	Mass	Mean	**29/30**	**27/30**	**15/30**	**2/30**	**12/30**
38% C_2H_6 62% He	4	6.84E-07	0.85	0.99	0.14	0.04	0.02
	2	1.83E-08					
	12	7.43E-09					
	15	6.33E-08					
	26	2.73E-07					
	27	4.40E-07					
	28	1.68E-06					
	29	3.79E-07					
	30	4.46E-07					
51.2% C_2H_6 48.8% He	4	5.52E-07	0.85	1.00	0.14	0.04	0.01
	2	1.89E-08					
	12	6.41E-09					
	15	7.06E-08					
	26	3.06E-07					
	27	4.92E-07					
	28	1.84E-06					
	29	4.21E-07					
	30	4.94E-07					
57.9% C_2H_6 42.1% He	4	4.18E-07	0.86	1.01	0.15	0.04	0.01
	2	2.18E-08					
	12	6.88E-09					
	15	7.86E-08					
	26	3.38E-07					
	27	5.41E-07					
	28	1.99E-06					
	29	4.56E-07					
	30	5.34E-07					
		Avr.:	*0.86*	*1.02*	*0.15*	*0.05*	*0.02*

Table A.9. Mass spectrometer calibration data for C_2H_4 in He
(check- empty reactor)

			C_2H_4	C_2H_4	C_2H_4	C_2H_4
		Ref.:*	*1.54*	*1.61*	*8.55*	*0.03*
Experiment	Mass	Mean	**28/27**	**28/26**	**28/25**	**12/27**
10.4% C_2H_4 89.6% He	4	1.154E-06	2.38	2.59	18.73	0.02
	12	6.226E-09				
	25	3.269E-08				
	26	2.368E-07				
	27	2.573E-07				
	28	6.122E-07				
	29	1.531E-08				
15.3% C_2H_4 84.7% He	4	1.073E-06	2.23	2.44	16.87	0.03
	12	9.208E-09				
	25	4.485E-08				
	26	3.098E-07				
	27	3.385E-07				
	28	7.565E-07				
	29	1.965E-08				
21% C_2H_4 79% He	4	1.025E-06	2.15	2.35	16.64	0.02
	12	9.460E-09				
	25	5.616E-08				
	26	3.979E-07				
	27	4.347E-07				
	28	9.345E-07				
	29	2.314E-08				
29% C_2H_4 71% He	4	9.255E-07	2.06	2.24	16.26	0.02
	12	1.239E-08				
	25	8.240E-08				
	26	5.993E-07				
	27	6.508E-07				
	28	1.340E-06				
	29	3.320E-08				

Table A.9. (Cont'd.)

			C_2H_4	C_2H_4	C_2H_4	C_2H_4
		Ref.:*	*1.54*	*1.61*	*8.55*	*0.03*
Experiment	Mass	Mean	**28/27**	**28/26**	**28/25**	**12/27**
40.6% C_2H_4 59.4% He	4	7.555E-07	2.05	2.25	16.97	0.01
	12	1.119E-08				
	25	9.032E-08				
	26	6.820E-07				
	27	7.478E-07				
	28	1.533E-06				
	29	3.816E-08				
48% C_2H_4 52% He	4	6.704E-07	2.04	2.25	16.98	0.02
	12	1.416E-08				
	25	1.070E-07				
	26	8.087E-07				
	27	8.893E-07				
	28	1.817E-06				
	29	4.677E-08				
61.2% C_2H_4 38.8% He	4	4.902E-07	2.02	2.23	16.77	0.01
	12	1.615E-08				
	25	1.326E-07				
	26	9.995E-07				
	27	1.101E-06				
	28	2.224E-06				
	29	5.849E-08				
		Avr.:	*2.13*	*2.33*	*17.03*	*0.02*

Table A.10. Mass spectrometer calibration data for O_2 in He
(check - reactor filled with Cr-O catalyst)

				O_2	O_2/He
		Ref.:*		*0.014*	
Experiment	Mass	Mean	**28/32**	**16/32**	**32/4**
5% O_2 95% He	4	1.024E-06	1.33	0.09	0.09
	16	8.254E-09			
	28	1.270E-07			
	32	9.571E-08			
9.5% O_2 90.5% He	4	9.105E-07	0.68	0.07	0.19
	16	1.152E-08			
	28	1.171E-07			
	32	1.724E-07			
20.2% O_2 79.8% He	4	7.864E-07	0.36	0.06	0.42
	16	2.067E-08			
	28	1.179E-07			
	32	3.297E-07			
29.9% O_2 70.1% He	4	6.856E-07	0.24	0.06	0.71
	16	2.951E-08			
	28	1.173E-07			
	32	4.849E-07			
40.4% O_2 59.6% He	4	5.568E-07	0.18	0.06	1.16
	16	3.812E-08			
	28	1.156E-07			
	32	6.476E-07			
50.5% O_2 49.5% He	4	4.151E-07	0.14	0.06	1.76
	16	4.460E-08			
	28	1.038E-07			
	32	7.313E-07			
60% O_2 40% He	4	3.032E-07	0.12	0.06	2.51
	16	4.846E-08			
	28	9.100E-08			
	32	7.600E-07			
		Avr.:		*0.07*	

Table A.11. Mass spectrometer calibration data for CO_2 in He
(check - reactor filled with Cr-O catalyst)

			CO_2	CO_2	CO_2/He	CO_2	CO_2/He
		Ref.:*	*11.76*	*8.77*		*0.06*	
Experiment	Mass	Mean	**44/16**	**44/28**	**44/4**	**12/44**	**28/4**
3.4% CO_2 96.6% He	4	9.835E-07	10.33	1.57	0.22	0.04	0.14
	12	9.308E-09					
	16	2.124E-08					
	28	1.399E-07					
	44	2.194E-07					
7% CO_2 93% He	4	9.302E-07	10.97	1.90	0.28	0.04	0.14
	12	9.489E-09					
	16	2.390E-08					
	28	1.380E-07					
	44	2.621E-07					
10.6% CO_2 89.4% He	4	8.922E-07	11.46	2.28	0.36	0.03	0.16
	12	1.085E-08					
	16	2.802E-08					
	28	1.406E-07					
	44	3.212E-07					
14.1% CO_2 85.9% He	4	8.706E-07	11.72	2.68	0.43	0.03	0.16
	12	1.294E-08					
	16	3.212E-08					
	28	1.403E-07					
	44	3.764E-07					
21.3% CO_2 78.7% He	4	8.365E-07	12.10	3.45	0.61	0.03	0.18
	12	1.586E-08					
	16	4.216E-08					
	28	1.478E-07					
	44	5.100E-07					
24.8% CO_2 75.2% He	4	8.045E-07	12.34	3.90	0.74	0.03	0.19
	12	1.833E-08					
	16	4.818E-08					
	28	1.526E-07					
	44	5.944E-07					

Table A.11. (Cont'd.)

			CO_2	CO_2	CO_2/He	CO_2	CO_2/He
		Ref.:*	*11.76*	*8.77*		*0.06*	
Experiment	Mass	Mean	**44/16**	**44/28**	**44/4**	**12/44**	**28/4**
29.2% CO_2 70.8% He	4	7.711E-07	12.50	4.42	0.91	0.03	0.21
	12	2.078E-08					
	16	5.645E-08					
	28	1.595E-07					
	44	7.054E-07					
39.5% CO_2 60.5% He	4	6.692E-07	12.98	5.63	1.44	0.03	0.26
	12	2.626E-08					
	16	7.443E-08					
	28	1.715E-07					
	44	9.660E-07					
45.6% CO_2 54.4% He	4	6.024E-07	13.12	6.35	1.87	0.03	0.29
	12	3.013E-08					
	16	8.604E-08					
	28	1.777E-07					
	44	1.129E-06					
		Avr.:	*11.9*			*0.03*	

Table A.12. Mass spectrometer calibration data for CH_4 in He

(check – empty reactor)

			CH_4	CH_4	CH_4/He		CH_4/He
		Ref.:*	*1.17*	*6.41*			
Experiment	Mass	Mean	**16/15**	**16/14**	**16/4**	**12/15**	**15/4**
4.5% CH_4 95.5% He	4	8.179E-07	1.22	9.26	0.26	0.03	0.21
	12	4.405E-09					
	14	2.286E-08					
	15	1.735E-07					
	16	2.117E-07					
	28	7.789E-08					
11% CH_4 89% He	4	8.330E-07	1.23	9.80	0.30	0.02	0.24
	12	4.746E-09					
	14	2.515E-08					
	15	2.011E-07					
	16	2.464E-07					
	28	8.045E-08					
15% CH_4 85% He	4	7.838E-07	1.22	10.74	0.49	0.02	0.40
	12	6.331E-09					
	14	3.575E-08					
	15	3.142E-07					
	16	3.841E-07					
	28	7.665E-08					
20% CH_4 80% He	4	7.477E-07	1.22	11.21	0.68	0.02	0.56
	12	7.568E-09					
	14	4.547E-08					
	15	4.184E-07					
	16	5.097E-07					
	28	7.410E-08					
30% CH_4 70% He	4	7.300E-07	1.23	11.95	0.94	0.02	0.76
	12	8.925E-09					
	14	5.726E-08					
	15	5.563E-07					
	16	6.840E-07					
	28	7.625E-08					
41% CH_4 59% He	4	6.004E-07	1.23	12.46	1.83	0.02	1.50
	12	1.399E-08					
	14	8.835E-08					
	15	8.977E-07					
	16	1.101E-06					
	28	7.422E-08					

Table A.12. (Cont'd.)

			CH_4	CH_4	CH_4/He		CH_4/He
		Ref.:*	*1.17*	*6.41*			
Experiment	Mass	Mean	**16/15**	**16/14**	**16/4**	**12/15**	**15/4**
50% CH_4 50% He	4	5.517E-07	1.23	12.74	2.27	0.01	1.85
	12	1.419E-08					
	14	9.831E-08					
	15	1.019E-06					
	16	1.252E-06					
	28	7.281E-08					
60% CH_4 40% He	4	4.516E-07	1.24	13.21	3.52	0.01	2.85
	12	1.741E-08					
	14	1.204E-07					
	15	1.288E-06					
	16	1.591E-06					
	28	7.124E-08					
70% CH_4 30% He	4	3.586E-07	1.24	13.38	5.18	0.01	4.18
	12	2.042E-08					
	14	1.389E-07					
	15	1.500E-06					
	16	1.858E-06					
	28	7.043E-08					
		Avr.:	*1.23*	*11.64*		*0.018*	

Table A.13. Mass spectrometer calibration data for CO in He (empty reactor)

			CO	CO
		Ref.:*	*22.2*	*4.1*
Experiment	Mass	Mean	**28/12**	**12/29**
5%CO 95% He	4	9.439E-07	51.00	1.13
	12	4.216E-09		
	28	2.150E-07		
	29	3.717E-09		
10.4%CO 89.6% He	4	9.984E-07	49.07	1.17
	12	7.901E-09		
	28	3.877E-07		
	29	6.748E-09		
15.5%CO 84.5% He	4	8.591E-07	59.28	1.13
	12	8.289E-09		
	28	4.914E-07		
	29	7.327E-09		
19.3%CO 80.7% He	4	8.452E-07	59.82	1.12
	12	9.807E-09		
	28	5.867E-07		
	29	8.725E-09		
30%CO 70% He	4	7.531E-07	60.90	1.17
	12	1.247E-08		
	28	7.594E-07		
	29	1.063E-08		
42%CO 58% He	4	6.325E-07	62.09	1.16
	12	1.704E-08		
	28	1.058E-06		
	29	1.467E-08		
		Avr.:	*57.03*	*1.15*

Table A.14. Mass spectrometer calibration data for H_2 in He
(reactor filled with Cr-O catalyst)

			H_2	H_2/He
		Ref.:*	*0.1*	
Experiment	Mass	Mean	**1/2**	**2/4**
8%H_2 92% He	1	6.350E-07	1.67	0.42
	2	3.806E-07		
	4	9.070E-07		
10.2% H_2 89.8% He	1	7.147E-07	1.53	0.52
	2	4.686E-07		
	4	9.047E-07		
16%H_2 84% He	1	1.064E-06	1.39	0.92
	2	7.664E-07		
	4	8.311E-07		
20%H_2 80% He	1	1.245E-06	1.27	1.15
	2	9.834E-07		
	4	8.524E-07		
24%H_2 76% He	1	1.445E-06	1.23	1.39
	2	1.174E-06		
	4	8.455E-07		
31% H_2 69% He	1	1.834E-06	1.17	1.93
	2	1.561E-06		
	4	8.072E-07		
38%H_2 62% He	1	2.170E-06	1.13	2.56
	2	1.926E-06		
	4	7.510E-07		

* Reference data were obtained from the library of the Hiden Analytical HPR20 Mass Spectrometer's software 'MASsoft'.

A.4. MS Calibration Charts – with Mean Values

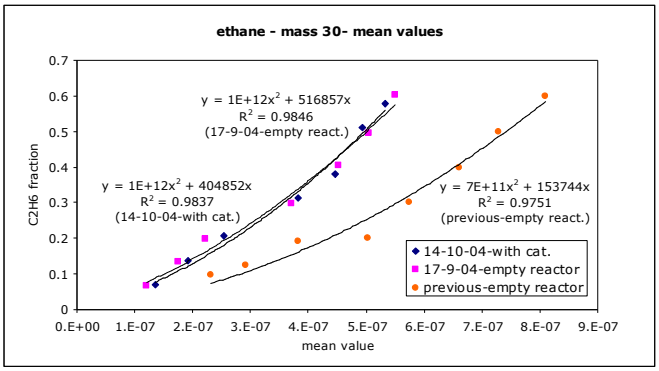

C_2H_6-mass 30

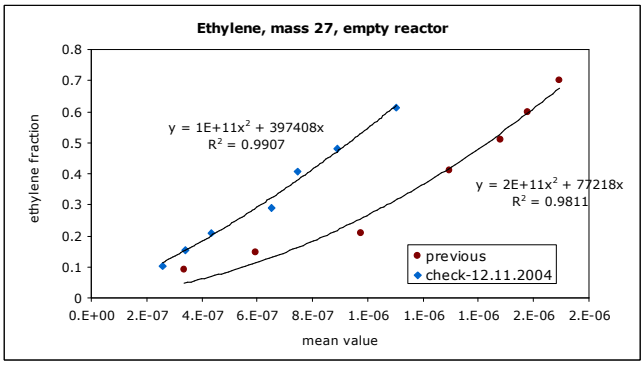

C_2H_4-mass 27

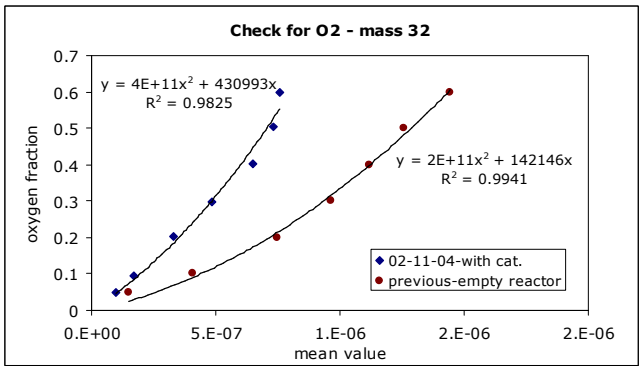

O_2-mass 32

Figure A.4.1. Mass spectrometer calibration data with mean values

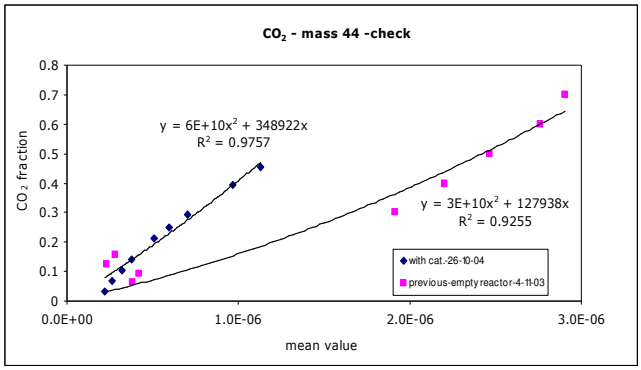

CO_2-mass 44

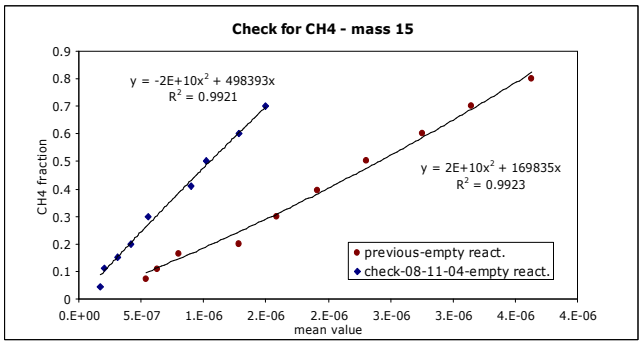

CH_4-mass 15

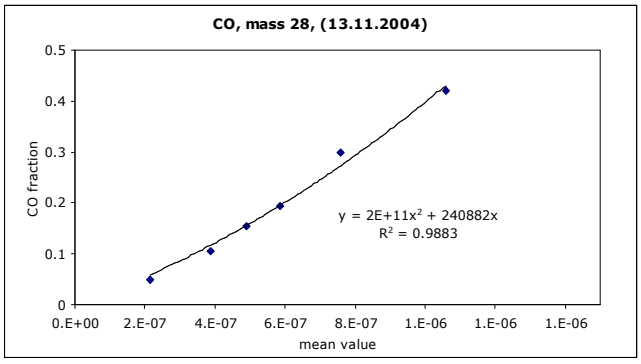

CO-mass 28

Figure A.4.1. (Cont'd.)

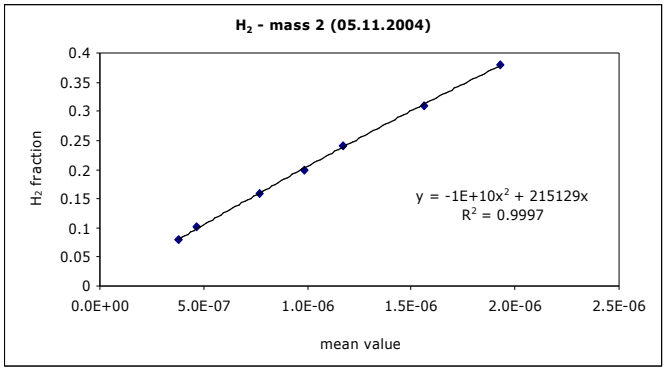

H_2-mass 2

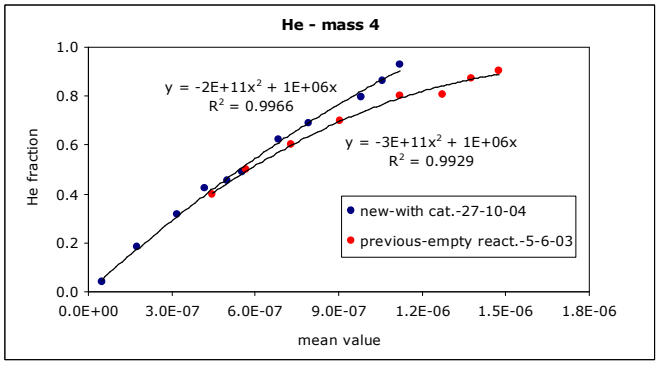

He-mass 4

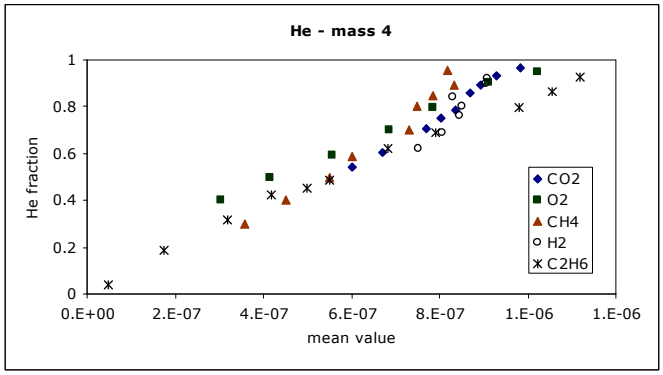

He-mass 4
(with data of various gases)

Figure A.4.1. (Cont'd.)

A.5. MS Calibration Charts – with Normalized Mean Values

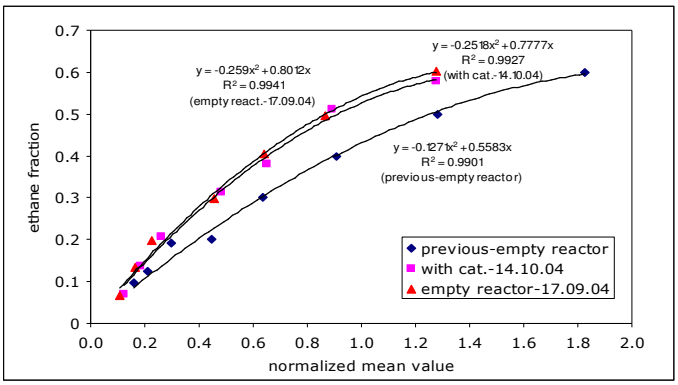

C_2H_6-mass 30

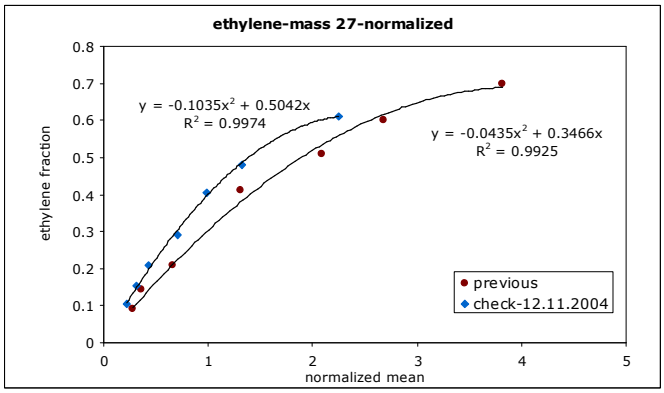

C_2H_4-mass 27

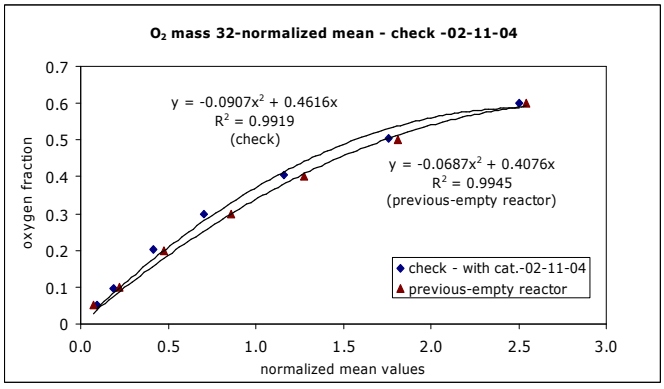

O_2-mass 32

Figure A.5.1. Mass spectrometer calibration data with normalized mean values

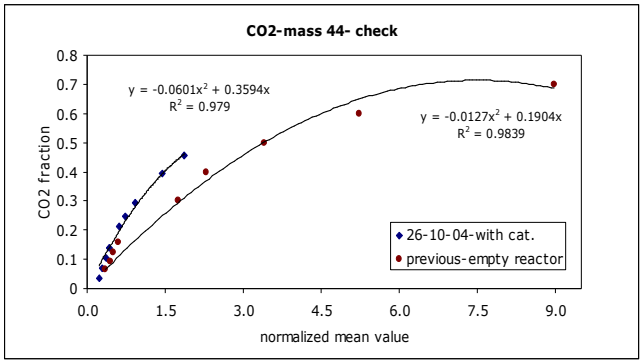

CO_2-mass 44

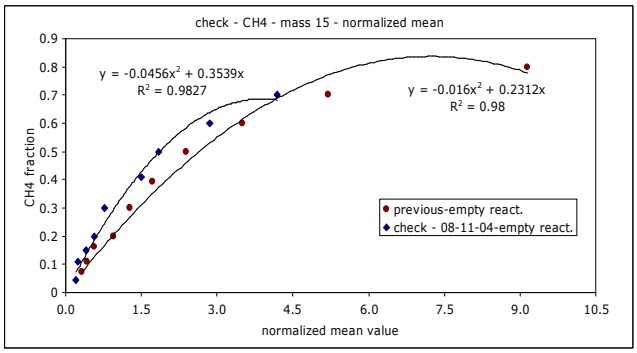

CH_4-mass 15

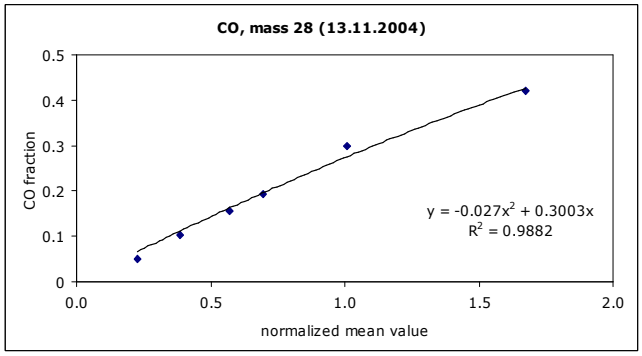

CO-mass 28

Figure A.5.1. (Cont'd.)

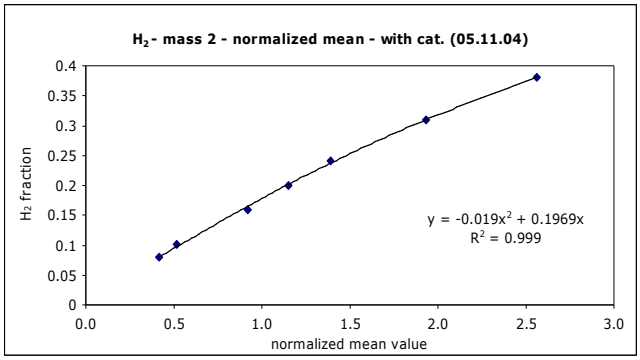

H_2-mass 2

Figure A.5.1. (Cont'd.)

APPENDIX B

DEFINITIONS OF 'GOODNESS OF FIT STATISTICS' FOR MATLAB 6.5 CURVE FITS

'**Sum of Squares Due to Error (SSE):** This statistic measures the total deviation of the response values from the fit to the response values. A value closer to 0 indicates a better fit.

R-Square: This statistic measures how successful the fit is in explaining the variation of the data. Put another way, R-square is the square of the correlation between the response values and the predicted response values. R-square can take on any value between 0 and 1, with a value closer to 1 indicating a better fit. For example, an R^2 value of 0.8234 means that the fit explains 82.34% of the total variation in the data about the average.

Degrees of Freedom Adjusted R-Square: This statistic uses the R-square statistic defined above, and adjusts it based on the residual degrees of freedom. The adjusted R-square statistic can take on any value less than or equal to 1, with a value closer to 1 indicating a better fit.

Root Mean Squared Error (RMSE): This statistic is also known as the fit standard error and the standard error of the regression. A *RMSE* value closer to 0 indicates a better fit.' [63]

APPENDIX C

EXPERIMENTAL DATA FOR STEADY-STATE EXPERIMENTS

C.1. Experimental data for Cr-O catalyst

Table C.1. Experimental data for Cr-O catalyst with ~5% O_2 - 30% C_2H_6 – 65% He feed composition

T (^oC)	X_{total}	$S_{ethylene}$	$Y_{ethylene}$	S_{CO2}	S_{CH4}
148	0	0	0	0	0
249	0.03	0.82	0.02	0.17	0.014
300	0.13	0.78	0.10	0.16	0.052
346	0.17	0.77	0.13	0.170	0.050
400	0.16	0.79	0.13	0.15	0.05
447	0.19	0.82	0.16	0.130	0.050

Table C.2. Experimental data for Cr-O catalyst with ~10% O_2 - 30% C_2H_6 – 60% He feed composition

T (^oC)	X_{total}	$S_{ethylene}$	$Y_{ethylene}$	S_{CO2}	S_{CH4}	S_{CO}
250	0.11	0.91	0.10	0.036	0.054	0.000
299	0.23	0.67	0.15	0.25	0.051	0.026
350	0.28	0.72	0.20	0.200	0.059	0.019
399	0.29	0.72	0.21	0.20	0.062	0.019

Table C.3. Experimental data for variation of O_2 mole fraction in feed with Cr-O catalyst (T = ~250°C)

Feed O_2	X_{total}	$S_{ethylene}$	$Y_{ethylene}$
0.05	0.03	0.82	0.02
0.10	0.11	0.91	0.1
0.15	0.16	0.19	0.03

Table C.4. Experimental data for Cr-O catalyst with ~10% CO_2 - 30% C_2H_6 – 60% He feed composition

T (°C)	X_{total}	$S_{ethylene}$	$Y_{ethylene}$	S_{CH4}
250	0.10	0.94	0.10	0.064
300	0.16	0.93	0.15	0.070
349	0.15	0.93	0.14	0.072
449	0.16	0.93	0.15	0.072

C.2. Experimental data for Cr-V-O catalyst

Table C.5. Experimental data for Cr-V-O catalyst with ~5% O_2 - 30% C_2H_6 – 65% He feed composition

T (°C)	X_{total}	$S_{ethylene}$	$Y_{ethylene}$	S_{CO2}	S_{CH4}	S_{CO}
150	0.044	0.573	0.025	0	0.012	0.415
200.3	0.028	0.806	0.023	0.007	0.028	0.160
250	0.035	0.930	0.033	0.028	0.039	0.000
299.7	0.033	0.940	0.031	0.024	0.034	0.000
350.4	0.028	0.816	0.023	0.034	0.014	0.136
399	0.043	0.845	0.036	0.032	0.032	0.091
449	0.067	0.520	0.035	0.056	0.011	0.417
499	0.124	0.576	0.071	0.052	0.020	0.352
525	0.135	0.668	0.090	0.068	0.021	0.243

Table C.6. Experimental data for Cr-V-O catalyst with ~10% O_2 - 30% C_2H_6 – 60% He feed composition

T (°C)	X_{total}	$S_{ethylene}$	$Y_{ethylene}$	S_{CO2}	S_{CH4}	S_{CO}
150.9	0.053	0.98	0.052	0.009	0.012	0
200.1	0.05	0.965	0.051	0.015	0.020	0
248.4	0.059	0.950	0.056	0.012	0.036	0
300.4	0.059	0.950	0.056	0.020	0.028	0
349.2	0.068	0.937	0.064	0.025	0.038	0
399.6	0.097	0.926	0.090	0.036	0.038	0
448.2	0.220	0.620	0.136	0.042	0.025	0.310
496.9	0.200	0.500	0.100	0.060	0.025	0.421

Table C.7. Experimental data for Cr-V-O catalyst with ~10% CO_2 - 30% C_2H_6 – 60% He feed composition

T (°C)	X_{total}	$S_{ethylene}$	$Y_{ethylene}$	S_{CH4}
200.7	0.028	0.959	0.027	0.0411
250.8	0.0054	1	0.0054	0
299.6	0.012	0.968	0.012	0.032
350.4	0.023	0.912	0.021	0.088
401.4	0.0197	0.947	0.019	0.053
450.5	0.038	0.94	0.035	0.060
500.6	0.032	0.947	0.03	0.053
549	0.032	0.97	0.031	0.030
592	0.019	1	0.019	0

Table C.8. Experimental data for Cr-V-O catalyst with ~45% CO_2 - 30% C_2H_6 – 25% He feed composition

T (°C)	X_{total}	$S_{ethylene}$	$Y_{ethylene}$
350.9	0.015	0.969	0.0145
401.5	0.007	0.896	0.006
450	0.001	1.000	0.001
500.3	0.005	1.000	0.005

C.3. Experimental data for V-MCM-41 catalyst

Table C.9. Experimental data for V-MCM-41 catalyst with ~5% O_2 - 30% C_2H_6 – 65% He feed composition

T (°C)	X_{total}	$S_{ethylene}$	$Y_{ethylene}$	S_{CO2}	S_{CO}
151.7	0.042	0	0.000	0.000	1.000
200.6	0.023	0.270	0.006	0.045	0.682
249.4	0.020	0.200	0.004	0.038	0.760
302	0.020	0.364	0.007	0.026	0.610
349.9	0.016	0.415	0.007	0.038	0.547
400.8	0.021	0.771	0.016	0.100	0.128
449.8	0.026	0.667	0.017	0.044	0.289
499.8	0.033	0.811	0.027	0.117	0.306

APPENDIX D

EXPERIMENTAL DATA FOR DYNAMIC EXPERIMENTS

D.1. Dynamic Experiments' Data for Cr-O Catalyst

D.1.1. Dynamic Experiments' Data for Cr-O Catalyst with C_2H_6 Pulses into O_2 and He Flow at 350°C

The response data for C_2H_6 pulses into O_2 and He flow over Cr-O catalyst at 350°C are presented in Figures D.1.1-D.1.4. The Gaussian fits and de-convolution of Gaussian fits for CO_2 and H_2O response data are given in Figures D.1.5 and D.1.6, respectively. The results of moment, variance, mean residence time, and standard deviation calculations for C_2H_6, C_2H_4, CO_2, and H_2O are tabulated in Tables D.1-D.4.

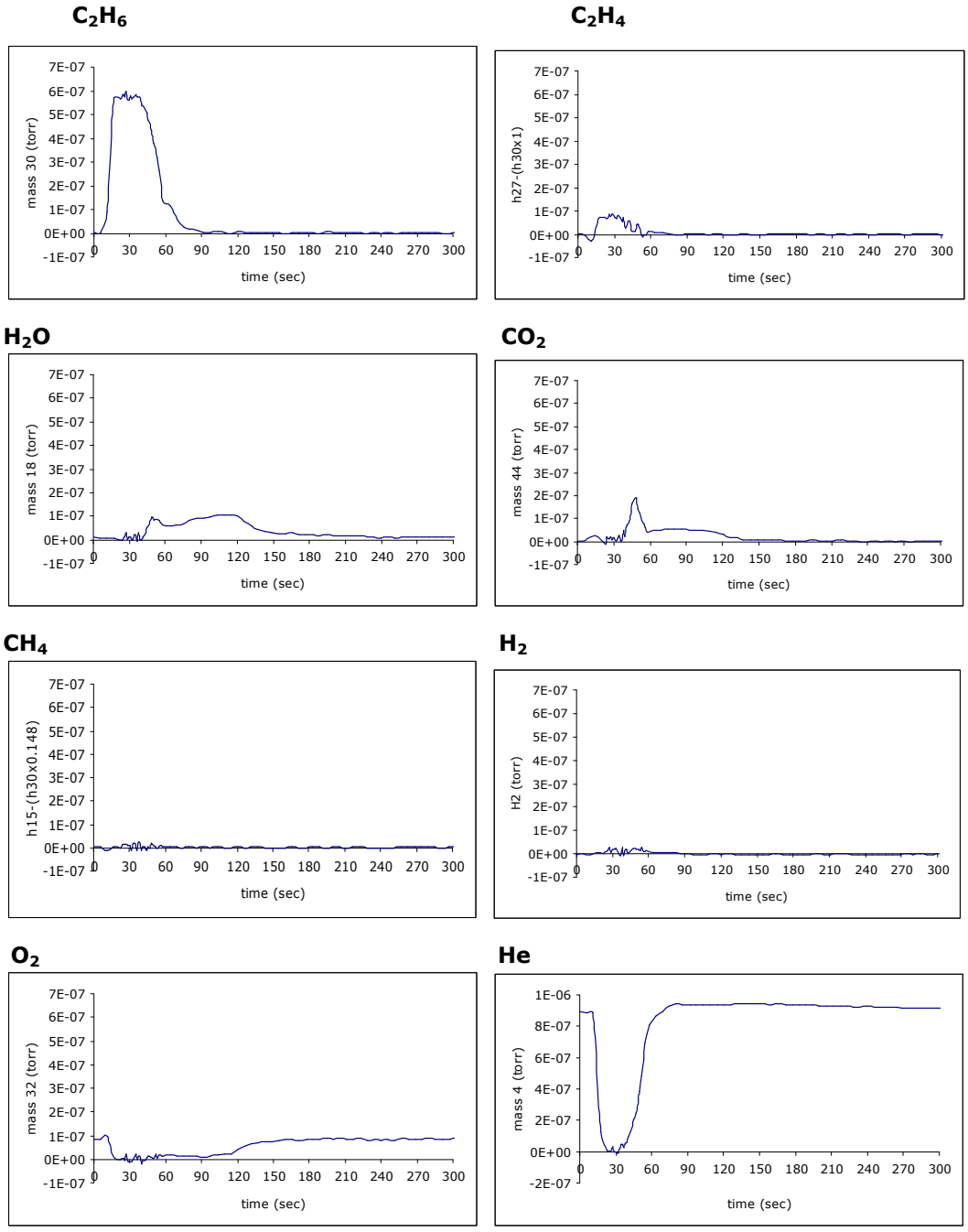

Figure D.1.1. 'Pulse 1' response data for C_2H_6 pulses into O_2 and He flow over Cr-O catalyst at 350°C

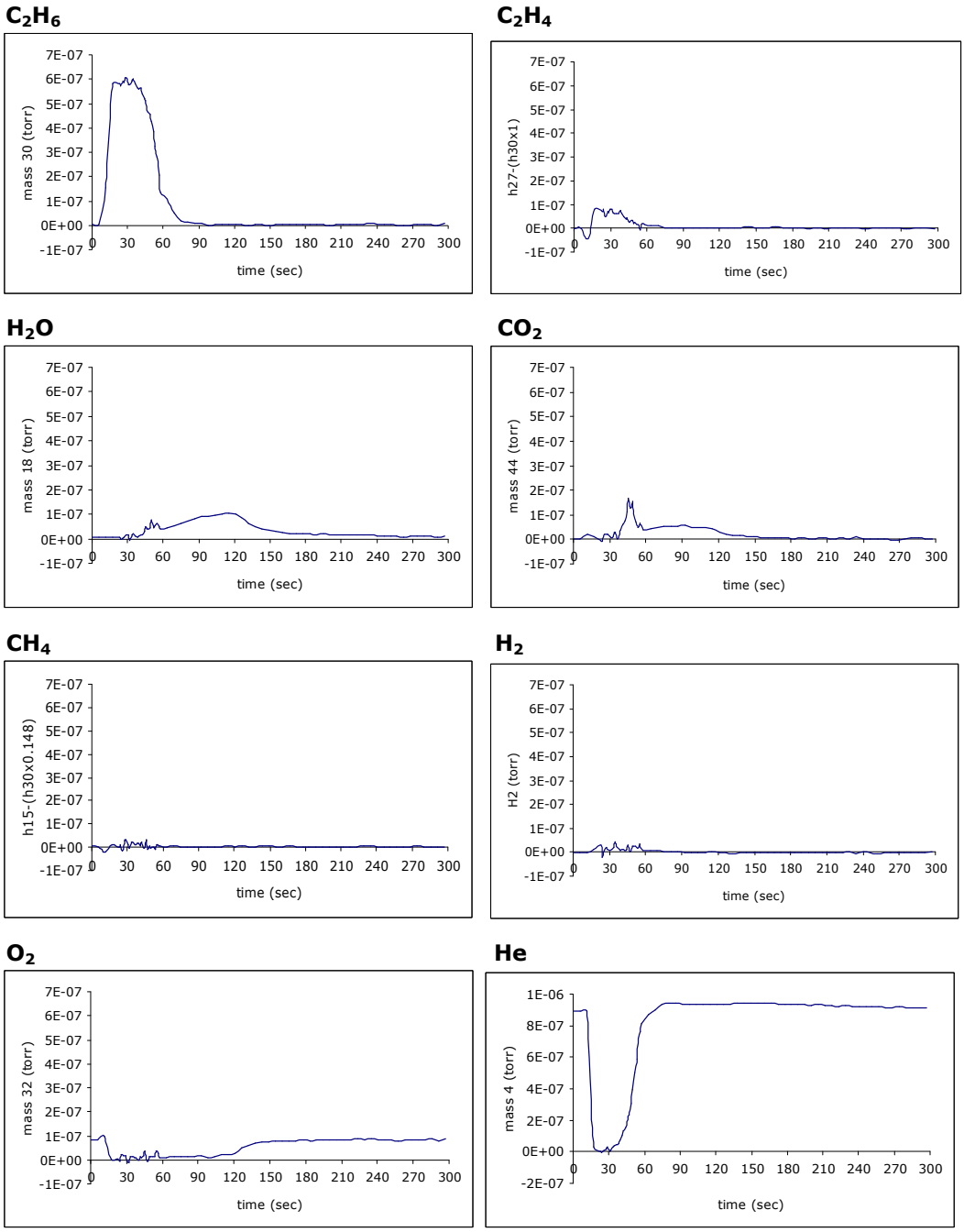

Figure D.1.2. 'Pulse 2' response data for C_2H_6 pulses into O_2 and He flow over Cr-O catalyst at 350°C

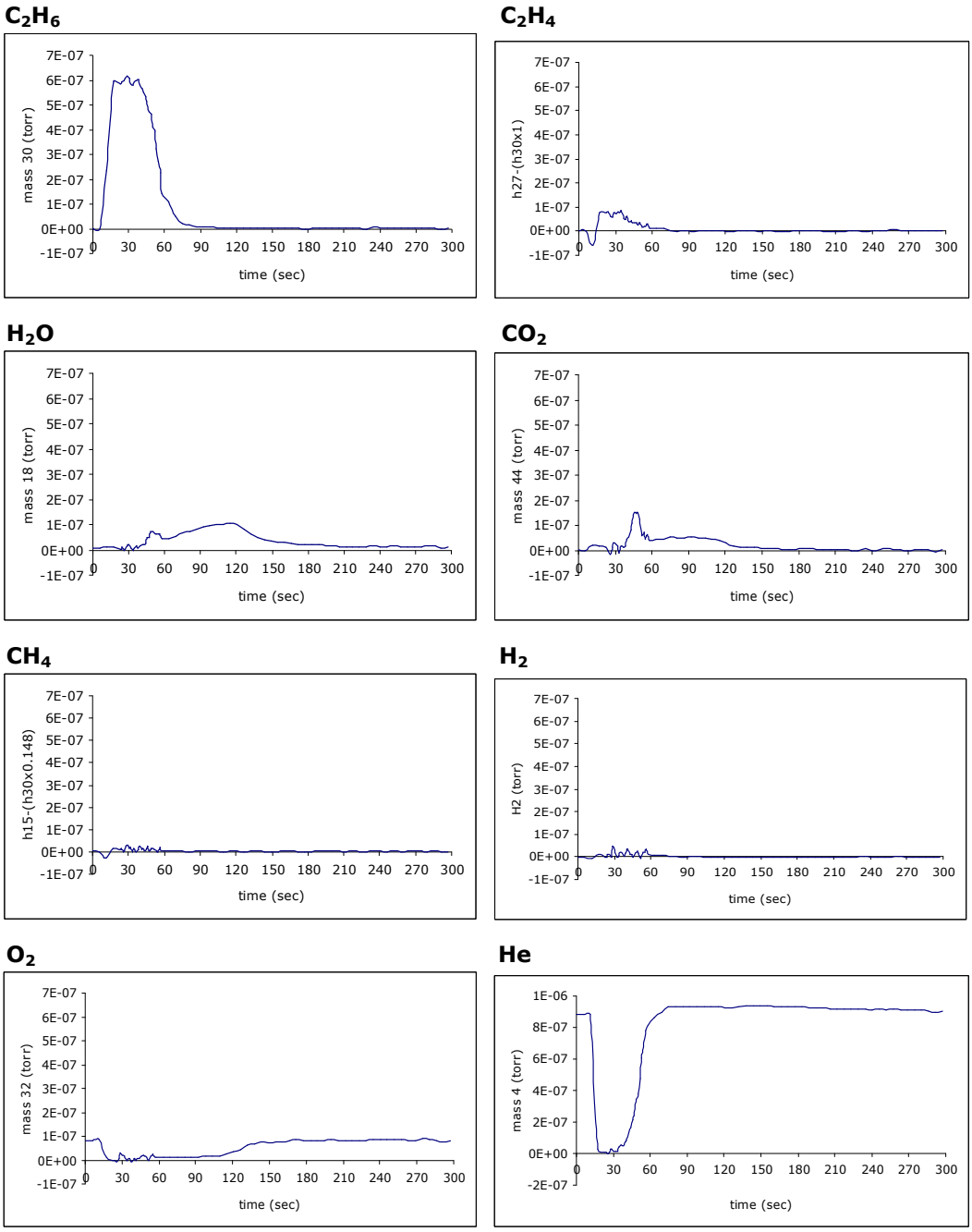

Figure D.1.3. 'Pulse 3' response data for C_2H_6 pulses into O_2 and He flow over Cr-O catalyst at 350°C

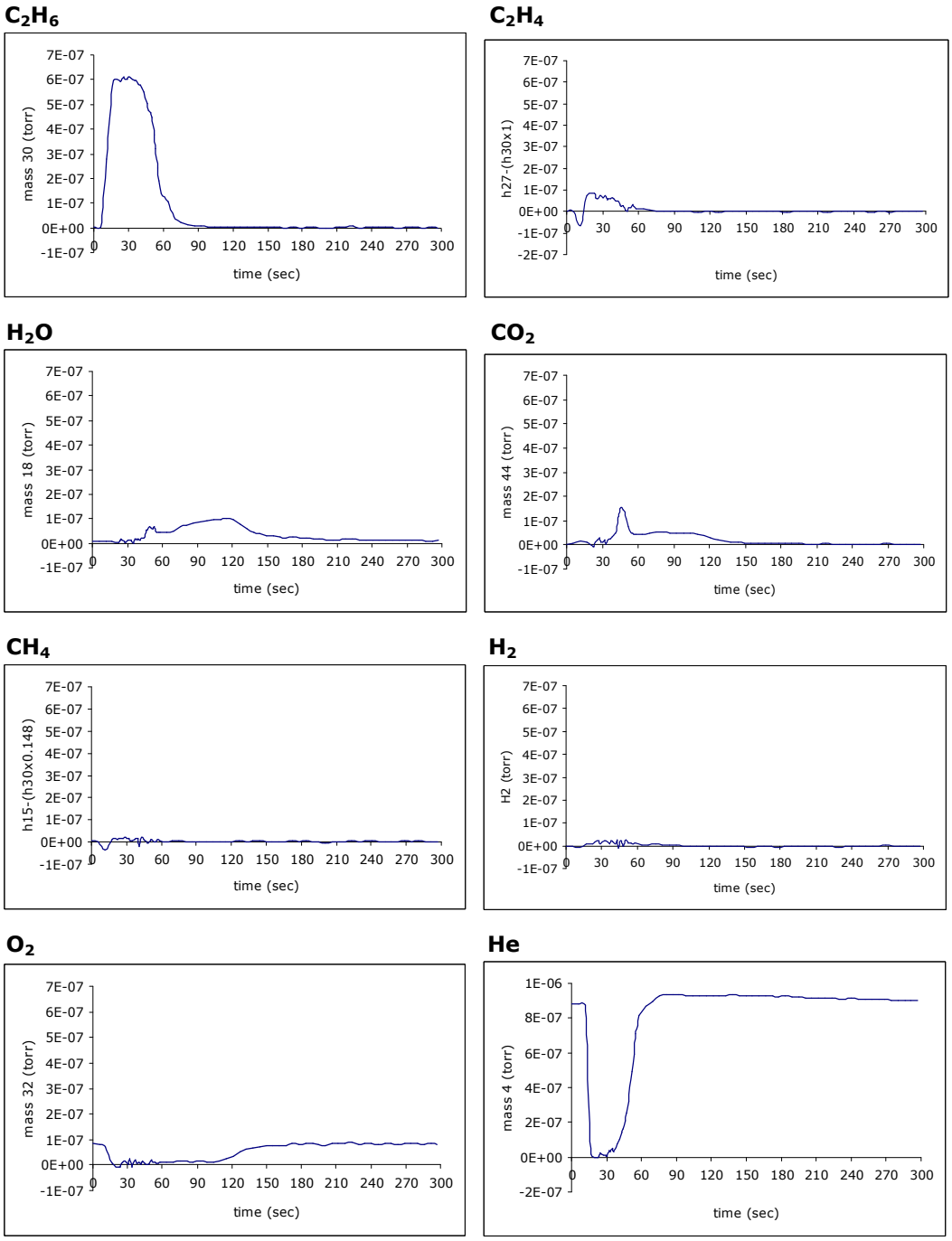

Figure D.1.4. 'Pulse 4' response data for C_2H_6 pulses into O_2 and He flow over Cr-O catalyst at 350°C

Pulse 1 – CO_2

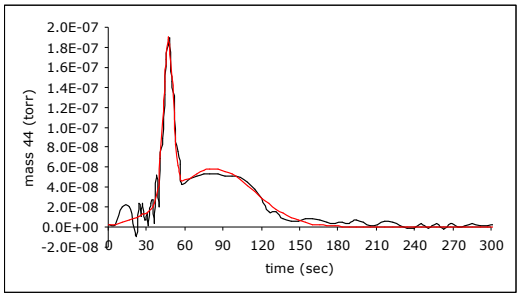

Pulse 1 - de-convoluted CO_2

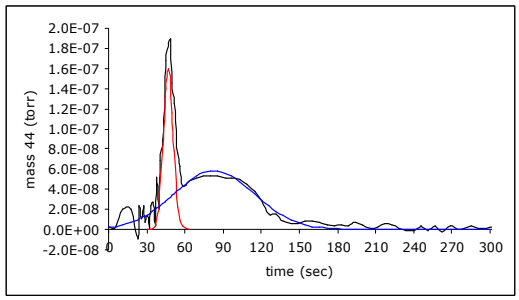

f(x)=1.595e-007*exp(-((x-47)/5.5)^2) + 5.822e-008*exp(-((x-83)/45)^2)

Goodness of fit:

SSE: 4.612e-015
R-square: 0.9682
Adjusted R-square: 0.9658
RMSE: 8.423e-009

Pulse 2 – CO_2

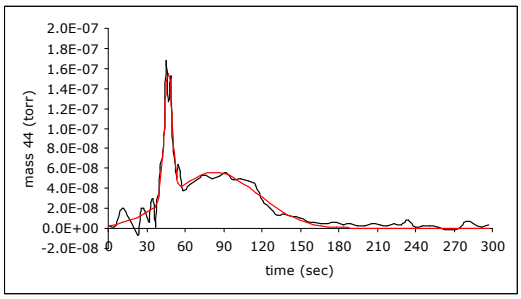

Pulse 2 - de-convoluted CO_2

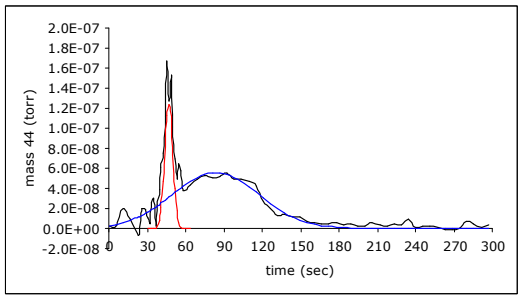

f(x)=1.233e-007*exp(-((x-47)/4.5)^2) + 5.577e-008 *exp(-((x-83.5)/48)^2)

Goodness of fit:

SSE: 4.919e-015
R-square: 0.9467
Adjusted R-square: 0.9426
RMSE: 8.767e-009

Pulse 3 – CO_2

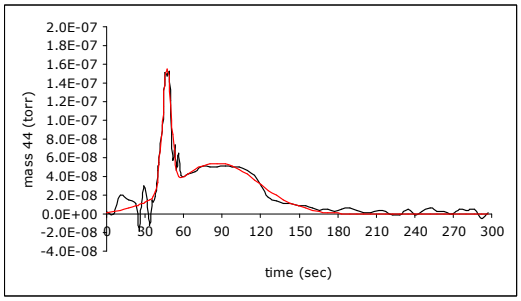

Pulse 3 - de-convoluted CO_2

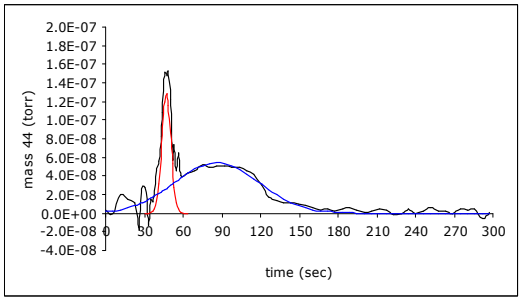

f(x)=1.285e-007*exp(-((x-47)/5)^2) + 5.434e-008*exp(-((x-86)/46)^2)

Goodness of fit:

SSE: 4.632e-015
R-square: 0.9531
Adjusted R-square: 0.9494
RMSE: 8.507e-009

Figure D.1.5. Gaussian fits and de-convolution of Gaussian fits for CO_2 response data for C_2H_6 pulses into O_2 and He flow over Cr-O catalyst at 350°C

Pulse 4 – CO_2

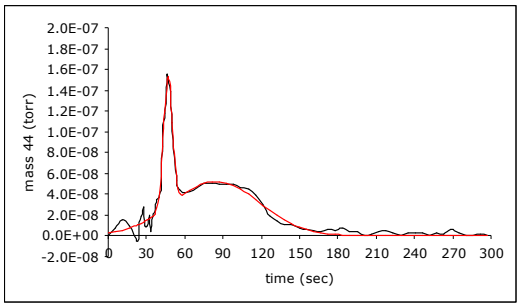

Pulse 4 - de-convoluted CO_2

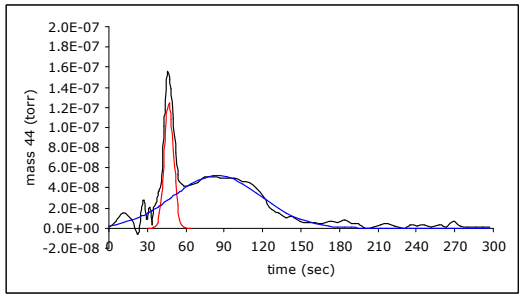

f(x)=1.25e-007*exp(-((x-47)/5)^2) + 5.226e-008*exp(-((x-84.5)/48.5)^2)

Goodness of fit:

SSE: 1.766e-015
R-square: 0.9809
Adjusted R-square: 0.9794
RMSE: 5.252e-009

Figure D.1.5. (Cont'd.)

Pulse 1 – H_2O

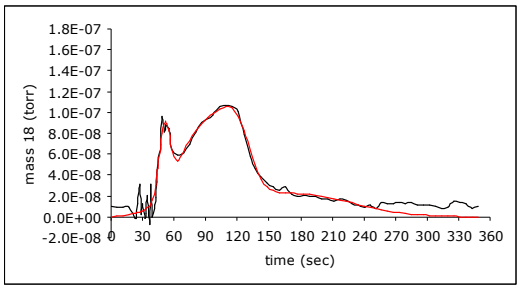

Pulse 1 - de-convoluted H_2O

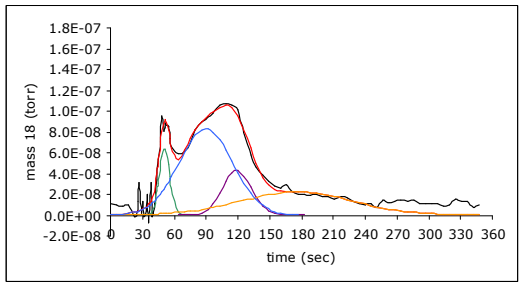

f(x)=6.414e-008*exp(-((x-51)/7)^2) + 8.306e-008*exp(-((x-90)/36)^2) +
4.269e-008*exp(-((x-119)/19)^2) + 2.209e-008*exp(-((x-175)/75)^2)

Goodness of fit:
SSE: 3.098e-015
R-square: 0.9577
Adjusted R-square: 0.9484
RMSE: 7.872e-009

Pulse 2 – H_2O

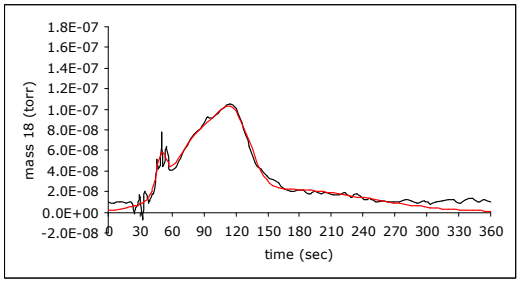

Pulse 2 - de-convoluted H_2O

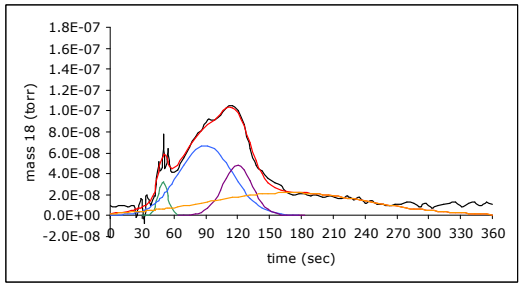

f(x)=3.228e-008*exp(-((x-50)/6.5)^2) + 6.678e-008*exp(-((x-90)/36)^2) +
4.795e-008*exp(-((x-120)/20)^2) + 2.183e-008*exp(-((x-169)/107)^2)

Goodness of fit:
SSE: 2.095e-015
R-square: 0.961
Adjusted R-square: 0.9524
RMSE: 6.472e-009

Pulse 3 – H_2O

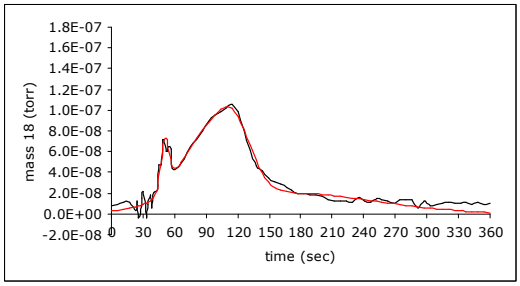

Pulse 3 - de-convoluted H_2O

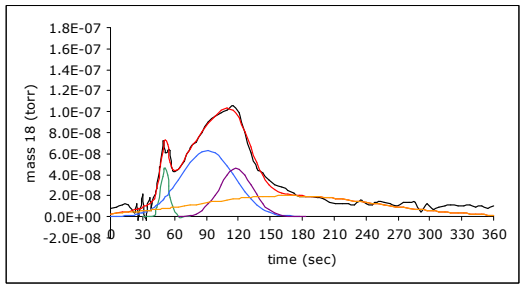

f(x)=4.662e-008*exp(-((x-51)/5.5)^2) + 6.287e-008*exp(-((x-91)/36)^2) +
4.565e-008*exp(-((x-118)/22.5)^2) + 2.002e-008*exp(-((x-167)/120)^2)

Goodness of fit:
SSE: 1.633e-015
R-square: 0.9709
Adjusted R-square: 0.9645
RMSE: 5.715e-009

Figure D.1.6. Gaussian fits and de-convolution of Gaussian fits for H_2O response data for C_2H_6 pulses into O_2 and He flow over Cr-O catalyst at 350°C

Pulse 4 – H_2O

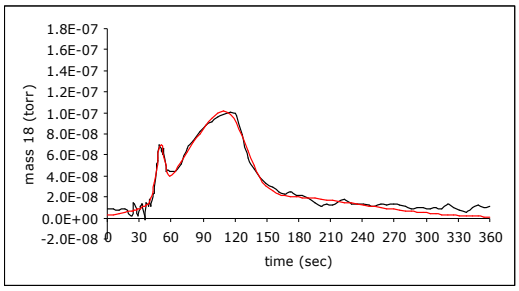

Pulse 4 - de-convoluted H_2O

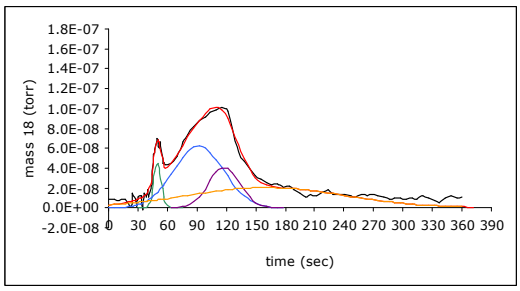

f(x)=4.49e-008*exp(-((x-50)/5.5)^2) + 6.214e-008*exp(-((x-92)/36)^2) +
4.094e-008*exp(-((x-118)/22.5)^2) + 2.035e-008*exp(-((x-160)/115)^2)

Goodness of fit:

SSE: 1.132e-015
R-square: 0.9783
Adjusted R-square: 0.9735
RMSE: 4.758e-009

Figure D.1.6. (Cont'd.)

Table D.1. C_2H_6 response data for C_2H_6 pulses into O_2 and He flow over Cr-O catalyst at 350°C

	Pulse 1	***Pulse 2***	***Pulse 3***	***Pulse 4***	***Avr:***
zeroth moment (m_0)	3.8E-05	3.9E-05	4.0E-05	4.0E-05	3.9E-05
m_1	1.4E-03	1.4E-03	1.5E-03	1.5E-03	1.4E-03
first moment ($\mu_0 = m_1/m_0$)	36.9	37.1	36.9	36.9	37.0
mean residence time (t_m)	36.9	37.1	36.9	36.9	37.0
m_2	5.6E-02	5.9E-02	6.0E-02	6.0E-02	5.9E-02
variance (σ^2), sec^2	133.0	134.4	137.3	136.7	135
standard deviation (σ), sec	12	12	12	12	12

Table D.2. C_2H_4 response data for C_2H_6 pulses into O_2 and He flow over Cr-O catalyst at 350°C

	Pulse 1	***Pulse 2***	***Pulse 3***	***Pulse 4***	***Avr:***
	Area1	*Area1*	*Area1*	*Area1*	
zeroth moment (m_0)	1.9E-06	1.9E-06	1.9E-06	1.9E-06	1.9E-06
m_1	6.4E-05	6.4E-05	6.5E-05	6.0E-05	6.3E-05
first moment ($\mu_0 = m_1/m_0$)	33.2	33.9	33.7	32.0	33.2
mean residence time (t_m)	33.2	33.9	33.7	32.0	33.2
m_2	2.3E-03	2.3E-03	2.3E-03	2.0E-03	2.2E-03
variance (σ^2), sec^2	64.3	68.9	67.5	54.4	64
standard deviation (σ),sec	8.0	8.3	8.2	7.4	8.0
% of total area	92.5	90.2	85.4	82.2	87.5

	Pulse 1	***Pulse 2***	***Pulse 3***	***Pulse 4***	***Avr:***
	Area2	*Area2*	*Area2*	*Area2*	
zeroth moment (m_0)	1.6E-07	2.1E-07	3.3E-07	4.0E-07	2.8E-07
m_1	9.9E-06	1.3E-05	1.9E-05	2.3E-05	1.6E-05
first moment ($\mu_0 = m_1/m_0$)	62.7	62.0	58.3	56.6	59.9
mean residence time (t_m)	62.7	62.0	58.3	56.6	59.9
m_2	6.2E-04	8.0E-04	1.1E-03	1.3E-03	9.7E-04
variance (σ^2), sec^2	26.8	28.3	28.2	25.1	27
standard deviation (σ),sec	5.2	5.3	5.3	5.0	5
% of total area	7.5	9.8	14.6	17.8	12

Total area (Area 1 + 2)	2.1E-06	2.1E-06	2.3E-06	2.3E-06	2.2E-06

Table D.3. CO_2 response data for C_2H_6 pulses into O_2 and He flow over Cr-O catalyst at 350°C

Gauss 1					
	Pulse 1	***Pulse 2***	***Pulse 3***	***Pulse 4***	***Avr:***
mean (η)	47	47	47	47	47.0
variance (σ^2)	15.1	10.1	12.5	12.5	12.6
standard deviation (σ)	3.9	3.2	3.5	3.5	3.5
peak amplitude	1.6E-07	1.2E-07	1.3E-07	1.3E-07	1.3E-07
Area under the curve	1.6E-06	9.8E-07	1.1E-06	1.1E-06	1.2E-06
% of total area	25	17	21	20	21

Gauss 2					
	Pulse 1	***Pulse 2***	***Pulse 3***	***Pulse 4***	***Avr:***
mean (η)	83	83.5	86	84.5	84.3
variance (σ^2)	1012.5	1152	1058	1176.1	1099.7
standard deviation (σ)	31.8	33.9	32.5	34.3	33.1
peak amplitude	5.8E-08	5.6E-08	5.4E-08	5.2E-08	5.5E-08
Area under the curve	4.6E-06	4.7E-06	4.4E-06	4.5E-06	4.6E-06
% of total area	75	83	79	80	79

Total area (Gauss 1+2)	6.2E-06	5.7E-06	5.6E-06	5.6E-06	5.7E-06

Table D.4. H_2O response data for C_2H_6 pulses into O_2 and He flow over Cr-O catalyst at 350°C

Gauss 1					
	Pulse 1	***Pulse 2***	***Pulse 3***	***Pulse 4***	***Avr:***
mean (η)	51	50	51	50	50.5
variance (σ^2)	3.5	3.3	2.8	2.8	3.1
standard deviation (σ)	1.9	1.8	1.7	1.7	1.7
peak amplitude	6.4E-08	3.2E-08	4.7E-08	4.5E-08	4.7E-08
Area under the curve	8.0E-07	3.7E-07	4.5E-07	4.4E-07	5.1E-07
% of total area	8	4	4	4	5

Gauss 2					
	Pulse 1	***Pulse 2***	***Pulse 3***	***Pulse 4***	***Avr:***
mean (η)	90	90	91	92	90.8
variance (σ^2)	18	18	18	18	18.0
standard deviation (σ)	4.2	4.2	4.2	4.2	4.2
peak amplitude	8.3E-08	6.7E-08	6.3E-08	6.2E-08	6.9E-08
Area under the curve	5.3E-06	4.3E-06	4.0E-06	4.0E-06	4.4E-06
% of total area	51	41	39	39	42

Gauss 3					
	Pulse 1	***Pulse 2***	***Pulse 3***	***Pulse 4***	***Avr:***
mean (η)	119	120	118	118	118.8
variance (σ^2)	9.5	10	11.3	11.3	10.5
standard deviation (σ)	3.1	3.2	3.4	3.4	3.2
peak amplitude	4.3E-08	4.8E-08	4.6E-08	4.1E-08	4.4E-08
Area under the curve	1.4E-06	1.7E-06	1.8E-06	1.6E-06	1.6E-06
% of total area	14	16	18	16	16

Gauss 4					
	Pulse 1	***Pulse 2***	***Pulse 3***	***Pulse 4***	***Avr:***
mean (η)	175	169	167	160	167.8
variance (σ^2)	37.5	53.5	60	57.5	52.1
standard deviation (σ)	6.1	7.3	7.7	7.6	7.2
peak amplitude	2.2E-08	2.2E-08	2.0E-08	2.0E-08	2.1E-08
Area under the curve	2.9E-06	4.1E-06	4.1E-06	4.0E-06	3.8E-06
% of total area	28	39	40	40	37

Total area (Gauss1+2+3+4)	1.0E-05	1.0E-05	1.0E-05	1.0E-05	1.0E-05

D.1.2. Dynamic Experiments' Data for Cr-O Catalyst with C_2H_6 Pulses into O_2 and He Flow at 401°C

The response data for C_2H_6 pulses into O_2 and He flow over Cr-O catalyst at 401°C are presented in Figures D.1.7-D.1.10. The Gaussian fits and de-convolution of Gaussian fits for CO_2 and H_2O response data are given in Figures D.1.11 and D.1.12, respectively. The results of moment, variance, mean residence time, and standard deviation calculations for C_2H_6, C_2H_4, CO_2, and H_2O are tabulated in Tables D.5-D.8.

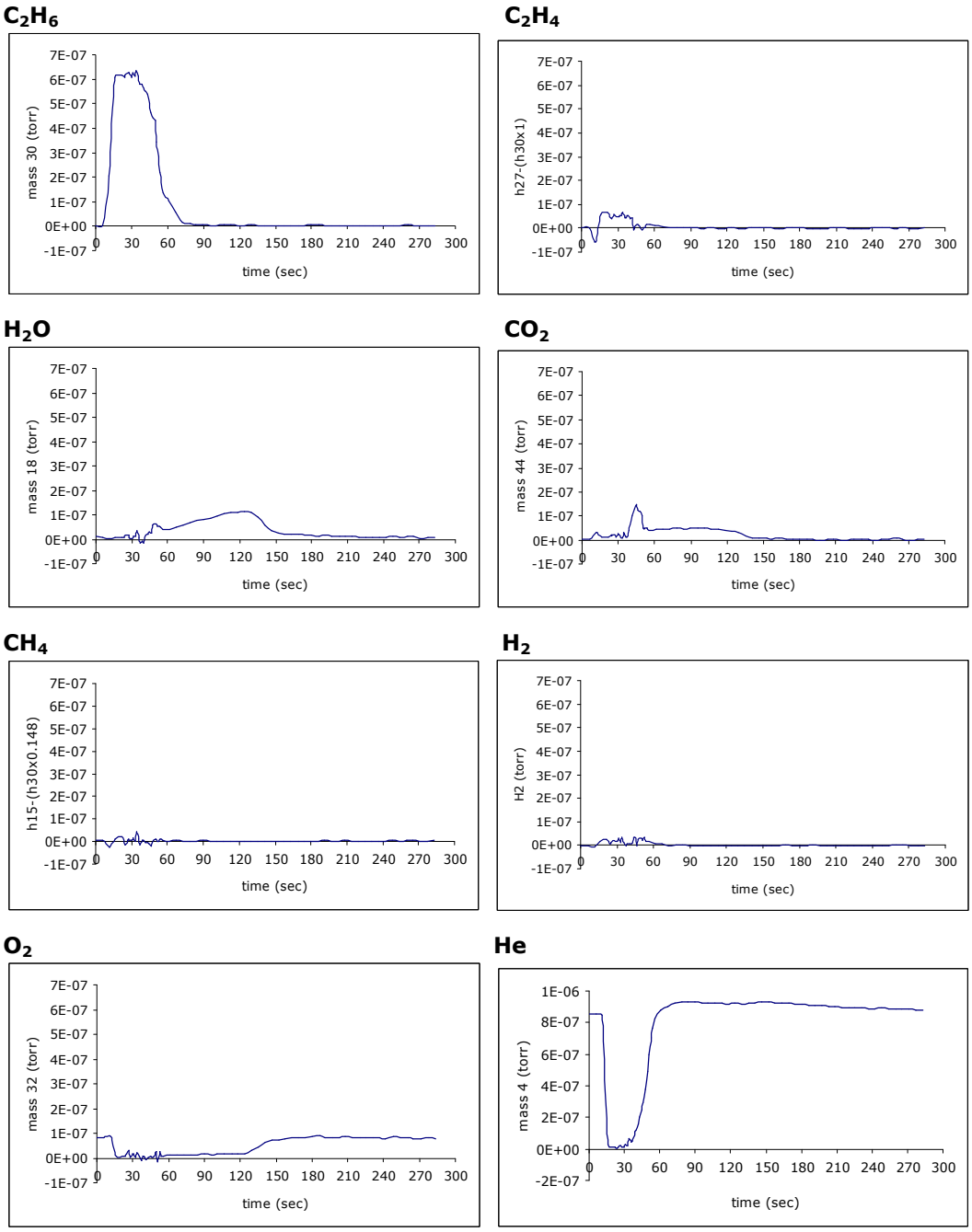

Figure D.1.7. 'Pulse 1' response data for C_2H_6 pulses into O_2 and He flow over Cr-O catalyst at 401°C

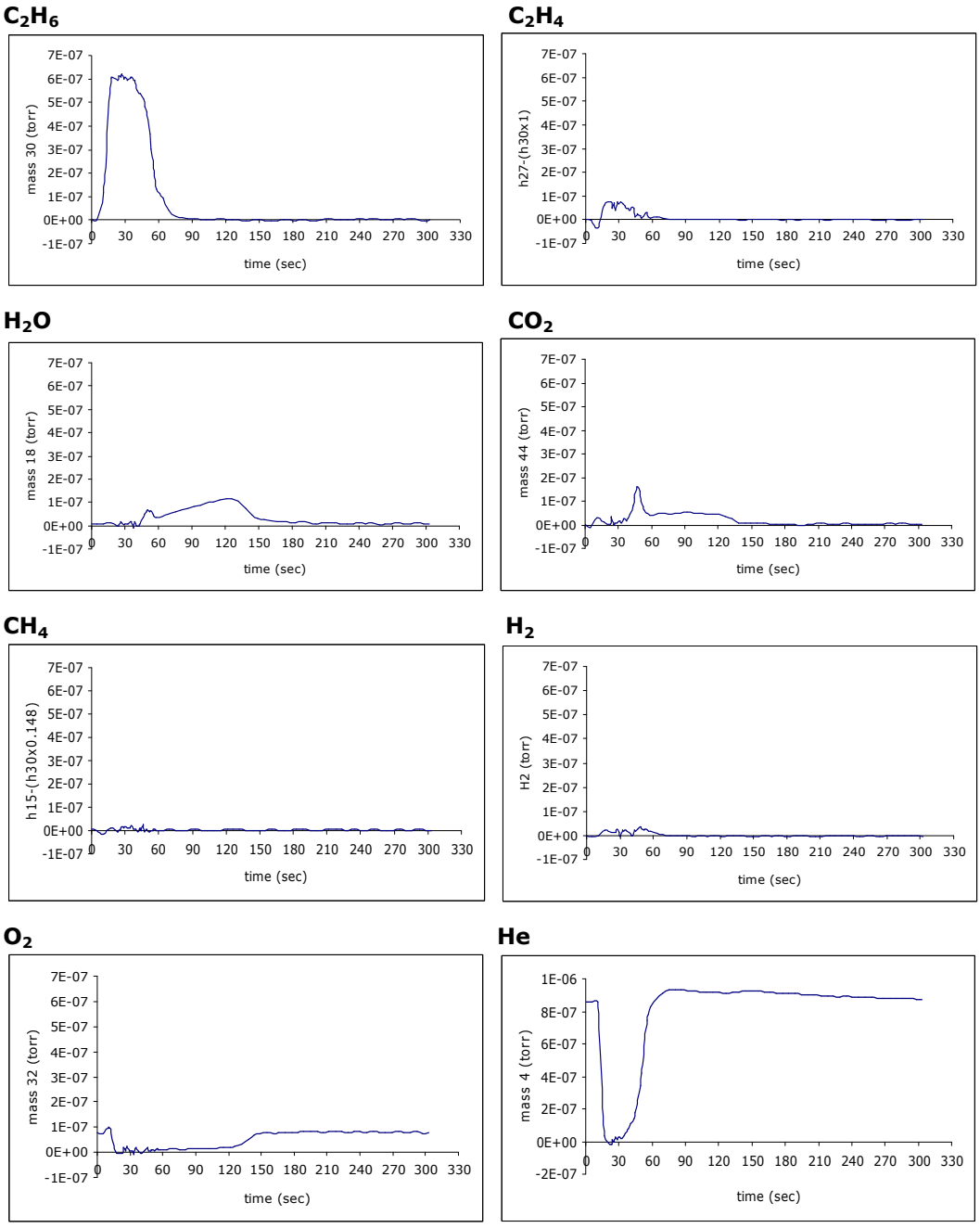

Figure D.1.8. 'Pulse 2' response data for C_2H_6 pulses into O_2 and He flow over Cr-O catalyst at 401°C

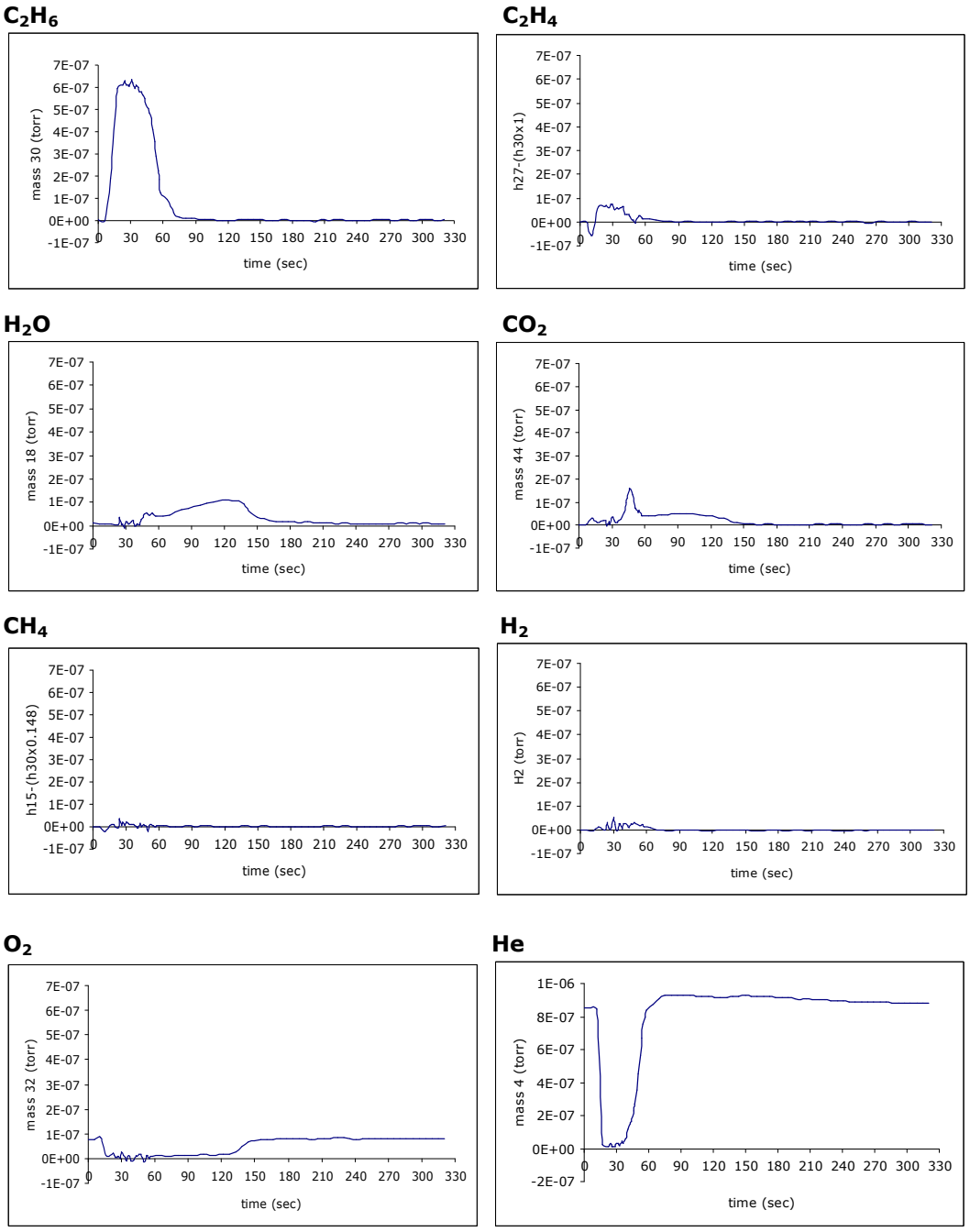

Figure D.1.9. 'Pulse 3' response data for C_2H_6 pulses into O_2 and He flow over Cr-O catalyst at 401°C

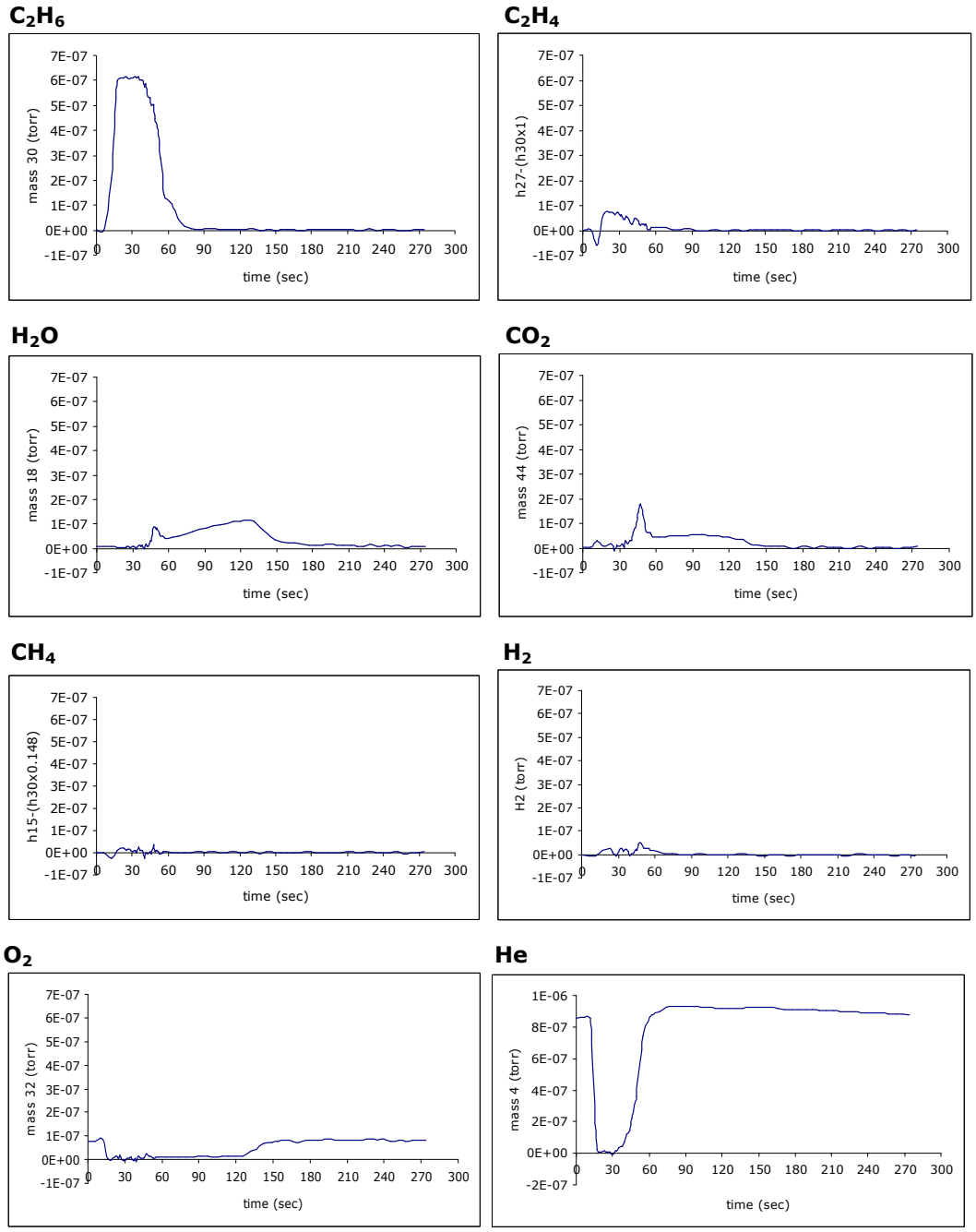

Figure D.1.10. 'Pulse 4' response data for C_2H_6 pulses into O_2 and He flow over Cr-O catalyst at 401°C

Pulse 1 – CO_2

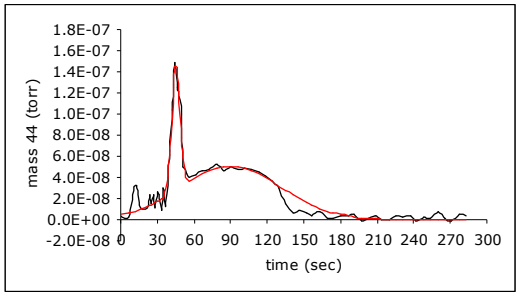

Pulse 1 - de-convoluted CO_2

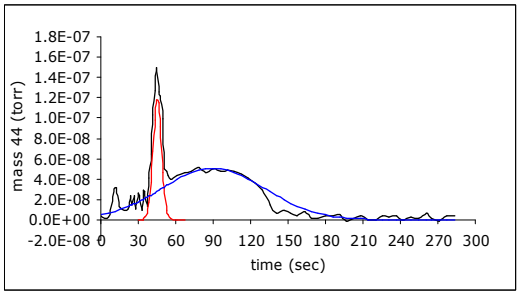

f(x) = 1.192e-007*exp(-((x-45.3)/4.8)^2) + 5.058e-008*exp(-((x-90)/58)^2)

Goodness of fit:
SSE: 3.576e-015
R-square: 0.955
Adjusted R-square: 0.9513
RMSE: 7.657e-009

Pulse 2 – CO_2

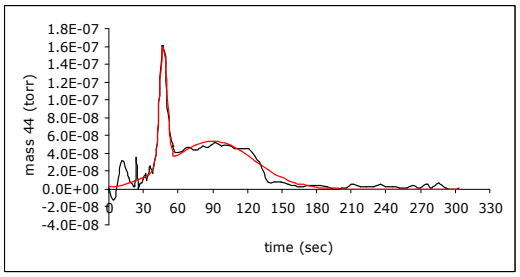

Pulse 2 - de-convoluted CO_2

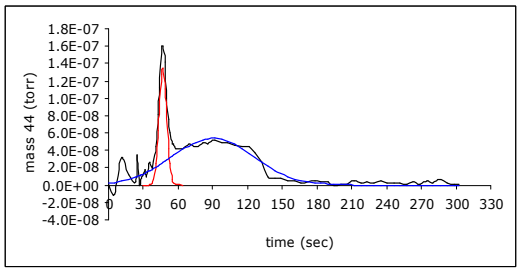

f(x) = 1.342e-007*exp(-((x-47)/4.6)^2) + 5.405e-008*exp(-((x-90)/50)^2)

Goodness of fit:
SSE: 3.31e-015
R-square: 0.9653
Adjusted R-square: 0.9627
RMSE: 7.136e-009

Pulse 3 – CO_2

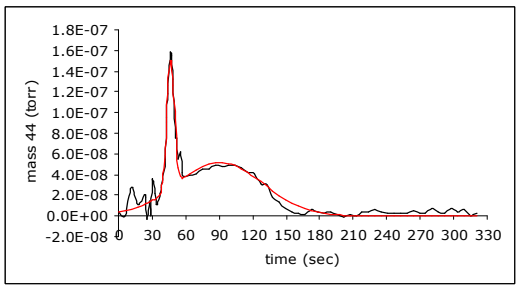

Pulse 3 - de-convoluted CO_2

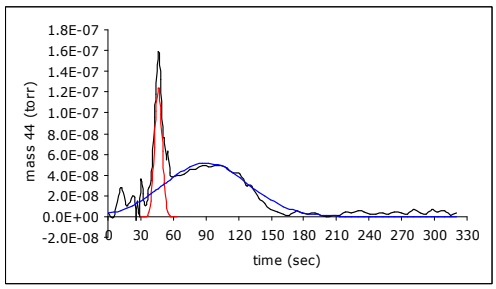

f(x) = 1.271e-007*exp(-((x-46.5)/4.7)^2) + 5.179e-008*exp(-((x-90.5)/54.3)^2)

Goodness of fit:
SSE: 4.141e-015
R-square: 0.9547
Adjusted R-square: 0.9513
RMSE: 7.804e-009

Figure D.1.11. Gaussian fits and de-convolution of Gaussian fits for CO_2 response data for C_2H_6 pulses into O_2 and He flow over Cr-O catalyst at 401°C

Pulse 4 – CO_2

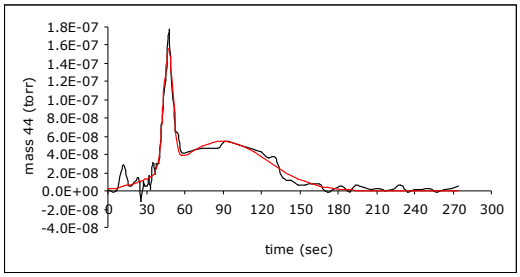

Pulse 4 - de-convoluted CO_2

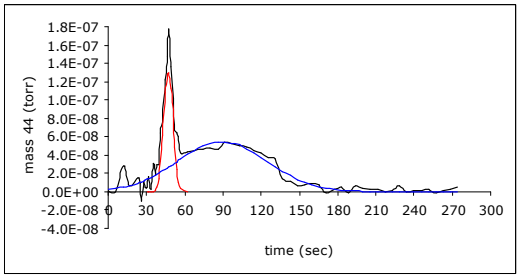

f(x)=1.307e-007*exp(-((x-47.2)/5)^2)+5.448e-008*exp(-((x-89.5)/49.9)^2)

Goodness of fit:

SSE: 3.84e-015
R-square: 0.96
Adjusted R-square: 0.9566
RMSE: 8.068e-009

Figure D.1.11. (Cont'd.)

Pulse 1 – H_2O

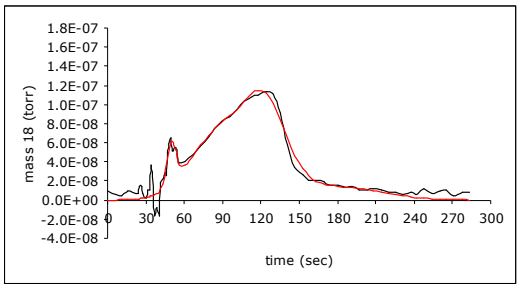

Pulse 1 - de-convoluted H_2O

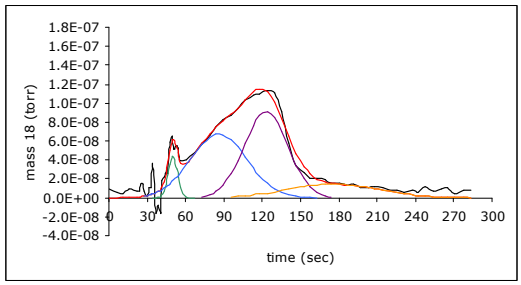

f(x)=4.35e-008*exp(-((x-50)/5)^2)+ 6.768e-008*exp(-((x-86)/31)^2) +
9.13e-008*exp(-((x-123)/24)^2)+1.441e-008*exp(-((x-175)/50)^2)

Goodness of fit:
SSE: 4.426e-015
R-square: 0.9406
Adjusted R-square: 0.9287
RMSE: 8.97e-009

Pulse 2 – H_2O

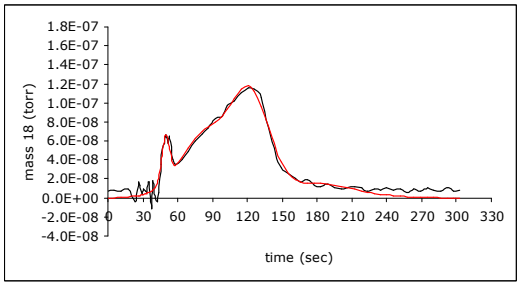

Pulse 2 - de-convoluted H_2O

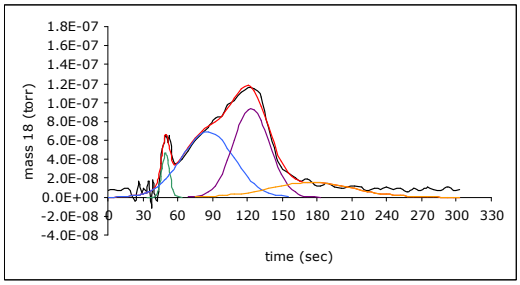

f(x)=4.664e-008*exp(-((x-50)/4.6)^2) + 6.87e-008*exp(-((x-86)/32)^2) +
9.347e-008*exp(-((x-123.5)/22)^2) + 1.539e-008*exp(-((x-175)/50)^2)

Goodness of fit:
SSE: 3.433e-015
R-square: 0.9546
Adjusted R-square: 0.9462
RMSE: 7.628e-009

Pulse 3 – H_2O

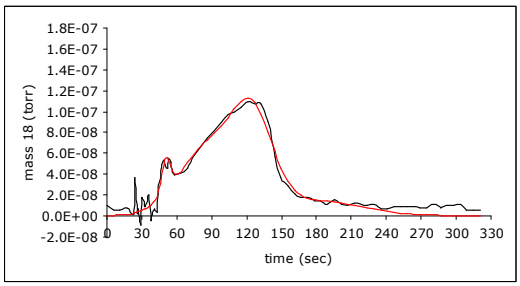

Pulse 3 - de-convoluted H_2O

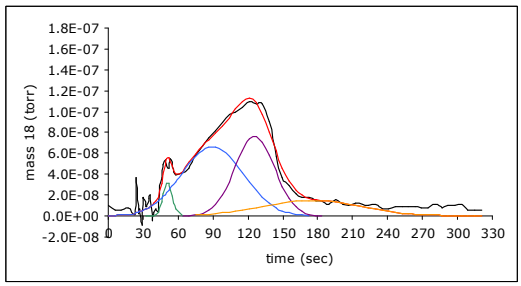

f(x)= 3.206e-008*exp(-((x-51)/5.7)^2) + 6.642e-008*exp(-((x-89.5)/37.6)^2)
+7.637e-008*exp(-((x-125.9)/24)^2) + 1.504e-008*exp(-((x-175)/60)^2)

Goodness of fit:
SSE: 4.133e-015
R-square: 0.9429
Adjusted R-square: 0.9328
RMSE: 8.164e-009

Figure D.1.12. Gaussian fits and de-convolution of Gaussian fits for H_2O response data for C_2H_6 pulses into O_2 and He flow over Cr-O catalyst at 401°C

Pulse 4 – H_2O

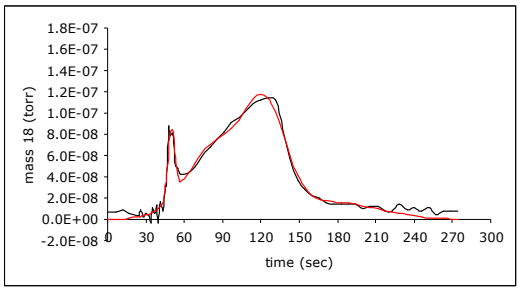

Pulse 4 - de-convoluted H_2O

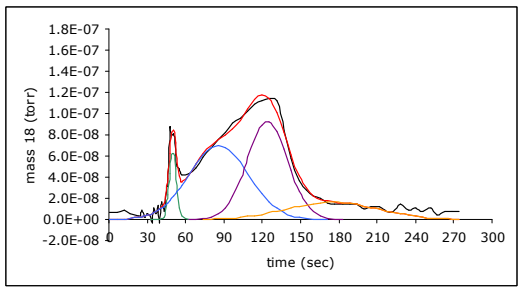

f(x)=6.391e-008*exp(-((x-50)/4)^2) + 6.974e-008*exp(-((x-86)/33)^2) +
9.218e-008*exp(-((x-124)/22.5)^2) + 1.639e-008*exp(-((x-175)/50)^2)

Goodness of fit:

SSE: 2.068e-015
R-square: 0.9739
Adjusted R-square: 0.9685
RMSE: 6.246e-009

Figure D.1.12. (Cont'd.)

Table D.5. C_2H_6 response data for C_2H_6 pulses into O_2 and He flow over Cr-O catalyst at 401°C

	Pulse 1	***Pulse 2***	***Pulse 3***	***Pulse 4***	***Avr:***
zeroth moment (m_0)	3.8E-05	3.9E-05	3.9E-05	4.1E-05	3.9E-05
m_1	1.4E-03	1.4E-03	1.4E-03	1.5E-03	1.4E-03
first moment ($\mu_1 = m_1/m_0$)	35.4	36.7	36.6	36.7	36.3
mean residence time (t_m)	35.4	36.7	36.6	36.7	36.3
m_2	5.3E-02	5.8E-02	5.8E-02	6.0E-02	5.7E-02
variance (σ^2), sec^2	122.0	129.9	130.6	128.6	127.8
standard deviation (σ)	11	11	11	11	11.3

Table D.6. C_2H_4 response data for C_2H_6 pulses into O_2 and He flow over Cr-O catalyst at 401°C

	Pulse 1	***Pulse 2***	***Pulse 3***	***Pulse 4***	***Avr:***
	Area1	*Area1*	*Area1*	*Area1*	
zeroth moment (m_0)	1.4E-06	1.6E-06	1.6E-06	1.7E-06	1.6E-06
m_1	4.4E-05	5.3E-05	5.2E-05	5.7E-05	5.2E-05
first moment ($\mu_1 = m_1/m_0$)	31.7	32.6	32.2	33.8	32.6
mean residence time (t_m)	31.7	32.6	32.2	33.8	32.6
m_2	1.5E-03	1.8E-03	1.8E-03	2.0E-03	1.8E-03
variance (σ^2), sec^2	55.0	53.6	51.6	75.2	58.9
standard deviation (σ)	7.4	7.3	7.2	8.7	7.6
% of total area	85.4	82.0	80.6	87.2	83.8

	Pulse 1	***Pulse 2***	***Pulse 3***	***Pulse 4***	***Avr:***
	Area2	*Area2*	*Area2*	*Area2*	
zeroth moment (m_0)	2.4E-07	3.6E-07	3.9E-07	2.5E-07	3.1E-07
m_1	1.4E-05	2.2E-05	2.3E-05	1.7E-05	1.9E-05
first moment ($\mu_1 = m_1/m_0$)	59.6	59.6	59.4	68.3	61.7
mean residence time (t_m)	59.6	59.6	59.4	68.3	61.7
m_2	8.6E-04	1.3E-03	1.4E-03	1.2E-03	1.2E-03
variance (σ^2), sec^2	62.5	66.8	52.0	113.0	73.6
standard deviation (σ)	7.9	8.2	7.2	10.6	8.5
% of total area	15	18	19	13	16.2

Total area (Area 1 + 2)	1.6E-06	2.0E-06	2.0E-06	1.9E-06	1.9E-06

Table D.7. CO_2 response data for C_2H_6 pulses into O_2 and He flow over Cr-O catalyst at 401°C

Gauss 1					
	Pulse 1	***Pulse 2***	***Pulse 3***	***Pulse 4***	***Avr:***
mean (η)	45.3	47	46.5	47.2	46.5
variance (σ^2)	11.5	10.6	11.0	12.5	11.4
standard deviation (σ)	3.4	3.3	3.3	3.5	3.4
peak amplitude	1.2E-07	1.3E-07	1.3E-07	1.3E-07	1.3E-07
Area under the curve	1.0E-06	1.1E-06	1.1E-06	1.2E-06	1.1E-06
% of total area	17	19	18	19	18

Gauss 2					
	Pulse 1	***Pulse 2***	***Pulse 3***	***Pulse 4***	***Avr:***
mean (η)	90	90	90.5	89.5	90.0
variance (σ^2)	1682	1250	1245	1245	1355.5
standard deviation (σ)	41.0	35.4	35.3	35.3	36.7
peak amplitude	5.1E-08	5.4E-08	5.2E-08	5.4E-08	5.3E-08
Area under the curve	5.1E-06	4.8E-06	4.9E-06	4.8E-06	4.9E-06
% of total area	83	81	82	81	82

Total area (Gauss 1+2)	6.1E-06	5.9E-06	6.0E-06	5.9E-06	6.0E-06

Table D.8. H_2O response data for C_2H_6 pulses into O_2 and He flow over Cr-O catalyst at 401°C

Gauss 1					
	Pulse 1	***Pulse 2***	***Pulse 3***	***Pulse 4***	***Avr:***
mean (η)	50	50	51	50	50.3
variance (σ^2)	12.5	10.6	16.2	8.0	11.8
standard deviation (σ)	3.5	3.3	4.0	2.8	3.4
peak amplitude	4.4E-08	4.7E-08	3.2E-08	6.4E-08	4.7E-08
Area under the curve	3.9E-07	3.8E-07	3.2E-07	4.5E-07	3.9E-07
% of total area	4	4	3	5	4

Gauss 2					
	Pulse 1	***Pulse 2***	***Pulse 3***	***Pulse 4***	***Avr:***
mean (η)	86	86	89.5	86	86.9
variance (σ^2)	480.5	512	706.9	544.5	561.0
standard deviation (σ)	21.9	22.6	26.6	23.3	23.6
peak amplitude	6.8E-08	6.9E-08	6.6E-08	7.0E-08	6.8E-08
Area under the curve	3.7E-06	3.9E-06	4.4E-06	4.1E-06	4.0E-06
% of total area	40	42	46	42	43

Gauss 3					
	Pulse 1	***Pulse 2***	***Pulse 3***	***Pulse 4***	***Avr:***
mean (η)	123	123.5	125.9	124	124.1
variance (σ^2)	288	242	288	253.1	267.8
standard deviation (σ)	17.0	15.6	17.0	15.9	16.4
peak amplitude	9.1E-08	9.3E-08	7.6E-08	9.2E-08	8.8E-08
Area under the curve	3.9E-06	3.6E-06	3.2E-06	3.7E-06	3.6E-06
% of total area	42	39	34	38	38

Gauss 4					
	Pulse 1	***Pulse 2***	***Pulse 3***	***Pulse 4***	***Avr:***
mean (η)	175	175	175	175	175.0
variance (σ^2)	1250	1250	1800	1250	1387.5
standard deviation (σ)	35.4	35.4	42.4	35.4	37.1
peak amplitude	1.4E-08	1.5E-08	1.5E-08	1.6E-08	1.5E-08
Area under the curve	1.3E-06	1.4E-06	1.6E-06	1.5E-06	1.4E-06
% of total area	14	15	17	15	15

Total area (Gauss1+2+3+4)	9.3E-06	9.3E-06	9.6E-06	9.7E-06	9.4E-06

D.1.3. Dynamic Experiments' Data for Cr-O Catalyst with C_2H_6 Pulses into O_2 and He Flow at 450°C

The response data for C_2H_6 pulses into O_2 and He flow over Cr-O catalyst at 450°C are presented in Figures D.1.13-D.1.17. The Gaussian fits and de-convolution of Gaussian fits for CO_2 and H_2O response data are given in Figures D.1.18 and D.1.19, respectively. The results of moment, variance, mean residence time, and standard deviation calculations for C_2H_6, C_2H_4, CO_2, and H_2O are tabulated in Tables D.9-D.12.

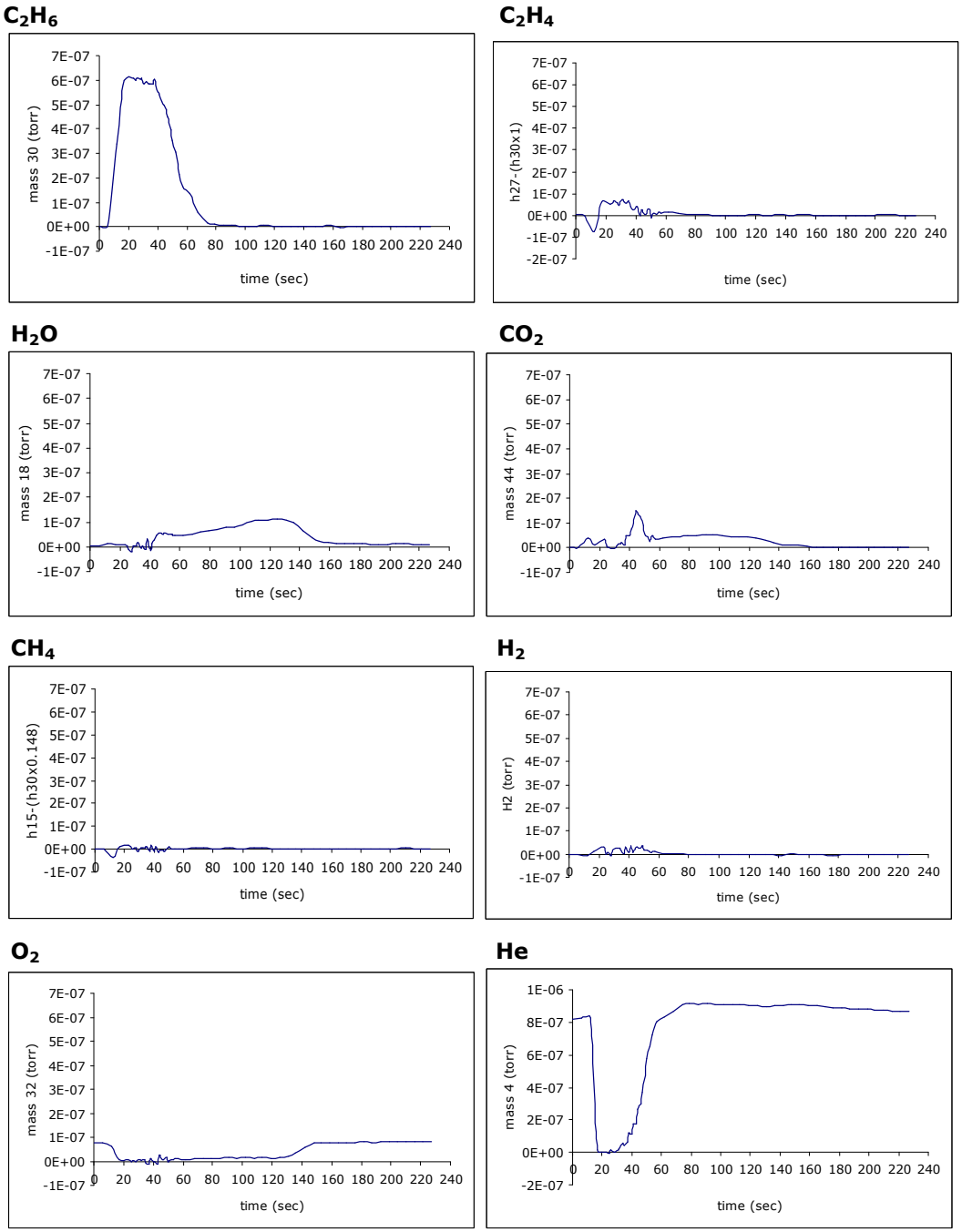

Figure D.1.13. 'Pulse 1' response data for C_2H_6 pulses into O_2 and He flow over Cr-O catalyst at 450°C

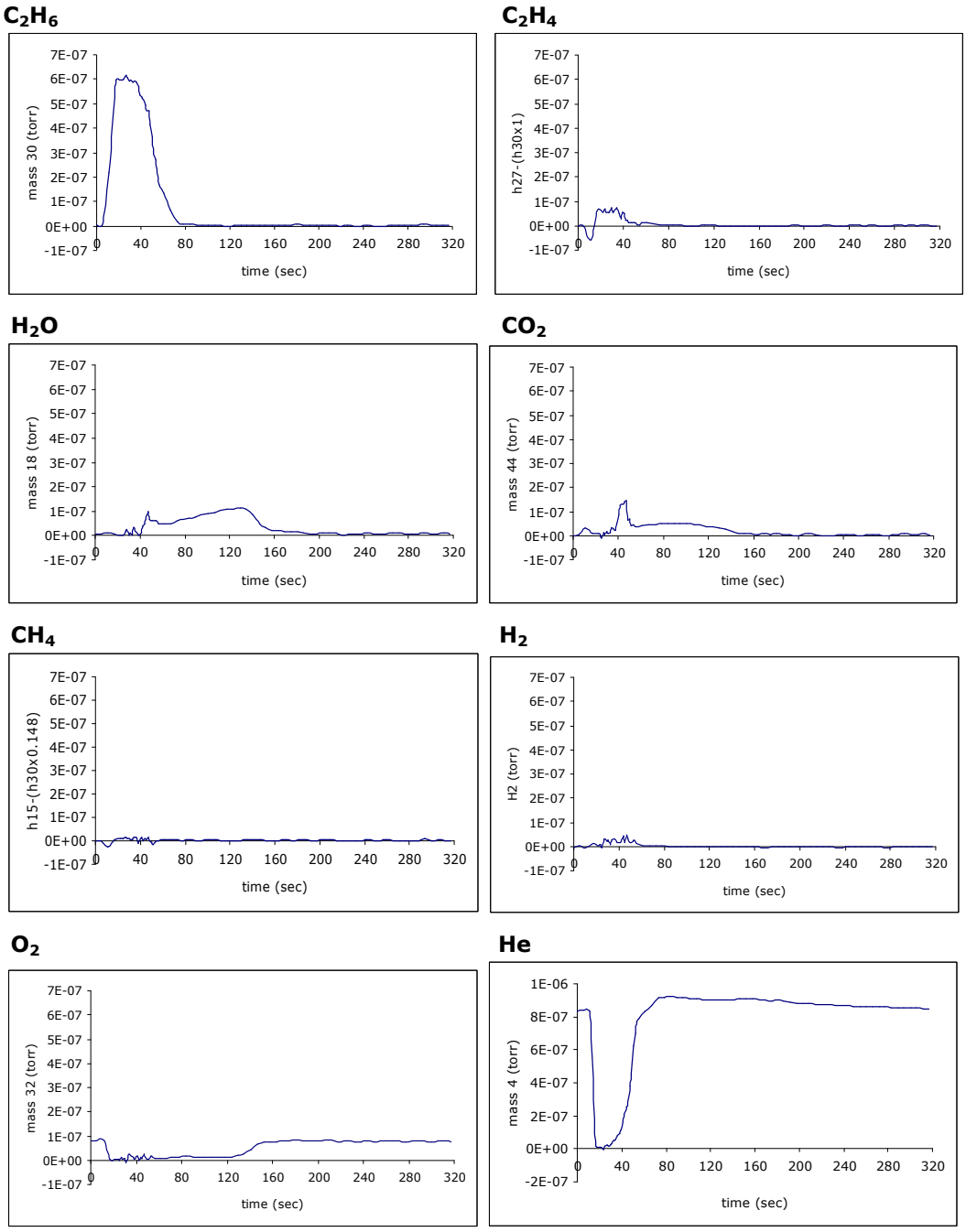

Figure D.1.14. 'Pulse 2' response data for C_2H_6 pulses into O_2 and He flow over Cr-O catalyst at 450°C

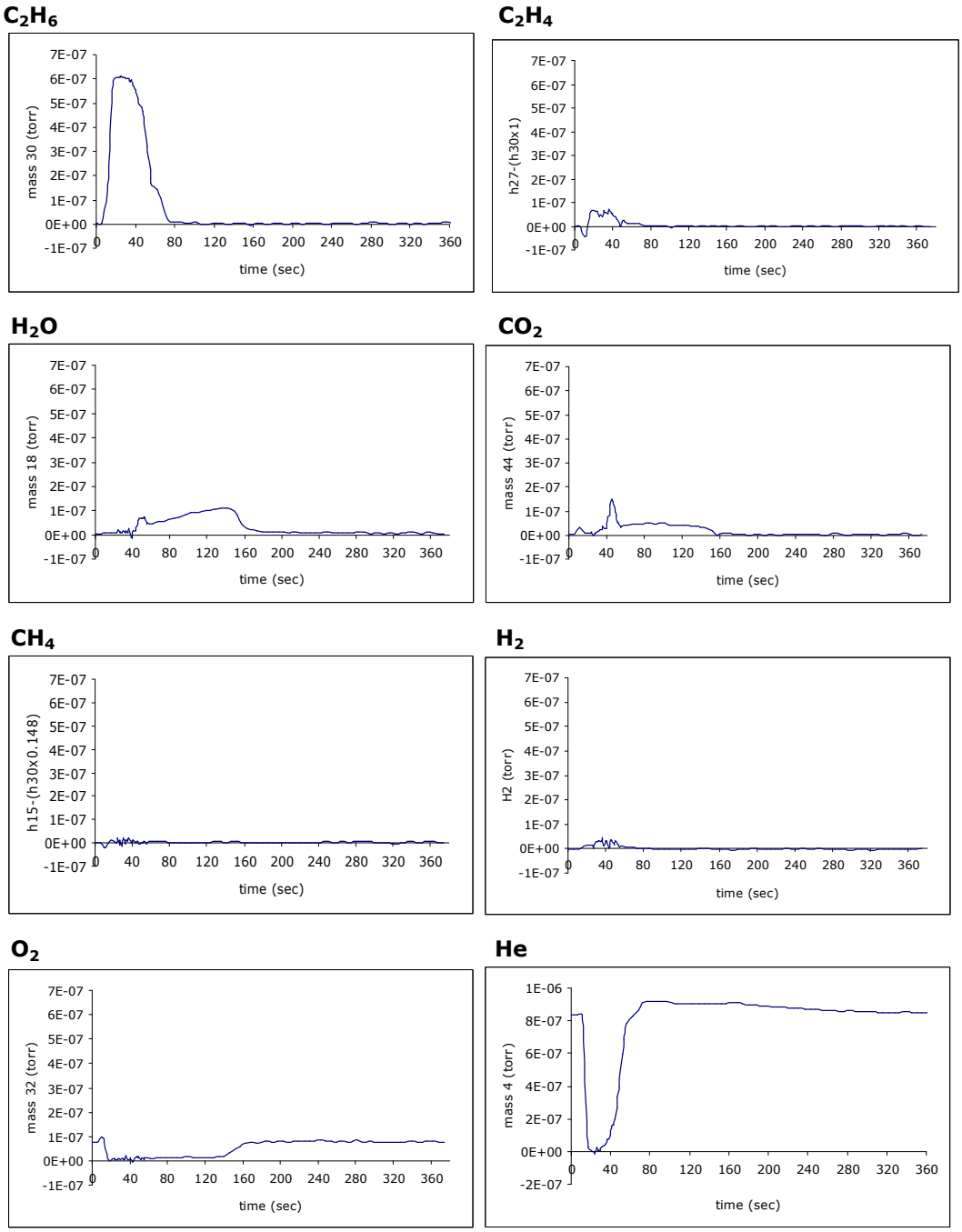

Figure D.1.15. 'Pulse 3' response data for C_2H_6 pulses into O_2 and He flow over Cr-O catalyst at 450°C

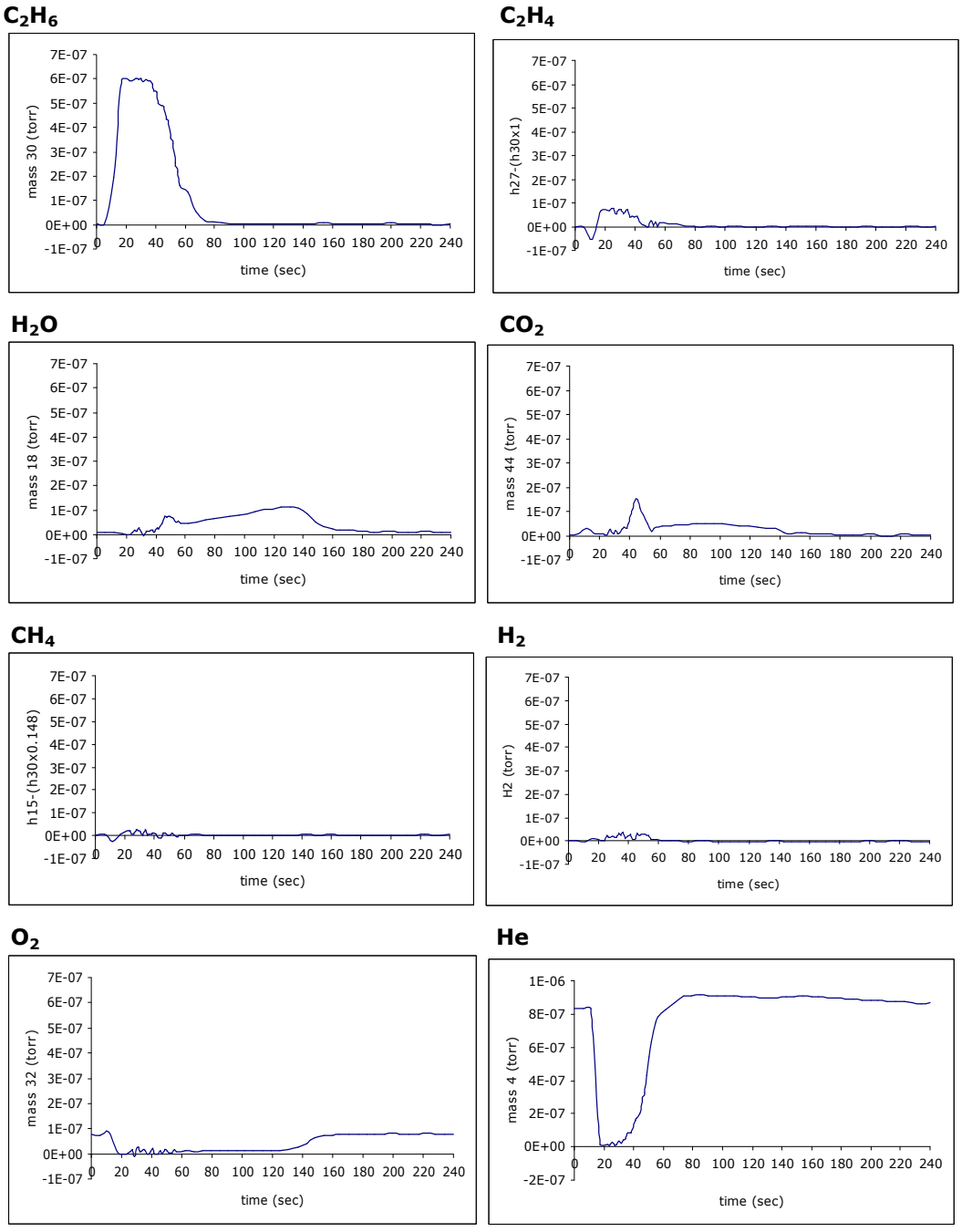

Figure D.1.16. 'Pulse 4' response data for C_2H_6 pulses into O_2 and He flow over Cr-O catalyst at 450°C

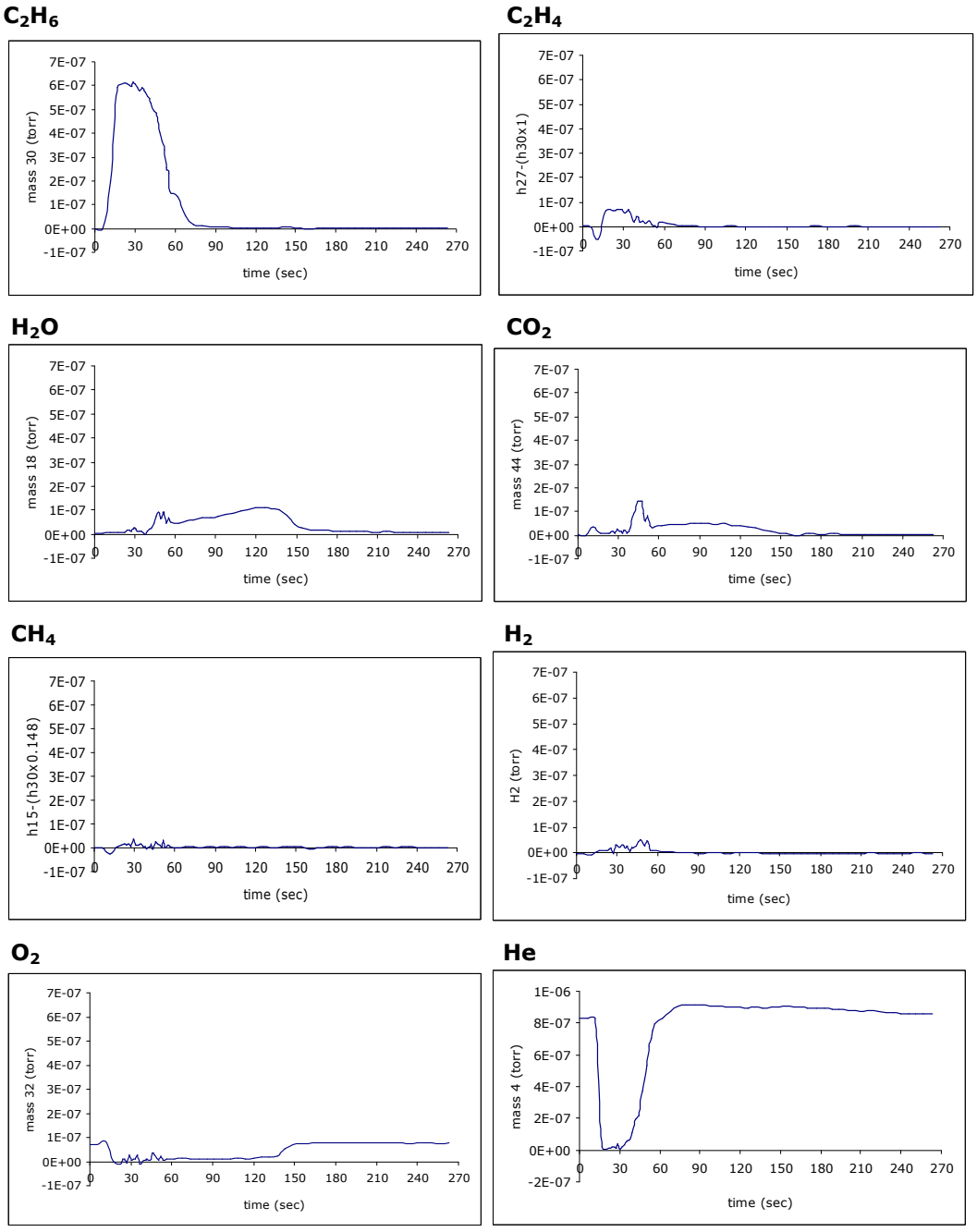

Figure D.1.17. 'Pulse 5' response data for C_2H_6 pulses into O_2 and He flow over Cr-O catalyst at 450°C

Pulse 1 – CO_2

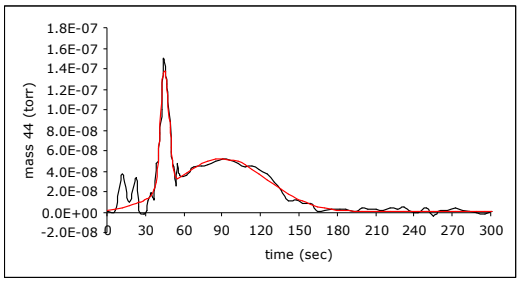

Pulse 1 - de-convoluted CO_2

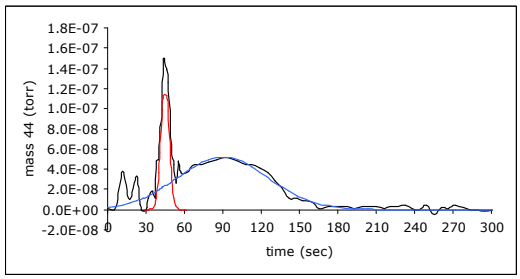

f(x)=1.187e-007*exp(-((x-45)/4.6)^2) + 5.209e-008*exp(-((x-90)/50)^2)

Goodness of fit:

SSE: 3.976e-015
R-square: 0.942
Adjusted R-square: 0.9363
RMSE: 8.83e-009

Pulse 2 – CO_2

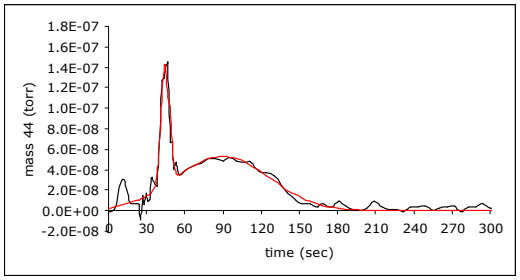

Pulse 2 - de-convoluted CO_2

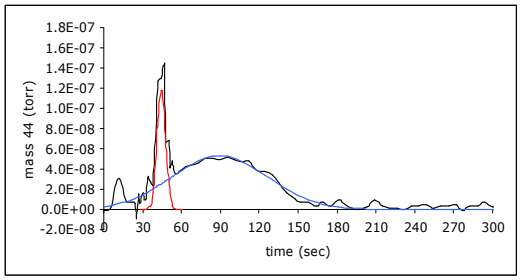

f(x)=1.189e-007*exp(-((x-44.5)/4.6)^2) + 5.3e-008*exp(-((x-89.5)/52)^2)

Goodness of fit:

SSE: 4.463e-015
R-square: 0.9454
Adjusted R-square: 0.9413
RMSE: 8.161e-009

Pulse 3 – CO_2

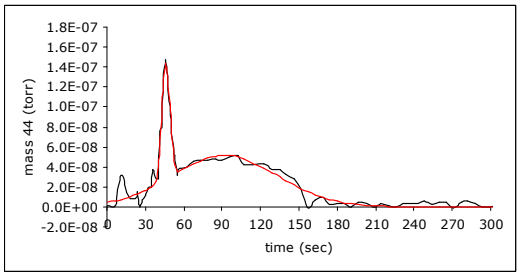

Pulse 3 - de-convoluted CO_2

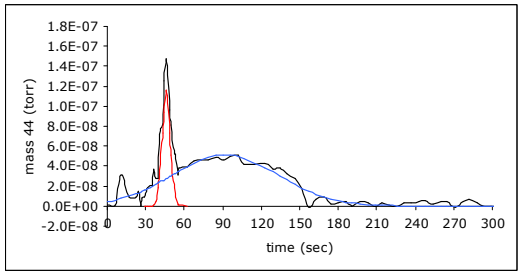

f(x)=1.158e-007*exp(-((x-46)/4.4)^2) + 5.125e-008*exp(-((x-92.1)/58.2)^2)

Goodness of fit:

SSE: 2.986e-015
R-square: 0.9631
Adjusted R-square: 0.9606
RMSE: 6.309e-009

Figure D.1.18. Gaussian fits and de-convolution of Gaussian fits for CO_2 response data for C_2H_6 pulses into O_2 and He flow over Cr-O catalyst at 450°C

Pulse 4 – CO_2

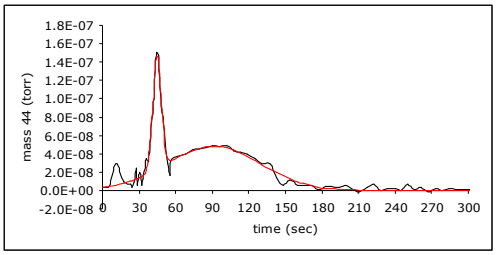

Pulse 4 - de-convoluted CO_2

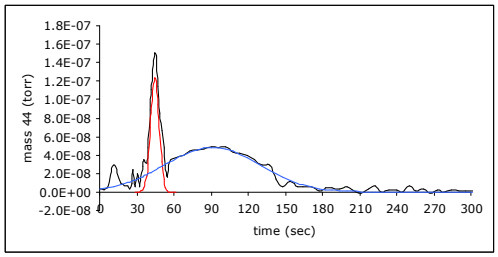

f(x)=1.245e-007 *exp(-((x-44.7)/4.8)^2) + 4.814e-008*exp(-((x-90.9)/54.4)^2)

Goodness of fit:

SSE: 2.152e-015
R-square: 0.9719
Adjusted R-square: 0.9697
RMSE: 5.798e-009

Pulse 5 – CO_2

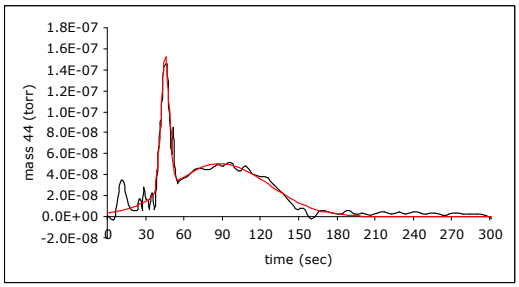

Pulse 5 - de-convoluted CO_2

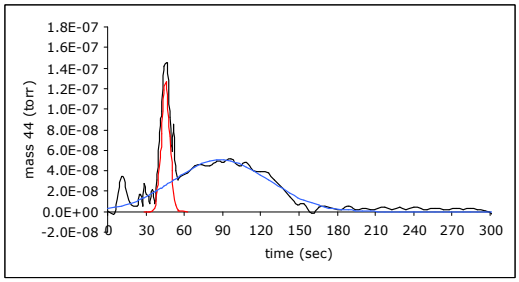

f(x)=1.272e-007*exp(-((x-45.3)/4.6)^2) + 5.083e-008*exp(-((x-89)/52.9)^2)

Goodness of fit:

SSE: 4.123e-015
R-square: 0.9504
Adjusted R-square: 0.9465
RMSE: 8.027e-009

Figure D.1.18. (Cont'd.)

Pulse 1 – H_2O

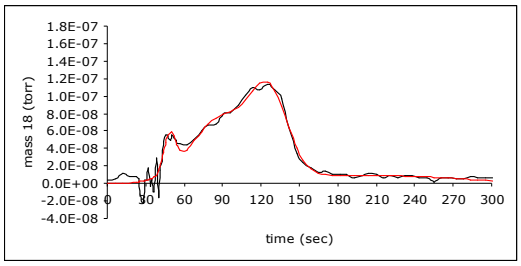

Pulse 1 - de-convoluted H_2O

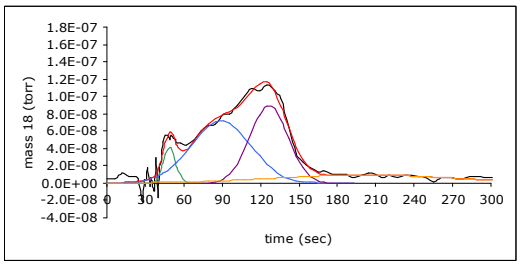

f(x)=4.148e-008*exp(-((x-49)/6.6)^2) + 7.184e-008*exp(-((x-89.2)/32.9)^2) +
8.98e-008*exp(-((x-126.6)/20.8)^2) + 9.274e-009*exp(-((x-201)/98)^2)

Goodness of fit:

SSE: 3.922e-015
R-square: 0.9509
Adjusted R-square: 0.9416
RMSE: 8.224e-009

Pulse 2 – H_2O

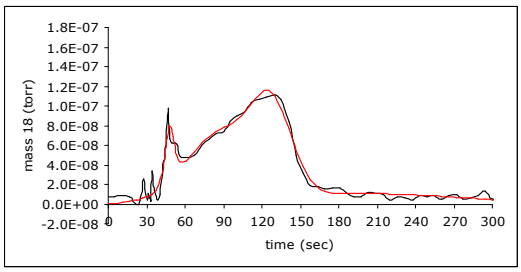

Pulse 2 - de-convoluted H_2O

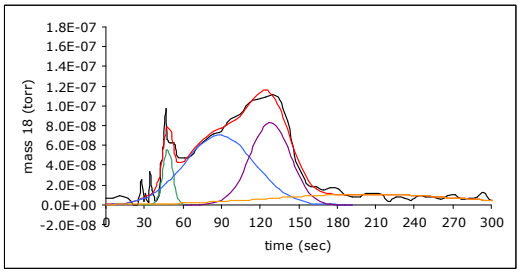

f(x)=5.512e-008*exp(-((x-48.1)/5.5)^2)+7.056e-008*exp(-((x-88.5)/38)^2)+
8.346e-008*exp(-((x-128)/22)^2) + 1.043e-008*exp(-((x-203)/105)^2)

Goodness of fit:

SSE: 3.638e-015
R-square: 0.9563
Adjusted R-square: 0.9484
RMSE: 7.722e-009

Pulse 3 – H_2O

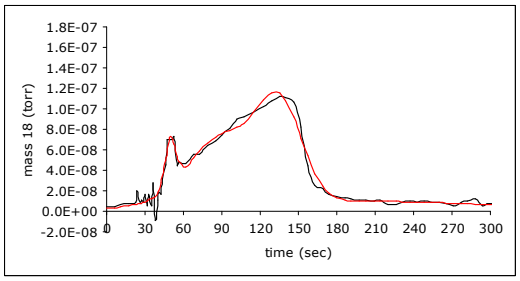

Pulse 3 - de-convoluted H_2O

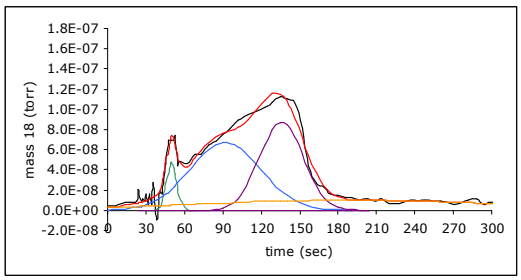

f(x)=4.792e-008 *exp(-((x-50)/5.5)^2) + 6.704e-008*exp(-((x-92)/38.9)^2) +
8.675e-008 *exp(-((x-136)/24)^2) + 9.943e-009*exp(-((x-190)/170)^2)

Goodness of fit:

SSE: 2.551e-015
R-square: 0.9674
Adjusted R-square: 0.9615
RMSE: 6.521e-009

Figure D.1.19. Gaussian fits and de-convolution of Gaussian fits for H_2O response data for C_2H_6 pulses into O_2 and He flow over Cr-O catalyst at 450°C

Pulse 4 – H_2O

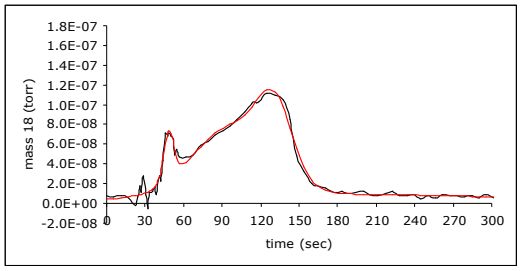

Pulse 4 - de-convoluted H_2O

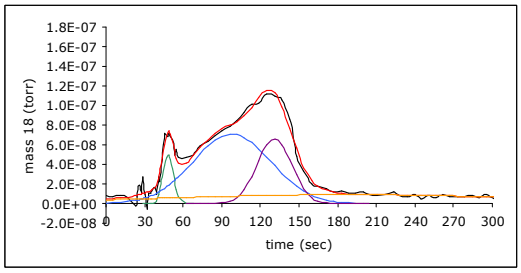

f(x)=4.943e-008*exp(-((x-48.5)/5.7)^2) + 7.088e-008*exp(-((x-98)/42.7)^2) +
6.578e-008*exp(-((x-131)/19)^2) + 9.098e-009*exp(-((x-188)/202)^2)

Goodness of fit:

SSE: 1.706e-015
R-square: 0.9774
Adjusted R-square: 0.9732
RMSE: 5.378e-009

Pulse 5 – H_2O

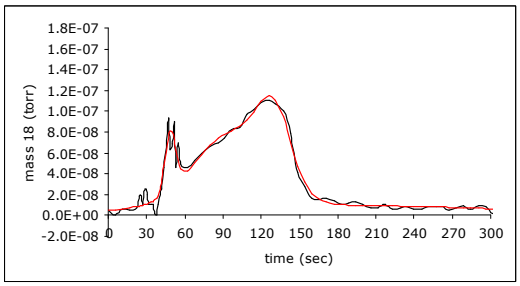

Pulse 5 - de-convoluted H_2O

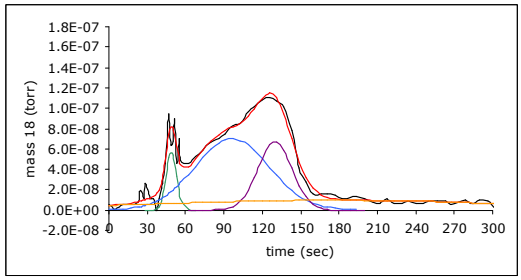

f(x)= 5.679e-008*exp(-((x-49)/5.8)^2) + 7.006e-008*exp(-((x-96.5)/41)^2) +
6.737e-008*exp(-((x-130)/18.7)^2) + 9.641e-009*exp(-((x-174)/200)^2)

Goodness of fit:

SSE: 3.515e-015
R-square: 0.9568
Adjusted R-square: 0.9489
RMSE: 7.654e-009

Figure D.1.19. (Cont'd.)

Table D.9. C_2H_6 response data for C_2H_6 pulses into O_2 and He flow over Cr-O catalyst at 450°C

	Pulse 1	***Pulse 2***	***Pulse 3***	***Pulse 4***	***Pulse 5***	***Avr:***
zeroth moment (m_0)	3.9E-05	3.9E-05	4.3E-05	3.9E-05	3.9E-05	4.0E-05
m_1	1.4E-03	1.4E-03	1.6E-03	1.4E-03	1.4E-03	1.4E-03
first moment ($\mu_0 = m_1/m_0$)	36.3	35.7	36.4	36.2	36.2	36.2
mean residence time (t_m)	36.3	35.7	36.4	36.2	36.2	36.2
m_2	5.7E-02	5.4E-02	6.2E-02	5.6E-02	5.7E-02	5.7E-02
variance (σ^2), sec^2	132.7	129.6	131.0	128.1	131.4	130.6
standard deviation (σ)	11.5	11.4	11.4	11.3	11.5	11.4

Table D.10. C_2H_4 response data for C_2H_6 pulses into O_2 and He flow over Cr-O catalyst at 450°C

	Pulse 1	***Pulse 2***	***Pulse 3***	***Pulse 4***	***Pulse 5***	***Avr:***
	Area1	*Area1*	*Area1*	*Area1*	*Area1*	
zeroth moment (m_0)	1.4E-06	1.5E-06	1.5E-06	1.6E-06	1.4E-06	1.5E-06
m_1	4.3E-05	4.8E-05	4.8E-05	5.2E-05	4.6E-05	4.7E-05
first moment ($\mu_0 = m_1/m_0$)	31.8	32.4	32.8	32.6	32.0	32.3
mean residence time (t_m)	31.8	32.4	32.8	32.6	32.0	32.3
m_2	1.4E-03	1.6E-03	1.6E-03	1.8E-03	1.6E-03	1.6E-03
variance (σ^2), sec^2	45.0	60.4	50.9	65.2	58.8	56.1
standard deviation (σ), sec	6.7	7.8	7.1	8.1	7.7	7.5
% of total area	83.9	85.6	75.0	89.6	88.0	84.4

	Pulse 1	***Pulse 2***	***Pulse 3***	***Pulse 4***	***Pulse 5***	***Avr:***
	Area2	*Area2*	*Area2*	*Area2*	*Area2*	
zeroth moment (m_0)	2.6E-07	2.5E-07	4.8E-07	1.9E-07	2.0E-07	2.8E-07
m_1	1.6E-05	1.6E-05	2.8E-05	1.2E-05	1.3E-05	1.7E-05
first moment ($\mu_0 = m_1/m_0$)	61.2	63.7	57.0	63.5	63.7	61.8
mean residence time (t_m)	61.2	63.7	57.0	63.5	63.7	61.8
m_2	9.9E-04	1.0E-03	1.6E-03	7.5E-04	8.1E-04	1.0E-03
variance (σ^2), sec^2	63.9	81.8	83.0	22.9	26.3	55.6
standard deviation (σ), sec	8.0	9.0	9.1	4.8	5.1	7.2
% of total area	16.1	14.4	25.0	10.4	12.0	15.6

Total area (Area 1 + 2)	1.6E-06	1.7E-06	1.9E-06	1.8E-06	1.6E-06	1.7E-06

Table D.11. CO_2 response data for C_2H_6 pulses into O_2 and He flow over Cr-O catalyst at 450°C

Gauss 1						
	Pulse 1	***Pulse 2***	***Pulse 3***	***Pulse 4***	***Pulse 5***	***Avr:***
mean (η)	45	44.5	46	44.7	45.0	45
variance (σ^2)	2.3	2.3	2.2	2.4	2.3	2.3
standard deviation (σ)	1.5	1.5	1.5	1.5	1.5	1.5
peak amplitude	1.2E-07	1.2E-07	1.2E-07	1.2E-07	1.3E-07	1.2E-07
Area under the curve	9.7E-07	9.7E-07	9.0E-07	1.1E-06	1.0E-06	9.9E-07
% of total area	21	20	17	23	22	21

Gauss 2						
	Pulse 1	***Pulse 2***	***Pulse 3***	***Pulse 4***	***Pulse 5***	***Avr:***
mean (η)	90	89.5	92.1	90.9	90.0	91
variance (σ^2)	25	26	29.1	27.2	25.0	26
standard deviation (σ)	5.0	5.1	5.4	5.2	5.0	5
peak amplitude	5.2E-08	5.3E-08	5.1E-08	4.8E-08	5.1E-08	5.1E-08
Area under the curve	4.6E-06	4.8E-06	5.2E-06	4.6E-06	4.7E-06	4.8E-06
% of total area	83	83	85	81	82	83

Total area (Gauss1+2):	5.6E-06	5.8E-06	6.1E-06	5.7E-06	5.8E-06	5.8E-06

Table D.12. H_2O response data for C_2H_6 pulses into O_2 and He flow over Cr-O catalyst at 450°C

Gauss 1						
	Pulse 1	***Pulse 2***	***Pulse 3***	***Pulse 4***	***Pulse 5***	***Avr:***
mean (η)	49	48.1	50	48.5	49.0	49
variance (σ^2)	3.3	2.8	2.8	2.9	2.9	3
standard deviation (σ)	1.8	1.7	1.7	1.7	1.7	2
peak amplitude	4.1E-08	5.5E-08	4.8E-08	4.9E-08	5.7E-08	5.0.E-08
Area under the curve	4.9E-07	5.4E-07	4.7E-07	5.0E-07	5.8E-07	5.1E-07
% of total area	5	5	4	5	5	5

Gauss 2						
	Pulse 1	***Pulse 2***	***Pulse 3***	***Pulse 4***	***Pulse 5***	***Avr:***
mean (η)	89.2	88.5	92	98	96.5	93
variance (σ^2)	16.5	19	19	21.4	20.5	19
standard deviation (σ)	4.1	4.4	4.4	4.6	4.5	4
peak amplitude	7.2E-08	7.1E-08	6.7E-08	7.1E-08	7.0E-08	7.0E-08
Area under the curve	4.2E-06	4.7E-06	4.6E-06	5.4E-06	5.1E-06	4.8E-06
% of total area	44	45	41	50	48	46

Gauss 3						
	Pulse 1	***Pulse 2***	***Pulse 3***	***Pulse 4***	***Pulse 5***	***Avr:***
mean (η)	126.6	128	136	131	130.0	130.3
variance (σ^2)	10.4	11	12.0	9.5	9.4	10.5
standard deviation (σ)	3.2	3.3	3.5	3.1	3.1	3.2
peak amplitude	9.0E-08	8.3E-08	8.7E-08	6.6E-08	6.7E-08	7.9E-08
Area under the curve	3.3E-06	3.3E-06	3.7E-06	2.2E-06	2.2E-06	2.9E-06
% of total area	35	31	32	21	21	28

Gauss 4						
	Pulse 1	***Pulse 2***	***Pulse 3***	***Pulse 4***	***Pulse 5***	***Avr:***
mean (η)	201	203	190	188	174	191.2
variance (σ^2)	49	52.5	85	101	100	77.5
standard deviation (σ)	7.0	7.2	9.2	10.0	10.0	8.7
peak amplitude	9.3E-09	1.0E-08	9.9E-09	9.1E-09	9.6E-09	9.7E-09
Area under the curve	1.6E-06	1.9E-06	2.6E-06	2.6E-06	2.7E-06	2.3E-06
% of total area	17	18	23	24	26	22

Total area (Gauss1+2+3+4)	9.6E-06	1.0E-05	1.1E-05	1.1E-05	1.1E-05	1.1E-05

D.1.4. Dynamic Experiments' data for Cr-O catalyst with C_2H_6 pulses into He flow at 448°C

The response data for C_2H_6 pulses into He flow over Cr-O catalyst at 448°C are presented in Figures D.1.20-D.1.36. The results of moment, variance, mean residence time, and standard deviation calculations for C_2H_6 and C_2H_4 are tabulated in Tables D.13 and D.14, respectively.

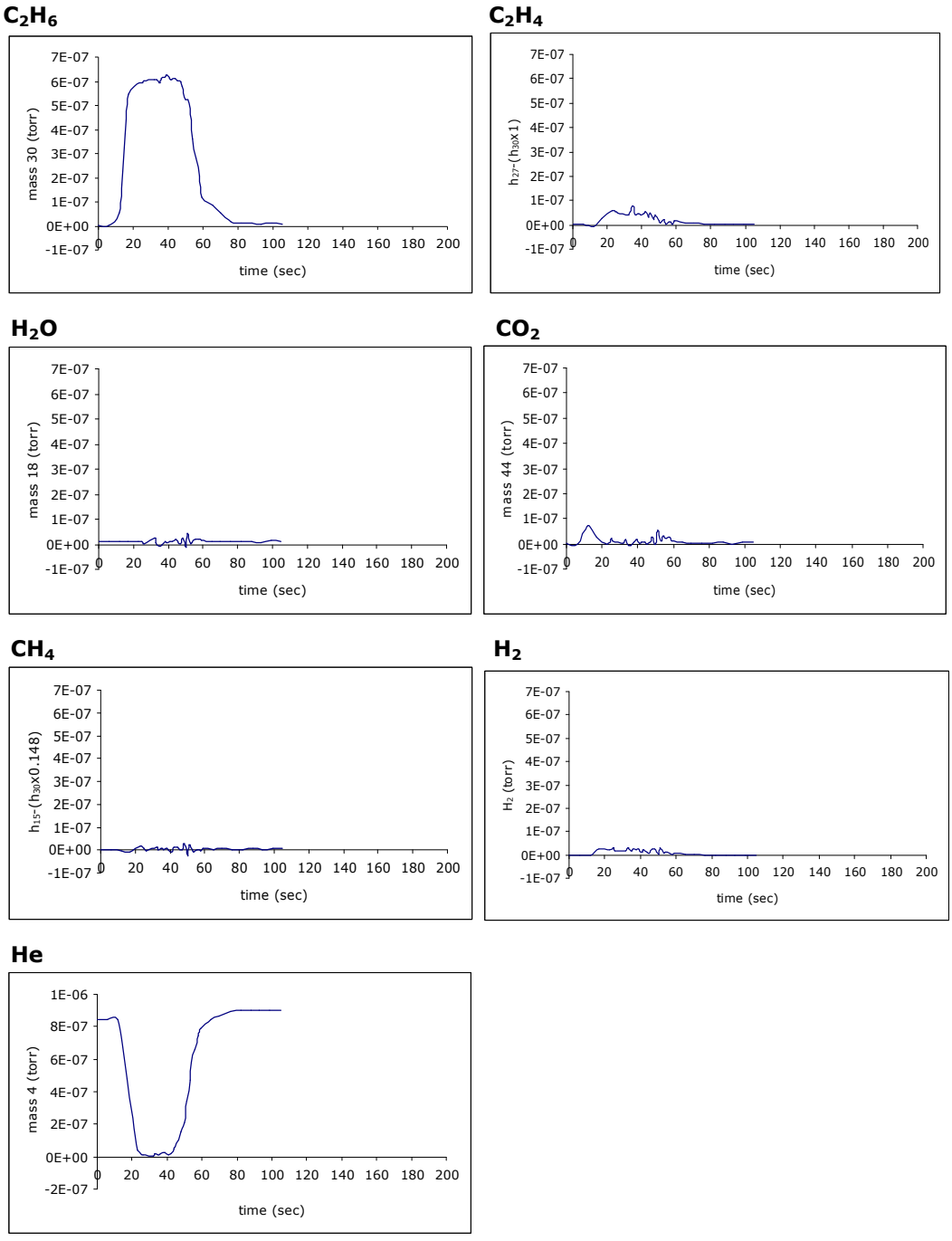

Figure D.1.20. 'Pulse 1' response data for C_2H_6 pulses into He flow over Cr-O catalyst at 448°C

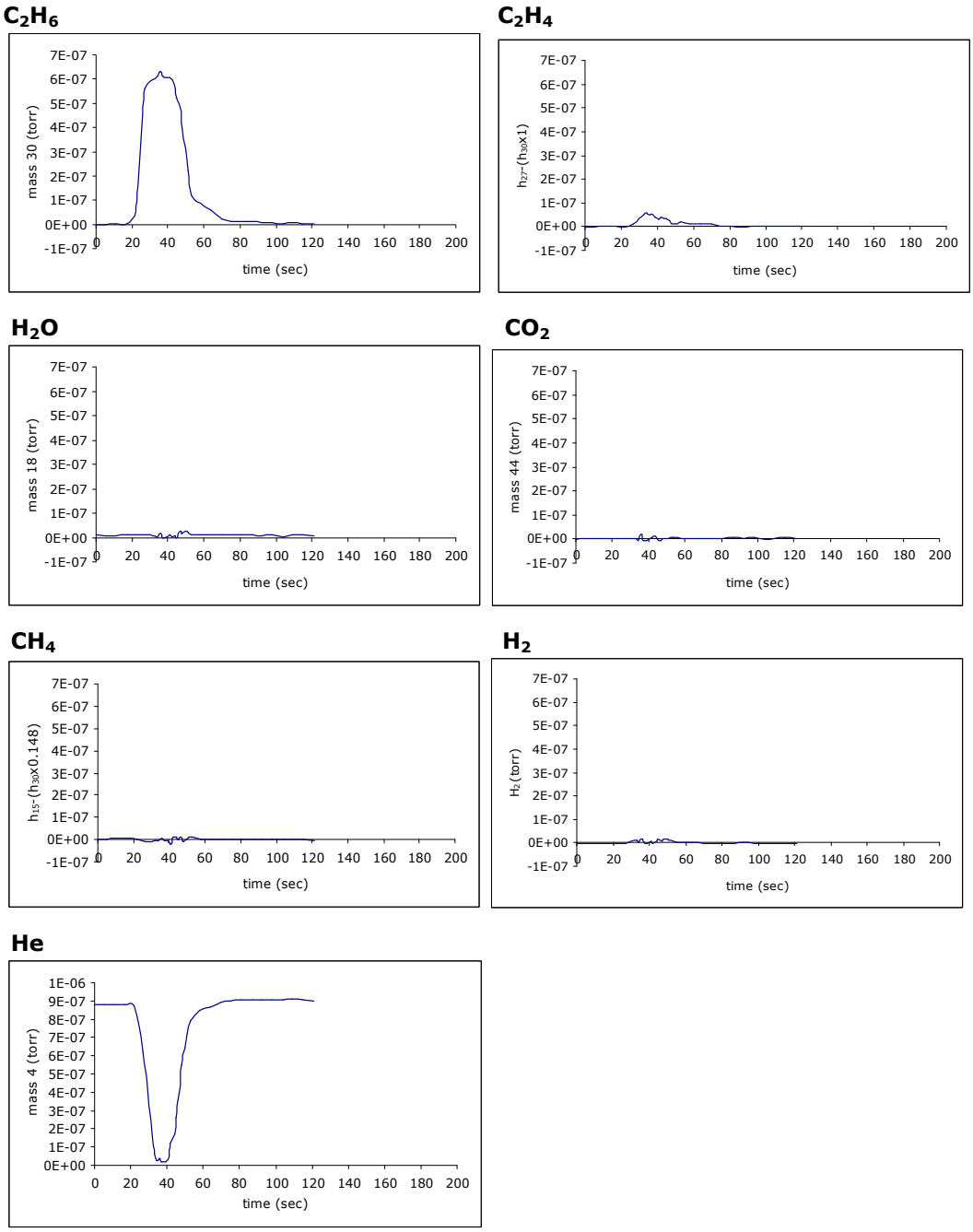

Figure D.1.21. 'Pulse 2' response data for C_2H_6 pulses into He flow over Cr-O catalyst at 448°C

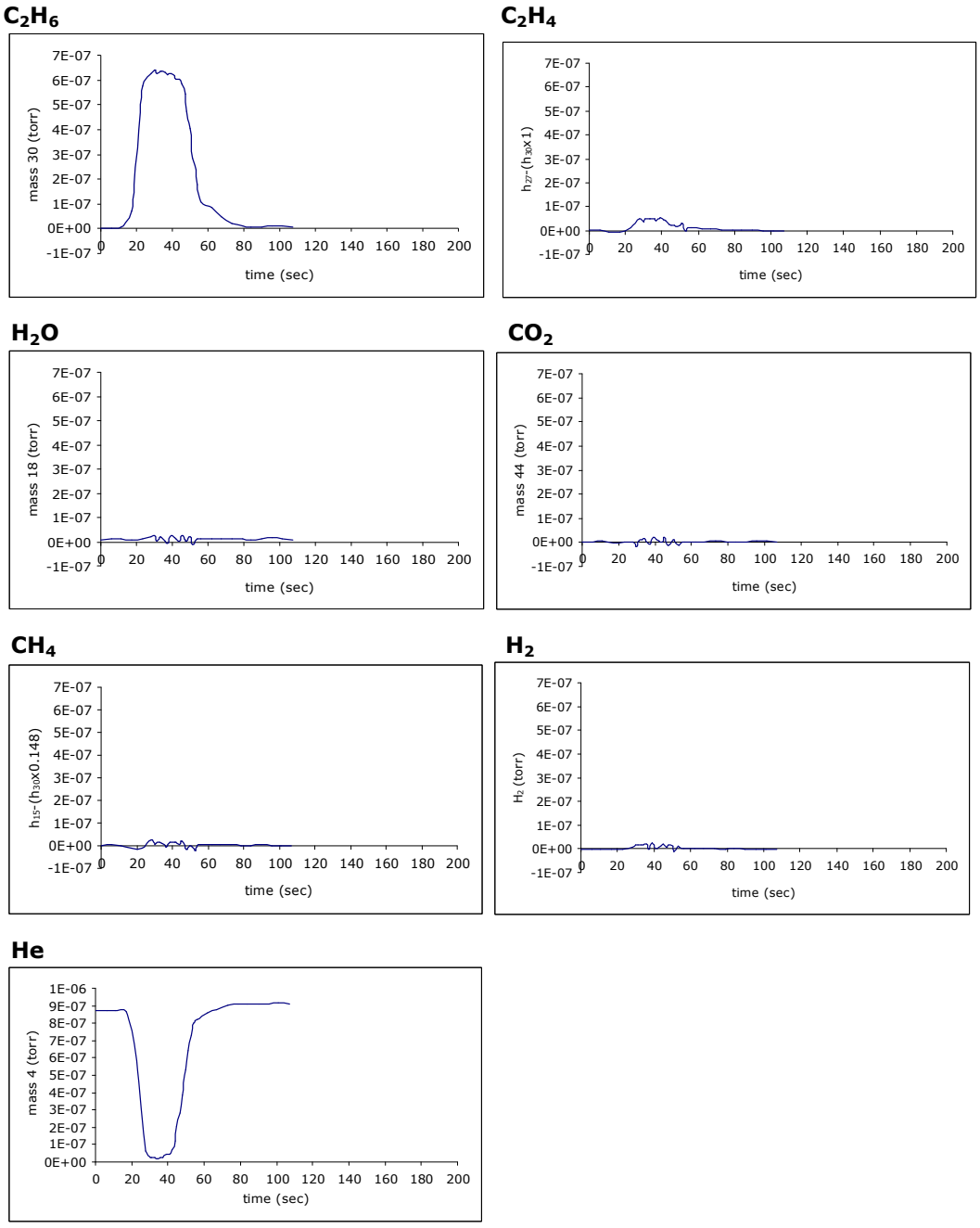

Figure D.1.22. 'Pulse 3' response data for C_2H_6 pulses into He flow over Cr-O catalyst at 448°C

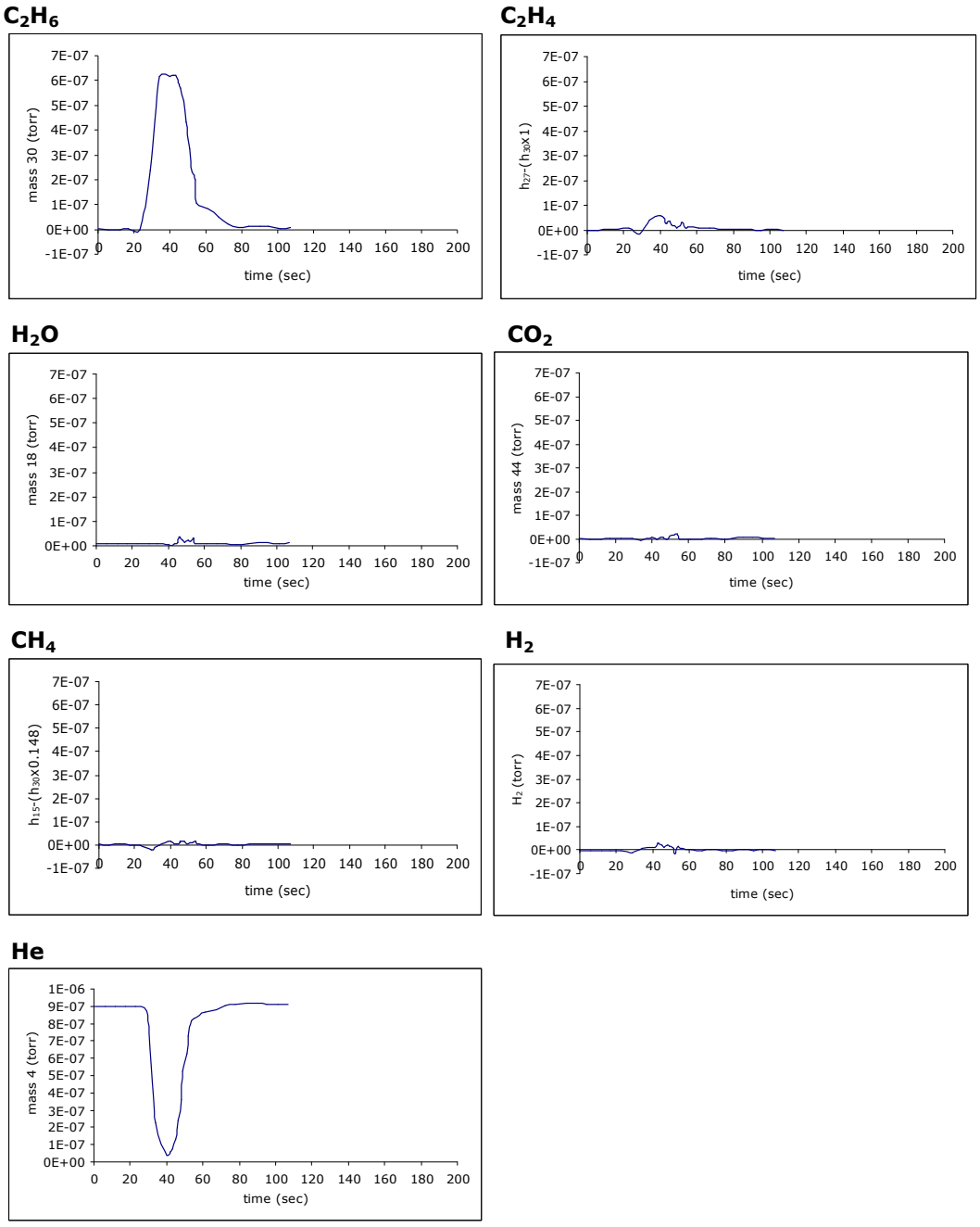

Figure D.1.23. 'Pulse 4' response data for C_2H_6 pulses into He flow over Cr-O catalyst at 448°C

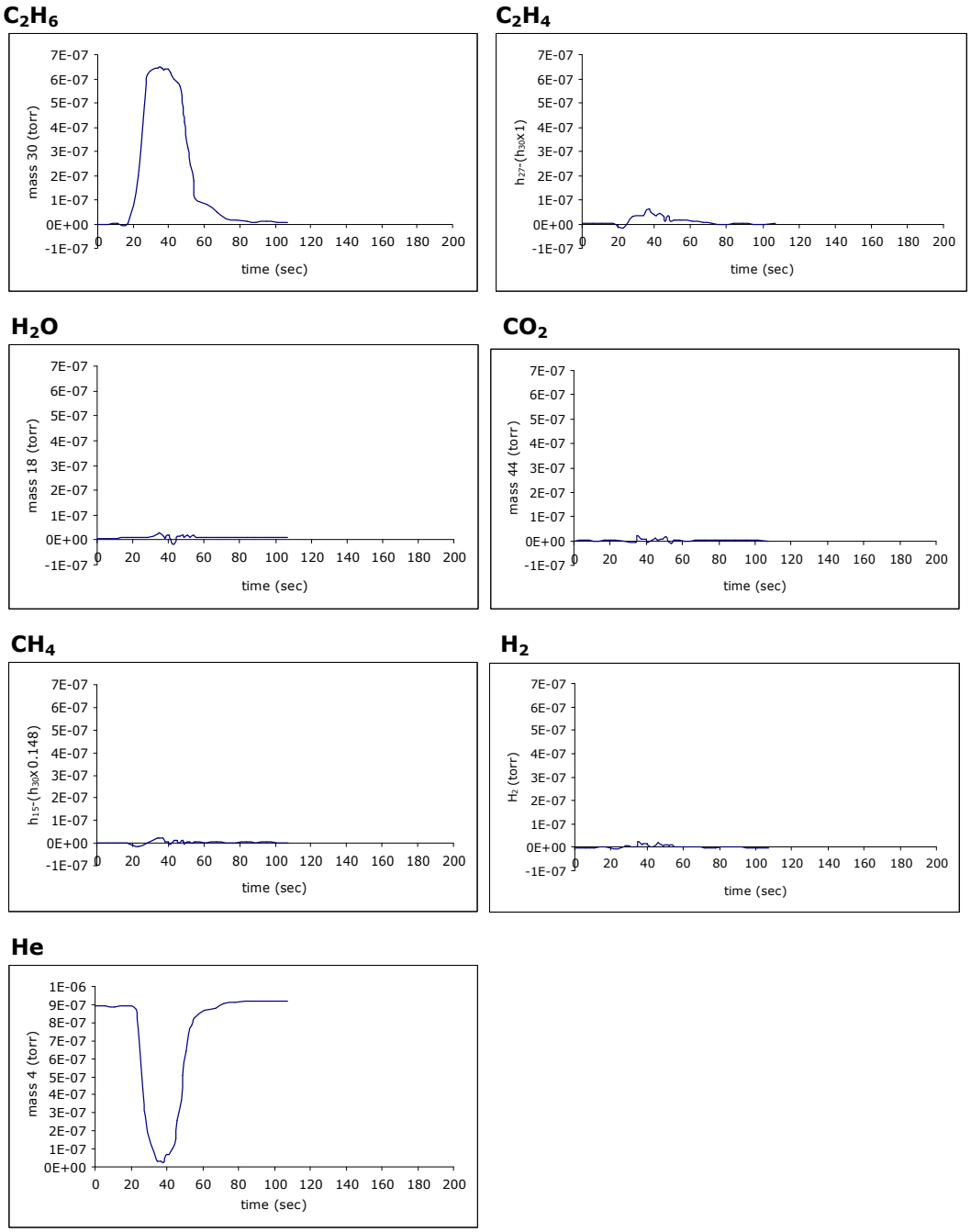

Figure D.1.24. 'Pulse 5' response data for C_2H_6 pulses into He flow over Cr-O catalyst at 448°C

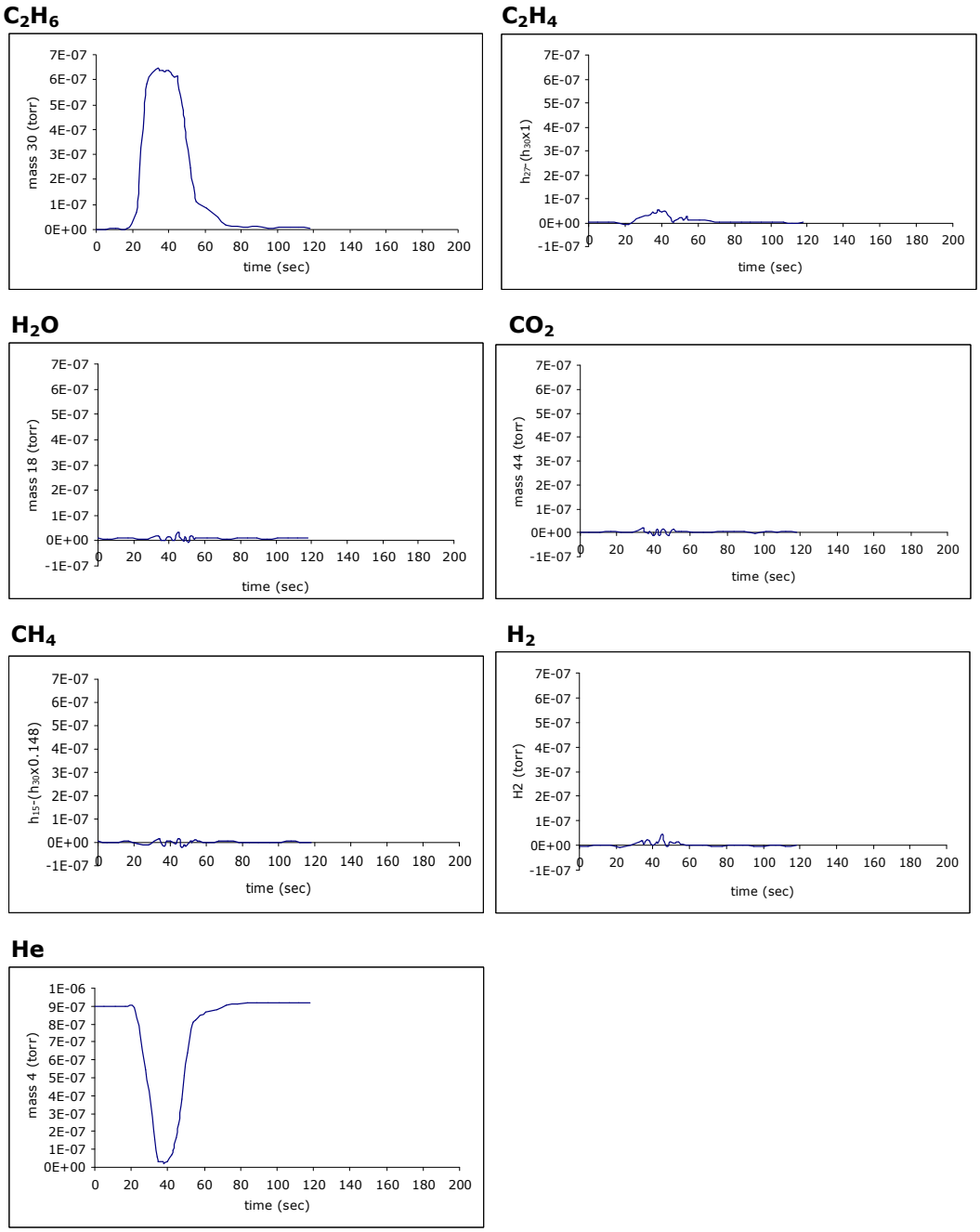

Figure D.1.25. 'Pulse 6' response data for C_2H_6 pulses into He flow over Cr-O catalyst at 448°C

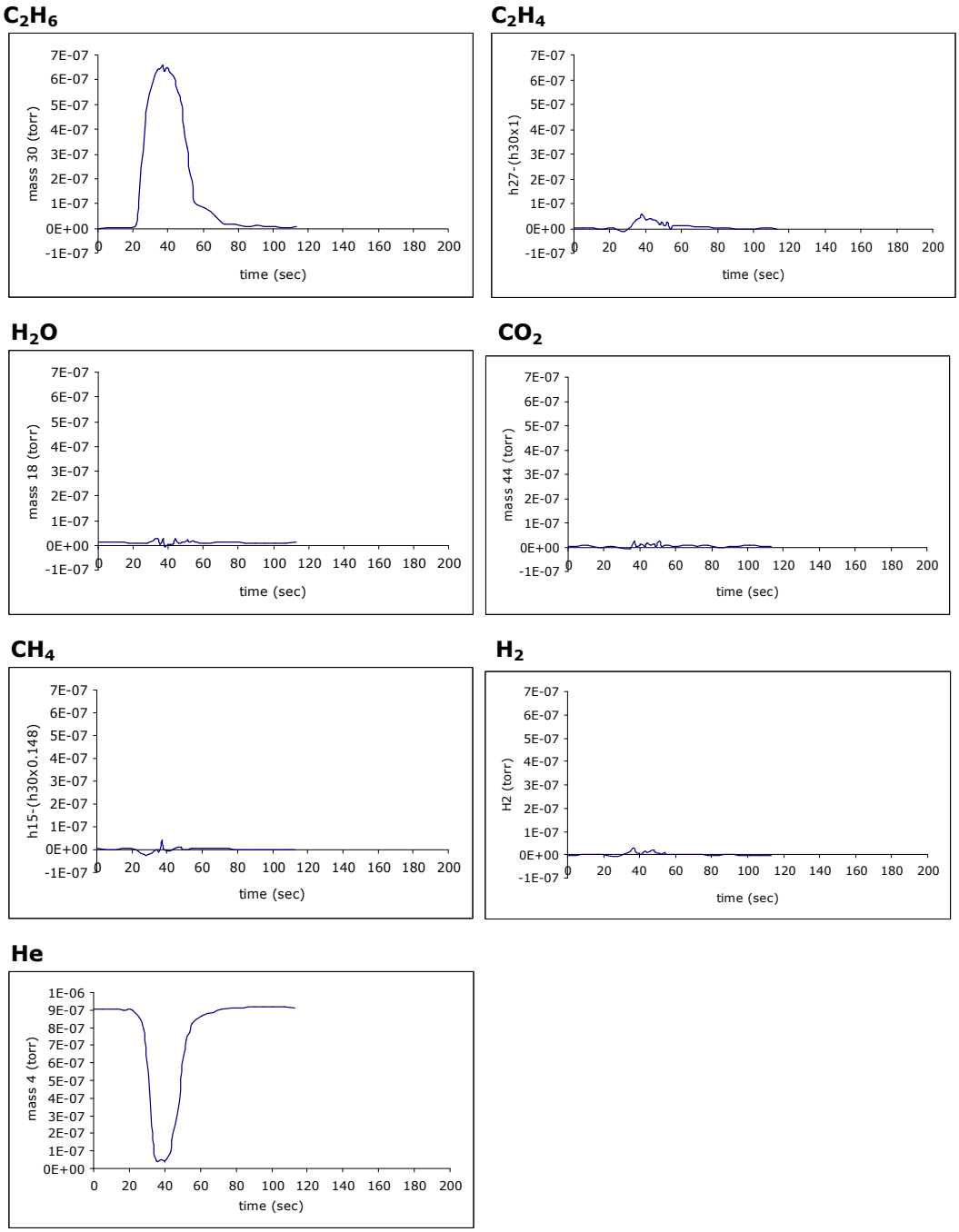

Figure D.1.26. 'Pulse 7' response data for C_2H_6 pulses into He flow over Cr-O catalyst at 448°C

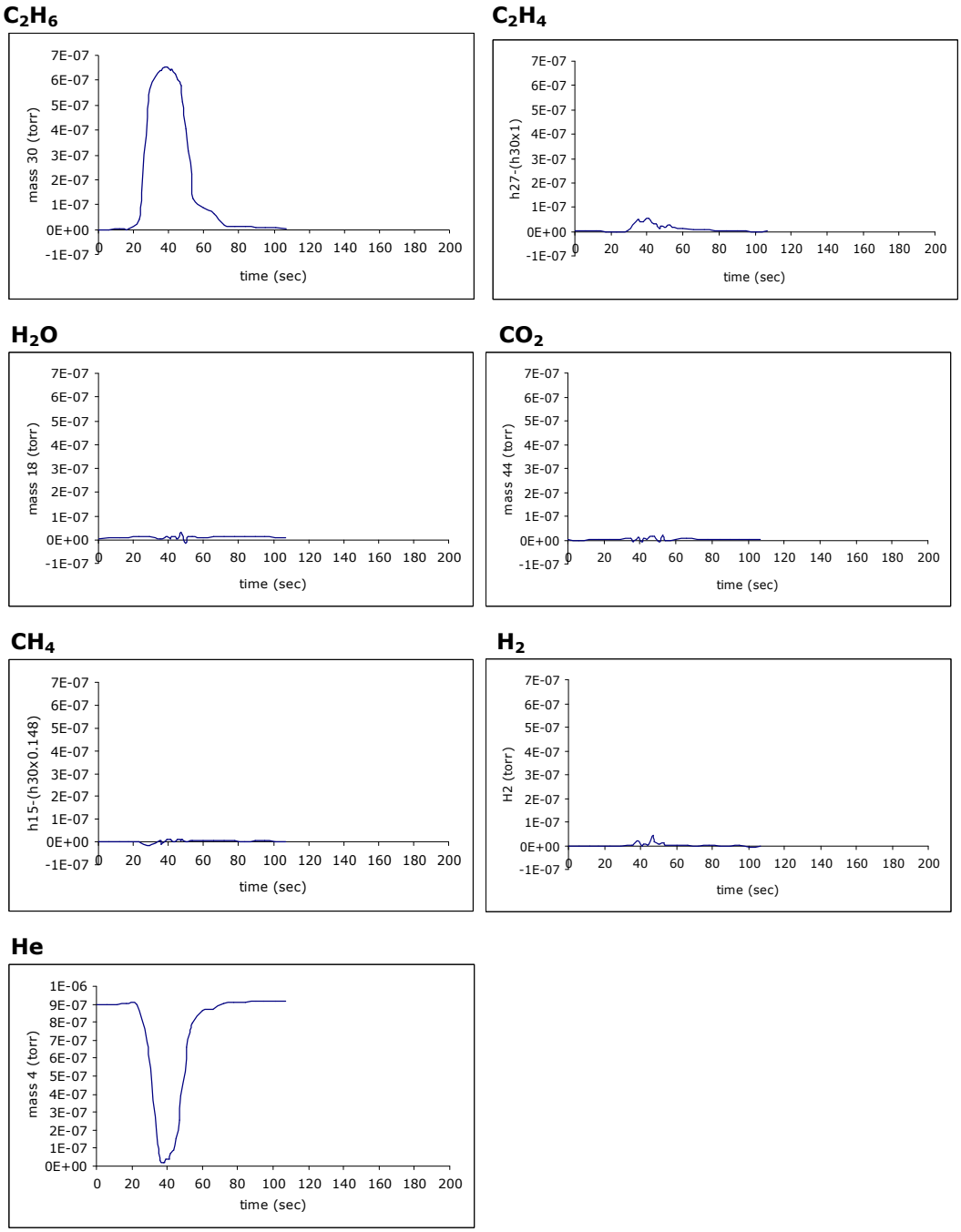

Figure D.1.27. 'Pulse 8' response data for C_2H_6 pulses into He flow over Cr-O catalyst at 448°C

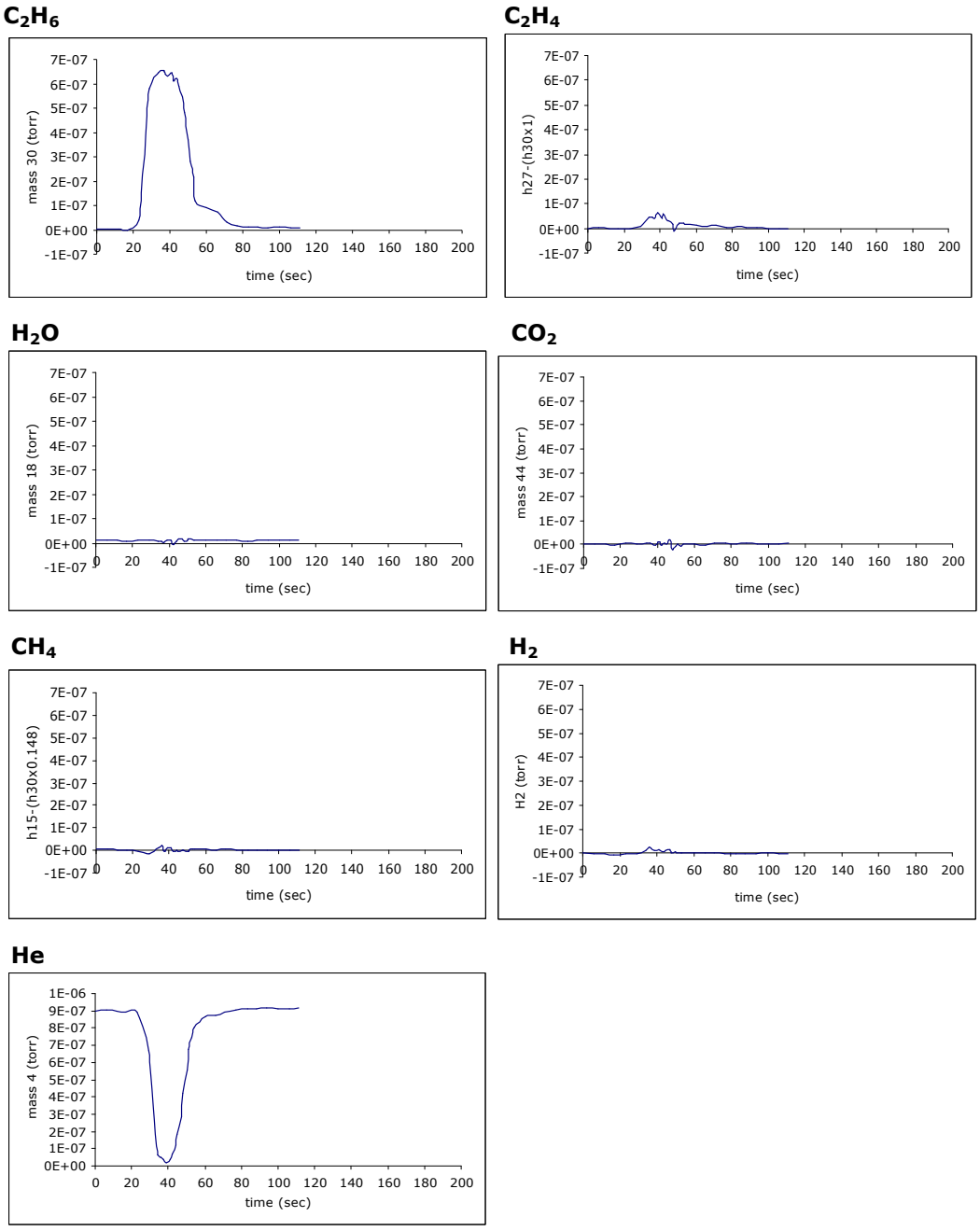

Figure D.1.28. 'Pulse 9' response data for C_2H_6 pulses into He flow over Cr-O catalyst at 448°C

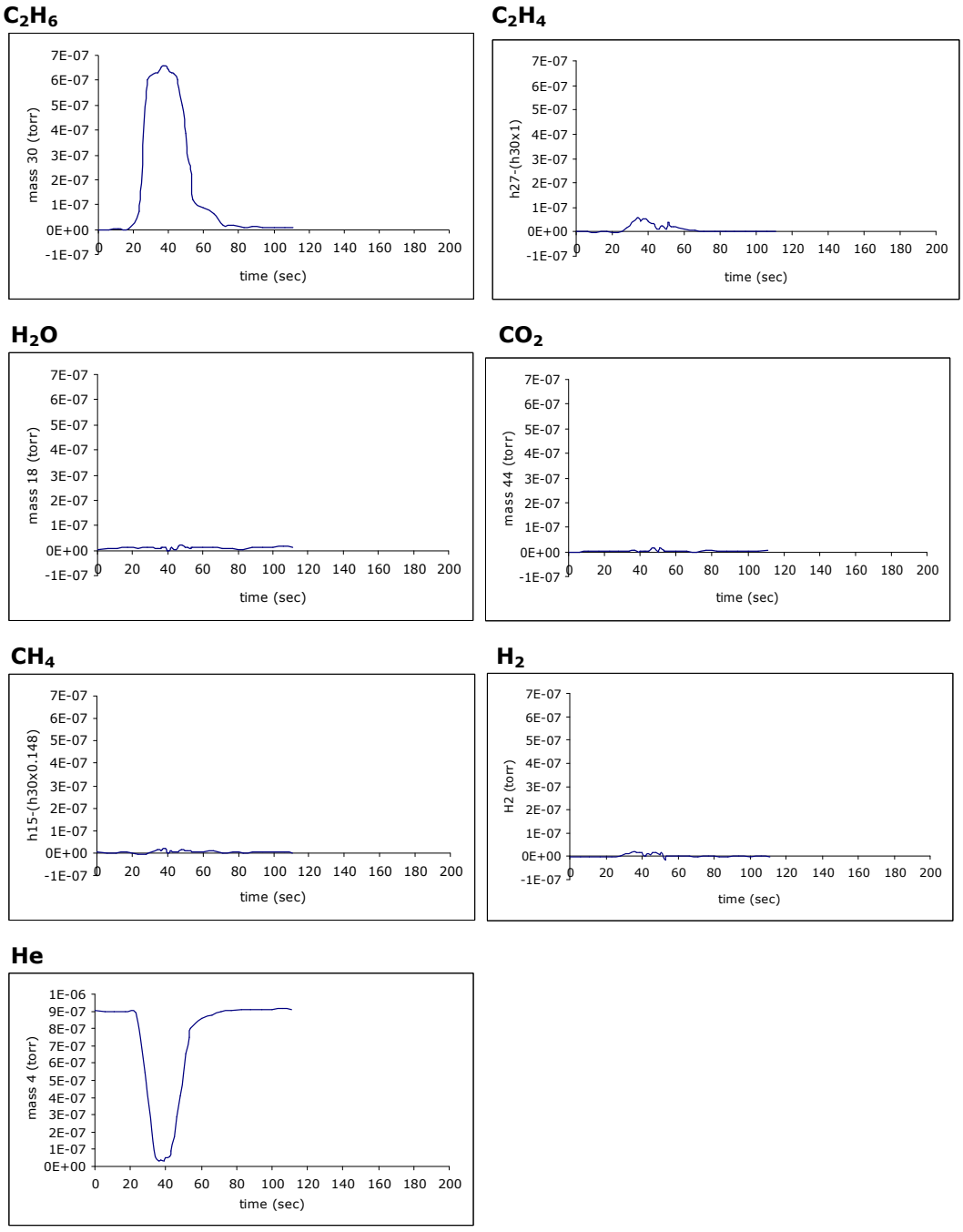

Figure D.1.29. 'Pulse 10' response data for C_2H_6 pulses into He flow over Cr-O catalyst at 448°C

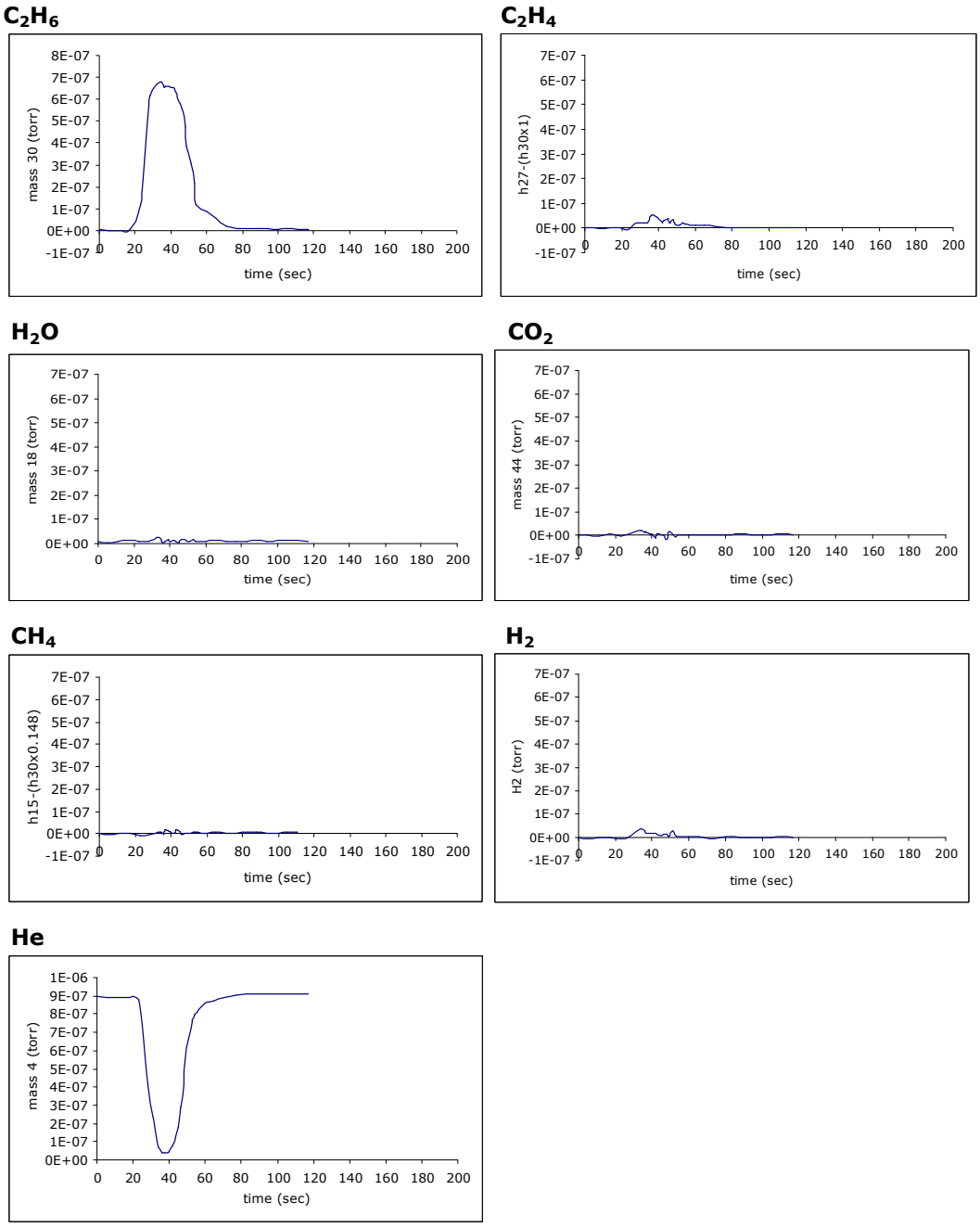

Figure D.1.30. 'Pulse 11' response data for C_2H_6 pulses into He flow over Cr-O catalyst at 448°C

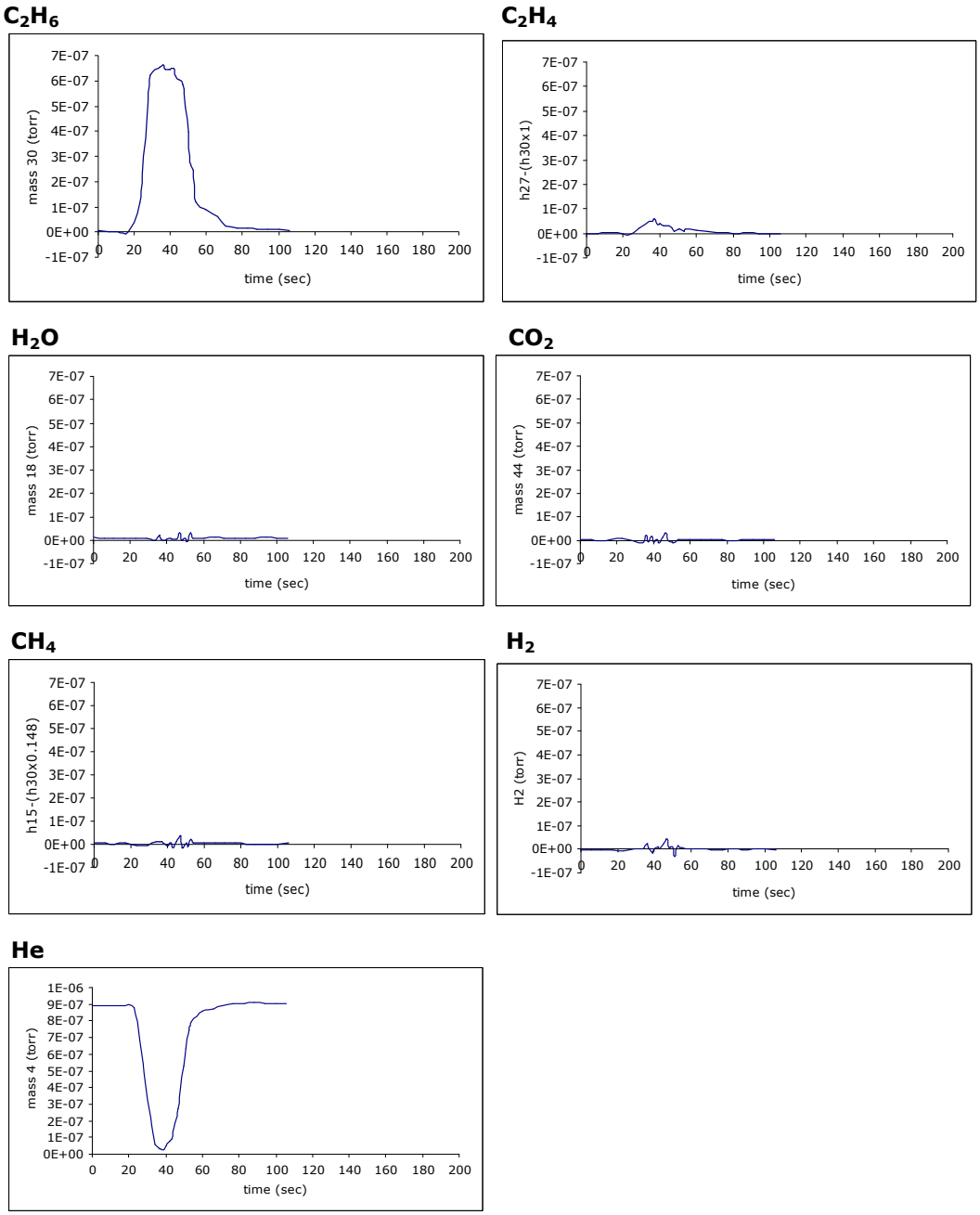

Figure D.1.31. 'Pulse 12' response data for C_2H_6 pulses into He flow over Cr-O catalyst at 448°C

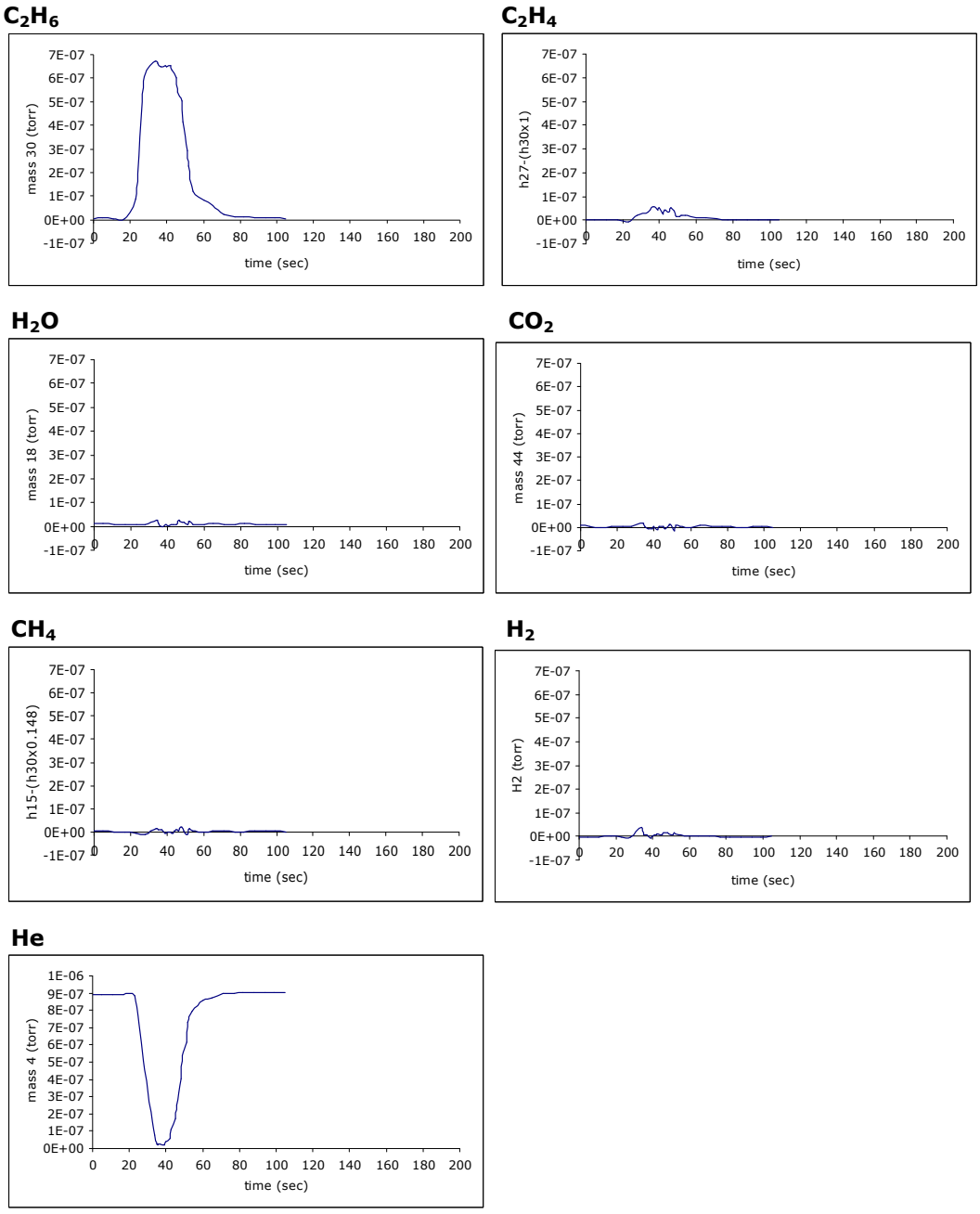

Figure D.1.32. 'Pulse 13' response data for C_2H_6 pulses into He flow over Cr-O catalyst at 448°C

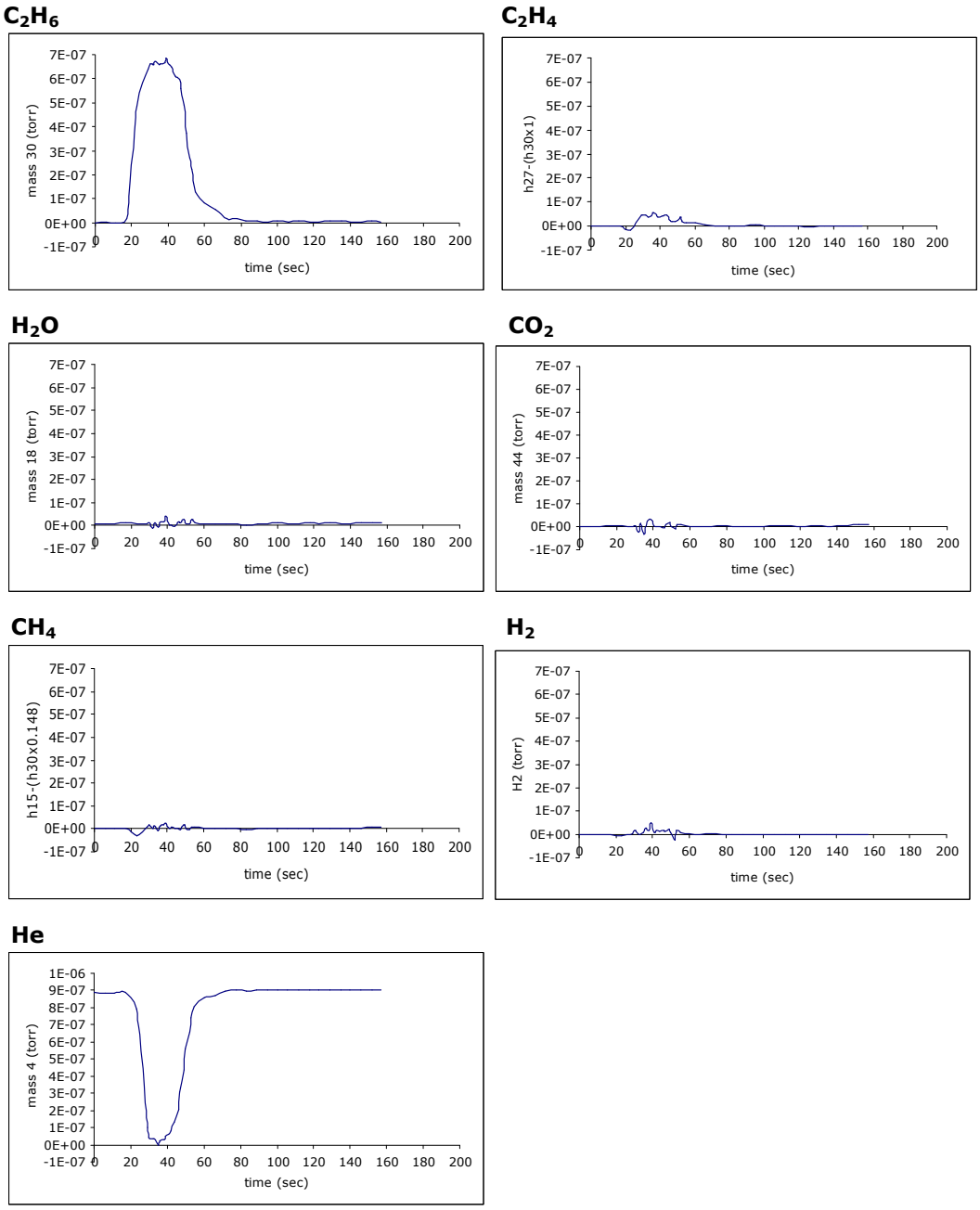

Figure D.1.33. 'Pulse 14' response data for C_2H_6 pulses into He flow over Cr-O catalyst at 448°C

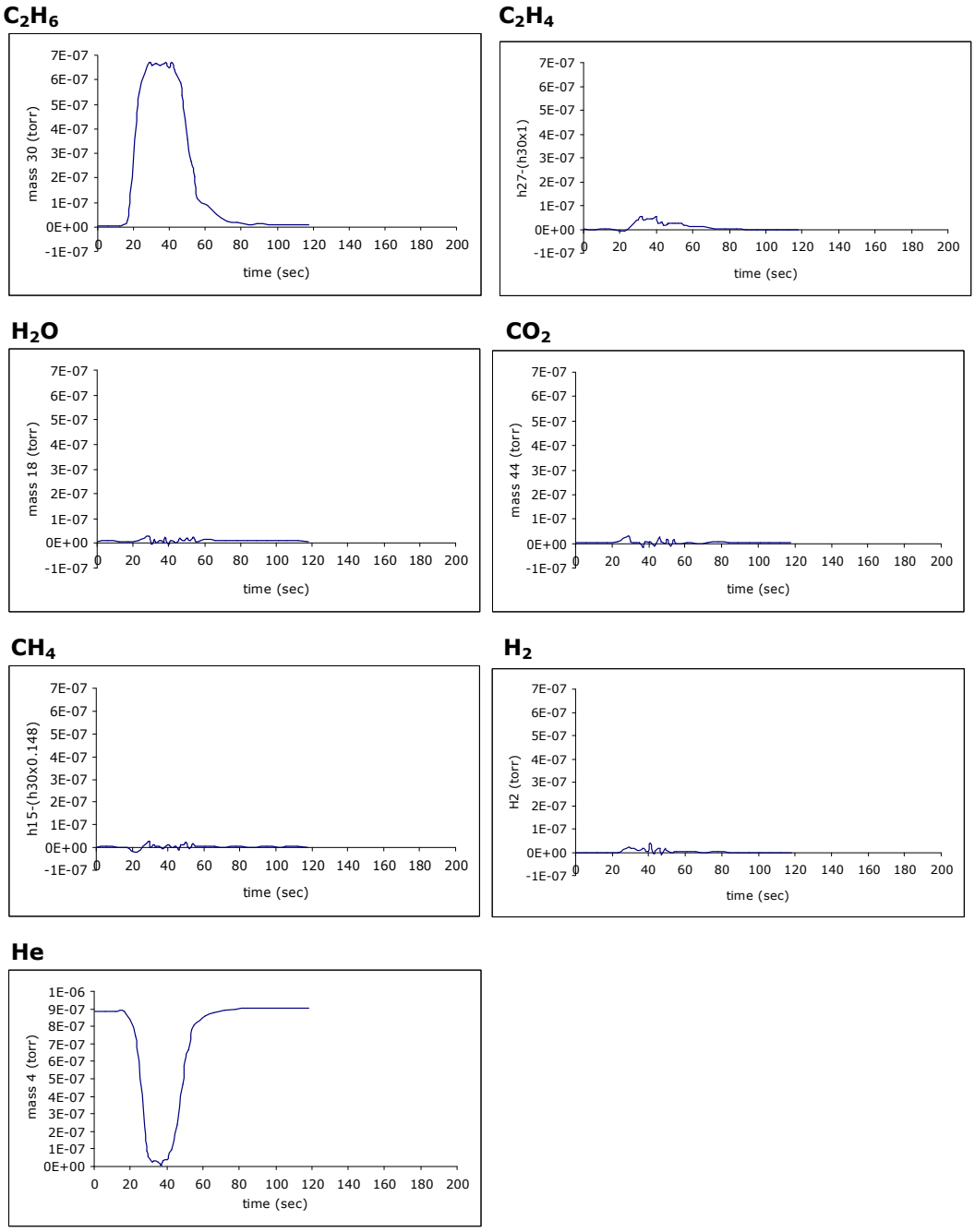

Figure D.1.34. 'Pulse 15' response data for C_2H_6 pulses into He flow over Cr-O catalyst at 448°C

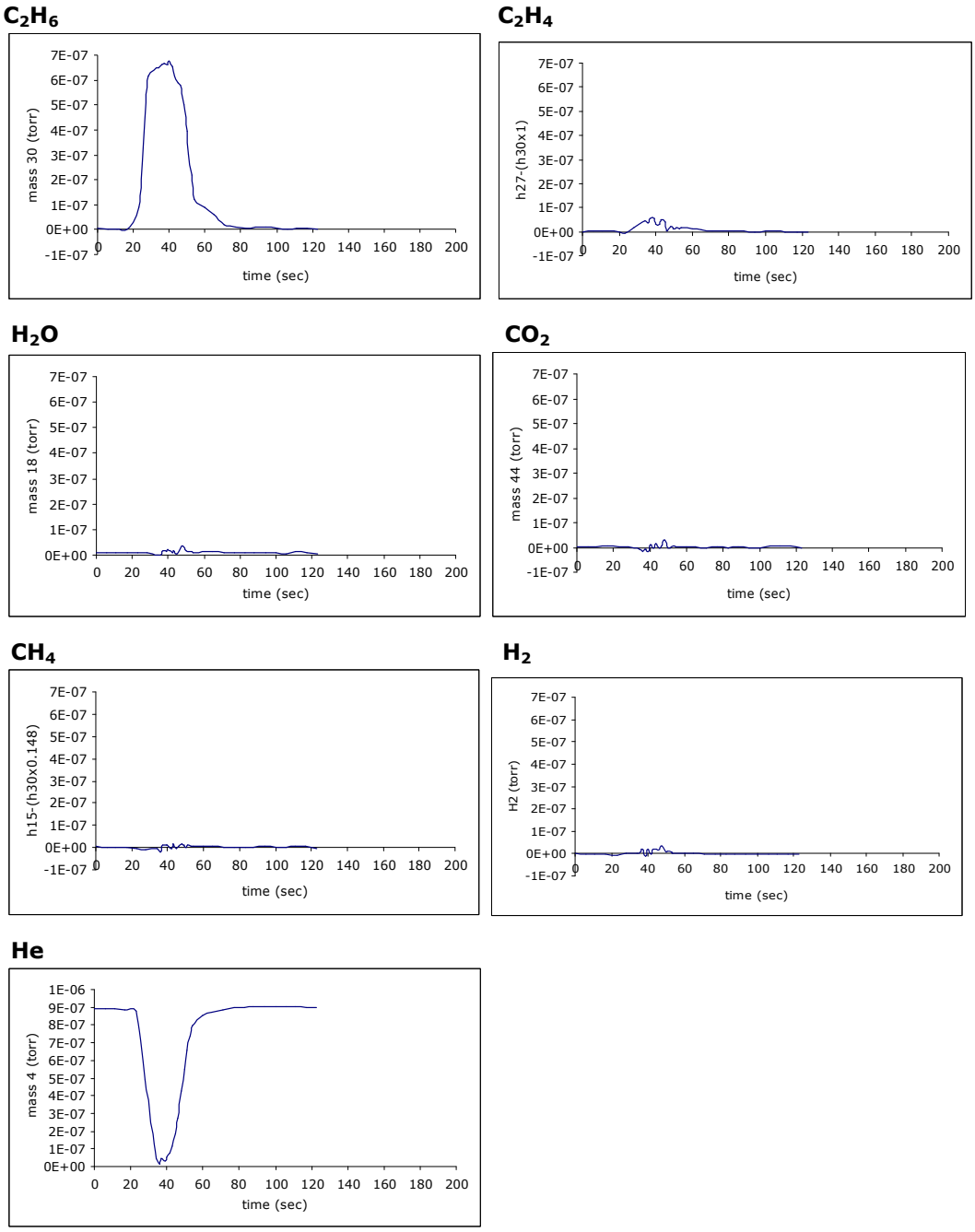

Figure D.1.35. 'Pulse 16' response data for C_2H_6 pulses into He flow over Cr-O catalyst at 448°C

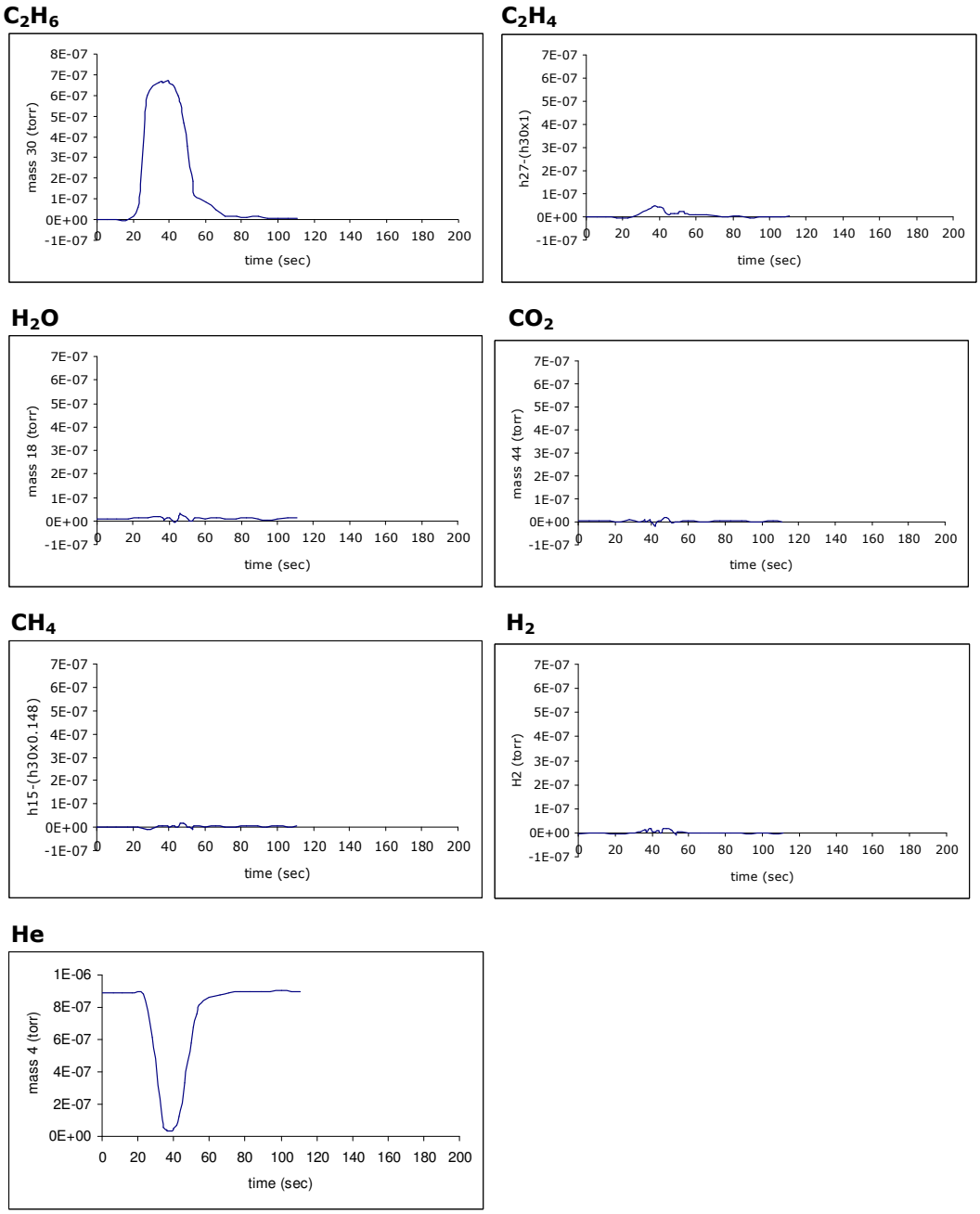

Figure D.1.36. 'Pulse 17' response data for C_2H_6 pulses into He flow over Cr-O catalyst at 448°C

Table D.13. C_2H_6 response data for C_2H_6 pulses into He flow over Cr-O catalyst at 448°C

	Pulse 1	***Pulse 2***	***Pulse 3***	***Pulse 4***	***Pulse 5***	***Pulse 6***	***Pulse 7***	***Pulse 8***
zeroth moment (m_0)	3.8E-05	2.8E-05	3.5E-05	2.1E-05	2.9E-05	3.0E-05	2.9E-05	3.0E-05
m_1	1.5E-03	1.1E-03	1.4E-03	9.4E-04	1.2E-03	1.2E-03	1.2E-03	1.3E-03
first moment ($\mu_1 = m_1/m_0$)	39.6	40.4	39.3	45.0	41.3	41.6	42.1	42.2
mean residence time (t_m)	39.6	40.4	39.3	45.0	41.3	41.6	42.1	42.2
m_2	6.5E-02	4.7E-02	5.7E-02	4.4E-02	5.2E-02	5.4E-02	5.4E-02	5.5E-02
variance (σ^2), sec^2	132.3	65.5	90.8	60.6	76.1	70.4	65.5	66.0
standard deviation (σ)	11.5	8.1	9.5	7.8	8.7	8.4	8.1	8.1

	Pulse 9	***Pulse 10***	***Pulse 11***	***Pulse 12***	***Pulse 13***	***Pulse 14***	***Pulse 15***	***Pulse 16***
zeroth moment (m_0)	3.0E-05	3.1E-05	3.2E-05	3.1E-05	3.2E-05	3.4E-05	3.8E-05	3.1E-05
m_1	1.3E-03	1.3E-03	1.3E-03	1.3E-03	1.3E-03	1.3E-03	1.5E-03	1.3E-03
first moment ($\mu_1 = m_1/m_0$)	42.6	42.0	41.6	42.1	41.4	39.2	39.7	41.5
mean residence time (t_m)	42.6	42.0	41.6	42.1	41.4	39.2	39.7	41.5
m_2	5.6E-02	5.8E-02	5.9E-02	5.7E-02	5.8E-02	5.5E-02	6.4E-02	5.6E-02
variance (σ^2), sec^2	79.2	77.5	84.2	79.9	78.1	78.9	94.2	69.1
standard deviation (σ)	8.9	8.8	9.2	8.9	8.8	8.9	9.7	8.3

	Pulse 17	***Avr.***
zeroth moment (m_0)	3.3E-05	3.1E-05
m_1	1.4E-03	1.3E-03
first moment ($\mu_1 = m_1/m_0$)	41.6	41.4
mean residence time (t_m)	41.6	41.4
m_2	5.9E-02	5.6E-02
variance (σ^2), sec^2	82.0	79.4
standard deviation (σ)	9.1	8.9

Table D.14. C_2H_4 response data for C_2H_6 pulses into He flow over Cr-O catalyst at 448°C

	Pulse 1	***Pulse 2***	***Pulse 3***	***Pulse 4***	***Pulse 5***	***Pulse 6***
	Area1	*Area1*	*Area1*	*Area1*	*Area1*	*Area1*
zeroth moment (m_0)	1.5E-06	1.0E-06	1.0E-06	5.6E-07	9.7E-07	6.6E-07
m_1	5.5E-05	4.0E-05	3.9E-05	2.5E-05	3.8E-05	2.5E-05
first moment ($\mu_1 = m_1/m_0$)	36.8	40.2	37.2	44.2	39.1	38.6
mean residence time (t_m)	36.8	40.2	37.2	44.2	39.1	38.6
m_2	2.1E-03	1.7E-03	1.5E-03	1.1E-03	1.5E-03	9.9E-04
variance (σ^2), sec^2	77.7	37.3	43.9	23.4	31.1	13.7
standard deviation (σ)	8.8	6.1	6.6	4.8	5.6	3.7
% of total area	86	85	81	72	75	55

	Pulse 1	***Pulse 2***	***Pulse 3***	***Pulse 4***	***Pulse 5***	***Pulse 6***
	Area2	*Area2*	*Area2*	*Area2*	*Area2*	*Area2*
zeroth moment (m_0)	2.5E-07	1.8E-07	2.5E-07	2.2E-07	3.3E-07	5.4E-07
m_1	1.7E-05	1.2E-05	1.6E-05	1.4E-05	1.8E-05	3.1E-05
first moment ($\mu_1 = m_1/m_0$)	68.1	66.4	65.7	63.4	55.1	57.1
mean residence time (t_m)	68.1	66.4	65.7	63.4	55.1	57.1
m_2	1.2E-03	7.9E-04	1.1E-03	9.2E-04	1.0E-03	1.8E-03
variance (σ^2), sec^2	120.8	26.7	126.3	106.4	26.4	150.6
standard deviation (σ)	11.0	5.2	11.2	10.3	5.1	12.3
% of total area	14	15	19	28	25	45

Total area (Area 1 + 2)	1.8E-06	1.2E-06	1.3E-06	7.9E-07	1.3E-06	1.2E-06

Table D.14. (Cont'd.)

	Pulse 7	***Pulse 8***	***Pulse 9***	***Pulse 10***	***Pulse 11***	***Pulse 12***
	Area1	*Area1*	*Area1*	*Area1*	*Area1*	*Area1*
zeroth moment (m_0)	5.8E-07	7.2E-07	6.8E-07	6.8E-07	7.0E-07	7.3E-07
m_1	2.4E-05	2.9E-05	2.7E-05	2.6E-05	2.8E-05	2.8E-05
first moment ($\mu_1 = m_1/m_0$)	41.4	39.6	39.6	38.4	40.6	39.0
mean residence time (t_m)	41.4	39.6	39.6	38.4	40.6	39.0
m_2	1.0E-03	1.1E-03	1.1E-03	1.0E-03	1.2E-03	1.1E-03
variance (σ^2), sec^2	23.6	11.7	15.9	12.1	23.2	17.9
standard deviation (σ)	4.9	3.4	4.0	3.5	4.8	4.2
% of total area	72	53	58	59	64	69

	Pulse 7	***Pulse 8***	***Pulse 9***	***Pulse 10***	***Pulse 11***	***Pulse 12***
	Area2	*Area2*	*Area2*	*Area2*	*Area2*	*Area2*
zeroth moment (m_0)	2.3E-07	6.4E-07	5.0E-07	4.7E-07	3.8E-07	3.3E-07
m_1	1.5E-05	3.6E-05	2.9E-05	2.5E-05	2.3E-05	1.8E-05
first moment ($\mu_1 = m_1/m_0$)	65.7	55.8	59.0	53.1	60.0	55.0
mean residence time (t_m)	65.7	55.8	59.0	53.1	60.0	55.0
m_2	1.0E-03	2.1E-03	1.8E-03	1.3E-03	1.4E-03	1.0E-03
variance (σ^2), sec^2	55.2	105.9	114.9	30.9	114.1	40.3
standard deviation (σ)	7.4	10.3	10.7	5.6	10.7	6.4
% of total area	28	47	42	41	36	31

Total area (Area 1 + 2)	8.1E-07	1.4E-06	1.2E-06	1.2E-06	1.1E-06	1.1E-06

Table D.14. (Cont'd.)

	Pulse 13	***Pulse 14***	***Pulse 15***	***Pulse 16***	***Pulse 17***	***Avr.***
	Area1	*Area1*	*Area1*	*Area1*	*Area1*	
zeroth moment (m_0)	7.9E-07	7.9E-07	6.0E-07	7.1E-07	6.0E-07	7.8E-07
m_1	3.2E-05	3.0E-05	2.2E-05	2.8E-05	2.3E-05	3.1E-05
first moment ($\mu_1 = m_1/m_0$)	39.8	38.0	36.2	39.3	38.2	39.2
mean residence time (t_m)	39.8	38.0	36.2	39.3	38.2	39.2
m_2	1.3E-03	1.2E-03	8.0E-04	1.1E-03	8.8E-04	1.2E-03
variance (σ^2), sec^2	26.5	27.3	18.9	15.0	9.3	25.2
standard deviation (σ)	5.1	5.2	4.3	3.9	3.0	4.8
% of total area	72	65	52	60	53	67

	Pulse 13	***Pulse 14***	***Pulse 15***	***Pulse 16***	***Pulse 17***	***Avr.***
	Area2	*Area2*	*Area2*	*Area2*	*Area2*	
zeroth moment (m_0)	3.1E-07	4.2E-07	5.5E-07	4.7E-07	5.2E-07	3.9E-07
m_1	1.9E-05	2.3E-05	2.8E-05	2.6E-05	2.8E-05	2.2E-05
first moment ($\mu_1 = m_1/m_0$)	59.7	53.9	51.6	55.1	54.2	58.8
mean residence time (t_m)	59.7	53.9	51.6	55.1	54.2	58.8
m_2	1.1E-03	1.2E-03	1.5E-03	1.5E-03	1.6E-03	1.3E-03
variance (σ^2), sec^2	50.3	26.3	30.1	81.7	71.8	75.2
standard deviation (σ)	7.1	5.1	5.5	9.0	8.5	8.3
% of total area	28	35	48	40	47	33

Total area (Area 1 + 2)	1.1E-06	1.2E-06	1.2E-06	1.2E-06	1.1E-06	1.2E-06

D.2. Dynamic Experiments' Data for Cr-V-O Catalyst

D.2.1. Dynamic Experiments' Data for Cr-V-O Catalyst with C_2H_6 Pulses into O_2 and He Flow at 400°C

The response data for C_2H_6 pulses into O_2 and He flow over Cr-V-O catalyst at 400°C are presented in Figures D.2.1-D.2.7. The results of moment, variance, mean residence time, and standard deviation calculations for C_2H_6, C_2H_4, and H_2O are tabulated in Tables D.15-D.17.

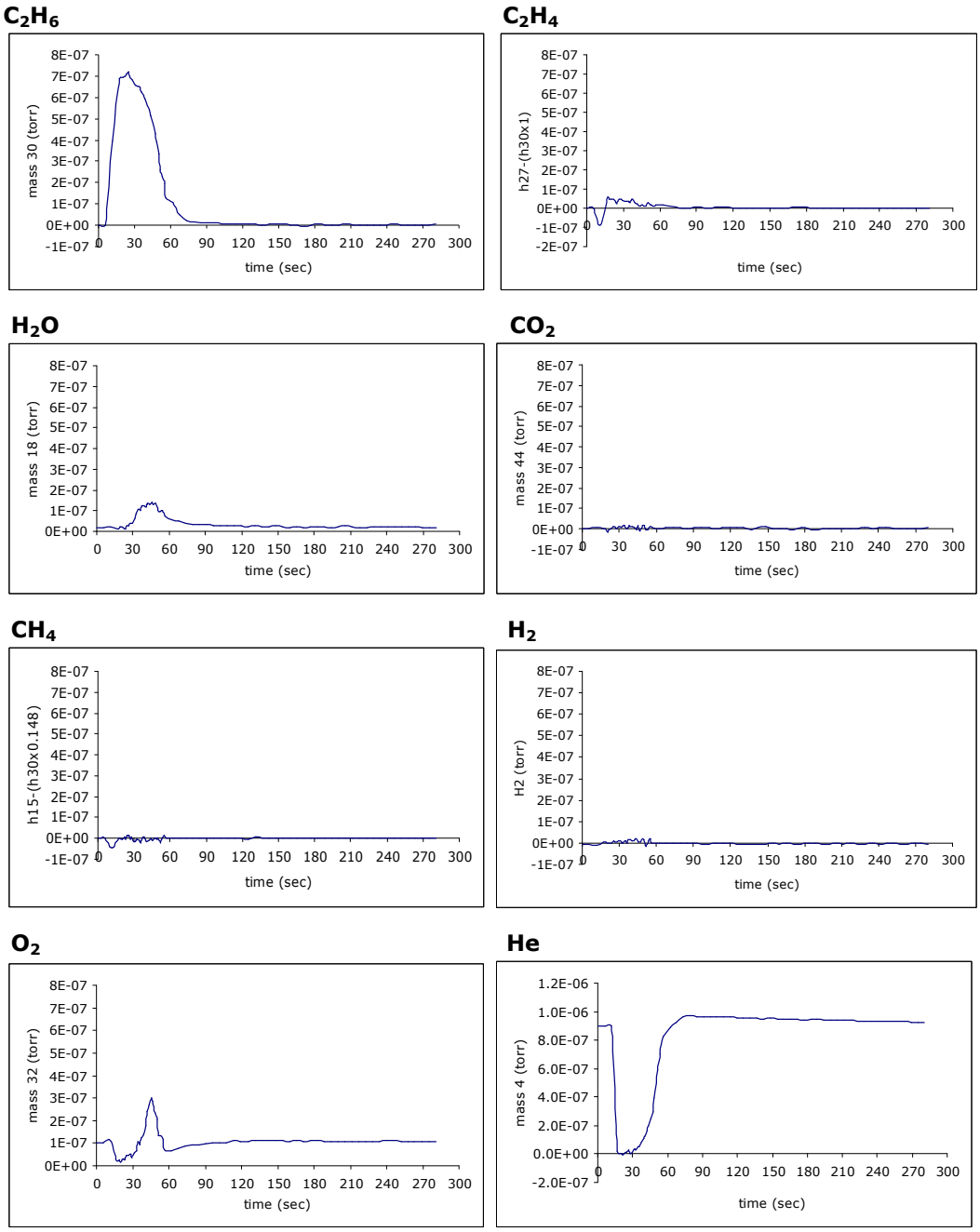

Figure D.2.1. 'Pulse 1' response data for C_2H_6 pulses into O_2 and He flow over Cr-V-O catalyst at 400°C

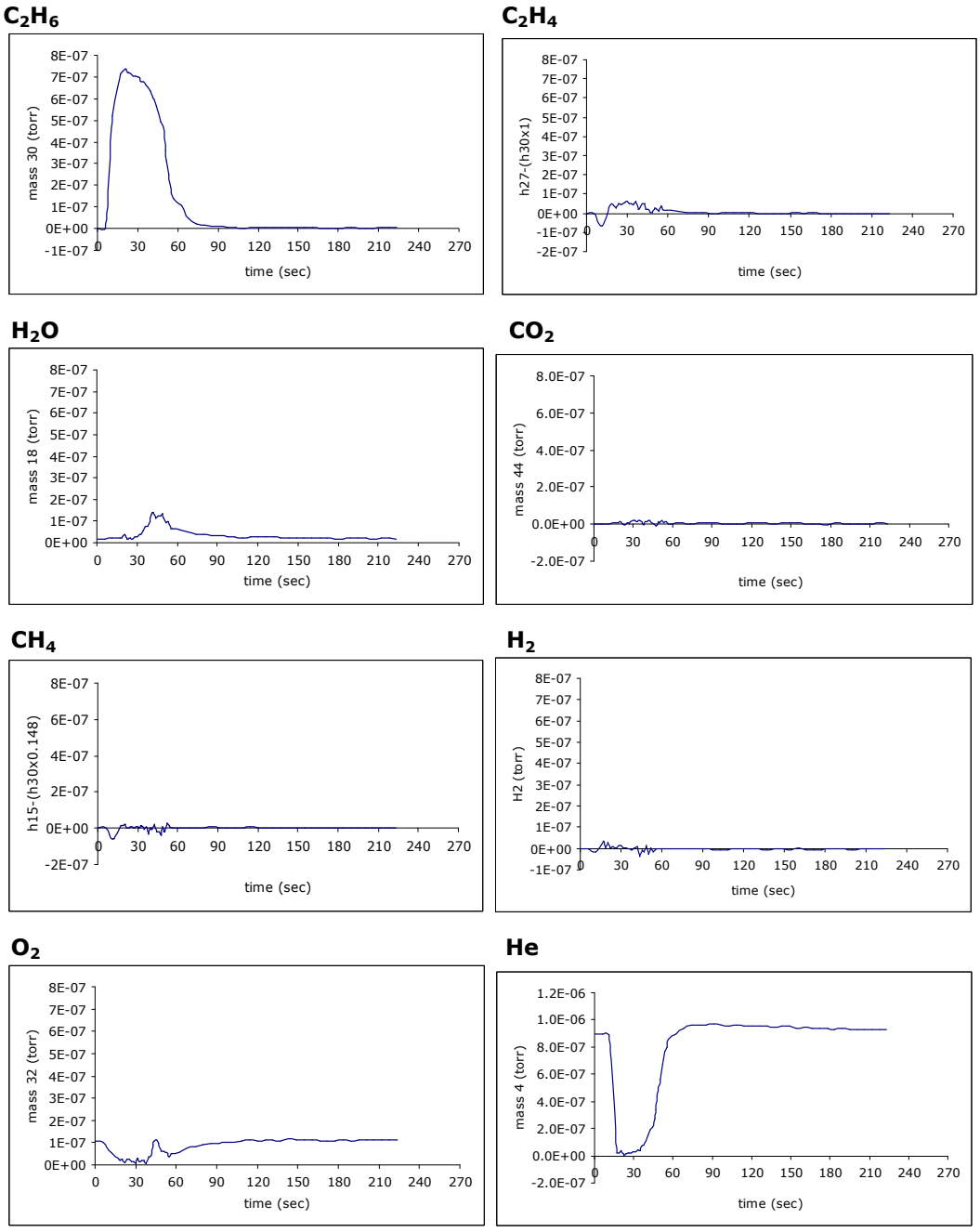

Figure D.2.2. 'Pulse 2' response data for C_2H_6 pulses into O_2 and He flow over Cr-V-O catalyst at 400°C

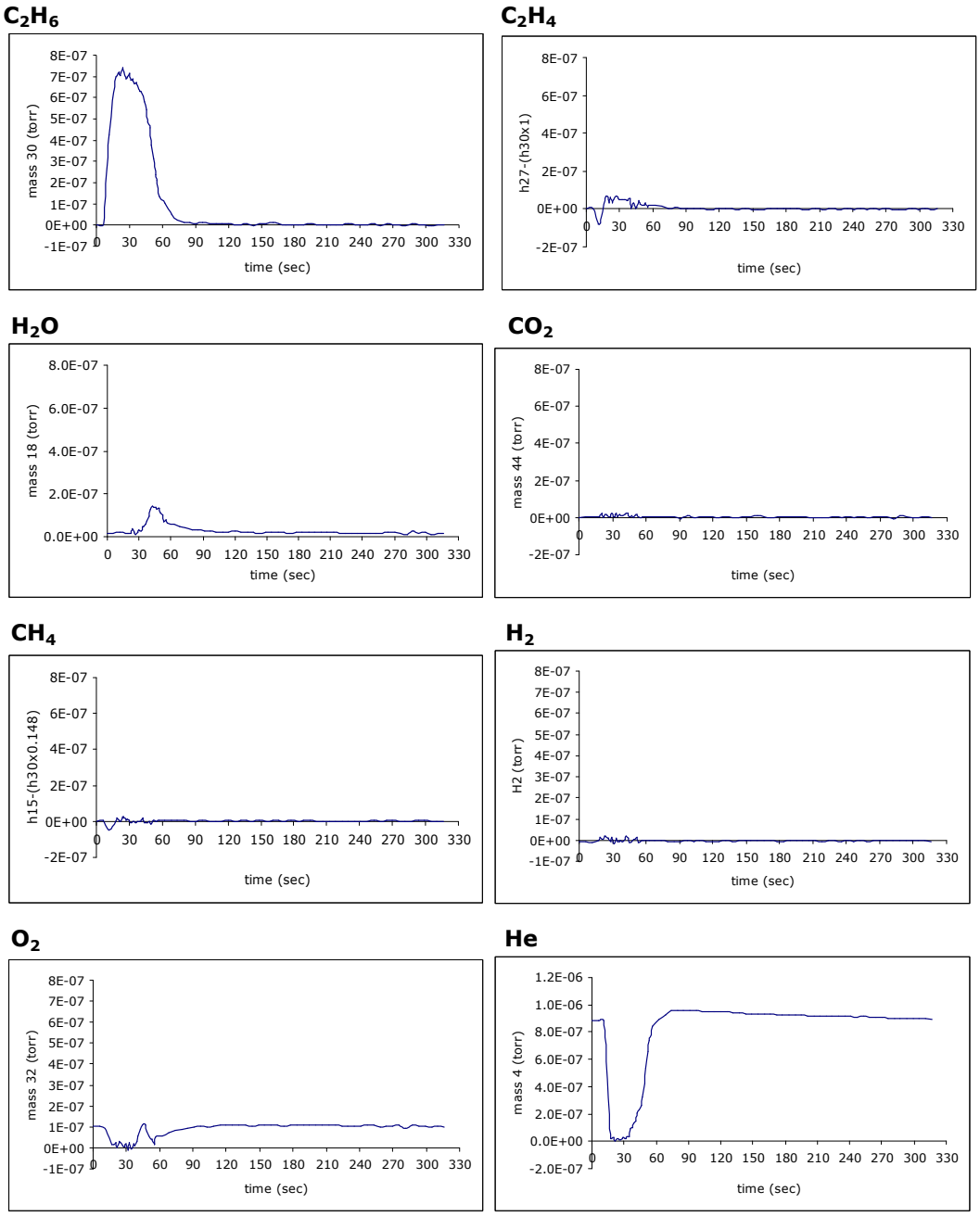

Figure D.2.3. 'Pulse 3' response data for C_2H_6 pulses into O_2 and He flow over Cr-V-O catalyst at 400°C

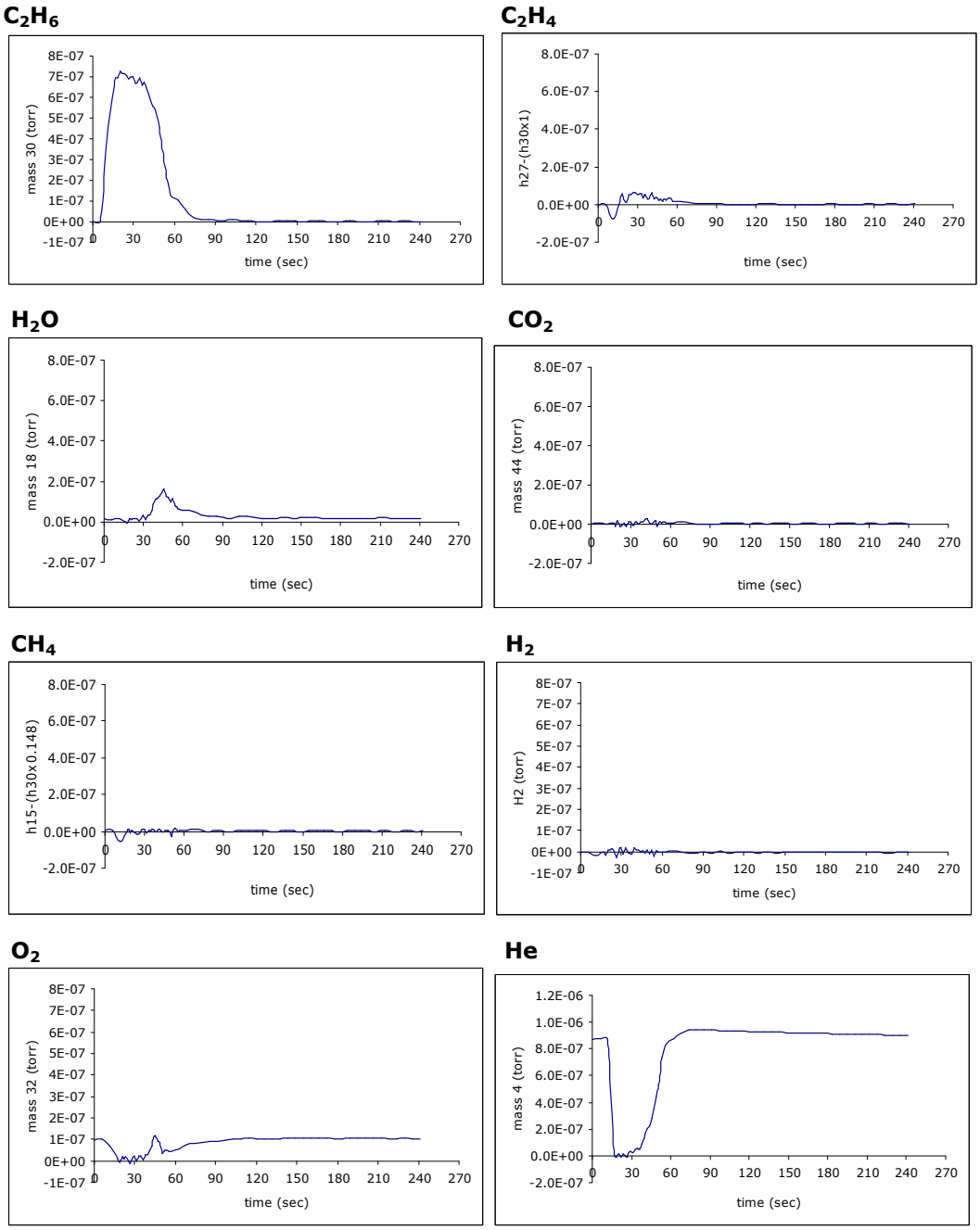

Figure D.2.4. 'Pulse 4' response data for C_2H_6 pulses into O_2 and He flow over Cr-V-O catalyst at 400°C

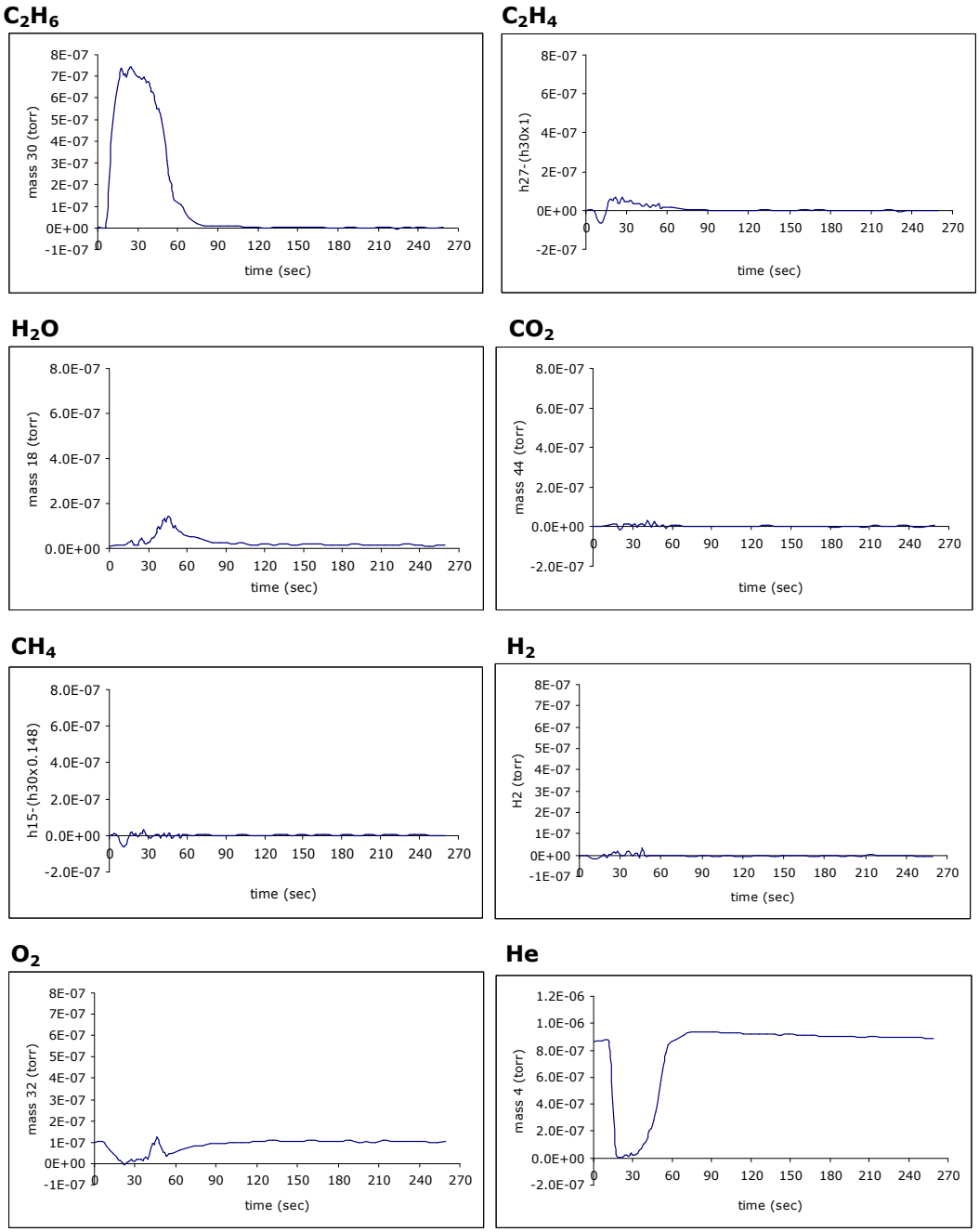

Figure D.2.5. 'Pulse 5' response data for C_2H_6 pulses into O_2 and He flow over Cr-V-O catalyst at 400°C

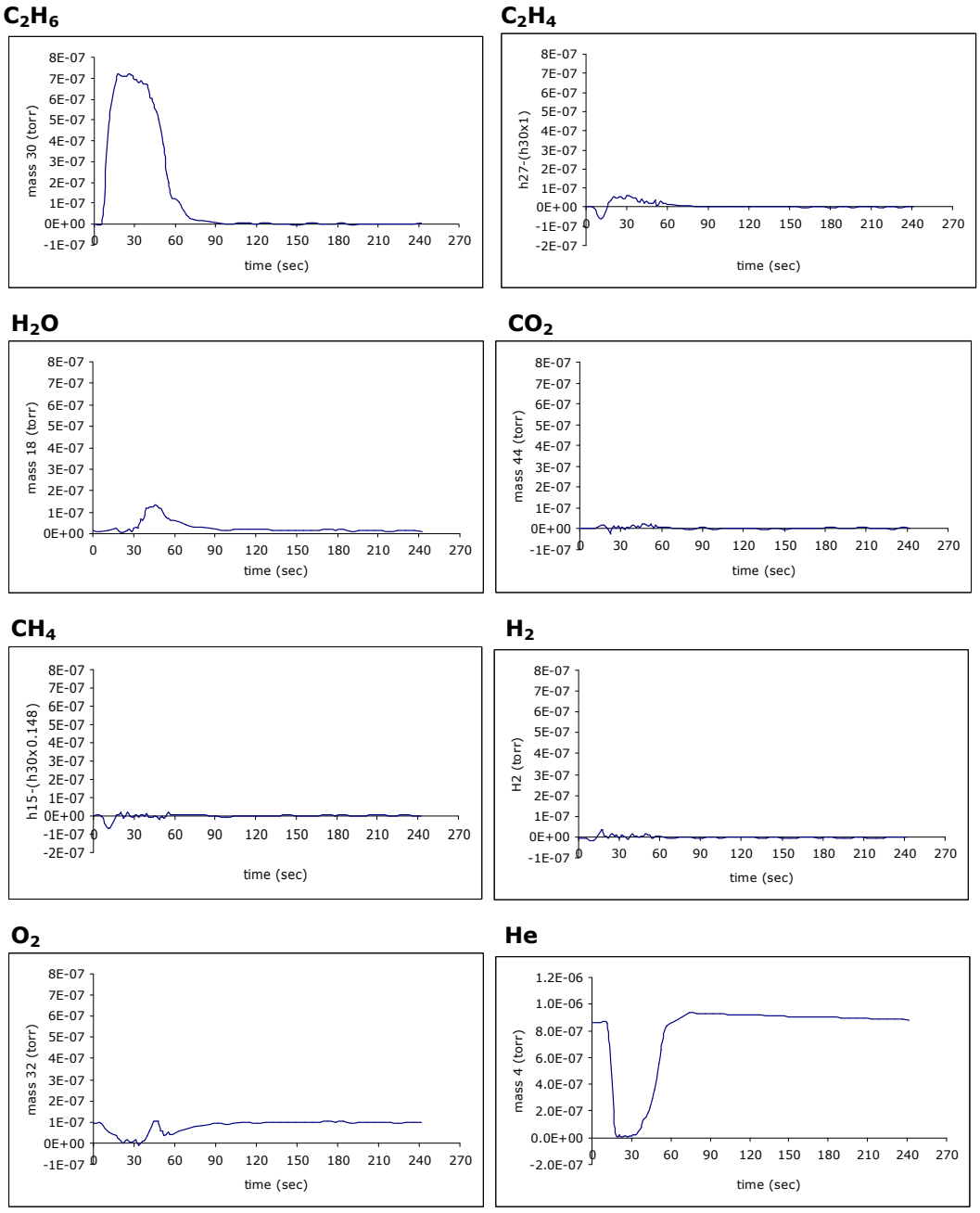

Figure D.2.6. 'Pulse 6' response data for C_2H_6 pulses into O_2 and He flow over Cr-V-O catalyst at 400°C

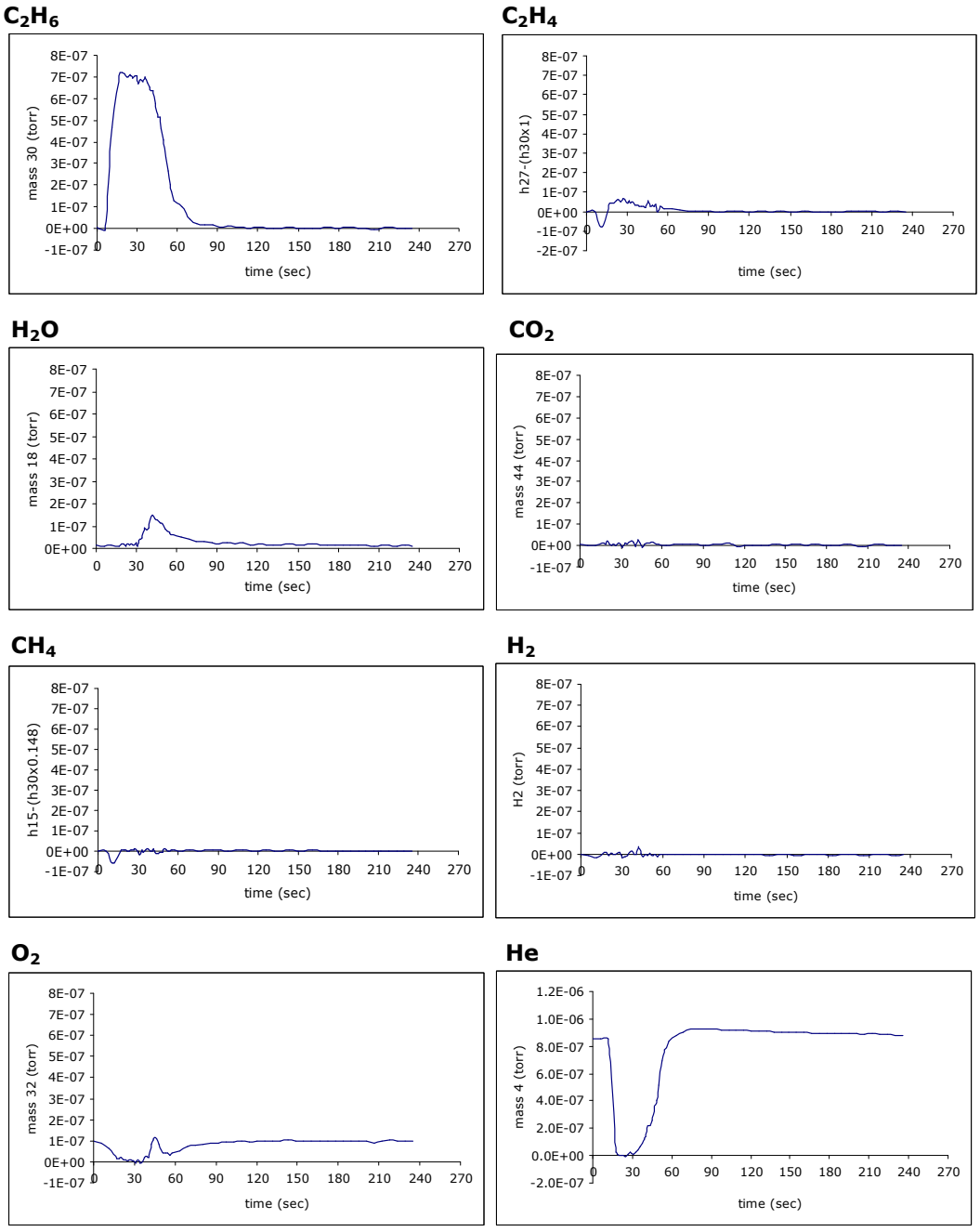

Figure D.2.7. 'Pulse 7' response data for C_2H_6 pulses into O_2 and He flow over Cr-V-O catalyst at 400°C

Table D.15. C_2H_6 response data for C_2H_6 pulses into O_2 and He flow over Cr-V-O catalyst at 400°C

	Pulse 1	***Pulse 2***	***Pulse 3***	***Pulse 4***	***Pulse 5***	***Pulse 6***	***Pulse 7***	***Avr:***
zeroth moment (m_0)	4.4E-05	4.7E-05	4.7E-05	4.7E-05	4.7E-05	4.7E-05	4.6E-05	4.6E-05
m_1	1.5E-03	1.6E-03	1.6E-03	1.6E-03	1.6E-03	1.6E-03	1.5E-03	1.6E-03
first moment ($\mu_1 = m_1/m_0$)	33.4	33.7	33.9	33.7	33.8	33.9	33.8	33.7
mean residence time (t_m)	33.4	33.7	33.9	33.7	33.8	33.9	33.8	33.7
m_2	5.5E-02	6.0E-02	6.1E-02	6.0E-02	6.1E-02	6.1E-02	5.9E-02	6.0E-02
variance (σ^2), sec^2	144.2	143.8	147.5	145.6	145.1	144.6	142.3	144.7
standard deviation (σ)	12.0	12.0	12.1	12.1	12.0	12.0	11.9	12.0

Table D.16. C_2H_4 response data for C_2H_6 pulses into O_2 and He flow over Cr-V-O catalyst at 400°C

	Pulse 1	***Pulse 2***	***Pulse 3***	***Pulse 4***	***Pulse 5***	***Pulse 6***	***Pulse 7***	***Avr:***
	Area1	*Area1*	*Area1*	*Area1*	*Area1*	*Area1*	*Area1*	
zeroth moment (m_0)	9.6E-07	1.2E-06	1.2E-06	1.3E-06	1.5E-06	1.4E-06	1.5E-06	1.3E-06
m_1	2.8E-05	3.8E-05	3.4E-05	4.2E-05	4.8E-05	4.6E-05	4.8E-05	4.1E-05
first moment ($\mu_1 = m_1/m_0$)	29.6	31.1	28.4	32.0	33.1	32.8	33.0	31.4
mean residence time (t_m)	29.6	31.1	28.4	32.0	33.1	32.8	33.0	31.4
m_2	9.1E-04	1.3E-03	1.0E-03	1.5E-03	1.8E-03	1.6E-03	1.7E-03	1.4E-03
variance (σ^2), sec^2	69.5	62.7	45.6	71.3	115.6	86.1	99.4	78.6
standard deviation (σ)	8.3	7.9	6.8	8.4	10.7	9.3	10.0	8.8
% of total area	87.6	70.4	63.2	64.4	81.8	75.7	76.8	74.3

	Pulse 1	***Pulse 2***	***Pulse 3***	***Pulse 4***	***Pulse 5***	***Pulse 6***	***Pulse 7***	***Avr:***
	Area2	*Area2*	*Area2*	*Area2*	*Area2*	*Area2*	*Area2*	
zeroth moment (m_0)	1.4E-07	5.1E-07	7.0E-07	7.3E-07	3.3E-07	4.5E-07	4.4E-07	4.7E-07
m_1	7.4E-06	2.9E-05	3.8E-05	4.2E-05	2.1E-05	2.7E-05	2.7E-05	2.7E-05
first moment ($\mu_1 = m_1/m_0$)	54.9	56.5	54.1	57.1	65.0	60.5	60.3	58.4
mean residence time (t_m)	54.9	56.5	54.1	57.1	65.0	60.5	60.3	58.4
m_2	4.1E-04	1.7E-03	2.1E-03	2.5E-03	1.4E-03	1.7E-03	1.6E-03	1.6E-03
variance (σ^2), sec^2	38.8	54.3	62.7	88.7	85.2	70.6	64.9	66.5
standard deviation (σ)	6.2	7.4	7.9	9.4	9.2	8.4	8.1	8.1
% of total area	12.4	29.6	36.8	35.6	18.2	24.3	23.2	25.7

Total area (Area 1+2)	1.1E-06	1.7E-06	1.9E-06	2.1E-06	1.8E-06	1.8E-06	1.9E-06	1.8E-06

Table D.17. H_2O response data for C_2H_6 pulses into O_2 and He flow over Cr-V-O catalyst at 400°C

	Pulse 1	***Pulse 2***	***Pulse 3***	***Pulse 4***	***Pulse 5***	***Pulse 6***	***Pulse 7***	***Avr:***
zeroth moment (m_0)	6.0E-06	5.0E-06	5.2E-06	5.2E-06	5.0E-06	5.3E-06	5.4E-06	5.3E-06
m_1	2.8E-04	2.5E-04	2.6E-04	2.6E-04	2.4E-04	2.6E-04	2.7E-04	2.6E-04
first moment ($\mu_1 = m_1/m_0$)	47.7	49.8	50.0	49.7	48.3	49.0	49.6	49.1
mean residence time (t_m)	47.7	49.8	50.0	49.7	48.3	49.0	49.6	49.1
m_2	1.5E-02	1.4E-02	1.4E-02	1.4E-02	1.3E-02	1.4E-02	1.5E-02	1.4E-02
variance (σ^2), sec^2	247.6	255.1	244.4	196.5	261.6	199.1	240.0	234.9
standard deviation (σ)	15.7	16.0	15.6	14.0	16.2	14.1	15.5	15.3

D.2.2. Dynamic Experiments' Data for Cr-V-O Catalyst with O_2 Pulses into C_2H_6 and He Flow at 400°C

The response data for O_2 pulses into C_2H_6 and He flow over Cr-V-O catalyst at 400°C are presented in Figures D.2.8-D.2.21. The results of moment, variance, mean residence time, and standard deviation calculations for O_2, H_2O, and CO are tabulated in Tables D.18-D.20.

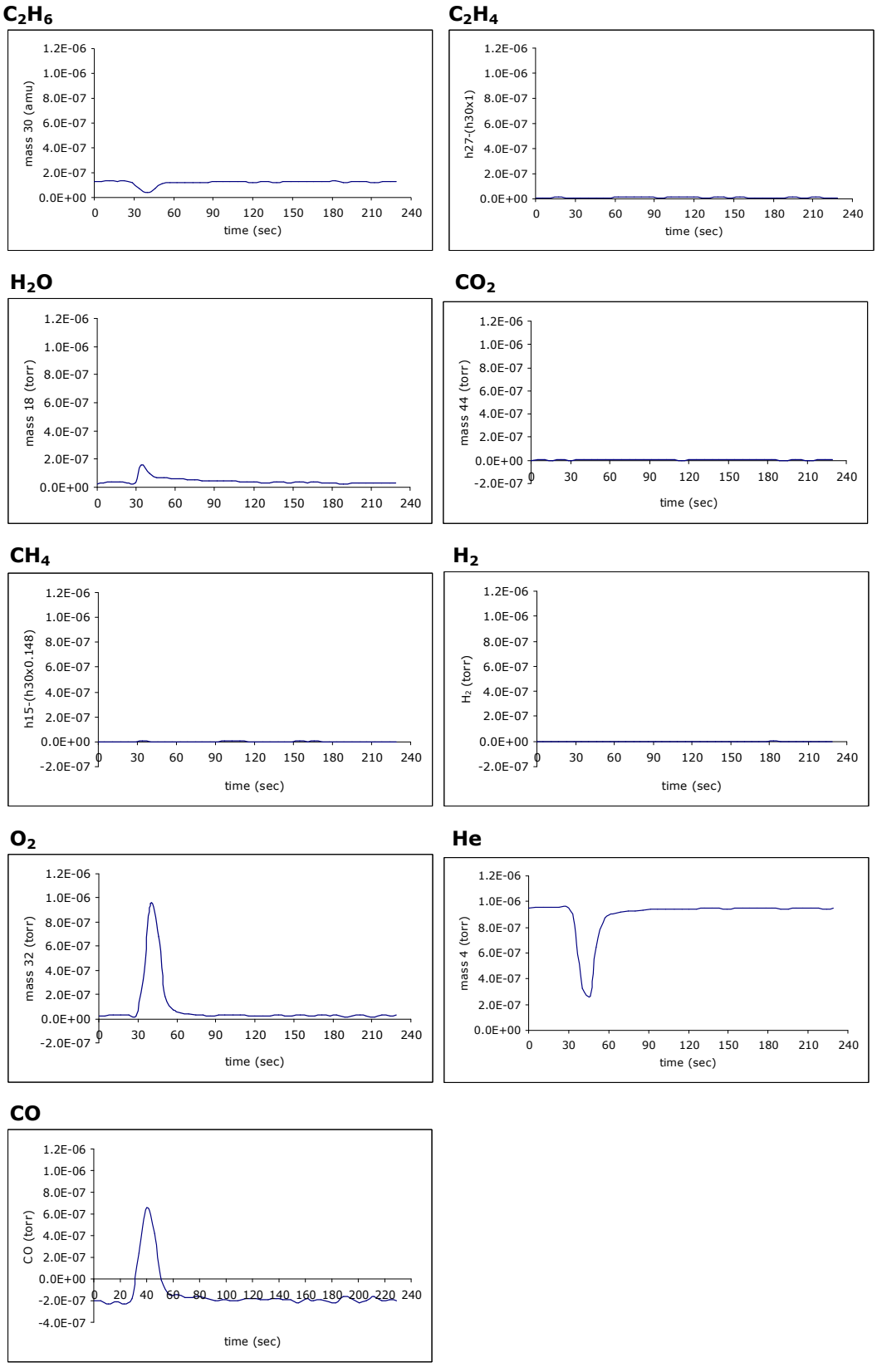

Figure D.2.8. 'Pulse 2' response data for O_2 pulses into C_2H_6 and He flow over Cr-V-O catalyst at 400°C

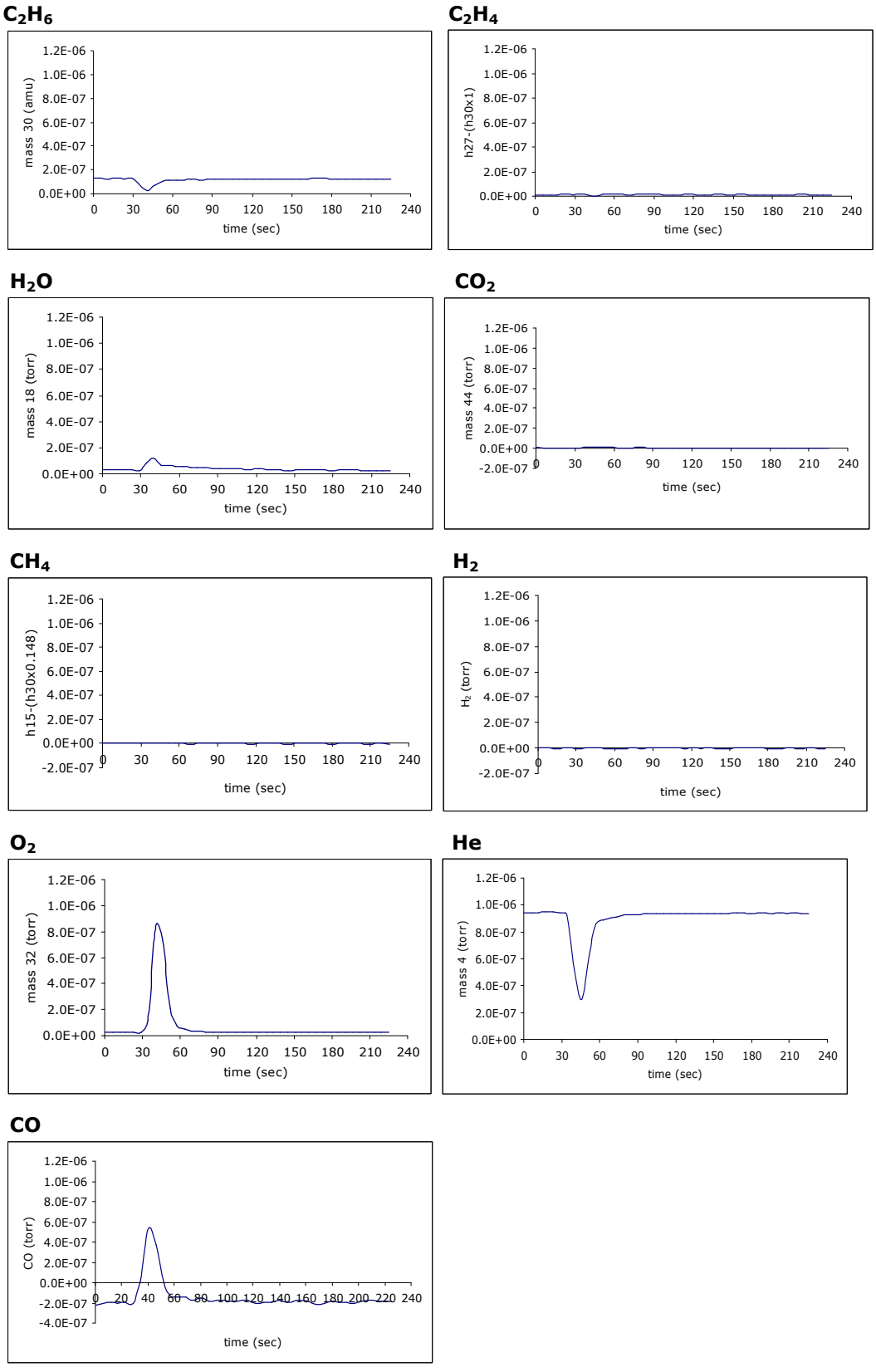

Figure D.2.9. 'Pulse 3' response data for O_2 pulses into C_2H_6 and He flow over Cr-V-O catalyst at 400°C

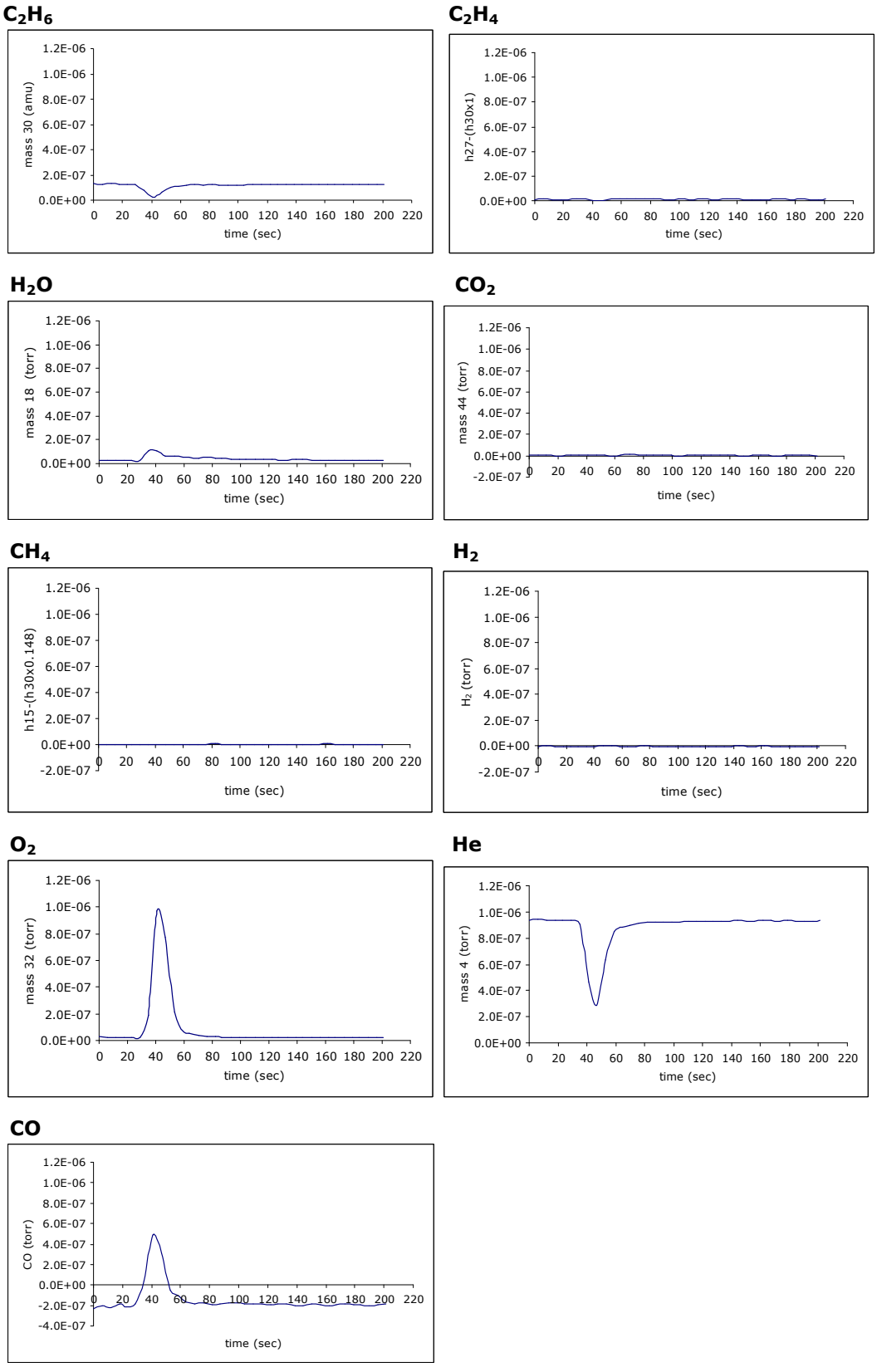

Figure D.2.10. 'Pulse 4' response data for O_2 pulses into C_2H_6 and He flow over Cr-V-O catalyst at 400°C

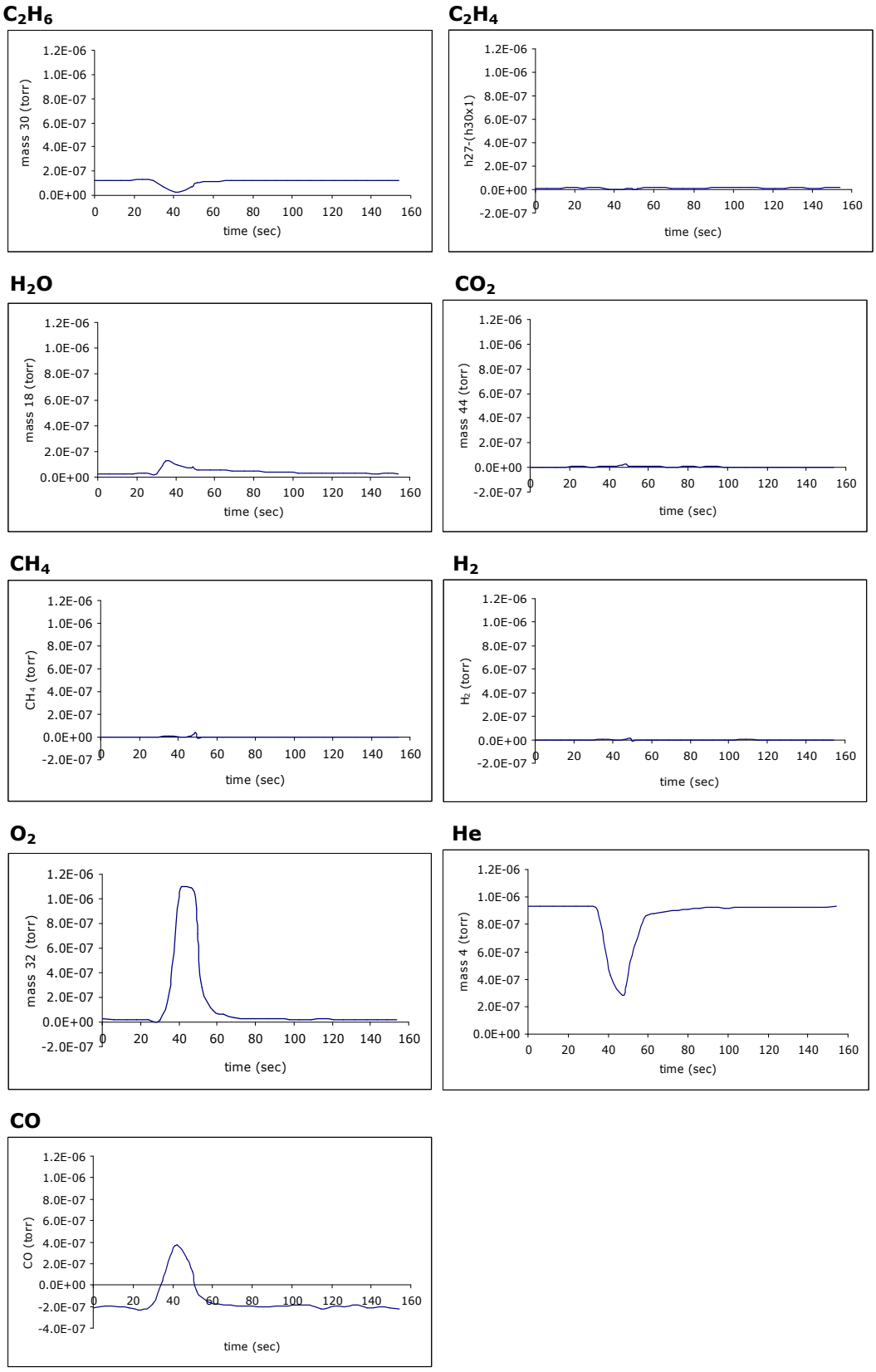

Figure D.2.11. 'Pulse 5' response data for O_2 pulses into C_2H_6 and He flow over Cr-V-O catalyst at 400°C

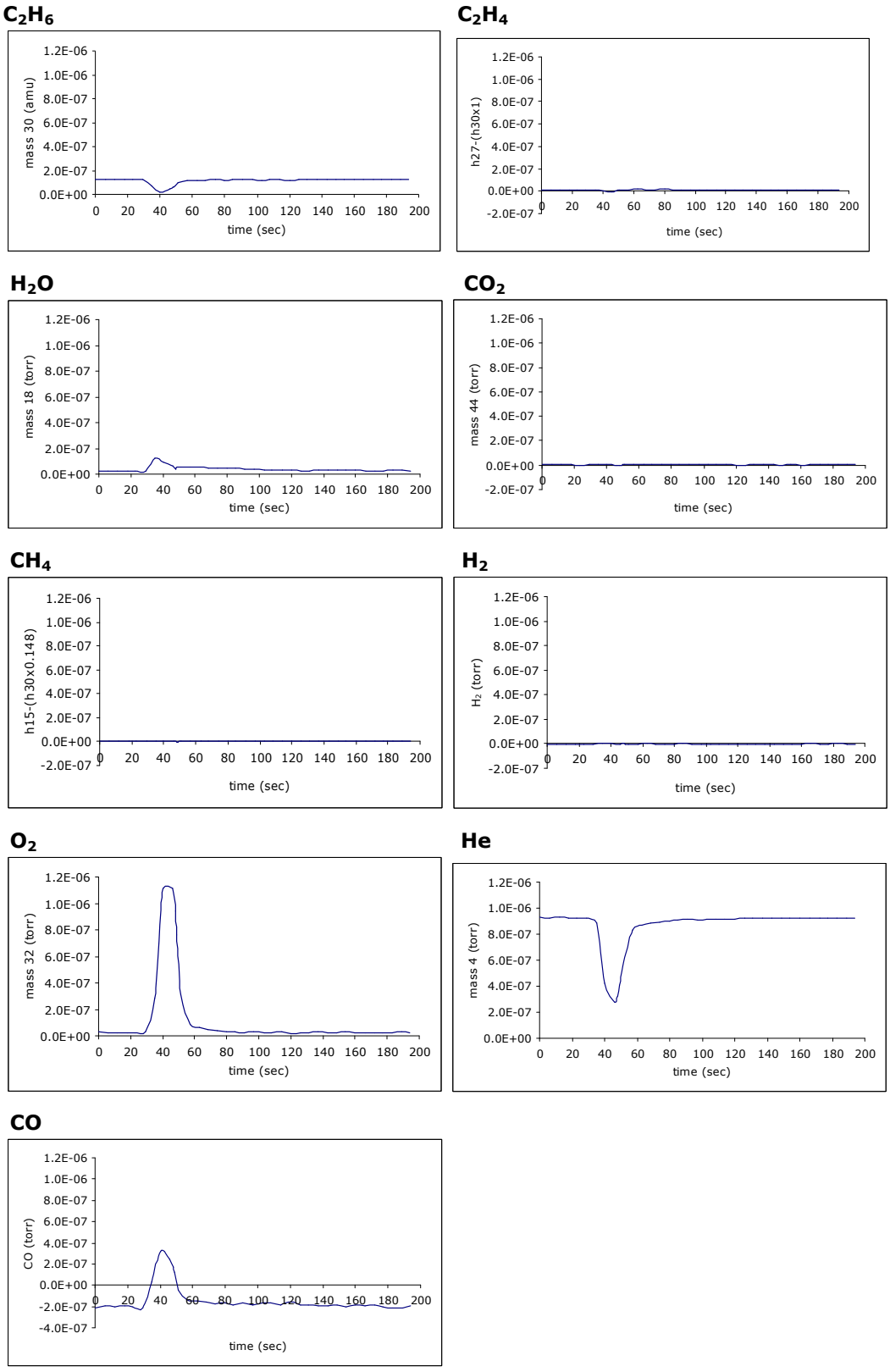

Figure D.2.12. 'Pulse 6' response data for O_2 pulses into C_2H_6 and He flow over Cr-V-O catalyst at 400°C

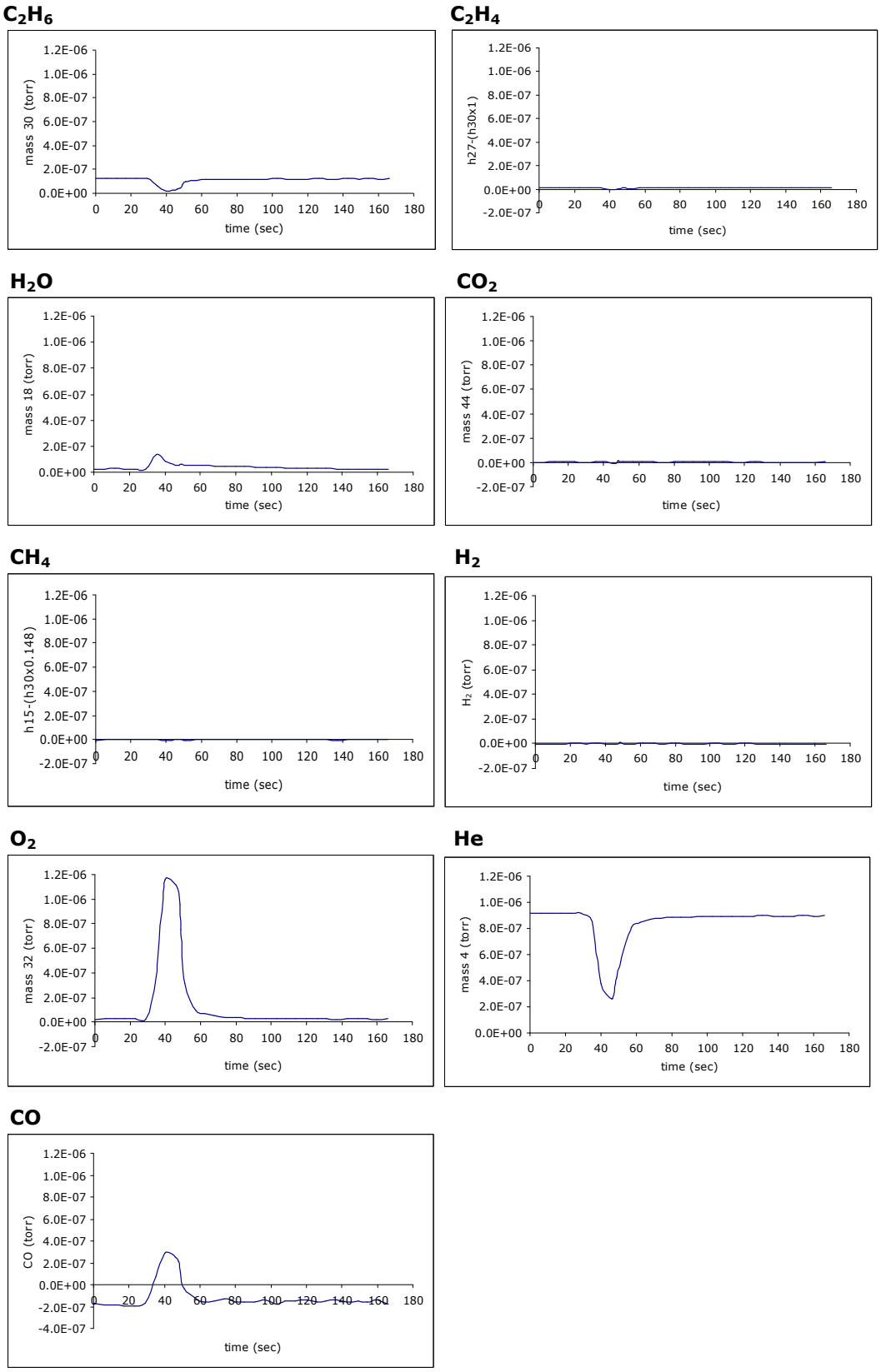

Figure D.2.13. 'Pulse 7' response data for O_2 pulses into C_2H_6 and He flow over Cr-V-O catalyst at 400°C

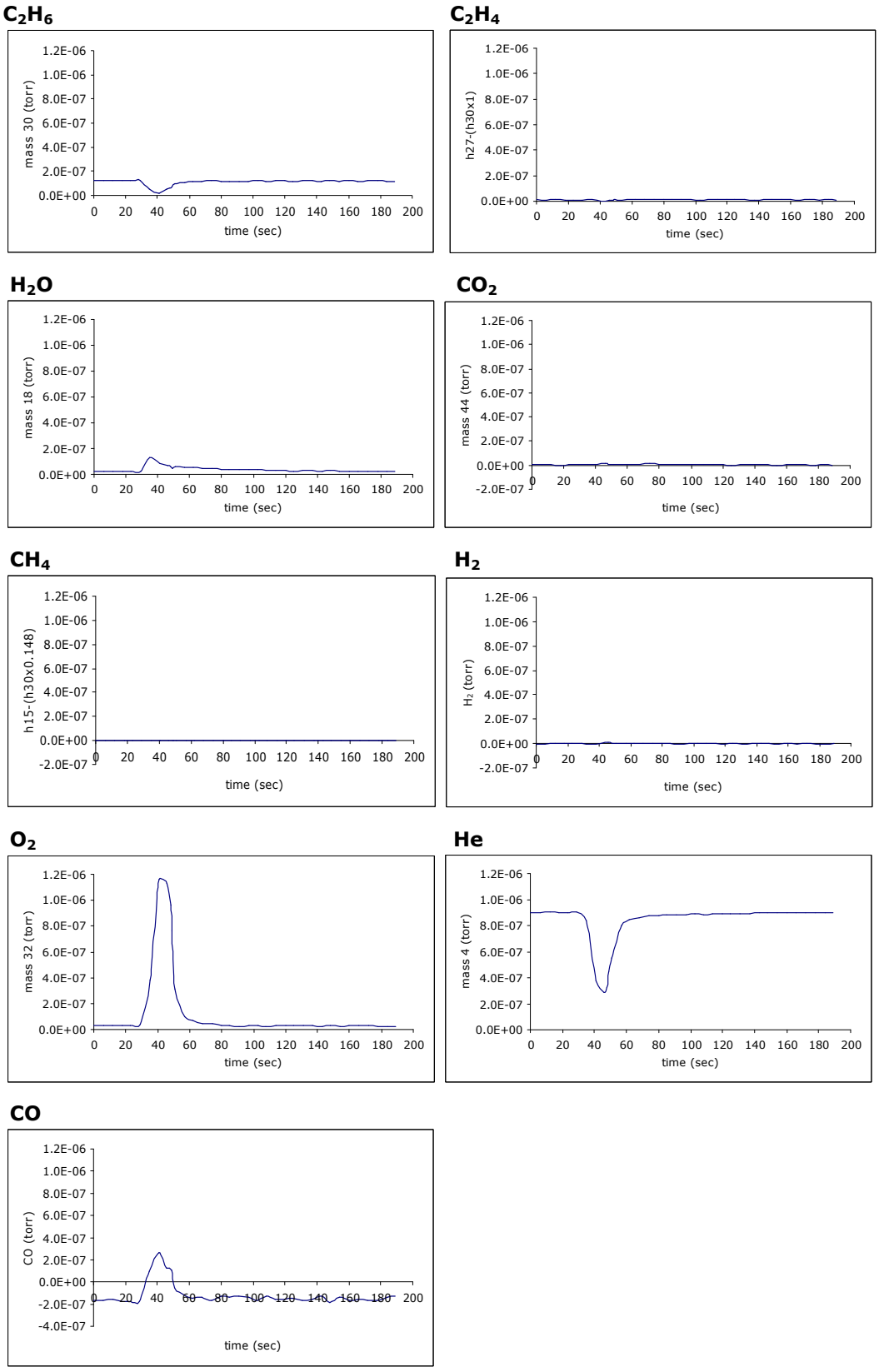

Figure D.2.14. 'Pulse 8' response data for O_2 pulses into C_2H_6 and He flow over Cr-V-O catalyst at 400°C

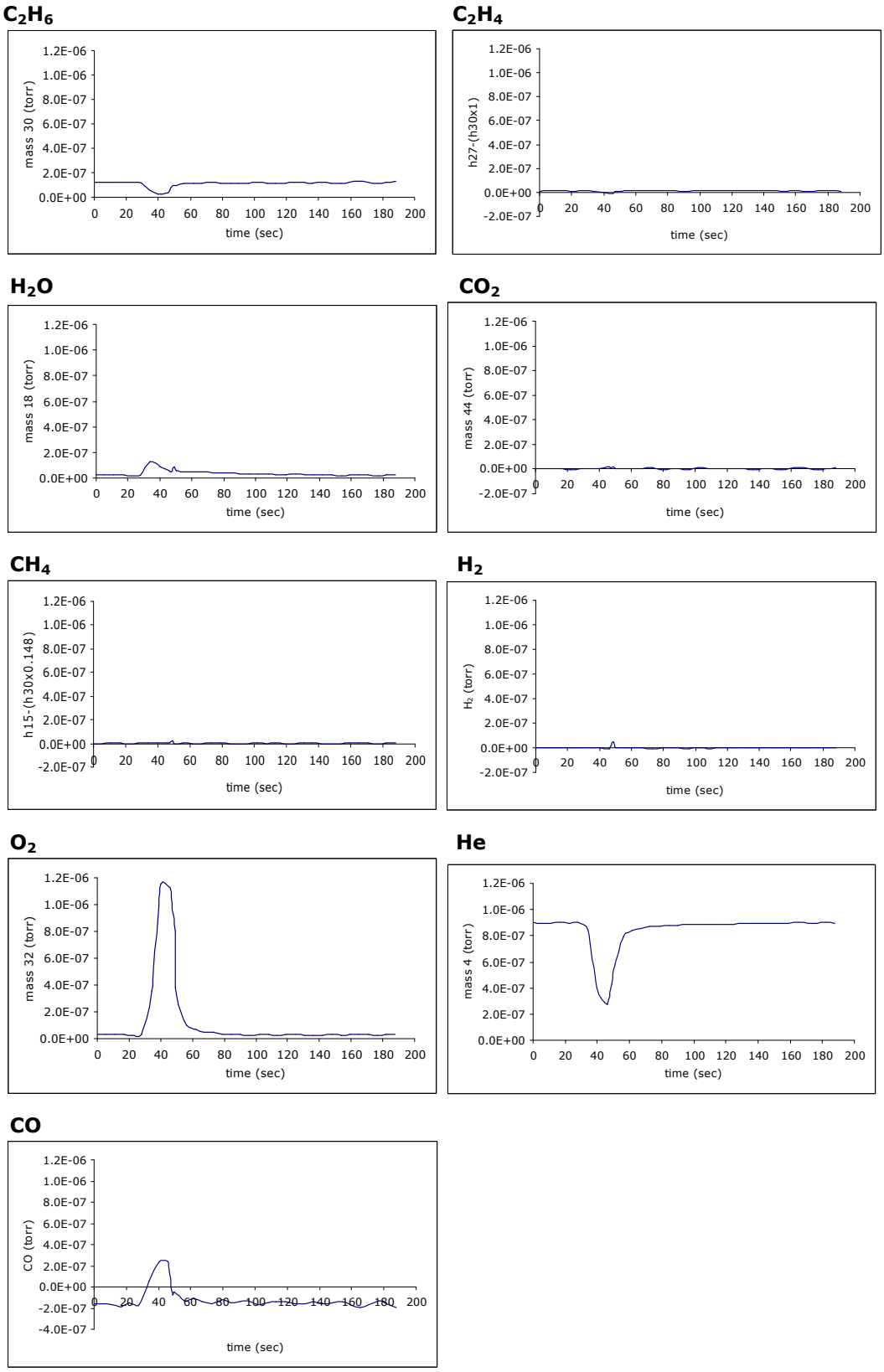

Figure D.2.15. 'Pulse 9' response data for O_2 pulses into C_2H_6 and He flow over Cr-V-O catalyst at 400°C

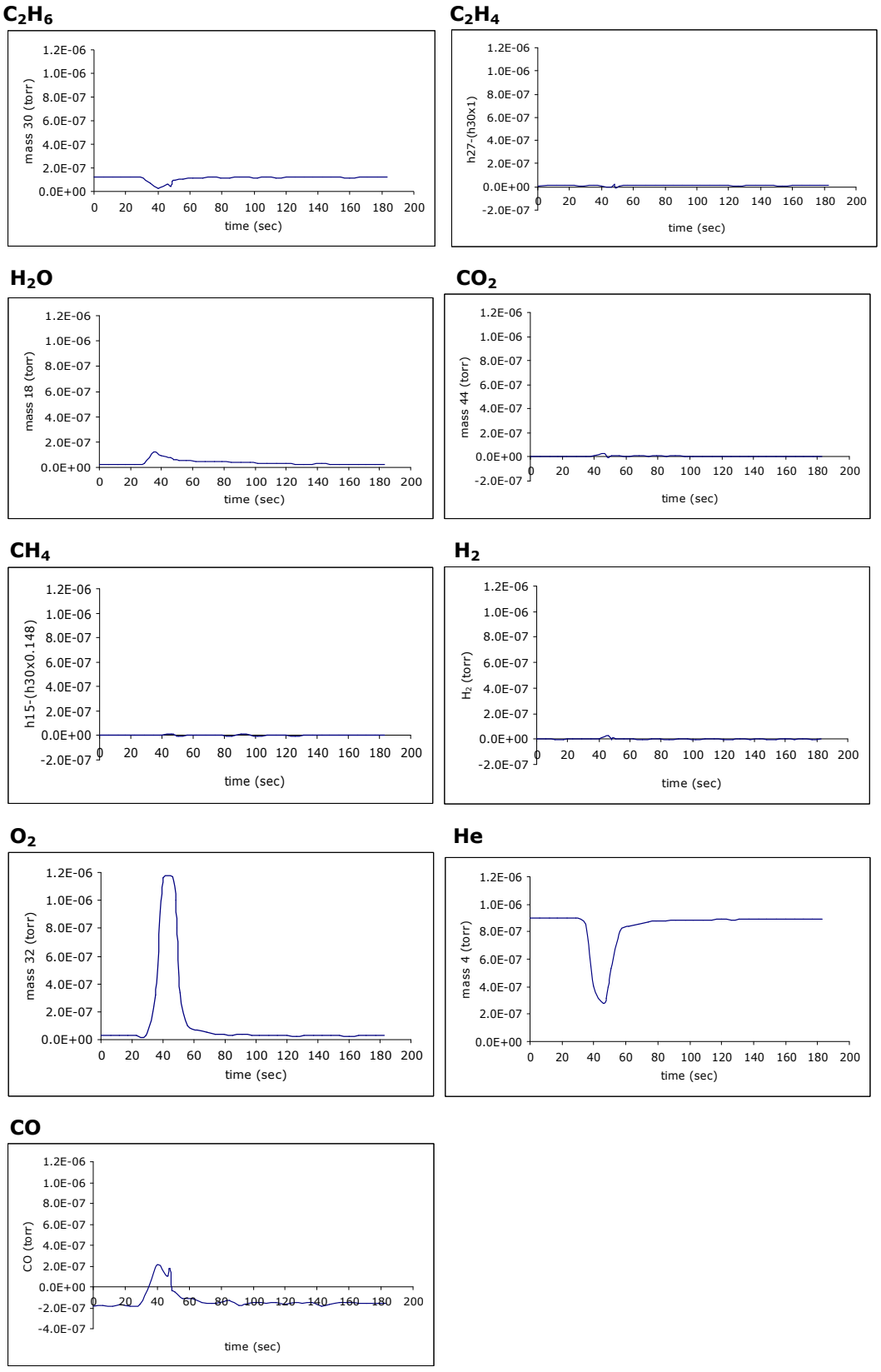

Figure D.2.16. 'Pulse 10' response data for O_2 pulses into C_2H_6 and He flow over Cr-V-O catalyst at 400°C

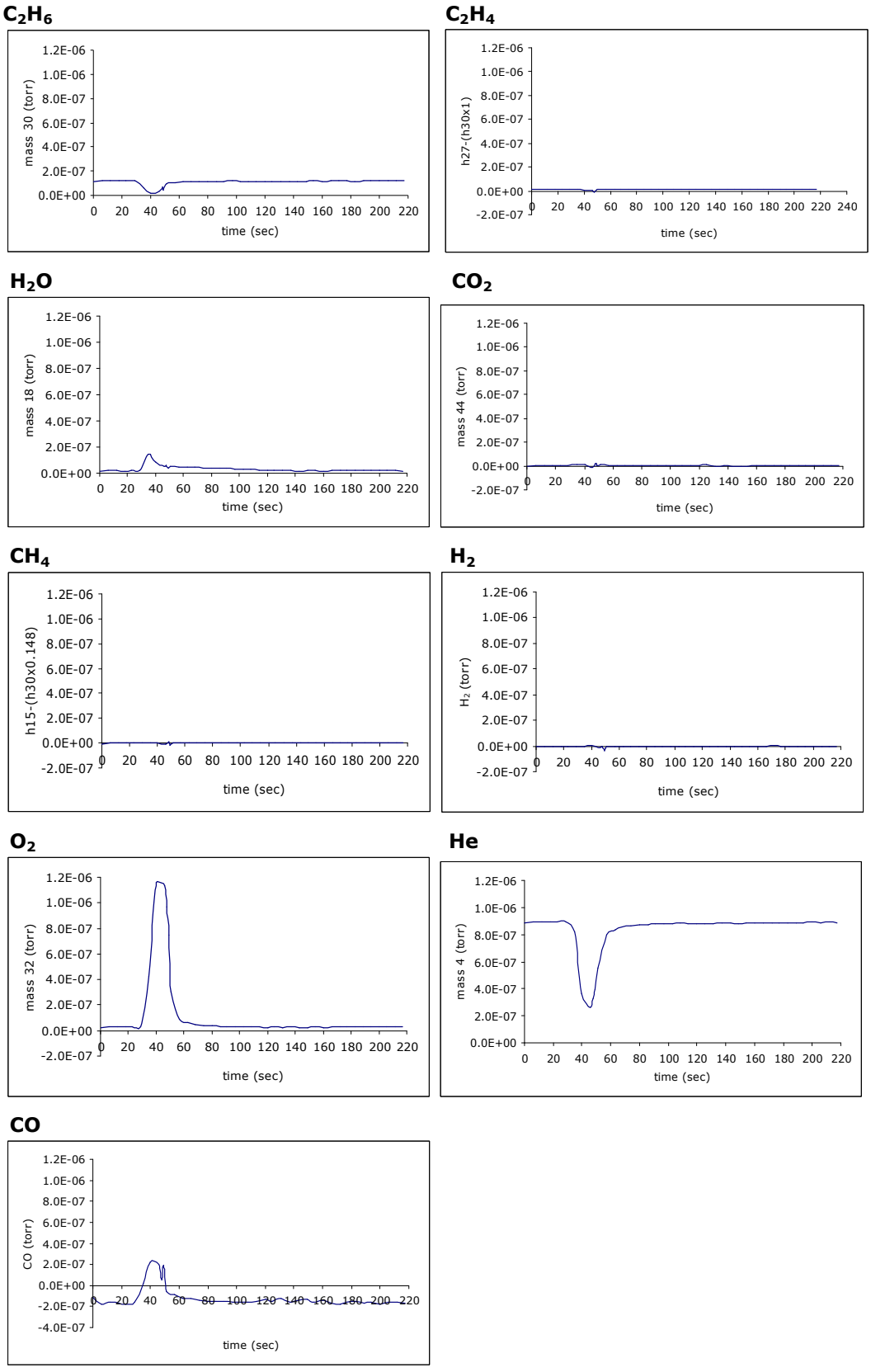

Figure D.2.17. 'Pulse 11' response data for O_2 pulses into C_2H_6 and He flow over Cr-V-O catalyst at 400°C

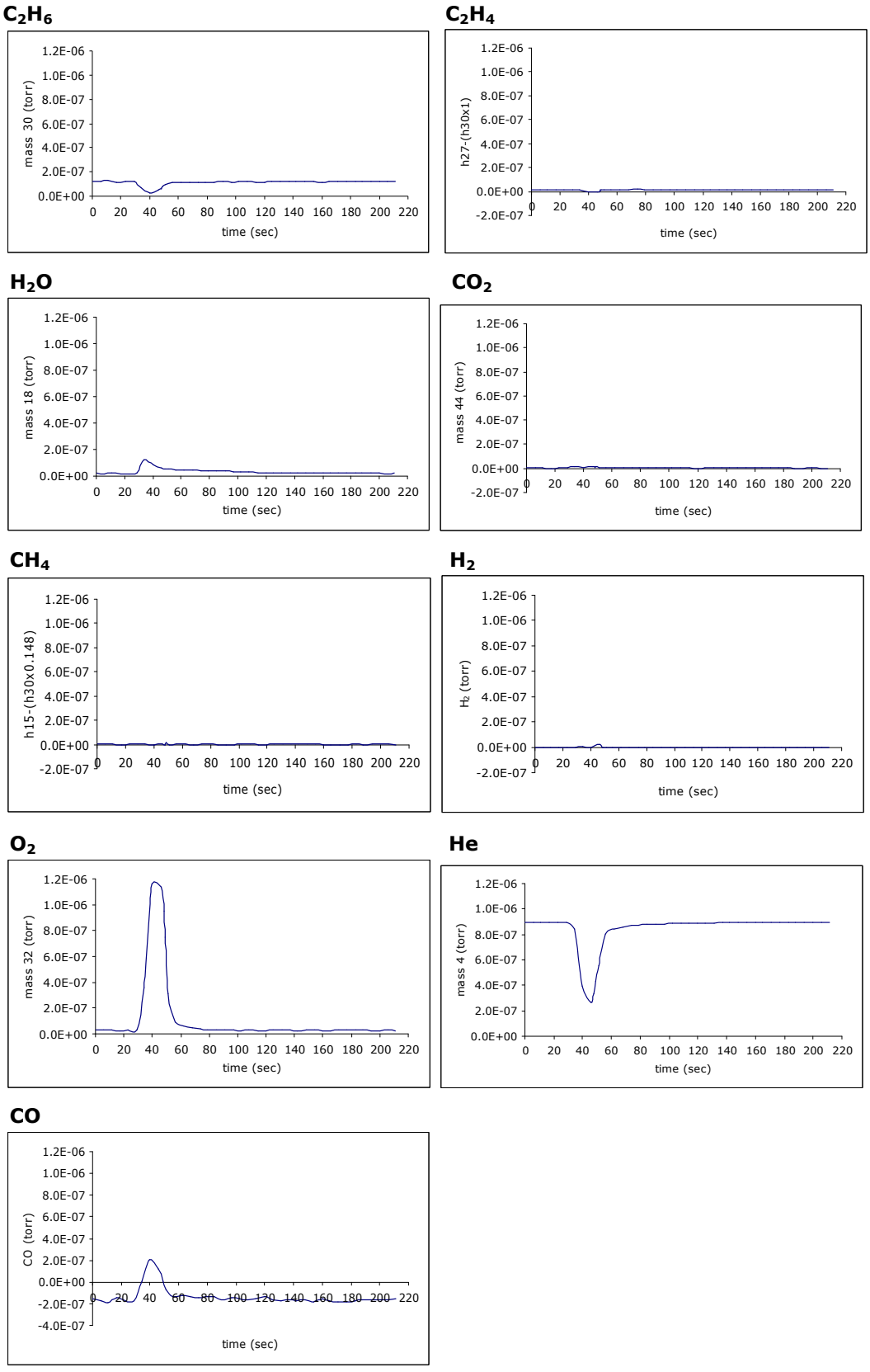

Figure D.2.18. 'Pulse 12' response data for O_2 pulses into C_2H_6 and He flow over Cr-V-O catalyst at 400°C

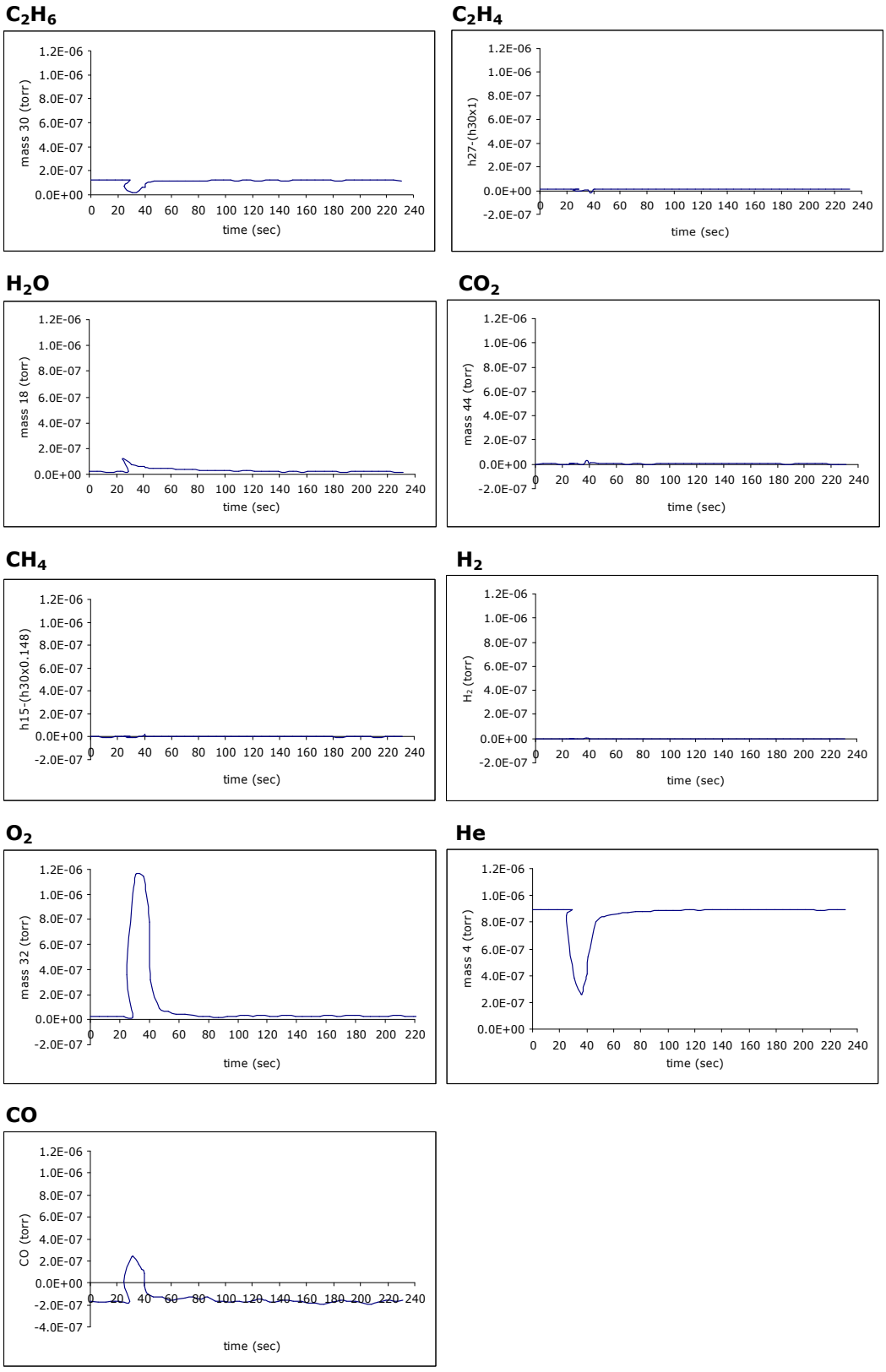

Figure D.2.19. 'Pulse 13' response data for O_2 pulses into C_2H_6 and He flow over Cr-V-O catalyst at 400°C

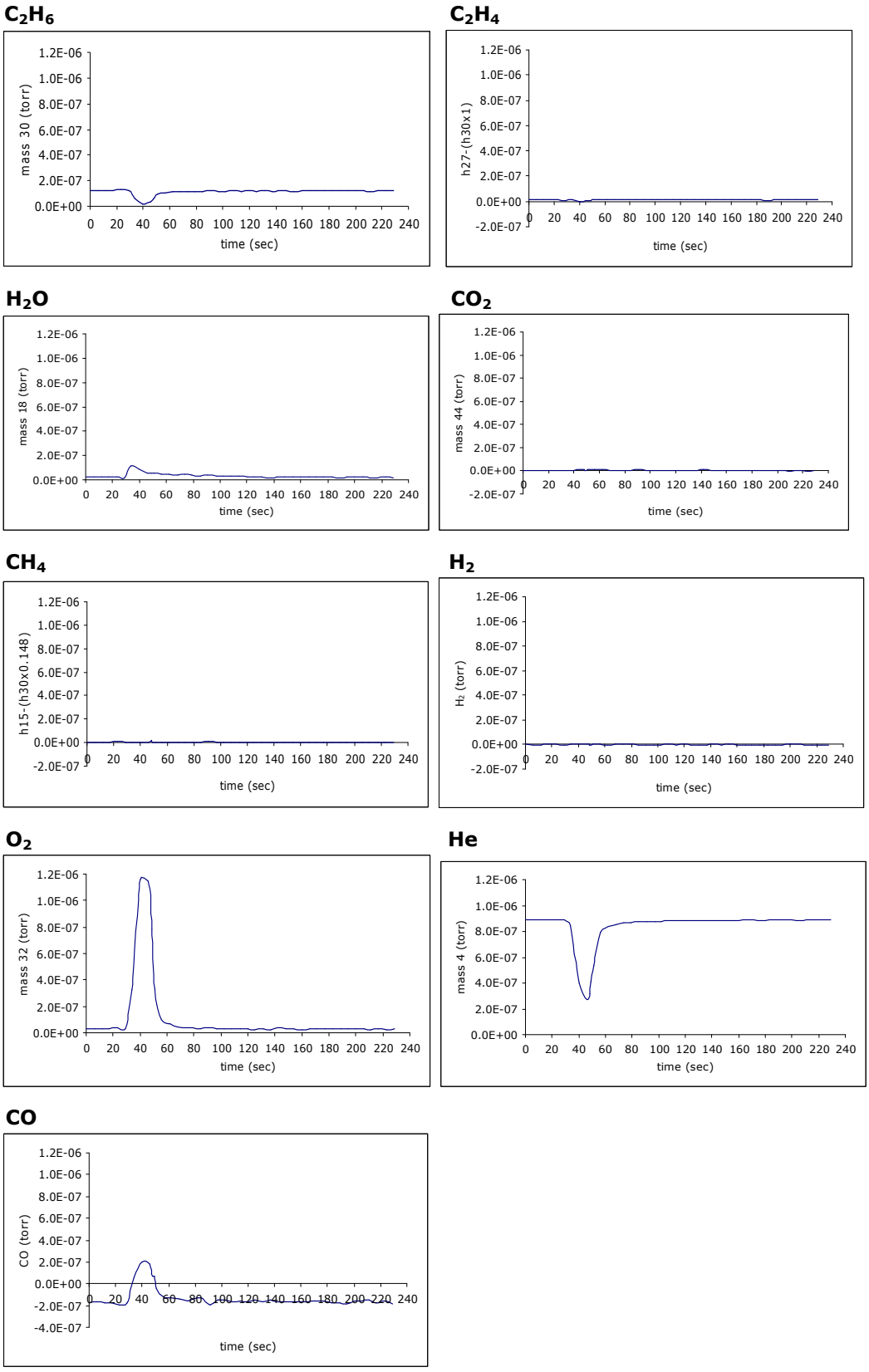

Figure D.2.20. 'Pulse 14' response data for O_2 pulses into C_2H_6 and He flow over Cr-V-O catalyst at 400°C

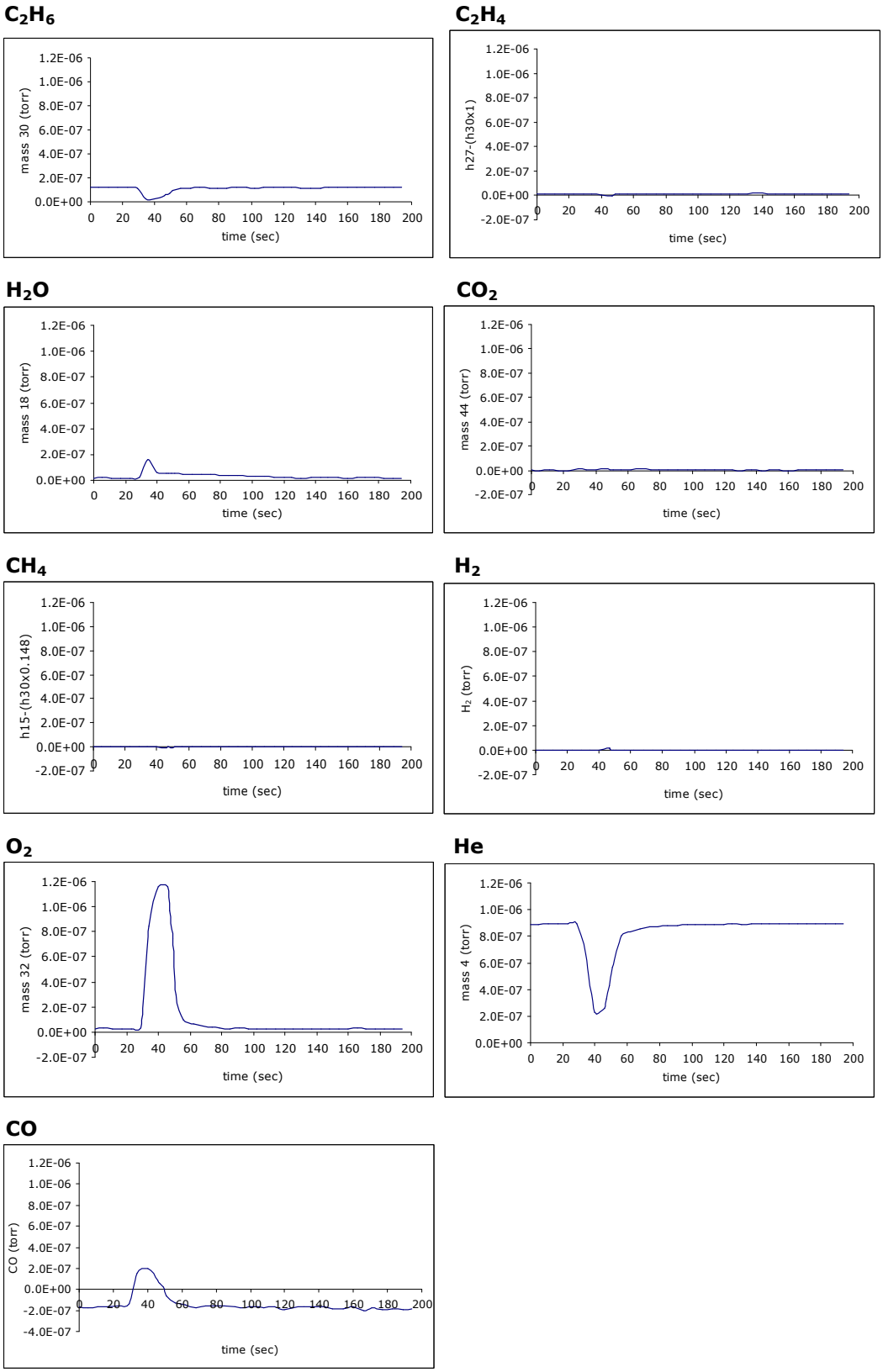

Figure D.2.21. 'Pulse 15' response data for O_2 pulses into C_2H_6 and He flow over Cr-V-O catalyst at 400°C

Table D.18. O_2 response data for O_2 pulses into C_2H_6 and He flow over Cr-V-O catalyst at 400°C

	Pulse 2	***Pulse 3***	***Pulse 4***	***Pulse 5***	***Pulse 6***	***Pulse 7***	***Pulse 8***
zeroth moment (m_0)	1.2E-05	1.2E-05	1.2E-05	2.1E-05	2.2E-05	2.2E-05	2.2E-05
m_1	5.3E-04	5.2E-04	5.4E-04	9.8E-04	9.9E-04	1.0E-03	1.0E-03
first moment ($\mu_1 = m_1/m_0$)	43.5	44.1	45.5	46.6	45.9	45.6	45.7
mean residence time (t_m)	43.5	44.1	45.5	46.6	45.9	45.6	45.7
m_2	2.3E-02	2.3E-02	2.5E-02	4.7E-02	4.6E-02	4.7E-02	4.7E-02
variance (σ^2), sec^2	34.1	57.4	43.5	30.4	31.3	32.9	29.9
standard deviation (σ)	5.8	7.6	6.6	5.5	5.6	5.7	5.5

	Pulse 9	***Pulse 10***	***Pulse 11***	***Pulse 12***	***Pulse 13***	***Pulse 14***	***Pulse 15***	***Avr:***
zeroth moment (m_0)	2.2E-05	2.4E-05	2.4E-05	2.2E-05	2.1E-05	2.4E-05	2.6E-05	1.9E-05
m_1	1.0E-03	1.1E-03	1.1E-03	1.0E-03	7.5E-04	1.1E-03	1.2E-03	8.5E-04
first moment ($\mu_1 = m_1/m_0$)	45.4	45.5	45.2	45.5	35.9	45.3	44.2	41.6
mean residence time (t_m)	45.4	45.5	45.2	45.5	35.9	45.3	44.2	41.6
m_2	4.6E-02	5.0E-02	4.9E-02	4.7E-02	2.7E-02	5.1E-02	5.3E-02	3.9E-02
variance (σ^2), sec^2	30.5	34.3	32.7	31.4	23.6	32.9	51.4	33.1
standard deviation (σ)	5.5	5.9	5.7	5.6	4.9	5.7	7.2	5.5

Table D.19. H_2O response data for O_2 pulses into C_2H_6 and He flow over Cr-V-O catalyst at 400°C

	Pulse 2	***Pulse 3***	***Pulse 4***	***Pulse 5***	***Pulse 6***	***Pulse 7***	***Pulse 8***
zeroth moment (m_0)	2.3E-06	2.0E-06	2.3E-06	2.8E-06	2.4E-06	2.4E-06	2.8E-06
m_1	1.4E-04	1.2E-04	1.3E-04	1.8E-04	1.3E-04	1.5E-04	1.6E-04
first moment ($\mu_1 = m_1/m_0$)	61.7	58.8	59.4	63.0	55.6	61.6	57.7
mean residence time (t_m)	61.7	58.8	59.4	63.0	55.6	61.6	57.7
m_2	1.0E-02	8.0E-03	9.5E-03	1.3E-02	8.6E-03	1.0E-02	1.1E-02
variance (σ^2), sec^2	674.8	517.6	665.7	689.8	465.3	563.8	577.3
standard deviation (σ)	26.0	22.8	25.8	26.3	21.6	23.7	24.0

	Pulse 9	***Pulse 10***	***Pulse 11***	***Pulse 12***	***Pulse 13***	***Pulse 14***	***Pulse 15***	***Avr:***
zeroth moment (m_0)	2.9E-06	3.1E-06	2.9E-06	2.3E-06	2.4E-06	2.3E-06	2.9E-06	2.6E-06
m_1	1.6E-04	1.8E-04	1.7E-04	1.4E-04	1.3E-04	1.4E-04	1.6E-04	1.5E-04
first moment ($\mu_1 = m_1/m_0$)	55.2	57.1	57.5	59.5	51.7	60.5	55.3	58.2
mean residence time (t_m)	55.2	57.1	57.5	59.5	51.7	60.5	55.3	58.2
m_2	1.0E-02	1.2E-02	1.1E-02	9.3E-03	8.0E-03	9.8E-03	1.1E-02	1.0E-02
variance (σ^2), sec^2	528.9	537.7	601.2	547.9	605.8	542.9	546.3	576.1
standard deviation (σ)	23.0	23.2	24.5	23.4	24.6	23.3	23.4	24.0

Table D.20. CO response data for O_2 pulses into C_2H_6 and He flow over Cr-V-O catalyst at 400°C

	Pulse 2	***Pulse 3***	***Pulse 4***	***Pulse 5***	***Pulse 6***	***Pulse 7***	***Pulse 8***
zeroth moment (m_0)	1.3E-05	1.2E-05	1.1E-05	1.2E-05	1.5E-05	9.6E-06	8.8E-06
m_1	5.7E-04	5.9E-04	5.8E-04	5.7E-04	8.7E-04	4.5E-04	4.3E-04
first moment ($\mu_1 = m_1/m_0$)	43.6	49.0	51.2	48.3	57.7	47.3	49.2
mean residence time (t_m)	43.6	49.0	51.2	48.3	57.7	47.3	49.2
m_2	2.6E-02	3.2E-02	3.4E-02	2.9E-02	6.1E-02	2.2E-02	2.3E-02
variance (σ^2), sec^2	89.9	256.7	413.4	146.2	730.6	106.1	168.4
standard deviation (σ)	9.5	16.0	20.3	12.1	27.0	10.3	13.0

	Pulse 9	***Pulse 10***	***Pulse 11***	***Pulse 12***	***Pulse 13***	***Pulse 14***	***Pulse 15***	***Avr:***
zeroth moment (m_0)	7.5E-06	8.2E-06	1.0E-05	6.6E-06	8.7E-06	8.0E-06	7.2E-06	9.9E-06
m_1	3.5E-04	3.9E-04	4.9E-04	3.1E-04	3.5E-04	3.8E-04	3.0E-04	4.7E-04
first moment ($\mu_1 = m_1/m_0$)	46.6	47.8	49.0	46.8	40.1	48.0	42.5	47.7
mean residence time (t_m)	46.6	47.8	49.0	46.8	40.1	48.0	42.5	47.7
m_2	1.7E-02	2.0E-02	2.6E-02	1.5E-02	1.6E-02	1.9E-02	1.3E-02	2.5E-02
variance (σ^2), sec^2	85.3	123.7	151.4	84.5	179.9	108.2	49.5	192.4
standard deviation (σ)	9.2	11.1	12.3	9.2	13.4	10.4	7.0	12.9

D.2.3. Dynamic Experiments' Data for Cr-V-O Catalyst with C_2H_6 Pulses into He Flow at 449°C

The response data for C_2H_6 pulses into He flow over Cr-V-O catalyst at 449°C are presented in Figures D.2.22-D.2.38. The results of moment, variance, mean residence time, and standard deviation calculations for C_2H_6, C_2H_4, and H_2O are tabulated in Tables D.21-D.23.

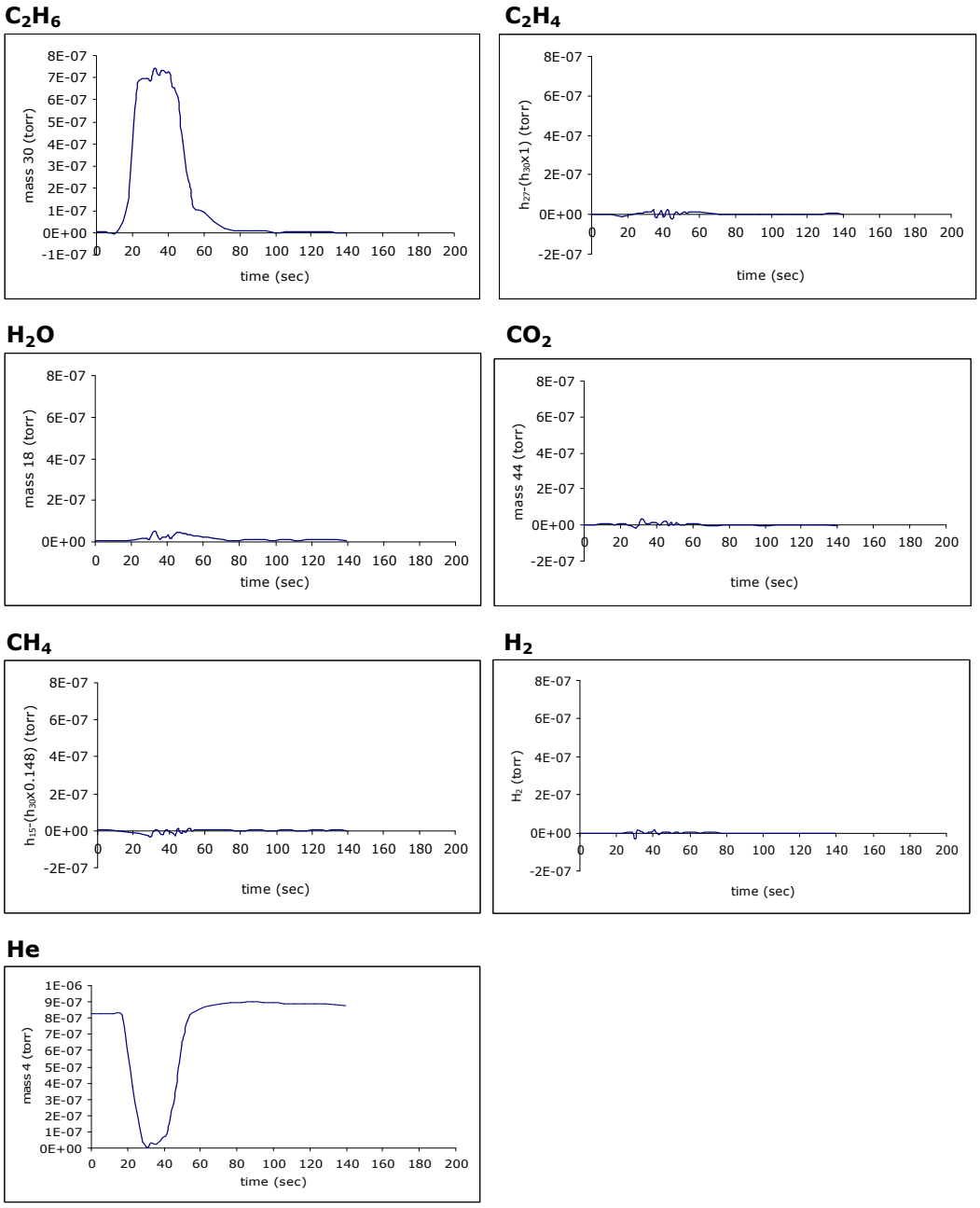

Figure D.2.22. 'Pulse 1' response data for C_2H_6 pulses into and He flow over Cr-V-O catalyst at 449°C

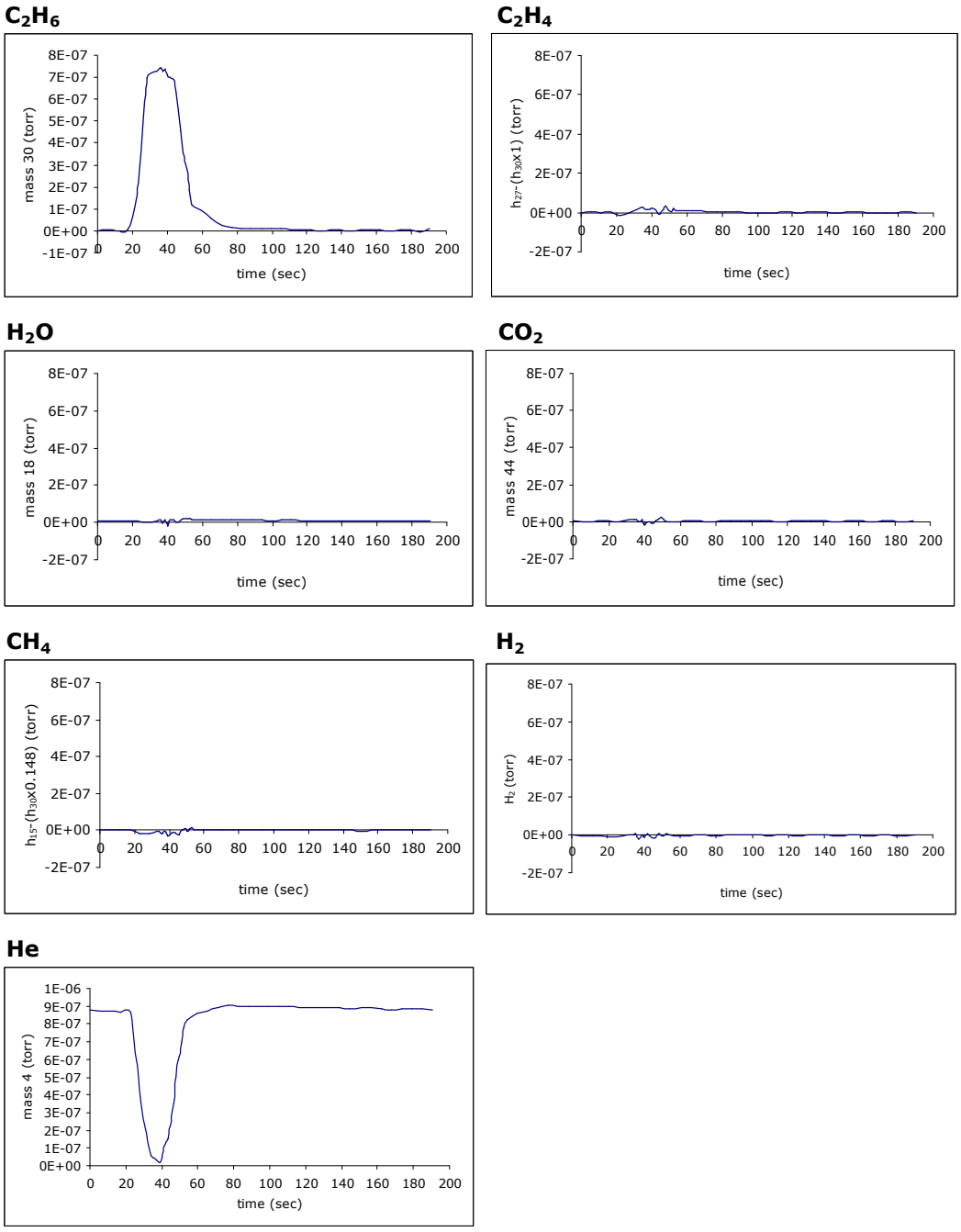

Figure D.2.23. 'Pulse 2' response data for C_2H_6 pulses into and He flow over Cr-V-O catalyst at 449°C

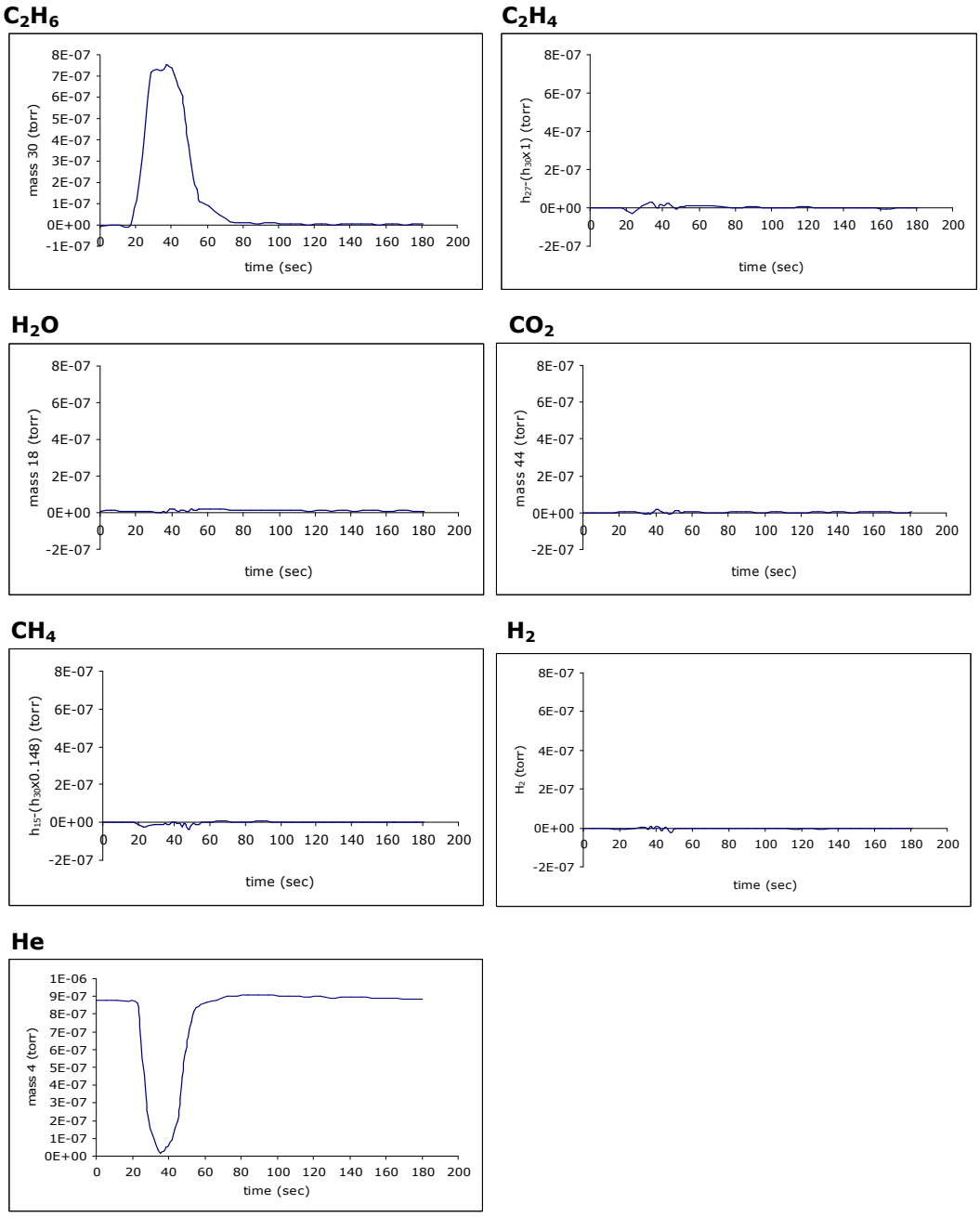

Figure D.2.24. 'Pulse 3' response data for C_2H_6 pulses into and He flow over Cr-V-O catalyst at 449°C

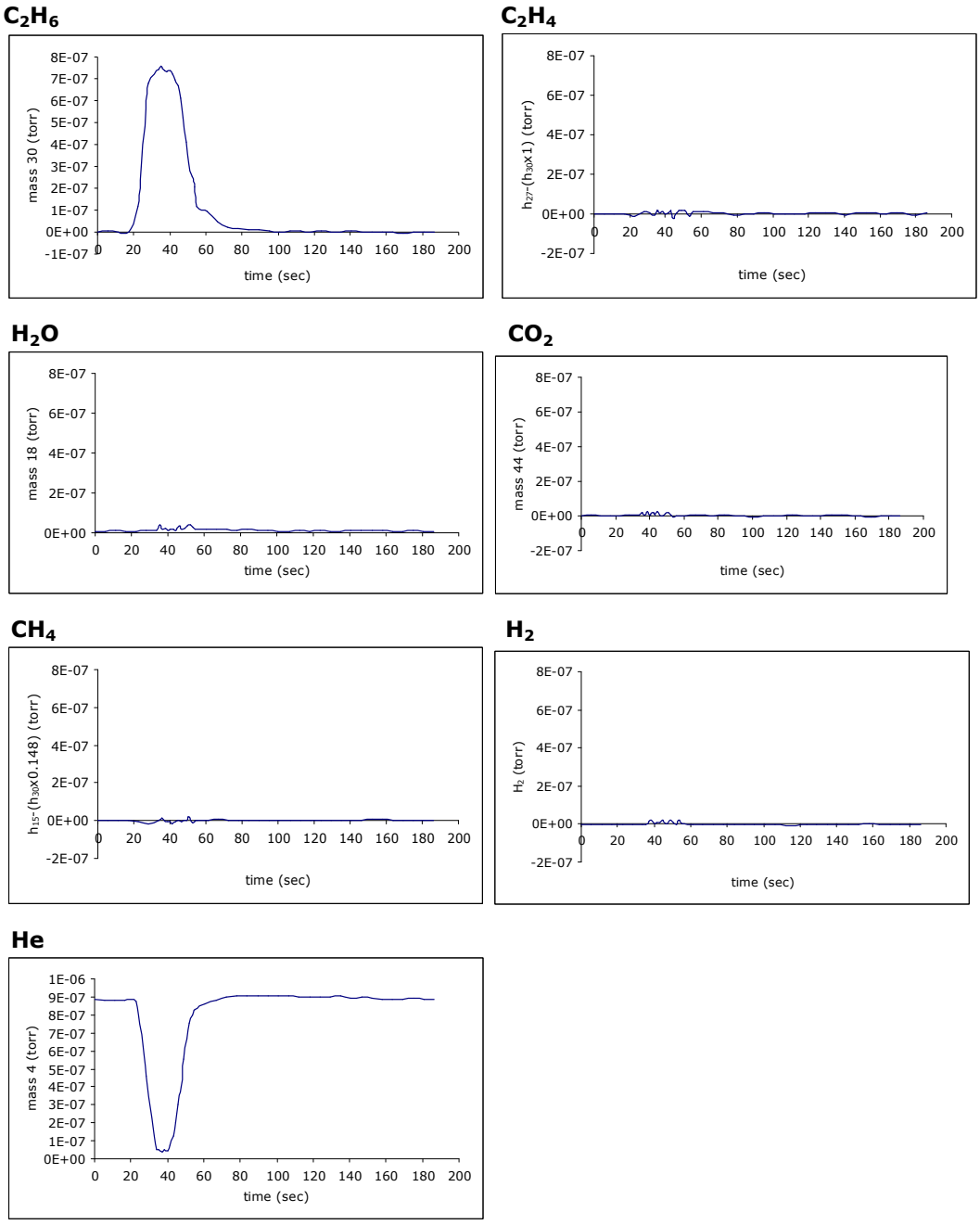

Figure D.2.25. 'Pulse 4' response data for C_2H_6 pulses into and He flow over Cr-V-O catalyst at 449°C

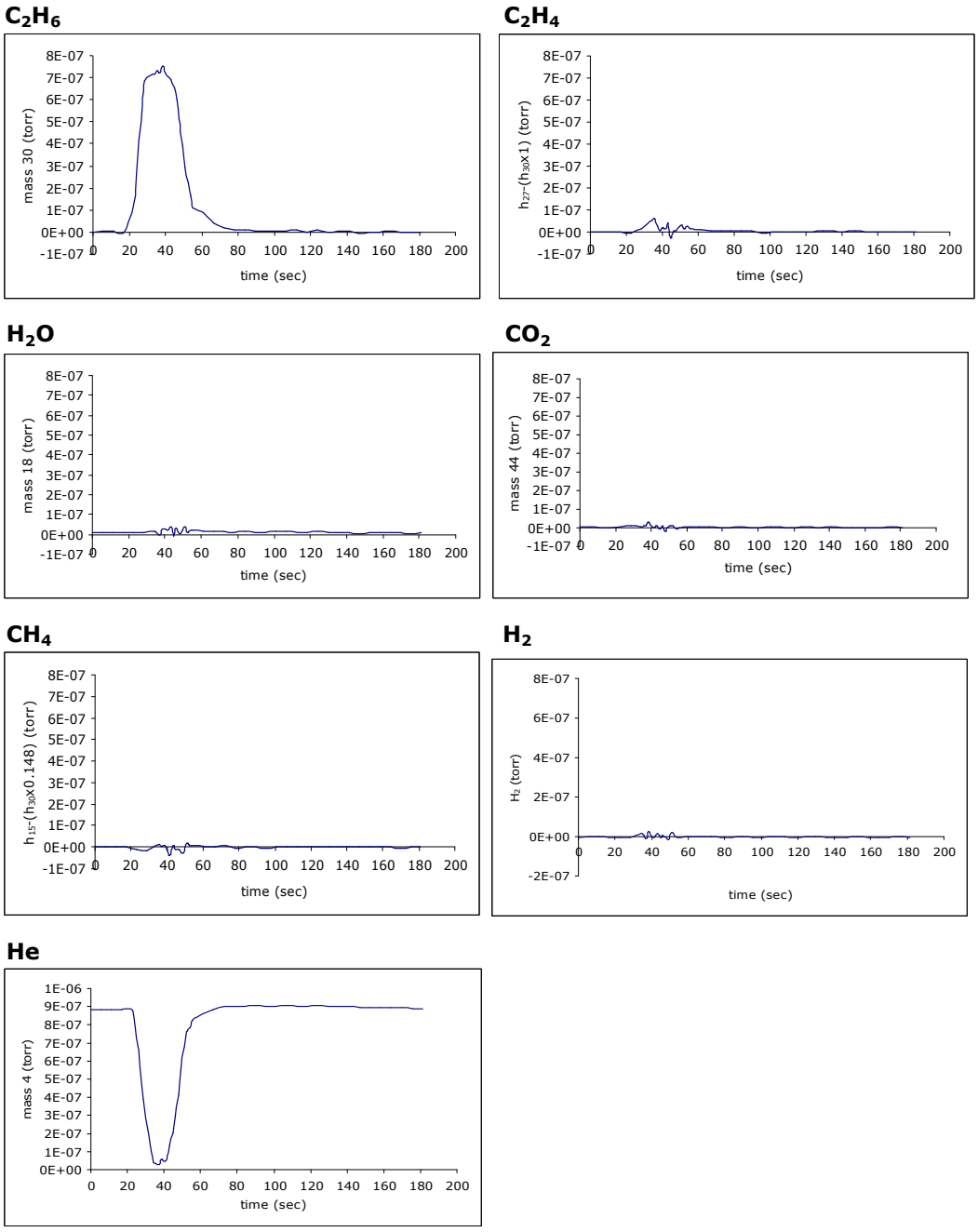

Figure D.2.26. 'Pulse 5' response data for C_2H_6 pulses into and He flow over Cr-V-O catalyst at 449°C

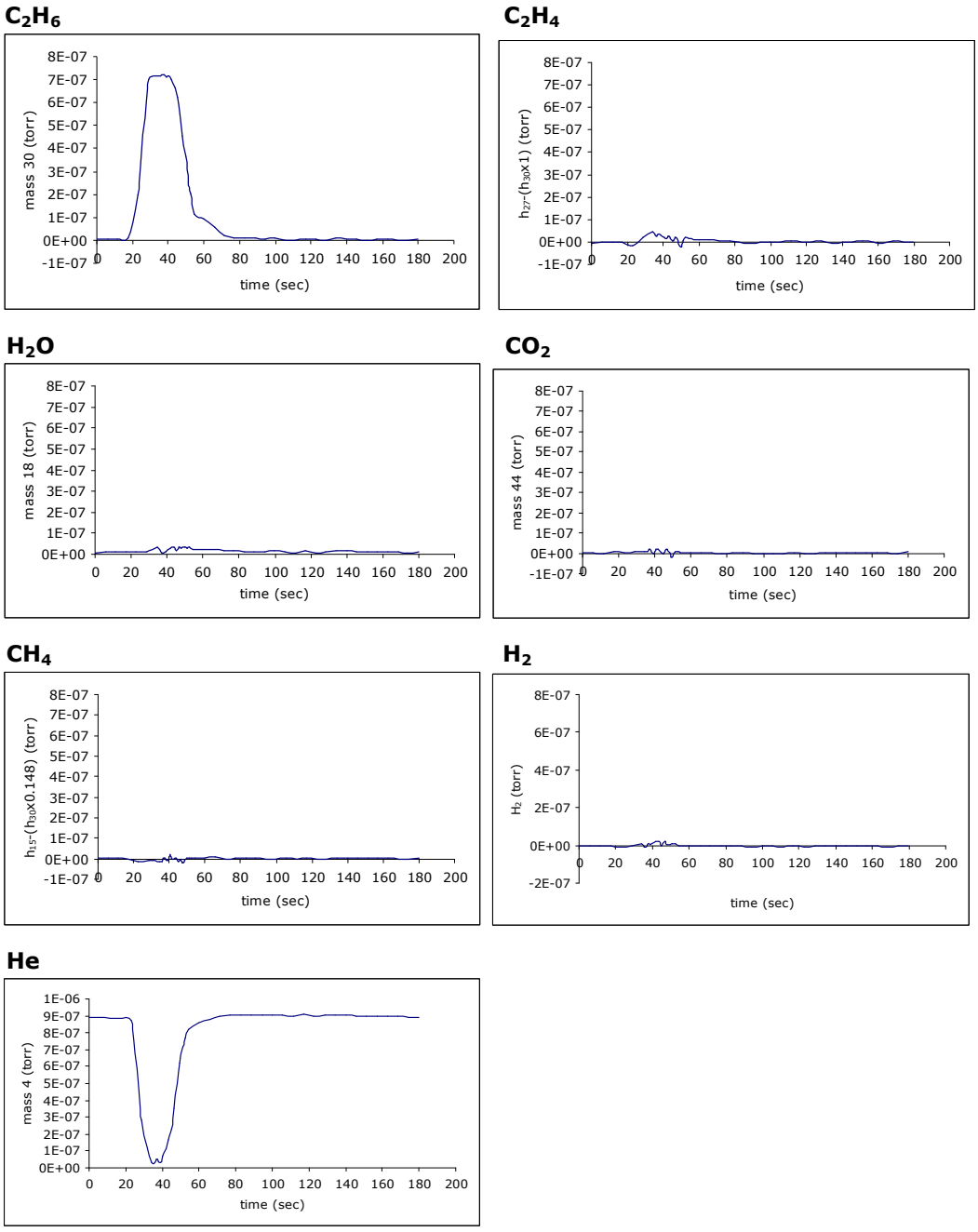

Figure D.2.27. 'Pulse 6' response data for C_2H_6 pulses into and He flow over Cr-V-O catalyst at 449°C

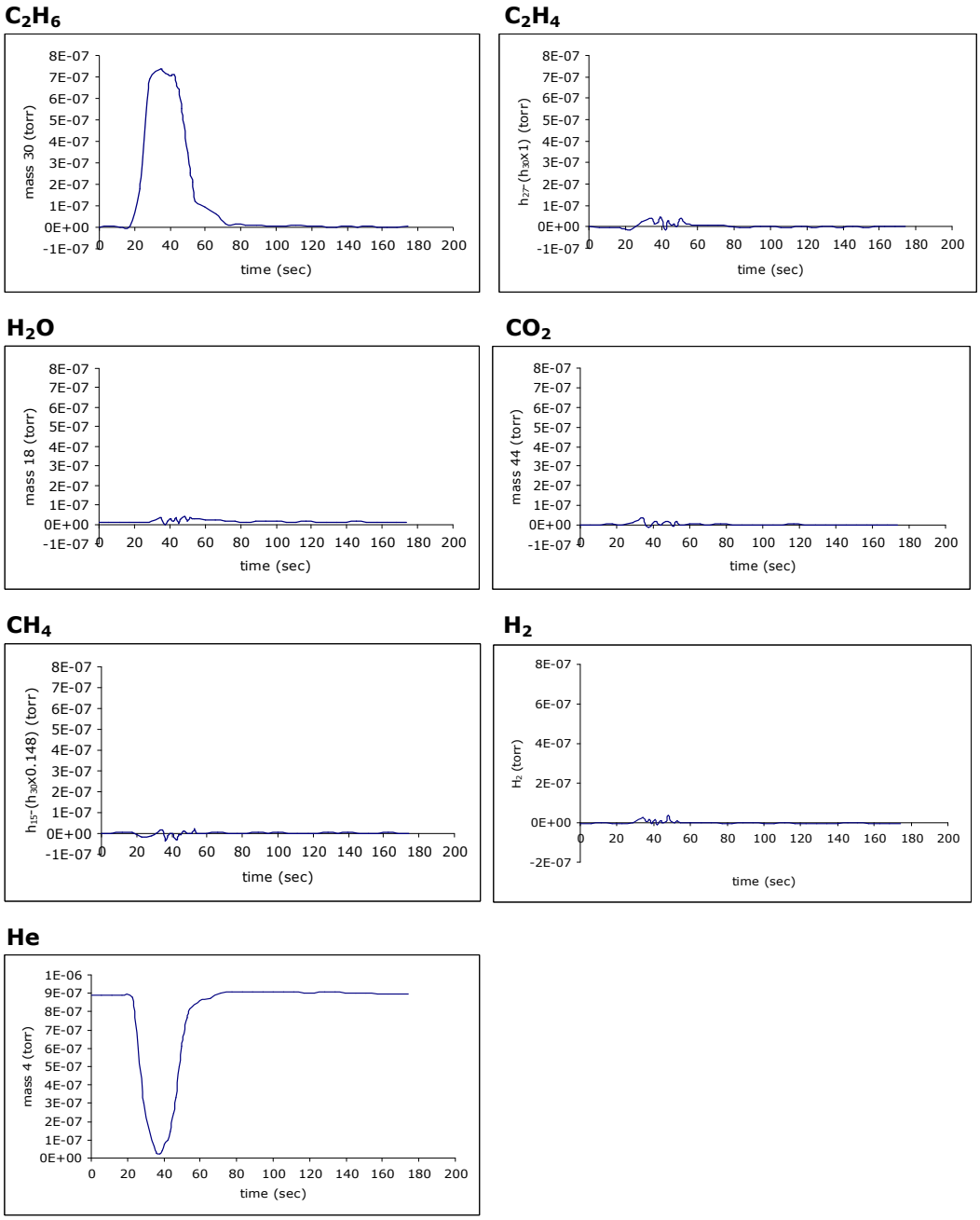

Figure D.2.28. 'Pulse 7' response data for C_2H_6 pulses into and He flow over Cr-V-O catalyst at 449°C

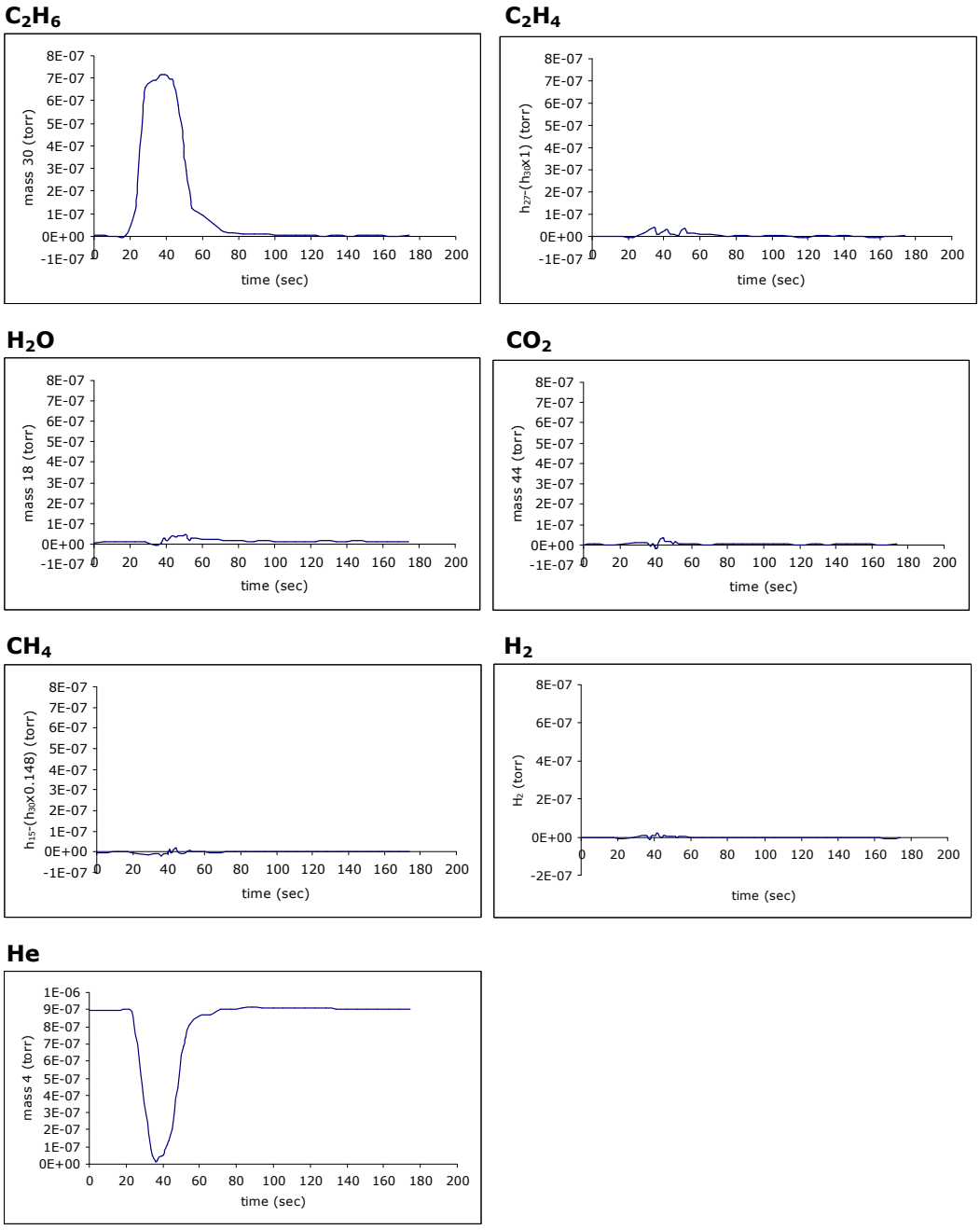

Figure D.2.29. 'Pulse 8' response data for C_2H_6 pulses into and He flow over Cr-V-O catalyst at 449°C

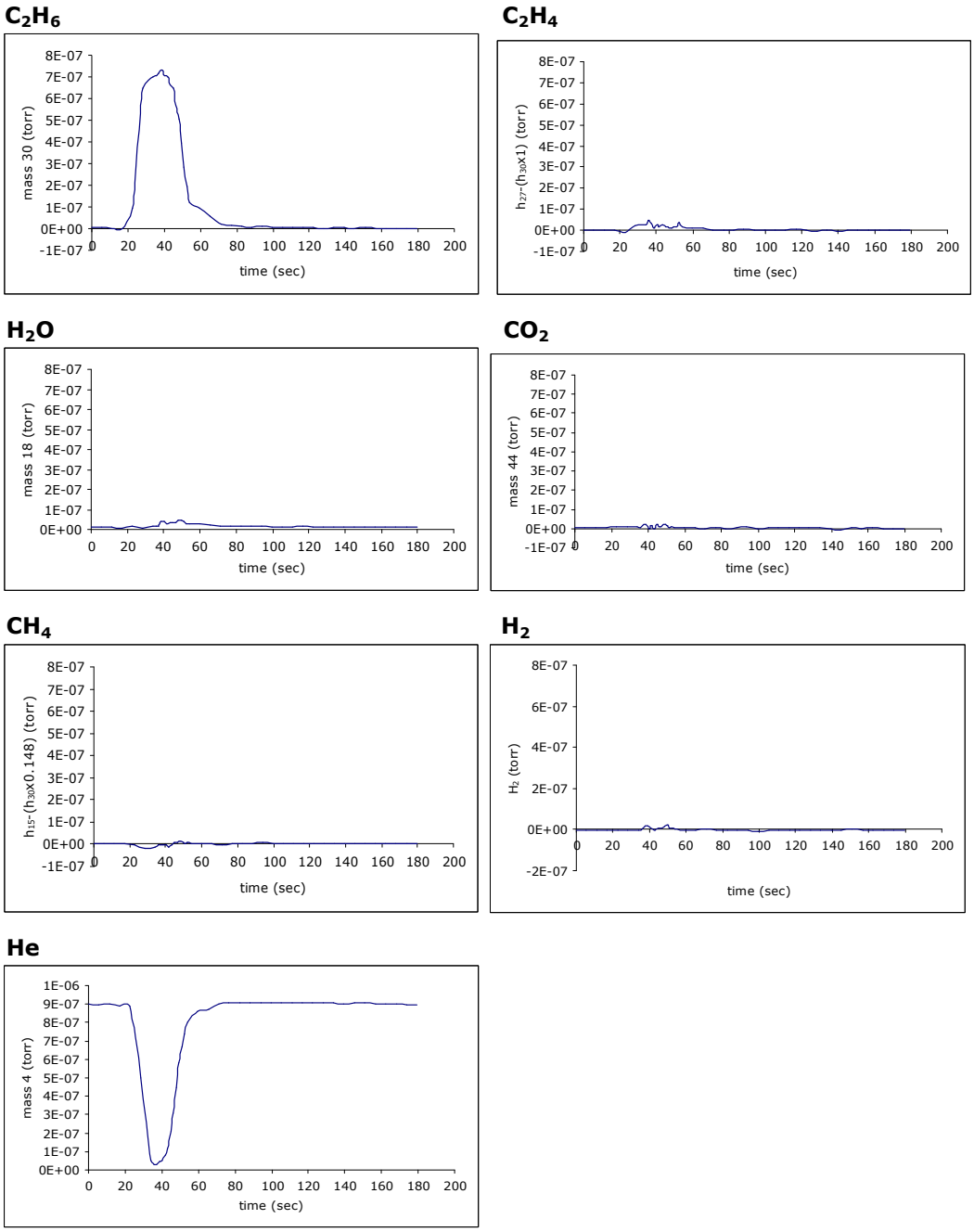

Figure D.2.30. 'Pulse 9' response data for C_2H_6 pulses into and He flow over Cr-V-O catalyst at 449°C

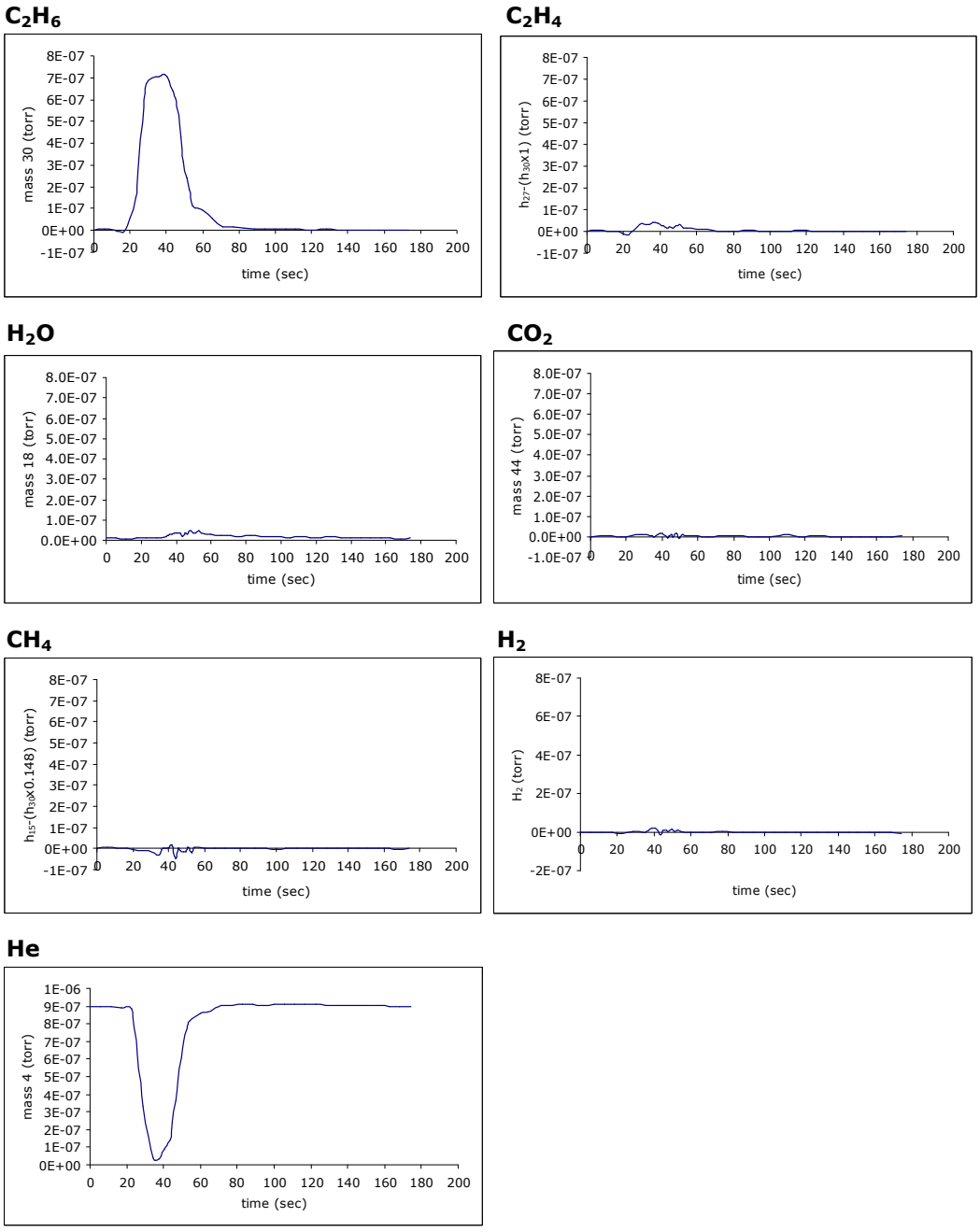

Figure D.2.31. 'Pulse 10' response data for C_2H_6 pulses into and He flow over Cr-V-O catalyst at 449°C

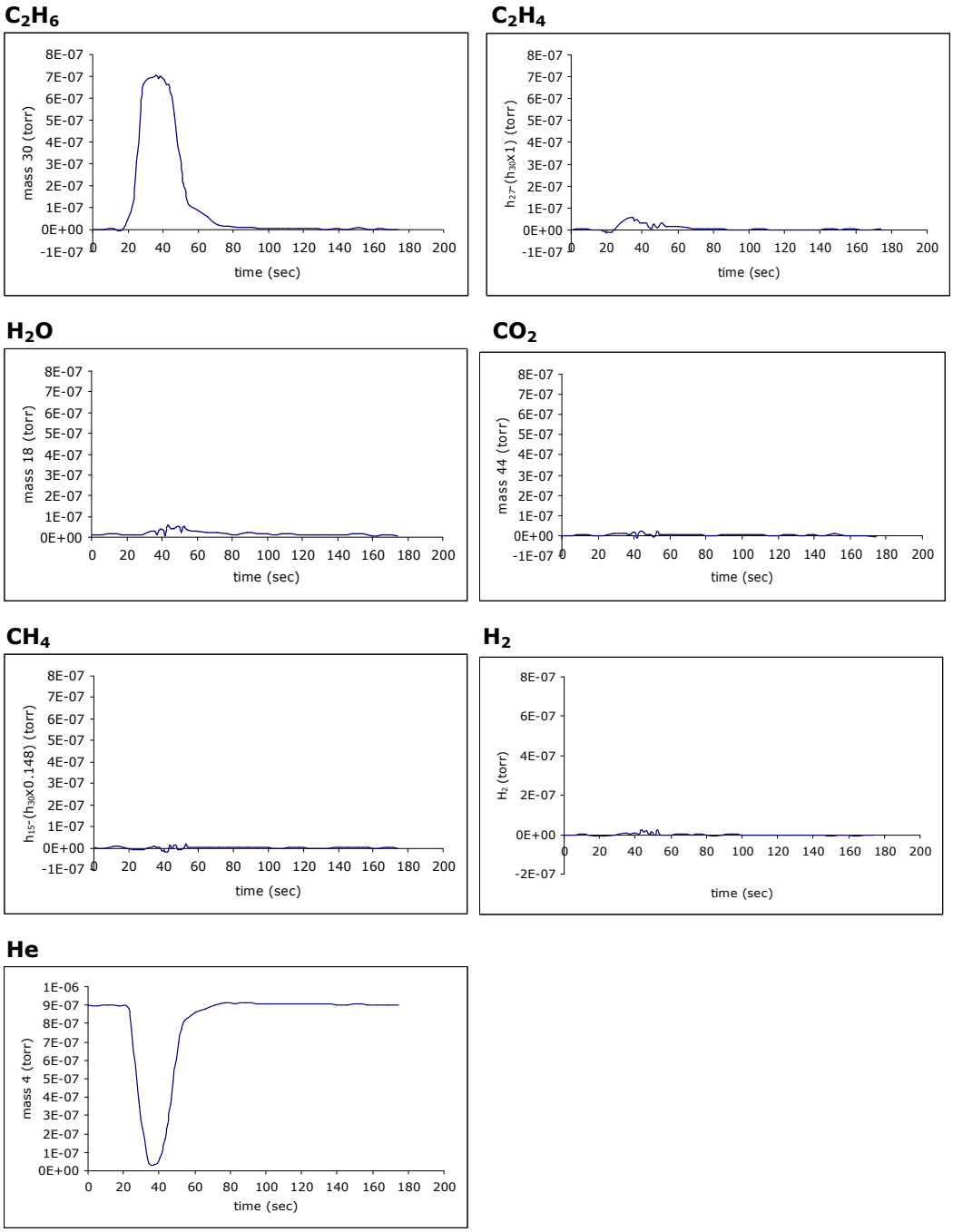

Figure D.2.32. 'Pulse 11' response data for C_2H_6 pulses into and He flow over Cr-V-O catalyst at 449°C

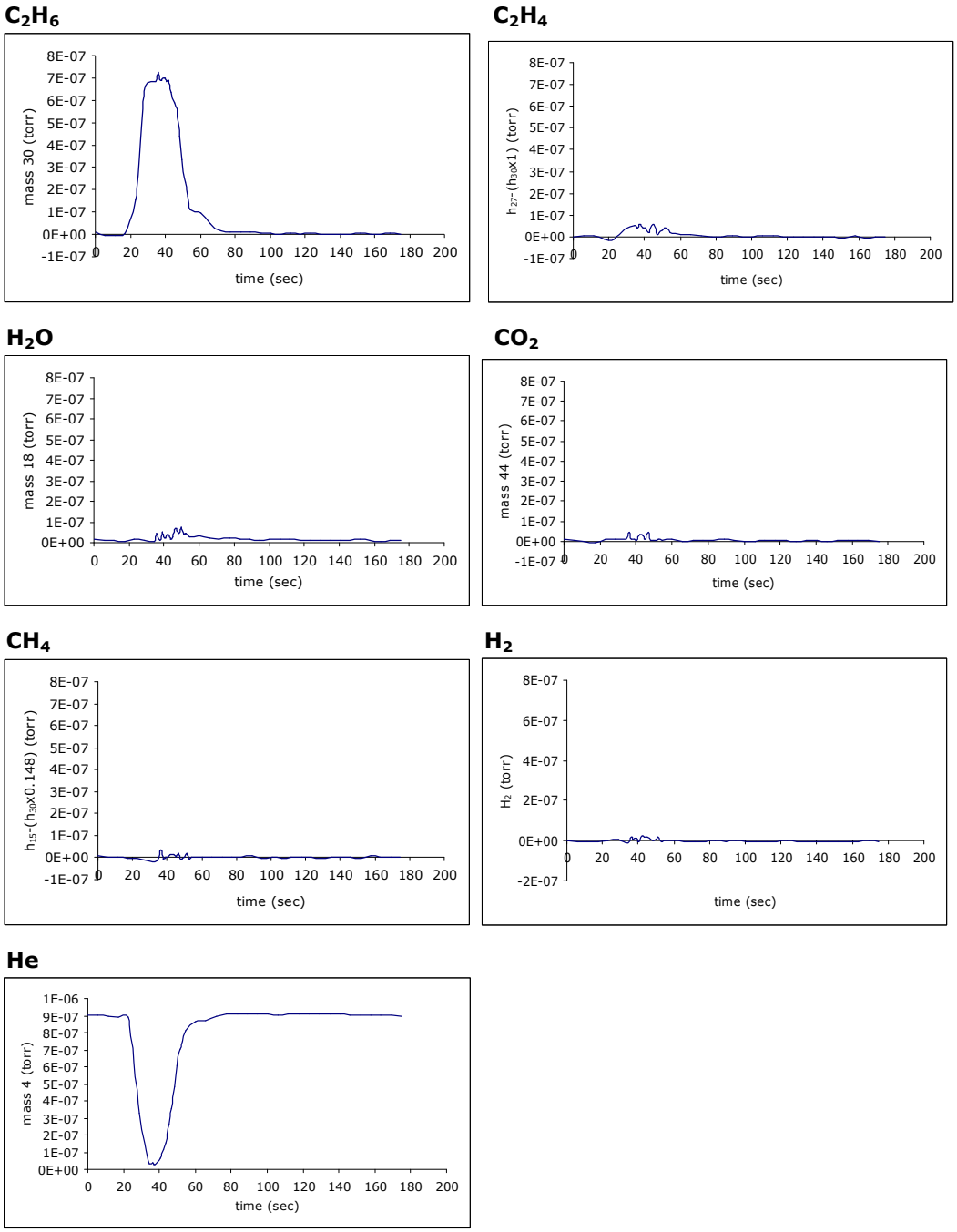

Figure D.2.33. 'Pulse 12' response data for C_2H_6 pulses into and He flow over Cr-V-O catalyst at 449°C

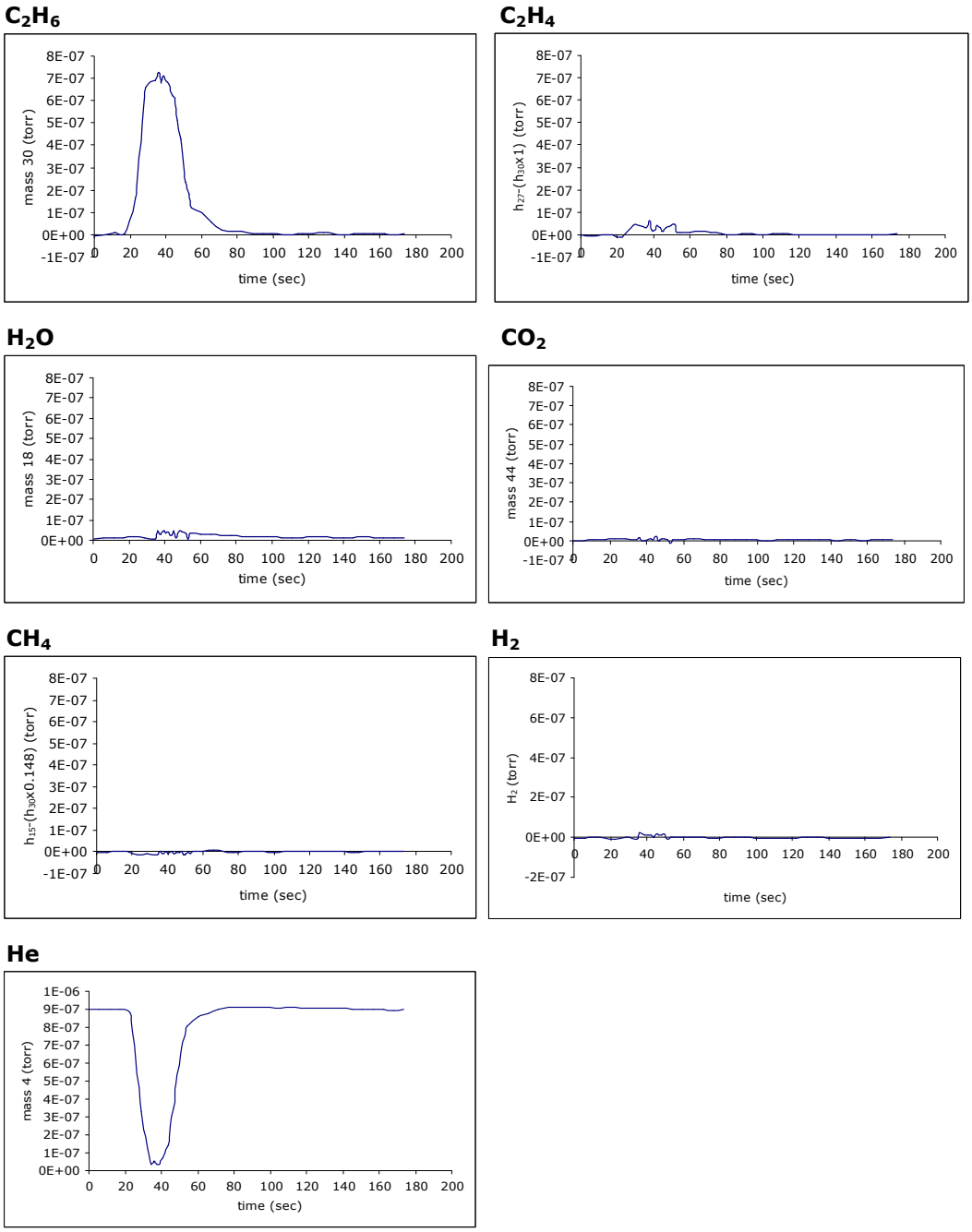

Figure D.2.34. 'Pulse 13' response data for C_2H_6 pulses into and He flow over Cr-V-O catalyst at 449°C

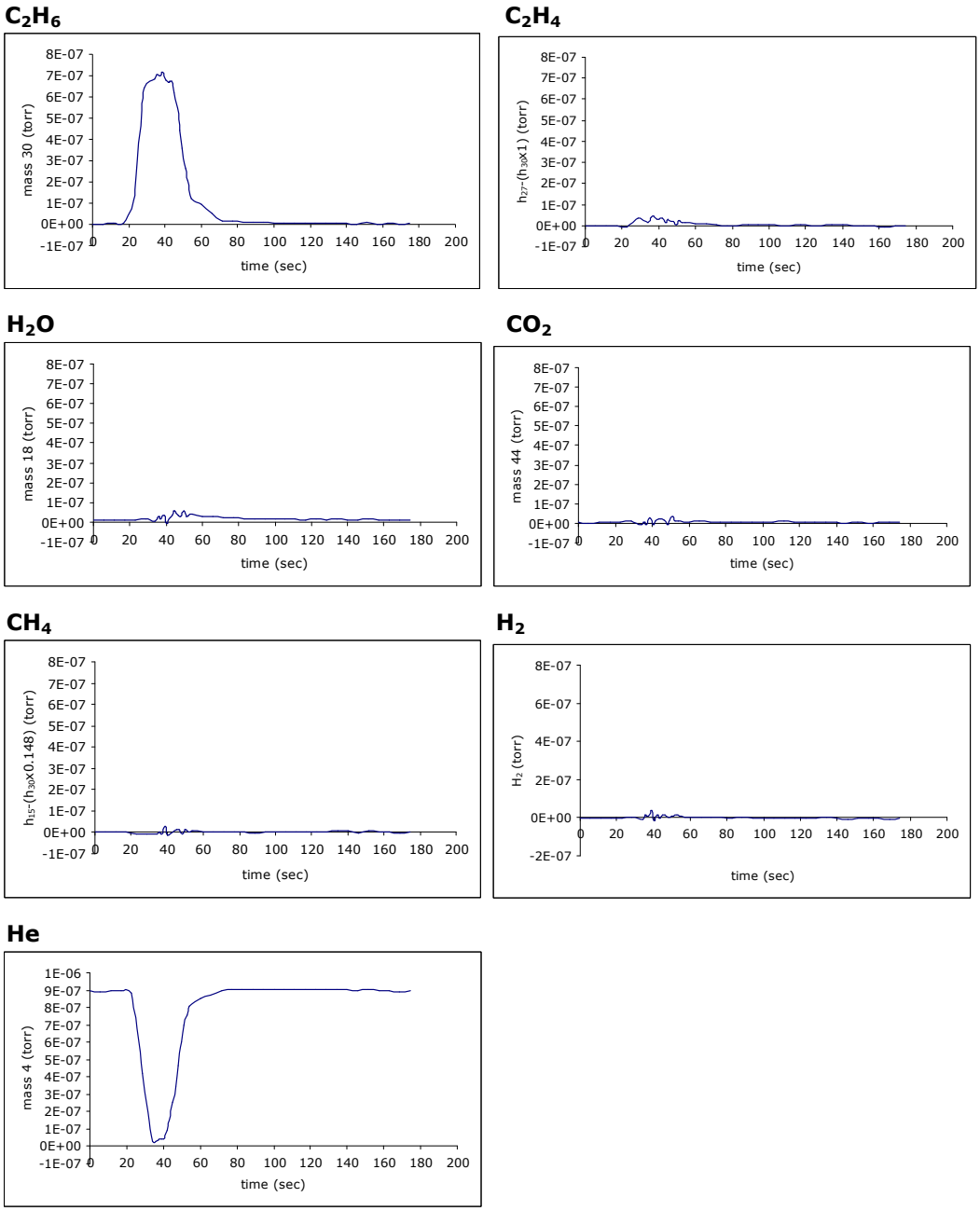

Figure D.2.35. 'Pulse 14' response data for C_2H_6 pulses into and He flow over Cr-V-O catalyst at 449°C

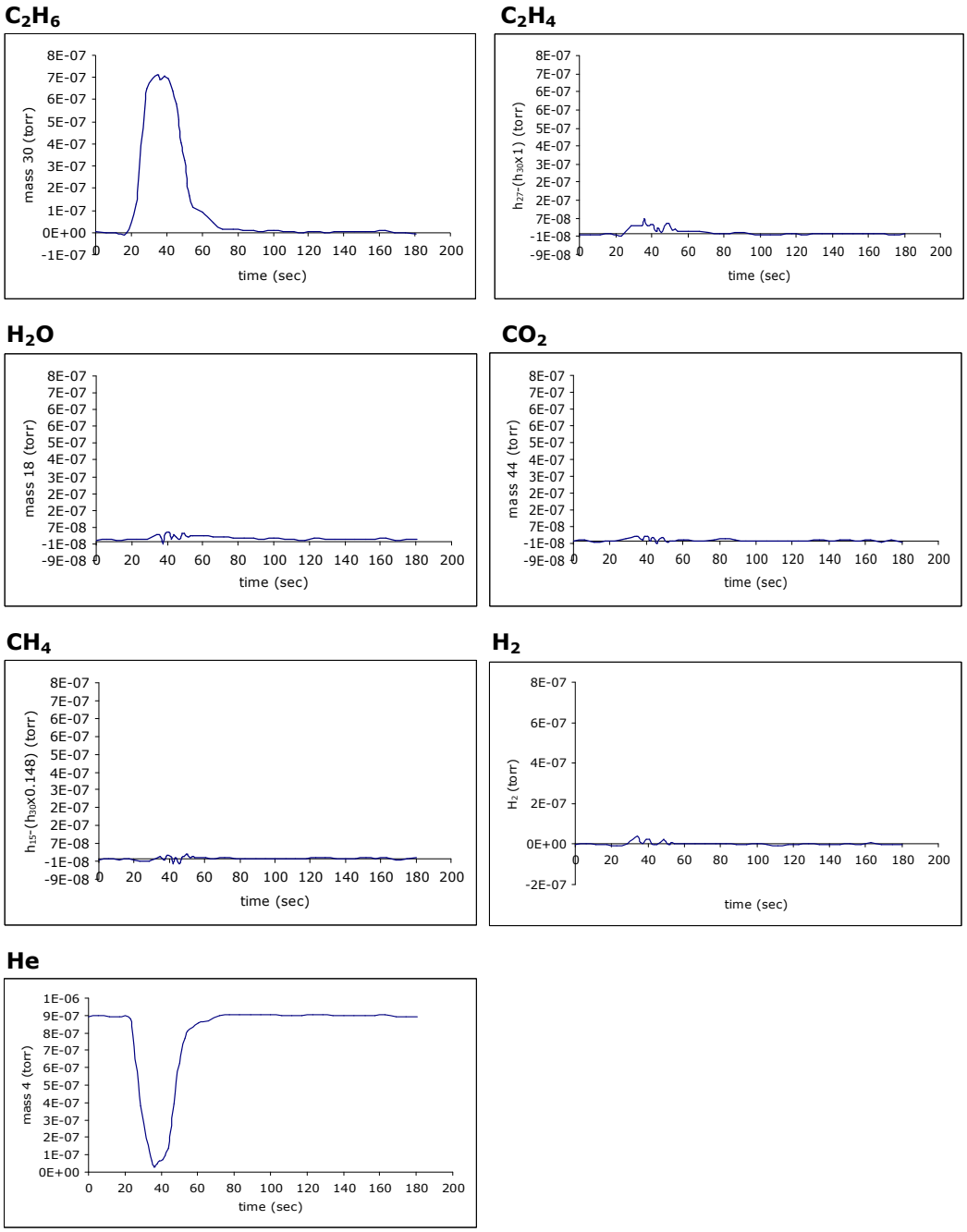

Figure D.2.36. 'Pulse 15' response data for C_2H_6 pulses into and He flow over Cr-V-O catalyst at 449°C

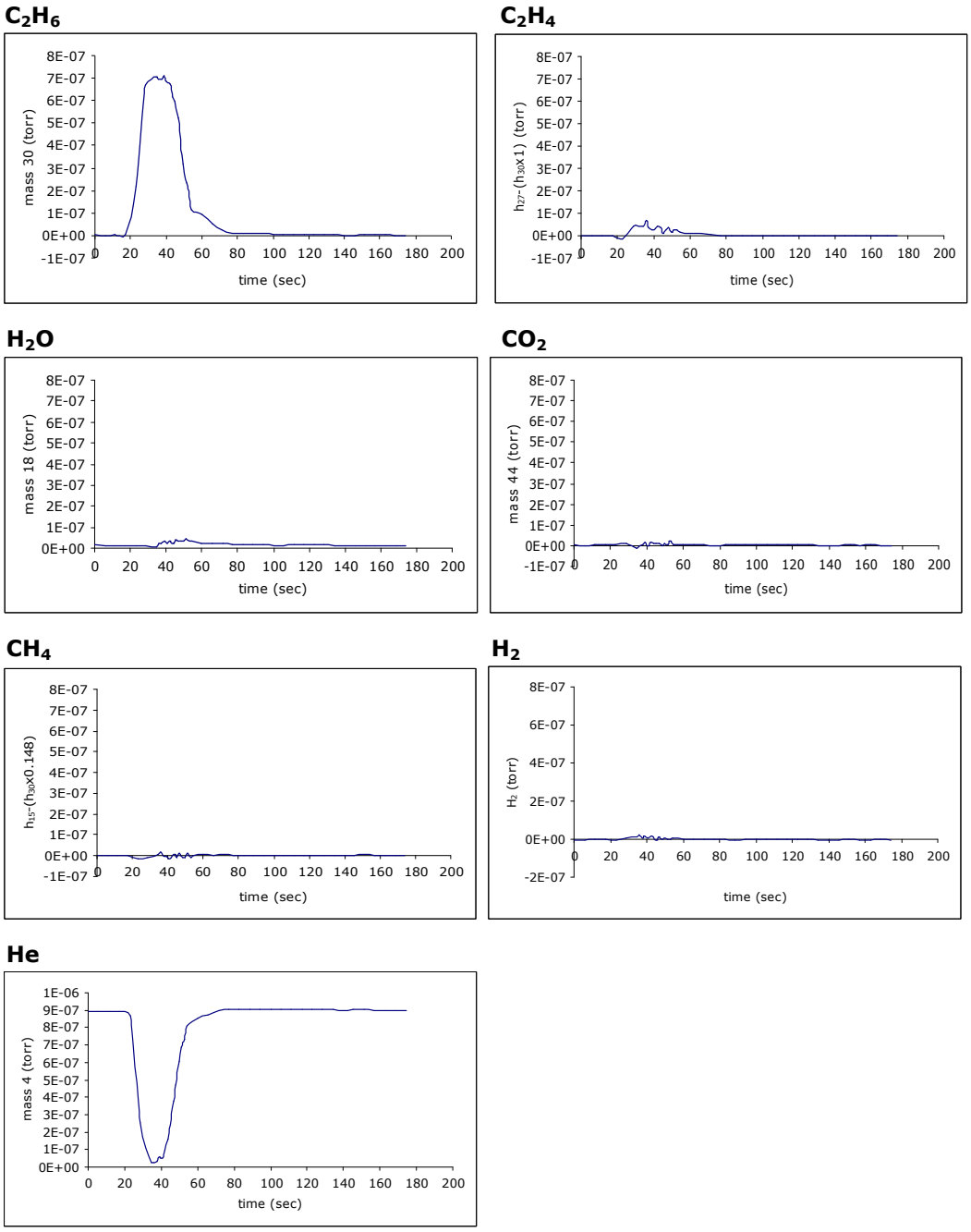

Figure D.2.37. 'Pulse 16' response data for C_2H_6 pulses into and He flow over Cr-V-O catalyst at 449°C

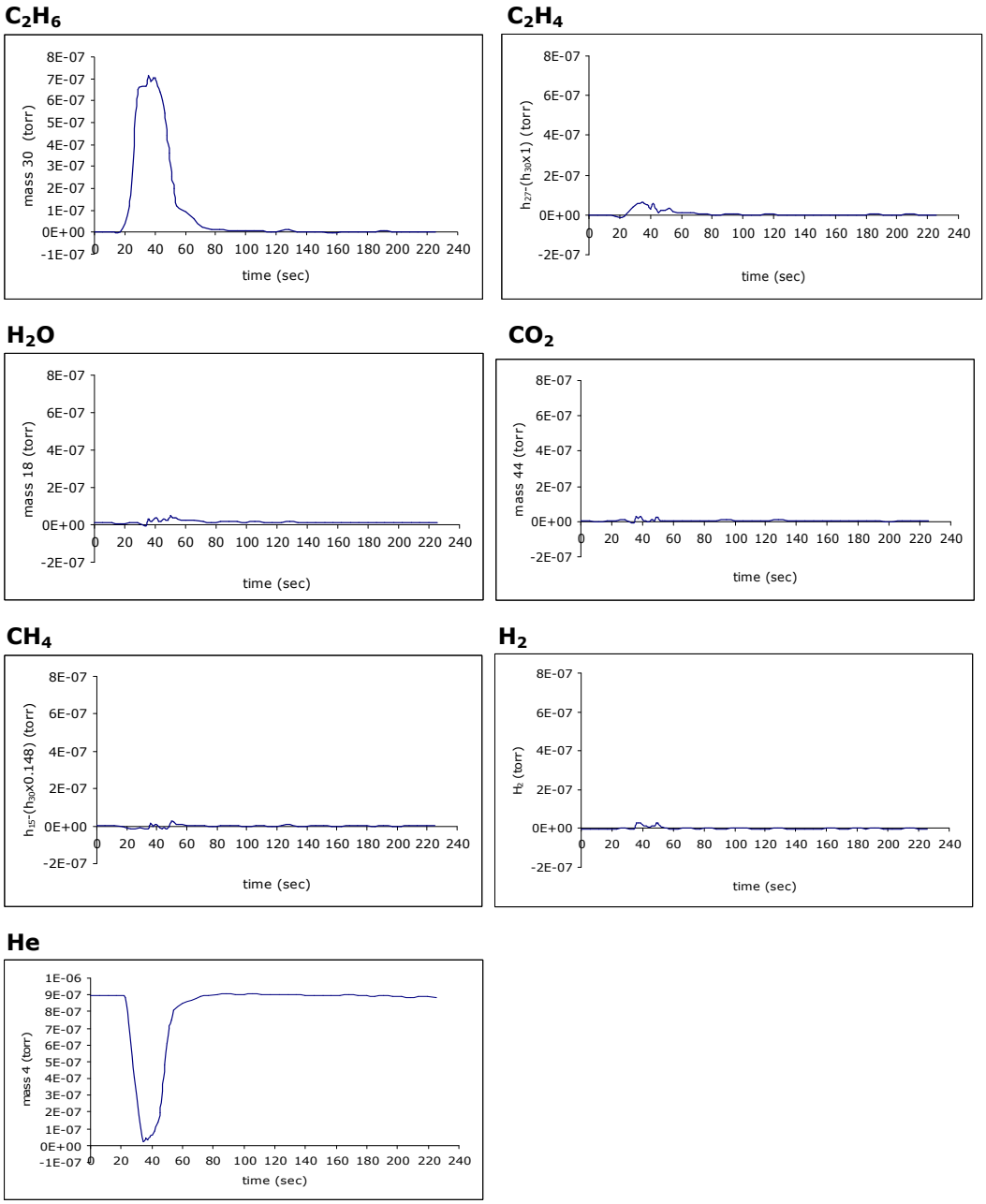

Figure D.2.38. 'Pulse 17' response data for C_2H_6 pulses into and He flow over Cr-V-O catalyst at 449°C

Table D.21. C_2H_6 response data for C_2H_6 pulses into He flow over Cr-V-O catalyst at 449°C

	Pulse 1	***Pulse 2***	***Pulse 3***	***Pulse 4***	***Pulse 5***	***Pulse 6***	***Pulse 7***	***Pulse 8***
zeroth moment (m_0)	3.7E-05	3.5E-05	3.3E-05	3.4E-05	3.3E-05	3.3E-05	3.5E-05	3.1E-05
m_1	1.4E-03	1.4E-03	1.4E-03	1.4E-03	1.4E-03	1.3E-03	1.5E-03	1.3E-03
first moment ($\mu_1 = m_1/m_0$)	38.2	41.1	41.2	41.3	41.5	41.0	41.4	41.8
mean residence time (t_m)	38.2	41.1	41.2	41.3	41.5	41.0	41.4	41.8
m_2	5.7E-02	6.2E-02	5.8E-02	5.9E-02	5.9E-02	5.7E-02	6.3E-02	5.6E-02
variance (σ^2), sec^2	79.4	83.0	76.2	65.6	72.0	70.4	83.7	64.2
standard deviation (σ)	8.9	9.1	8.7	8.1	8.5	8.4	9.1	8.0

	Pulse 9	***Pulse 10***	***Pulse 11***	***Pulse 12***	***Pulse 13***	***Pulse 14***	***Pulse 15***	***Pulse 16***
zeroth moment (m_0)	3.5E-05	3.3E-05	3.0E-05	2.8E-05	3.1E-05	3.2E-05	2.9E-05	3.3E-05
m_1	1.4E-03	1.3E-03	1.2E-03	1.2E-03	1.3E-03	1.3E-03	1.2E-03	1.4E-03
first moment ($\mu_1 = m_1/m_0$)	41.5	41.2	41.4	41.4	41.2	41.2	41.4	41.2
mean residence time (t_m)	41.5	41.2	41.4	41.4	41.2	41.2	41.4	41.2
m_2	6.3E-02	5.8E-02	5.3E-02	5.0E-02	5.5E-02	5.6E-02	5.3E-02	6.0E-02
variance (σ^2), sec^2	78.1	78.8	63.7	63.5	69.1	67.8	70.1	87.4
standard deviation (σ)	8.8	8.9	8.0	8.0	8.3	8.2	8.4	9.3

	Pulse 17	***Avr.***
zeroth moment (m_0)	3.3E-05	3.3E-05
m_1	1.4E-03	1.3E-03
first moment ($\mu_1 = m_1/m_0$)	41.4	41.1
mean residence time (t_m)	41.4	41.1
m_2	5.8E-02	5.8E-02
variance (σ^2), sec^2	76.7	73.5
standard deviation (σ)	8.8	8.6

Table D.22. C_2H_4 response data for C_2H_6 pulses into He flow over Cr-V-O catalyst at 449°C

	Pulse 5	***Pulse 6***	***Pulse 7***	***Pulse 8***	***Pulse 9***	***Pulse 10***	***Pulse 11***
	Area1	*Area1*	*Area1*	*Area1*	*Area1*	*Area1*	*Area1*
zeroth moment (m_0)	5.2E-07	5.1E-07	3.8E-07	3.8E-07	4.8E-07	6.7E-07	5.7E-07
m_1	2.0E-05	2.0E-05	1.4E-05	1.5E-05	1.9E-05	2.4E-05	2.1E-05
first moment ($\mu_1 = m_1/m_0$)	37.8	39.0	37.0	38.6	39.2	36.6	37.4
mean residence time (t_m)	37.8	39.0	37.0	38.6	39.2	36.6	37.4
m_2	7.5E-04	7.8E-04	5.2E-04	5.7E-04	7.4E-04	9.1E-04	8.0E-04
variance (σ^2), sec^2	14.1	19.6	9.7	18.2	19.3	18.6	11.7
standard deviation (σ)	3.8	4.4	3.1	4.3	4.4	4.3	3.4
% of total area	48	61	42	46	53	52	51

	Pulse 5	***Pulse 6***	***Pulse 7***	***Pulse 8***	***Pulse 9***	***Pulse 10***	***Pulse 11***
	Area2	*Area2*	*Area2*	*Area2*	*Area2*	*Area2*	*Area2*
zeroth moment (m_0)	5.7E-07	3.3E-07	5.1E-07	4.5E-07	4.2E-07	6.3E-07	5.5E-07
m_1	3.2E-05	1.9E-05	2.7E-05	2.4E-05	2.2E-05	3.2E-05	3.0E-05
first moment ($\mu_1 = m_1/m_0$)	55.5	59.1	52.0	54.1	53.6	51.1	53.7
mean residence time (t_m)	55.5	59.1	52.0	54.1	53.6	51.1	53.7
m_2	1.8E-03	1.2E-03	1.4E-03	1.3E-03	1.2E-03	1.7E-03	1.6E-03
variance (σ^2), sec^2	73.2	67.7	35.1	33.3	19.9	34.2	69.8
standard deviation (σ)	8.6	8.2	5.9	5.8	4.5	5.9	8.4
% of total area	52	39	58	54	47	48	49

Total area (Area 1 + 2)	1.1E-06	8.4E-07	8.9E-07	8.2E-07	9.0E-07	1.3E-06	1.1E-06

Table D.22. (Cont'd.)

	Pulse 12	***Pulse 13***	***Pulse 14***	***Pulse 15***	***Pulse 16***	***Pulse 17***	***Avr:***
	Area1	*Area1*	*Area1*	*Area1*	*Area1*	*Area1*	
zeroth moment (m_0)	9.1E-07	5.8E-07	7.6E-07	6.3E-07	6.2E-07	7.3E-07	5.9E-07
m_1	3.5E-05	2.2E-05	3.0E-05	2.4E-05	2.4E-05	2.7E-05	2.3E-05
first moment ($\mu_1 = m_1/m_0$)	38.7	38.2	39.0	38.2	38.3	37.8	38.1
mean residence time (t_m)	38.7	38.2	39.0	38.2	38.3	37.8	38.1
m_2	1.4E-03	8.5E-04	1.2E-03	9.3E-04	9.2E-04	1.0E-03	8.8E-04
variance (σ^2), sec^2	26.6	14.4	33.4	12.9	15.1	13.5	1.7E+01
standard deviation (σ)	5.2	3.8	5.8	3.6	3.9	3.7	4.1
% of total area	55	43	71	42	49	50	51

	Pulse 12	***Pulse 13***	***Pulse 14***	***Pulse 15***	***Pulse 16***	***Pulse 17***	***Avr:***
	Area2	*Area2*	*Area2*	*Area2*	*Area2*	*Area2*	
zeroth moment (m_0)	7.4E-07	7.5E-07	3.2E-07	8.7E-07	6.4E-07	7.2E-07	5.8E-07
m_1	4.0E-05	4.0E-05	1.7E-05	4.7E-05	3.4E-05	3.9E-05	3.1E-05
first moment ($\mu_1 = m_1/m_0$)	54.1	52.6	55.1	54.5	52.7	53.9	54.0
mean residence time (t_m)	54.1	52.6	55.1	54.5	52.7	53.9	54.0
m_2	2.2E-03	2.1E-03	9.7E-04	2.7E-03	1.8E-03	2.1E-03	1.7E-03
variance (σ^2), sec^2	56.1	57.1	29.6	108.8	48.5	87.4	5.5E+01
standard deviation (σ)	7.5	7.6	5.4	10.4	7.0	9.3	7.3
% of total area	45	57	29	58	51	50	49

Total area (Area 1 + 2)	1.6E-06	1.3E-06	1.1E-06	1.5E-06	1.3E-06	1.4E-06	1.2E-06

Table D.23. H_2O response data for C_2H_6 pulses into He flow over Cr-V-O catalyst at 449°C

	Pulse 5	***Pulse 6***	***Pulse 7***	***Pulse 8***	***Pulse 9***	***Pulse 10***	***Pulse 11***
zeroth moment (m_0)	1.0E-06	1.4E-06	7.0E-07	1.5E-06	1.5E-06	1.7E-06	2.0E-06
m_1	6.2E-05	7.5E-05	3.8E-05	9.1E-05	8.3E-05	9.7E-05	1.1E-04
first moment ($\mu_1 = m_1/m_0$)	61.9	53.1	54.9	61.0	54.3	56.3	57.4
mean residence time (t_m)	61.9	53.1	54.9	61.0	54.3	56.3	57.4
m_2	4.6E-03	4.6E-03	2.3E-03	6.6E-03	5.1E-03	6.3E-03	7.8E-03
variance (σ^2), sec^2	741.2	429.6	218.4	685.5	372.3	489.7	603.5
standard deviation (σ)	27.2	20.7	14.8	26.2	19.3	22.1	24.6

	Pulse 12	***Pulse 13***	***Pulse 14***	***Pulse 15***	***Pulse 16***	***Pulse 17***	***Avr.***
zeroth moment (m_0)	1.7E-06	1.8E-06	1.5E-06	1.6E-06	1.4E-06	1.4E-06	1.5E-06
m_1	9.4E-05	1.1E-04	8.7E-05	9.4E-05	8.0E-05	8.8E-05	8.6E-05
first moment ($\mu_1 = m_1/m_0$)	53.7	61.8	58.3	59.6	56.6	61.2	57.7
mean residence time (t_m)	53.7	61.8	58.3	59.6	56.6	61.2	57.7
m_2	5.5E-03	8.4E-03	6.0E-03	7.1E-03	5.2E-03	6.5E-03	5.8E-03
variance (σ^2), sec^2	267.3	901.3	570.2	920.5	499.9	814.9	578.0
standard deviation (σ)	16.3	30.0	23.9	30.3	22.4	28.5	23.6

CURRICULUM VITAE

PERSONAL INFORMATION

Surname, Name : Karamullaoğlu Gülsün

Nationality : Turkish (T.C.)

Date and Place of Birth : Sept. 16, 1974, Bursa

Marital Status : Single

e-mail : gulsun_k@yahoo.com

EDUCATION

- METU, Dept. of Chemical Engineering, M.S. June, 1999
- METU, Dept. of Chemical Engineering, B.S. July, 1996
- Bursa Özel Namık Sözeri High School, June, 1992

EXPERIENCE

- METU, Dept. of Chemical Engineering:
  Teaching assistant, 1996-2004

- 2nd Chemical Engineering Conference for Collaborative Research in Eastern Mediterranean:
  Editorial Assistance in Organizing Committee and Officer at Registration Desk,
  METU, May 20-24, 2001, Ankara.

- 2nd Chemical Engineering Conference for Collaborative Research in Eastern Mediterranean:
  Oral and poster presentation
  METU, May 20-24, 2001, Ankara.

- 4th National Chemical Engineering Congress:
  Oral presentation,
  İstanbul Univ., Sept.4-7, 2000, İstanbul.

- 14th International Congress of Chemical and Process Engineering- CHISA:
  Oral presentation,
  August 27-31, 2000, Praha, Czech Republic.

- TÜGSAS-Gemlik, Ammonia Factory:
  Apprenticeship,
  summer-1995, Gemlik, Bursa.

FOREIGN LANGUAGES

- English – high level,
  (Secondary school & university education)

- Italian – intermediate,
  (Certificated from Institute of Italian Culture in Ankara)

PUBLICATIONS

- G. Karamullaoglu, T. Dogu, 'Oxidative dehydrogenation of ethane over a monolith coated by molybdenum-vanadium-niobium mixed-oxide catalyst', *Chem. Eng. Comm.* 190 (2003) 1427.

- G. Karamullaoglu, S. Onen, T. Dogu, 'Oxidative dehydrogenation of ethane and isobutene with chromium-vanadium-niobium mixed oxide catalysts', *Chem. Eng. Proc.* 41 (2002) 337.

AWARDS

- Hasan Orbey Award in Graduate Studies,
  Department of Chemical Engineering, METU, 2002

- 2nd in place among graduates of the department,
  Department of Chemical Engineering, METU, 1996

- 1st in place among juniors for 1st and 2nd semester,
  Department of Chemical Engineering, METU, 1994-1995

- 2nd in place among sophomores for 1st and 2nd semester,
  Department of Chemical Engineering, METU, 1993-1994

- 1st in place among freshmen 2nd semester,
  Department of Chemical Engineering, METU, 1992

HOBBIES

- Attended dance lessons on Standard & Latin Dances, 1998-2000
- Personal projects:
  Designing cards, CD cover, editorial contribution in the design of the one issue DanceSport magazine
- Organizing parties among friends
- Painting in watercolor and gouache
- Reading books about memory, advertising and detective novels
- Watching romantic comedy films, animations, comedy and mystery serials